UQAC
Université du Québec
à Chicoutimi

Contamination en soufre et en semi-métaux de magmas mafiques par assimilation de sédiments et implications pour la formation de gisements de nickel-cuivre-éléments du groupe du platine. Exemple du Complexe de Duluth, Minnesota, États-Unis

Par Nadège Samalens

Thèse présentée à l'Université du Québec à Chicoutimi en vue de l'obtention du grade de Ph. D. en Sciences de la Terre et de l'atmosphère.

Québec, Canada

RÉSUMÉ

La contamination en soufre (S) du magma est une étape clef pour la formation de gisements de Ni-Cu-EGP (Éléments du Groupe du Platine). L'apport de S au magma depuis les roches sédimentaires encaissantes provoque la saturation en S du magma et l'individualisation d'un liquide sulfuré capable de collecter les éléments chalcophiles contenus dans le magma silicaté. Cependant, les modalités de cette contamination n'ont pas été préalablement élucidées et seront abordées dans cette thèse de doctorat.

L'unité basale de l'Intrusion de Partridge River (PRI) du Complexe de Duluth contient des gisements de Ni-Cu-EGP. Le soufre contenu dans ces derniers provient d'une unité de shales noirs riches en sulfures nommée la *Bedded Pyrrhotite Unit*, unité stratigraphique des roches encaissantes de la Formation de Virginia. De nombreux xénolithes de la *Bedded Pyrrhotite Unit* sont présents dans la zone basale du Complexe de Duluth.

Les xénolithes de la *Bedded Pyrrhotite Unit* montrent différents degrés de fusion partielle dans le magma mafique. Une étude pétrographique et texturale des xénolithes de la *Bedded Pyrrhotite Unit* a permis de mettre en évidence la présence de gouttelettes de sulfures dans le produit de fusion partielle des xénolithes. Le calcul de modèles d'assemblages de minéraux à l'équilibre montre que les xénolithes de la *Bedded Pyrrhotite Unit* enregistrent des températures dans le magma comprises entre ~800 et 1000°C; températures suffisantes pour la fusion des sulfures dans les xénolithes.

Les gouttelettes de sulfures dans le produit de fusion partielle des xénolithes de la *Bedded Pyrrhotite Unit* sont composées de pyrrhotite, chalcopyrite, cubanite et pentlandite. Les roches mafiques entourant les xénolithes, nommées norites, sont constituées d'un mélange de produit de fusion partielle des xénolithes de la *Bedded Pyrrhotite Unit* et de composants d'origine magmatique. Dans ces norites des gouttelettes de sulfures composées de pyrrhotite, chalcopyrite, cubanite et pentlandite sont également observées dans des poches de produit de fusion partielle. Ces observations démontrent que les gouttelettes de sulfures sont libérées depuis les xénolithes de la *Bedded Pyrrhotite Unit* dans le magma mafique via le produit de fusion partielle des xénolithes.

Les xénolithes de la *Bedded Pyrrhotite Unit* sont riches en S et en semi-métaux (Te, As, Bi, Sb et Sn). Une étude géochimique roche totale montre que les rapports $\delta^{34}S$ ainsi que le contenu en semi-métaux des sulfures dans les roches mafiques diminuent progressivement avec la distance aux xénolithes de la *Bedded Pyrrhotite Unit*.

Nous proposons, basé sur ces observations, un modèle de contamination en S et en semi-métaux du magma mafique par les xénolithes de la *Bedded Pyrrhotite Unit*. Les gouttelettes de liquide sulfuré dans le produit de fusion partielle des xénolithes de la *Bedded Pyrrhotite Unit* sont transférées depuis les xénolithes vers le magma mafique lors de la libération du produit de fusion partielle dans le magma. Les gouttelettes de liquide sulfuré ainsi transférées vont ensuite s'équilibrer avec le magma et entrainer sa contamination en S et en semi-métaux.

Enfin, une étude détaillée des phases sulfurées au LA-ICP-MS montre que les minéraux sulfurés ne contrôlent pas entièrement le budget en éléments chalcophiles. Les semi-métaux sont distribués dans les minéraux du groupe du platine (MGP) et certaines phases silicatées. Des composés riches en matière organique pourraient aussi jouer un rôle dans la concentration de ces éléments dans les shales noirs.

ABSTRACT

Sulfur (S) contamination of magma is a key process for the formation of Ni-Cu-PGE (Platinum-Group Element) deposits. Sulfur addition into the magma from sedimentary country rocks may allow S saturation of the magma and the individualization of sulfide liquid capable of collecting Ni, Cu and the PGE from the magma. However, mechanisms for S transfer have not been previously established and will be addressed in this doctoral thesis.

The basal unit of the Partridge River Intrusion (PRI) in the Duluth Complex contains Ni-Cu-PGE deposits. The source of S for these is thought to be a S-rich black shales unit, named Bedded Pyrrhotite Unit, stratigraphic unit within the Virginia Formation country rocks. Many xenoliths of the Bedded Pyrrhotite Unit are found in the basal unit of the Duluth Complex.

Xenoliths show different degrees of partial melting in the mafic magma. Petrographic and textural study of xenoliths of the Bedded Pyrrhotite Unit has shown the presence of sulfide droplets in the anatectic melt of the xenoliths. Mineral equilibria calculations of xenoliths of the Bedded Pyrrhotite Unit shows that xenoliths record temperatures between ~ 800 and 1000°C in the magma; temperatures sufficiently high to allow melting of the sulfides within.

The sulfide droplets within the xenolith anatectic melt consist of pyrrhotite, chalcopyrite, pentlandite and cubanite. The hybrid mafic rocks surrounding the xenoliths, named norites, are composed of anatectic melt mixed with components from the magma. Sulfide droplets that consist of pyrrhotite, chalcopyrite, pentlandite and cubanite occur in the anatectic melt in the norites. These observations show that sulfide droplets were entrained in the xenolith anatectic melt and transferred to the mafic magma.

Xenoliths of Bedded Pyrrhotite Unit are rich in S and semimetals (Te, As, Bi, Sb and Sn). Semimetals are chalcophile elements and therefore contamination of mafic magma with black shale xenoliths may produce sulfide melts enriched in these elements compared to sulfide melts formed from mafic magmas. A whole rock geochemical study shows that $\delta^{34}S$ and semimetals contents of sulfides in the mafic rocks decrease with distance from the xenoliths.

Based on these observations, we proposed a model of S and semimetals contamination of the mafic magma by xenoliths of the Bedded Pyrrhotite Unit. Sulfide droplets were entrained in the xenolith anatectic melt and transferred to mafic magma. Then sulfide droplets will equilibrate with the magma and cause its S and semimetals contamination.

A detailed study of sulfide phases by LA-ICP-MS shows that the entire chalcophile elements budget is not hosted by base metal sulfides. Semimetals must be hosted by platinum group minerals (PGM) and silicate phases, i.e. plagioclases and pyroxenes. Some other phases such as organic compounds may also host semimetals in the black shales.

REMERCIEMENTS

"Si haute soit la montagne, on y trouve un sentier" - Anonyme

Je tiens tout d'abord à remercier particulièrement ma directrice de thèse la professeure Sarah-Jane Barnes pour son encadrement, sa disponibilité, ses nombreux conseils et son aide précieuse pour la révision des trois articles. Je tiens également à remercier mon co-directeur Edward Sawyer pour sa disponibilité, les nombreuses discussions et conseils échangés ainsi que pour son aide pour la révision des trois articles. Je vous remercie à tous les deux de m'avoir fait confiance tout au long de ce projet. La réalisation de ce projet n'aurait pu être possible sans le support financier de la Chaire de Recherche du Canada en Métallogénie Magmatique et du Conseil de recherches en sciences naturelles et en génie du Canada. Je remercie également Dany Savard et toute l'équipe du laboratoire pour leur aide dans la réalisation de mes analyses. Je remercie également l'ensemble de mes collègues et l'ensemble du corps professoral de l'UQAC.

Enfin, je tiens à remercier les acteurs de fond de ce projet de doctorat. Tout d'abord mon amoureux Victor qui a joué les rôles de: mari, psychologue, technicien en informatique à maintes reprises, relecteur, accompagnateur sportif… Merci à toi d'avoir partagé cette curieuse aventure à mes côtés, ne changes jamais!

Je tiens également à remercier très fort ma famille pour leur soutien quotidien et constant. Merci à vous tous de m'avoir toujours poussé à aller de l'avant malgré les difficultés rencontrées et toujours témoigné un amour inconditionnel malgré les kilomètres nous séparant. Grâce à vous tous je suis dorénavant convaincue, avec preuves à l'appui, que l'environnement contribue pour au moins 50% à la réalisation et à la réussite d'un projet de doctorat! Je remercie également chaleureusement Malika, notre ange gardien, qui veille sur nous depuis notre arrivée au Canada, merci pour ton soutien et tout l'amour que tu manifestes à notre égard. Enfin, je remercie tous mes amis pour leur soutien, leurs visites et tous les messages d'amitiés partagés outre-frontières…

TABLE DES MATIÈRES

CHAPITRE 1 – Introduction

CHAPITRE 2 – The role of black shales as a source of sulfur and semimetals in magmatic nickel-copper deposits: Example from the Partridge River Intrusion, Duluth Complex, Minnesota, USA

CHAPITRE 5 – Conclusion

LISTE DES FIGURES

CHAPITRE 1

CHAPITRE 2

CHAPITRE 3

CHAPITRE 4

LISTE DES TABLEAUX

CHAPITRE 2

CHAPITRE 3

CHAPITRE 4

LISTE DES ANNEXES

CHAPITRE 1

INTRODUCTION

1.1 INTRODUCTION

Le chapitre d'introduction de cette thèse de doctorat a pour but de présenter le cadre de l'étude et l'approche méthodologique choisie. Ce chapitre s'articule autour de plusieurs parties dont les principales correspondent à la présentation du contexte de l'étude, la zone d'étude, la problématique, les hypothèses, les objectifs et la méthodologie de ce projet de doctorat.

1.2 CONTEXTE

La majeure partie du S des gisements mondiaux de sulfures de Ni-Cu-EGP (Éléments du Groupe du Platine) provient des roches encaissantes, c'est-à-dire de sources externes au magma (Naldrett, 1966; Mainwaring and Naldret ; 1977; Huppert et al., 1984; Lesher et al., 198 4; Lesher and Campbell, 1993; Lesher and Burnham, 1999; Lesher and Burnham, 2001; Ripley et Li, 2013). L'ajout de S au magma suite à l'assimilation de roches encaissantes riches en S par le magma est un mécanisme capable de provoquer sa saturation en sulfures (Mainwaring et Naldrett, 1977; Thériault et al., 2000; Lesher et Burnham, 2001; Ripley et Li, 2002). En effet, lors de la remontée d'un magma depuis le manteau vers des profondeurs crustales la solubilité en S du magma augmente. Une plus grande quantité de S dissout dans le magma est alors nécessaire lors de sa mise en place dans les niveaux crustaux pour obtenir sa saturation précoce en sulfures (Mavrogenes et O'Neill, 1999). Par conséquent, l'ajout de S au magma est un mécanisme

pouvant permettre la saturation en sulfures du magma lors de la mise en place d'une intrusion à des profondeurs crustales.

Suite à la saturation en S du magma, la ségrégation d'un liquide sulfuré peut survenir et entrainer la formation de gouttelettes de liquide sulfuré capable de collecter les métaux (Ni, Cu et EGP) et les autres éléments chalcophiles et ainsi permettre la formation de gisements de Ni-Cu-EGP.

Le Complexe de Duluth est un exemple intéressant pour l'étude des processus de contamination en S du magma. De nombreuses études montrent l'importance de la contamination du magma mafique par des xénolithes de roches encaissantes sédimentaires pour la formation des gisements de Ni-Cu-EGP du Complexe de Duluth (Ripley et Alawi, 1988; Thériault et al., 1997; Thériault et Barnes, 1998; Thériault et al., 2000; Queffurus et Barnes, 2014). De plus, de nombreux forages recoupent le contact entre les roches encaissantes et les roches mafiques de la base du Complexe de Duluth. Enfin, les gîtes minéraux associés au complexe montrent de grands intérêts économiques au niveau mondial (rapports Ni/Cu de 0,8 à 2,5) pour leurs forts tonnages (Figure 1.1) et ce malgré de faibles teneurs en Ni s'illustrant par des ratios S/Ni élevés (Barnes et Lightfoot, 2005).

Préalablement à la présentation des objectifs, de la méthodologie et des principaux résultats de cette étude, les concepts fondamentaux de formation des gisements de Ni-Cu-EGP sont présentés afin de permettre au lecteur d'intégrer le sujet de cette étude dans un processus général de formation de ces gisements.

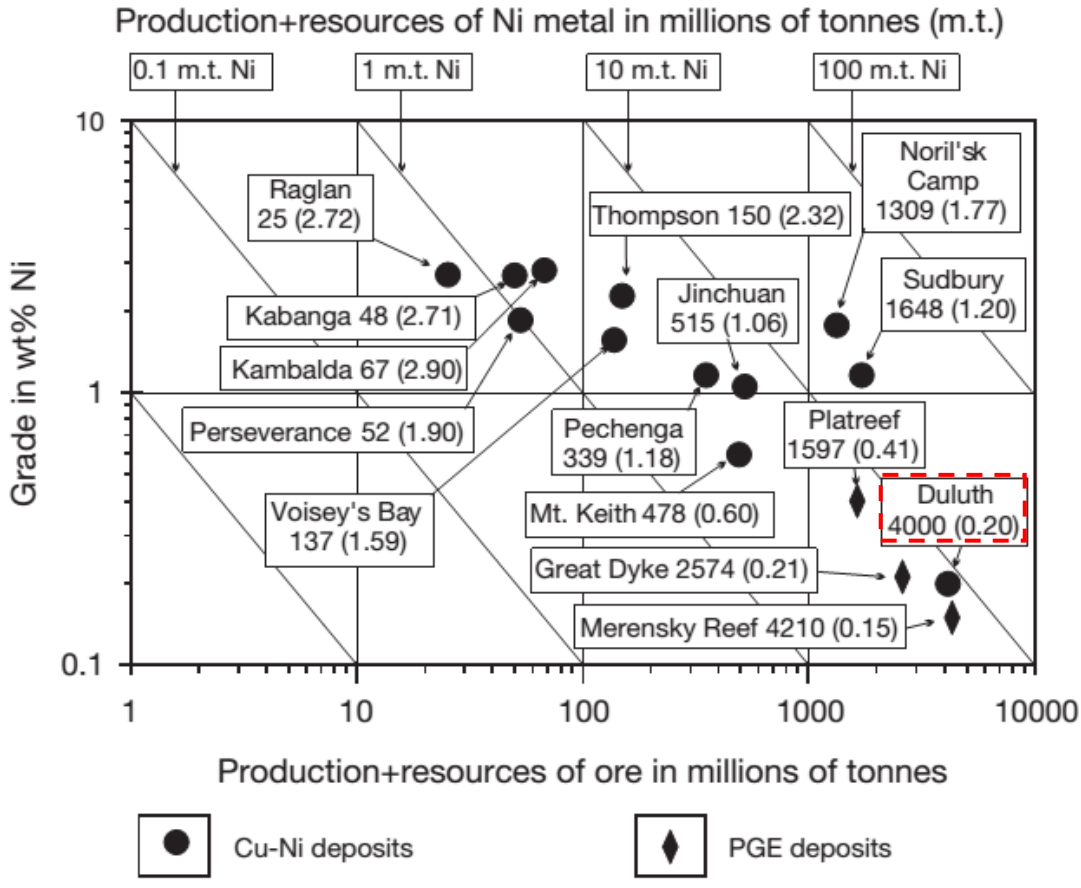

Figure 1.1: Principaux gisements de sulfures de Ni en fonction de leur tonnage et de leur grade (Modifiée d'après Naldrett, 2011).

1.2.1 CARACTÉRISTIQUES ET MISE EN PLACE DU MAGMA PRIMAIRE

La fusion partielle à haut degré d'un manteau lithosphérique ou asthénosphérique, c.à-.d., corrélée à la présence d'un panache mantellique, donne naissance à un magma mafique primaire. De forts taux de fusion partielle permettent la libération de Ni, Cu et EGP par la fusion des sulfures mantelliques et la libération de Ni par une importante contribution de l'olivine au liquide magmatique. Le magma primaire montre alors des rapports Cu/Pd compris entre 10^3 et 10^4 (Barnes et Lightfoot, 2005) et des teneurs en S dissout de 500 à 1000 ppm (Mavrogenes et O'Neill, 1999).

La remontée du magma primaire (décompression) vers la croûte doit être suffisamment rapide afin que le Ni ne soit pas incorporé dans l'olivine lors de sa cristallisation. Lors de cette décompression la solubilité en S du magma augmente et inhibe la saturation en sulfures et la formation d'un liquide sulfuré (Mavrogenes et O'Neill, 1999).

1.2.2 SÉGRÉGATION DU LIQUIDE SULFURÉ

Afin de ségréguer un liquide sulfuré le magma doit être saturé en sulfures. Différents paramètres physiques contrôlent la solubilité en S et par conséquent la saturation en sulfures du magma: la pression, la température, la fugacité en oxygène (fO_2), la fugacité en soufre (fS_2) et la composition du magma. L'apport de S au magma par des sources externes, telles que les roches sédimentaires encaissantes, peut également entrainer la saturation en sulfures du magma (Mavrogenes et O'Neill, 1999; Barnes et Lightfoot, 2005; Li et Ripley, 2005).

Une augmentation de pression entraine une diminution de la solubilité du S dans le magma (Haughton et al., 1974; Helz, 1977; Huang and Williams, 1980; Wendlandt, 1982; Mavrogenes et O'Neill, 1999). La ségrégation d'un liquide sulfuré est possible en profondeur, avant la remontée et la mise en place du magma à des niveaux crustaux (Barnes et Lightfoot, 2005). La diminution de pression, causée par la remontée du magma et sa mise en place dans la croûte, peut entrainer la dissolution des sulfures déjà présents dans le magma sous des conditions mantelliques (Wallace et Carmichael, 1992; Li et al., 1996; Barnes et Lightfoot, 2005). Par conséquent, le magma primaire n'est alors plus saturé en sulfures. De même, une diminution de température provoque une diminution de la solubilité du S dans le magma mais l'effet de la température est moins important que celui de la pression (Wendlandt, 1982 ; Mavrogenes et O'Neill, 1999).

Une augmentation de la fO_2 ou une diminution de la fS_2 du magma se traduit par une diminution de la solubilité du S dans le magma (Haughton et al., 1974; Wallace et Carmichael, 1992; Li et Ripley, 2005; Jugo et al., 2005; Jugo, 2009).

Un changement de composition du magma (Haughton et al., 1974; Li et Ripley, 2005; Liu et al., 2007) peut engendrer la ségrégation d'un liquide sulfuré dans le magma en modifiant la solubilité du S dans le magma. La concentration en FeO du magma est positivement corrélable à la solubilité du S dans le magma. L'augmentation des concentrations de SiO_2 dans le magma, par ajout de SiO_2 ou fractionnement du magma, abaisse la solubilité du S dans le magma en favorisant une diminution de la température du magma (Li et Ripley, 2005).

Cependant, la quantité de S que le magma pourra exsolver sera trop faible pour permettre la création de gisements de Ni-Cu-EGP (Lesher et Groves, 1986). Une autre

possibilité est alors l'ajout de S au magma se produisant lors de la contamination en S du magma par des fluides riches en H_2S dérivés des roches encaissantes et par l'assimilation de roches encaissantes riches en S dans le magma. L'ajout de S au magma entraine une diminution de la solubilité du S dans le magma.

1.2.2.1 CONTAMINATION EN S PAR DES FLUIDES DÉRIVÉS DES ROCHES ENCAISSANTES

Un premier mode de contamination en S du magma correspond à l'apport de S au magma par une phase fluide riche en H_2S dérivée des roches encaissantes (Naldrett, 1966; Mainwaring and Naldret; 1977). Des travaux expérimentaux de dévolatilisation des roches sédimentaires encaissantes ont été réalisés par Baker et al. (2001). Ce mécanisme a été proposé pour la formation de plusieurs gisements de sulfures magmatiques dont la zone minéralisée du Platreef dans le Complexe de Bushveld (Pronost et al., 2008), le Complexe de Duluth (Rao et Ripley, 1983; Ripley et Al-Jassar, 1987; Ripley et al., 2007) ou encore pour le gisement de Noril'sk (Ripley et al., 2003; Li et al., 2009; Pang et al., 2012).

Cependant, cette modalité de contamination est controversée. Selon Ripley et Alawi (1986), le volume de fluides riches en H_2S issu de la dévolatilisation des roches encaissantes du Complexe de Duluth est insuffisant pour la formation des gisements dans les proportions observées dans le complexe. Selon Andrews et Ripley (1989), le S serait conservé dans les roches encaissantes du Complexe de Duluth en tant que constituant de sulfures. Selon Duchesne (2004), dans les roches encaissantes sédimentaires de l'auréole métamorphique au contact du Complexe de Duluth les fluides créés sont conservés et ne contribuent pas à la contamination de l'intrusion mafique adjacente. Enfin, selon

Robertson et al., (2015) le mécanisme de transport de S par des fluides dérivés des roches encaissantes de l'auréole de métamorphisme de contact aurait un effet négligeable sur la contamination en S du magma en comparaison avec la libération de S induite suite à la fusion partielle ou à la dissolution de xénolithes de roches encaissantes dans le magma. En effet, les auteurs estiment que la diffusivité thermique dans un magma est supérieure à la diffusivité du S sous la forme d'un fluide riche en H_2S et suggèrent que le magma sera solidifié bien avant la mise en place du transport diffusif de S depuis les roches encaissantes de l'auréole de métamorphisme de contact.

1.2.2.2 ASSIMILATION DE ROCHES ENCAISSANTES RICHES EN S DANS LE MAGMA

Un second mode de contamination en S du magma correspond à l'assimilation par le magma primaire de roches encaissantes riches en S. Ce mécanisme intervient lors de la mise en place de l'intrusion à son site actuel. La chaleur et la dynamique du magma provoque l'érosion thermo-mécanique, l'arrachement et le transport de fragments de roches encaissantes dans le magma. L'inclusion des xénolithes de roches encaissantes dans le magma mafique provoque leur fusion.

Deux mécanismes sont à distinguer: l'assimilation totale de xénolithes dans des coulées volcaniques de type komatiites (Huppert et al., 1984; Lesher et al., 1984) et l'assimilation partielle de xénolithes avec la formation de « xenomelt » dans des intrusions mafiques et coulées volcaniques de type komatiites (Lesher and Campbell, 1993; Lesher and Burnham, 1999; Lesher and Burnham, 2001).

L'assimilation partielle se définit comme le mécanisme par lequel des composants exogènes, tels que le S, sont incorporés au magma mafique depuis les xénolithes suite à la libération de produit de fusion partielle, c.à-.d. de *xenomelt*, depuis les xénolithes dans le magma. Cette assimilation provoque une contamination du magma mafique en ces composants. De nombreux auteurs ont proposés ce mécanisme d'assimilation partielle pour les complexes de Kambalda (Lesher et Burnham, 2001), Voisey's Bay (Ripley et Li, 2002), Duluth (Ripley et Al-Jassar, 1987; Ripley et Alawi, 1988; Andrews et Ripley, 1989; Ripley et al., 1999; Thériault et al., 2000; Queffurus et Barnes, 2014; Williams et al., 2010; Robertson et al., 2015) et la zone minéralisée du Platreef dans le Complexe de Bushveld (Maier et al., 2008; Johnson et al., 2010).

1.2.3 COLLECTE DES EGP ET CRISTALLISATION DES SULFURES À PARTIR DU LIQUIDE SULFURÉ

Suite à la saturation en sulfures du magma, ce dernier ne peut plus contenir l'excédant de S en solution et des gouttelettes de liquide sulfuré immiscibles capable de collecter les éléments chalcophiles peuvent être ségréguées.

Les métaux communs (Fe, Cu, Ni), les semi-métaux (Te, As, Bi, Sb et Sn) et les EGP sont collectés dans le magma par le liquide sulfuré (Barnes et al., 2001; Brenan et Andrews, 2001). Cette collecte sera favorisée par l'intéraction de grands volumes de magmas silicaté et sulfuré se traduisant par le facteur R (liquide silicaté/liquide sulfuré) (Campbell and Naldrett, 1979). En effet, pour être enrichi en ces métaux, une faible quantité de liquide sulfuré doit avoir été en contact avec d'importants volumes de magma silicaté, c.à-.d., un facteur R élevé. Cette collecte dépend également du contenu en métaux

du magma (Borisov, 2005) et des coefficients de partage de ces éléments pour le liquide sulfuré.

Suite à la collecte de ces métaux, les gouttelettes de liquide sulfuré vont cristalliser (Kullerud et al., 1969; Naldrett, 1969; Li et al., 1992; Ebel and Naldrett, 1996; Barnes et al., 2006; Holwell et McDonald, 2010). Pour une température magmatique d'environ 1200°C, les gouttelettes de liquide sulfuré contiennent Fe, Ni, PGE et semi-métaux en solution. Au cours de la diminution de température, le fractionnement du liquide sulfuré se produit et entraine la cristallisation d'une phase mss (*monosulfide solid solution*) contenant Fe, IPGE (Os, Ir et Ru), Rh et Ni ainsi que la formation d'un liquide sulfuré riche en Cu, Pt, Pd, Au et semi-métaux (Li et al., 1996; Barnes et al., 2001; voir la synthèse dans Barnes et Lightfoot, 2005). À une température proche de 900°C, une phase iss (*intermediate solid solution*) riche en Cu cristallise et un liquide fractionné riche en Pt, Pd, Au et semi-métaux s'individualise (Peregoedova et al., 2004; Helmy et al., 2007). Enfin, pour des températures inférieures à 650°C les sulfures de métaux communs (pentlandite, pyrrhotite et chalcopyrite) exsolvent depuis les phases mss et iss. À des températures inférieures à 650°C des minéraux du groupe du platine (MGP) peuvent se former par exsolution (Barnes et al., 2008).

Le processus de cristallisation des gouttelettes de liquide sulfuré survient pendant et après leur transport et leur accumulation dans des lacunes structurales, c.à-.d., par exemple des dépressions au plancher des intrusions. Cette accumulation est une conséquence de la densité plus élevée des sulfures en comparaison avec le magma silicaté hôte et d'une diminution de la dynamique du magma.

Enfin, des épisodes de métamorphisme et d'hydrothermalisme peuvent modifier les sulfures des gisements suite à ces étapes de fractionnement (Farrow et Watkinson, 1992; Dare et al., 2010a; Dare et al., 2010b; Dare et al., 2011). De plus, suite à leur accumulation, les sulfures peuvent être déformés et déplacés de leur site de formation (Barnes et Lightfoot, 2005).

1.3 LE COMPLEXE DE DULUTH

1.3.1 ZONE D'ÉTUDE

Le contexte géologique général du Complexe de Duluth est présenté dans cette section. Le détail de chaque zone d'étude est présenté de façon spécifique dans chaque articles ; c.-à-d. les chapitres 2, 3 et 4 de cette thèse de doctorat.

Le Complexe de Duluth, situé à l'ouest des Grands Lacs dans le Minnesota aux États-Unis (Figure 1.2), est constitué de plusieurs intrusions mafiques. Ces intrusions se sont formées par plusieurs injections de magma corrélées à la présence d'un panache mantellique en contexte de rift continental (Severson et Hauck, 1997; Ojakangas et al., 2001; Miller et Severson, 2002). La mise en place du complexe a été datée à 1,1 Ga (Miller et al., 2002). Deux épisodes magmatiques distincts ont permis la formation, d'une part, des séquences felsiques et gabbroiques et, d'autre part, des séquences anorthositiques et litées, c.à-.d., des roches gabbroiques et troctolitiques du Complexe de Duluth (Figure 1.2).

L'Intrusion de Partridge River fera l'objet de cette étude. Elle comprend quatre gisements de Ni et de Cu principaux : *Wyman Creek*, *Wetlegs*, *NorthMet* (anciennement nommé *Dunka Road)* et *Mesaba* (anciennement nommé *Babbitt)*. L'Intrusion de Partridge River est constituée de huit unités magmatiques (Figure 1.3). L'unité basale I de l'intrusion

contient de nombreux xénolithes de roches encaissantes de la Formation de Virginia et la majorité des roches minéralisées de l'intrusion. Cette unité est composée de la succession de lithologies suivante: norites, gabbronorites et roches ultramafiques (troctolites) riches en EGP de la base vers le centre de l'intrusion (Hauck et al., 1997; Thériault et al., 1997; Miller et Severson, 2002; Severson et Hauck, 2008; Queffurus et Barnes, 2014).

Les gisements localisés dans l'unité basale de l'Intrusion de Partridge River sont principalement constitués de sulfures disséminés (Thériault et Barnes, 1998; Ripley, 2014). Cependant, de petites accumulations de sulfures massifs sont fréquemment observées en périphérie des xénolithes de roches encaissantes.

Les roches encaissantes de l'Intrusion de Partridge River appartiennent à deux unités de roches sédimentaires datées du paléoprotérozoïque et faisant partie de la séquence sédimentaire de Animikie: la Formation de Virginia (argilites noires, pélites, greywackes et siltites) (Lucente et Morey, 1983) au contact de l'Intrusion de Partridge River et la formation de Fer de Biwabik (Figure 1.2). Les sédiments de la Formation de Virginia sont métamorphisés sur une distance de plus de 100m à partir du contact avec l'intrusion; les roches les plus proches du contact, nommées diatexites, enregistrent des températures supérieures à 800°C (Labotka et al., 1981; Tracy et Frost, 1991; Sawyer, 2014).

Une unité importante dans cette étude est la *Bedded Pyrrhotite Unit* qui appartient à la Formation de Virginia. Cette unité est constituée de shales noirs particulièrement riches en S et en semi-métaux et est localisée proche du contact avec l'Intrusion de Partridge River (Severson et Hauck, 2008). De nombreux xénolithes dérivés de cette unité sont

présents dans l'unité basale I de l'Intrusion de Partridge River (Ripley et Alawi, 1988; Thériault et al., 2000; Severson et Hauck, 2008; Queffurus et Barnes, 2014).

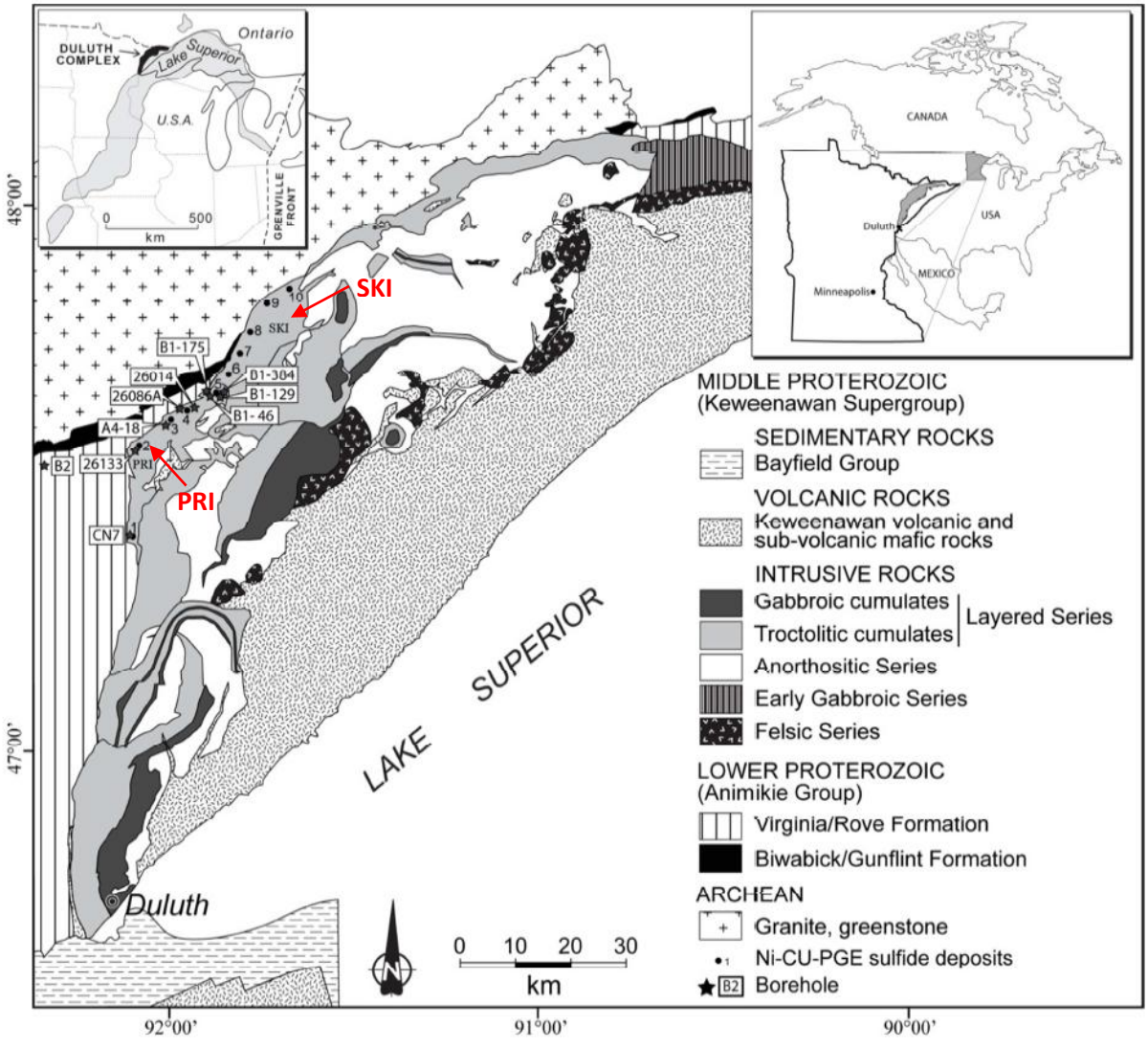

Figure 1.2: Carte géologique du Complexe de Duluth, nord est du Minnesota, États-Unis (Modifiée d'après Miller et Severson, 2002). Nomenclature des gisements: 1)Water Hen, 2)Wyman Creek, 3)Wetlegs, 4)NorthMet, 5)Mesaba, 6)Serpentine, 7)Dunka Pit, 8)Birch Lake, 9)Maturi, 10)Spruce Road. Abréviations: PRI = Partridge River Intrusion; SKI = South Kawishiwi Intrusion.

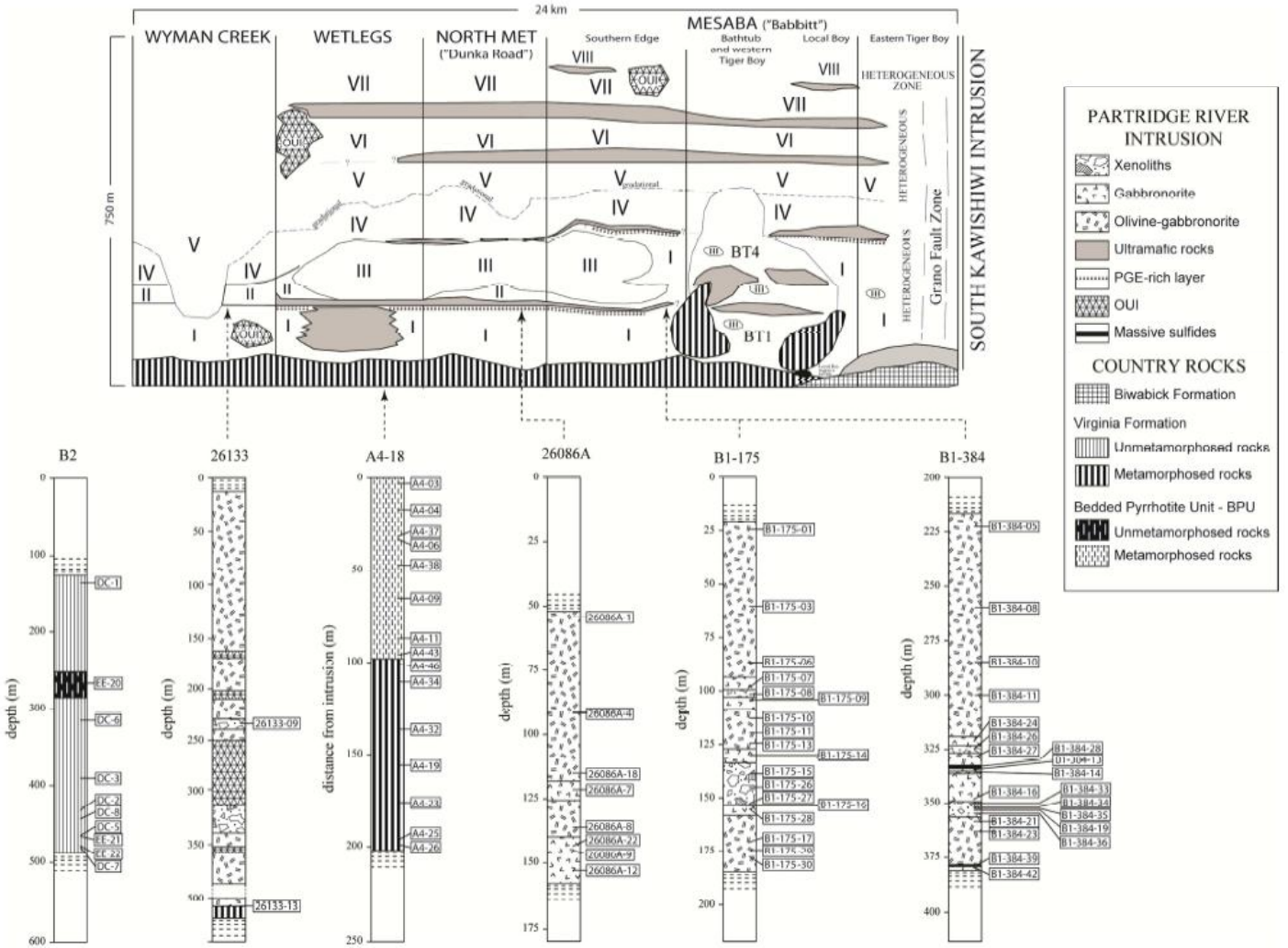

Figure 1.3: Coupe à travers de l'Intrusion de Partridge River (PRI) basée sur des données de forage (modifiée d'après Severson et Hauck, 2008; Queffurus et Barnes, 2014). Abréviations: BPU = Bedded Pyrrhotite Unit, OUI = Oxide-rich bodies.

1.3.2 CONTAMINATION *IN-SITU* EN S DU MAGMA

Deux modalités de contamination en S du magma ont été proposées pour le Complexe de Duluth. Une première modalité controversée est la contamination en S par des fluides dérivés des roches encaissantes (Rao et Ripley, 1983; Ripley et Al-Jassar, 1987; Baker et al., 2001; Ripley et al., 2007). A l'inverse, un modèle de contamination en S du magma suite à l'assimilation partielle de xénolithes de roches encaissantes riches en S dans le magma a été proposé par Thériault et Barnes (1998) et Queffurus et Barnes (2014).

Les valeurs élevées en $\delta^{34}S$, S/Se des roches mafiques à proximité des xénolithes et la présence de sulfures massifs autour des xénolithes sont interprétées comme des évidences de contamination *in-situ* en S du magma suite à l'assimilation de xénolithes riches en S dans le magma (Ripley, 1990; Thériault et Barnes, 1998; Queffurus et Barnes, 2014, Robertson et al., 2015).

Différentes étapes conduisent à la formation des minéralisations en sulfures des gisements de l'Intrusion de Partridge River du Complexe de Duluth:

1) Inclusion dans le magma et fusion partielle de xénolithes de roches sédimentaires encaissantes

Lors de la mise en place à son site actuel du magma mafique du Complexe de Duluth, la chaleur et la dynamique du magma provoque l'érosion thermo-mécanique, l'arrachement et le transport de fragments de roches encaissantes de la Formation de Virginia observés sous la forme de xénolithes dans les roches mafiques. L'inclusion de xénolithes de roches encaissantes dans le magma mafique provoque leur fusion partielle (Ripley et Alawi, 1988; Thériault et al., 1997; Thériault et Barnes, 1998; Thériault et al., 2000; Lesher et Burnham, 2001; Queffurus et Barnes, 2014).

2) Contamination *in-situ* en S du magma

La décroissance progressive des rapports S/Se et des valeurs de $\delta^{34}S$ depuis la zone basale de l'intrusion contenant de nombreux xénolithes vers le centre de l'intrusion est interprétée comme un argument en faveur de la contamination *in-situ* en S du magma depuis les xénolithes de roches encaissantes (Figure 1.4). Selon Queffurus et Barnes (2014), seuls les xénolithes riches en S issus de l'unité sédimentaire de la *Bedded Pyrrhotite Unit* de la Formation de Virginia permettent un apport de S suffisant au magma pour sa saturation en sulfures (Figures 1.4 b et c). En effet, comparativement avec les autres roches de la Formation de Virginia, les roches de la *Bedded Pyrrhotite Unit* ont les plus grandes valeurs pour les rapports S/Se et $\delta^{34}S$. Ces auteurs suggèrent que la libération de gouttelettes de sulfures depuis les xénolithes dans le magma mafique pourrait se produire via le produit de fusion partielle produit lors de l'assimilation des xénolithes dans le magma.

3) Injection de magma troctolitique non contaminé

Enfin, une nouvelle injection de magma peut se produire au dessus de la séquence minéralisée. Les gouttelettes de liquide sulfuré à la base de cette injection seraient alors mises en mouvement par la dynamique du magma hôte (Thériault et Barnes, 1998). Par la suite, le liquide sulfuré ainsi mobilisé réagirait avec le magma silicaté riche en métaux et pourrait alors cristalliser des horizons de sulfures riches en EGP (facteur R élevé: ratio liquide silicaté/liquide sulfuré) en percolant dans les cumulats partiellement consolidés.

Cependant, le mécanisme réel par lequel le S et les éléments chalcophiles, tels que les semi-métaux, sont transférés au magma à partir des roches encaissantes n'a pas clairement été élucidé et sera exploré et documenté dans cette thèse de doctorat.

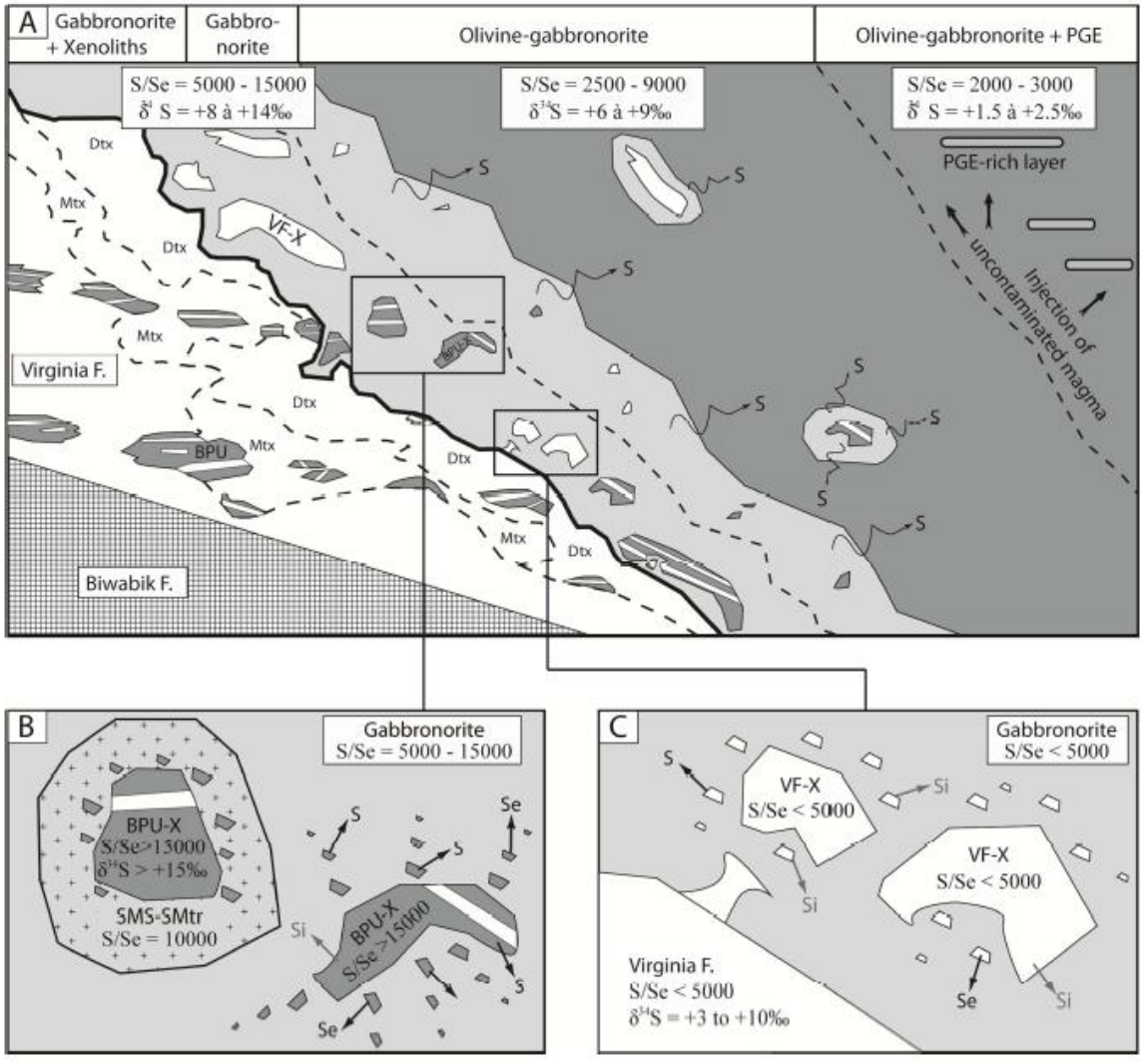

Figure 1.4: Modèle de contamination en S du magma par assimilation in-situ de xénolithes de roches sédimentaires de la BPU (Bedded Pyrrhotite Unit) (Modifiée d'après Queffurus et Barnes, 2014). Abréviations : VF-X=Xénolithes de la Formation de Virginia non issus de la BPU; BPU-X=Xénolithes de la Bedded Pyrrhotite Unit; Mtx=Métatexites; Dtx=Diatexites; SMS-SMtr=Sulfures massifs et matriciels.

1.4 PROBLÉMATIQUE

L'objet de ce doctorat est d'élucider les mécanismes de transfert du S au magma depuis les xénolithes de roches encaissantes riches en S de la *Bedded Pyrrhotite Unit* ainsi que d'étudier l'association potentielle du S avec d'autres éléments chalcophiles, tels que les semi-métaux, lors de ce transfert.

1.5 HYPOTHÈSES

La principale hypothèse de contamination en S du magma testée dans ce projet de doctorat serait un transfert de gouttelettes de liquide sulfuré depuis les xénolithes de la *Bedded Pyrrhotite Unit* vers le magma mafique lors de la migration du produit de fusion partielle des xénolithes dans le magma, à la vitesse du magma environnant. Des gouttelettes de sulfure, produites lors de la fusion partielle des sulfures contenus dans les xénolithes, seront alors observées dans le produit de fusion partielle des xénolithes et dans les roches mafiques environnantes.

De plus, les roches de la *Bedded Pyrrhotite Unit* sont enrichies en semi-métaux. Les xénolithes peuvent de la *Bedded Pyrrhotite Unit* alors être potentiellement une source de semi-métaux. Ces éléments pourraient être transférés au magma avec le S lors de l'assimilation des xénolithes de la *Bedded Pyrrhotite Unit* dans le magma.

1.6 OBJECTIFS

Cette étude se concentrera sur l'interaction entre les xénolithes de roches encaissantes et le magma dans l'unité inférieure de l'Intrusion de Partridge River du Complexe de Duluth. Les principaux objectifs de cette étude sont:

- Caractériser les différentes lithologies : Shales noirs métamorphisés hors de l'auréole de contact, les roches de la *Bedded Pyrrhotite Unit* de l'auréole de métamorphisme de contact, les xénolithes de la *Bedded Pyrrhotite Unit* partiellement fondus de roches encaissantes, les roches mafiques de l'unité basale I;
- Identifier les échanges chimiques entre les xénolithes et le magma se produisant lors de la fusion partielle des xénolithes dans le magma, c.-à-d. les éléments impliqués:
    - ✓ Concentration des éléments chalcophiles dans chaque lithologie;
    - ✓ Distribution des éléments chalcophiles entres les différents minéraux;
- Déterminer le/les mécanisme(s) d'apport du S au magma et estimer les conditions prévalant lors de l'assimilation des xénolithes de la *Bedded Pyrrhotite Unit*;
- Proposer un modèle de contamination en S du magma suite à l'assimilation des xénolithes de la *Bedded Pyrrhotite Unit* par le magma.

1.7 MÉTHODOLOGIE

1.7.1 SÉLECTION DES ÉCHANTILLONS

Les échantillons choisis sont représentatifs des lithologies de l'unité basale de l'Intrusion de Partridge River et de ses roches encaissantes. Les échantillons caractérisés dans la présente étude ont été collectés lors de précédents travaux sur le Complexe de Duluth (Thériault et al., 1997; Lafrance J., « communication écrite », 1998; Thériault et Barnes, 1998; Thériault et al., 2000; Nabil, 2003; Duchesne, 2004; Queffurus et Barnes, 2014). Ces échantillons proviennent de carottes de forages qui ont échantillonné la base de

l'Intrusion de Partridge River, le contact avec les roches sédimentaires encaissantes et les roches sédimentaires encaissantes de la Formation de Virginia.

1.7.2 ÉTUDE PÉTROGRAPHIQUE ET TEXTURALE

Les proportions et les textures des minéraux silicatés et sulfurés des lithologies énumérées ci-dessus ont été évaluées et caractérisées. Cette étude pétrographique et texturale permet de préciser la nature des lithologies impliquées dans la contamination en S du magma et de mettre en évidence les modalités de transfert du S depuis les xénolithes vers le magma hôte.

Ces observations ont été réalisées principalement par microscopie optique et microscopie électronique à balayage (MEB).

1.7.3 ANALYSES GÉOCHIMIQUES

En complément d'une banque de données géochimiques accessibles pour une grande partie des échantillons (Thériault et al., 1997; Lafrance J., « communication écrite », 1998; Thériault et Barnes, 1998; Thériault et al., 2000; Nabil, 2003; Duchesne, 2004; Queffurus et Barnes, 2014), des analyses géochimiques pour les éléments majeurs, traces, terres rares, isotopes et EGP ont été réalisées. Le détail des méthodes d'analyses est présenté dans la rubrique méthodologie de chaque chapitre scientifique, c.-à-d. les chapitres 2, 3 et 4 de cette thèse de doctorat.

1.7.4 MODÉLISATION THERMODYNAMIQUE

Grâce au logiciel de modélisation thermodynamique Perple_X, des pseudosections ont été réalisées à partir de données géochimiques sur roche totale afin de mettre en évidence les températures, les degrés de fusion partielle et la nature du protolithe des xénolithes de la *Bedded Pyrrhotite Unit* et ainsi caractériser les conditions qui prévalaient lors du transfert du S depuis les xénolithes vers le magma. Le détail des procédures de modélisation est présenté dans le deuxième article de cette thèse de doctorat, c.-à-d. le chapitre 3.

1.8 FORMAT DE LA THÈSE

La présente thèse de doctorat s'organise sous la forme d'un recueil de publications scientifiques. Cette thèse est divisée en cinq chapitres. Le premier chapitre correspond à une introduction permettant de situer l'étude dans un contexte scientifique général. Le deuxième chapitre correspond à un manuscrit intitulé « The role of black shales as a source of sulfur and semimetals in magmatic nickel-copper deposits: Example from the Partridge River Intrusion, Duluth Complex, Minnesota, USA » et publié en anglais dans la revue internationale spécialisée Ore Geology Reviews. Le troisième chapitre correspond à un manuscrit intitulé « Modeling the partial melting of sulfur-rich black shale xenoliths in the Duluth Complex, Minnesota, U.S.A.». Ce manuscrit a été accepté dans la revue Journal of Metamorphic Geology. Le quatrième chapitre correspond à un manuscrit intitulé «A Laser Ablation Inductively Coupled Plasma Mass Spectrometry study of the distribution of chalcophile elements in sedimentary and magmatic sulfides of the Duluth Complex, Minnesota, USA ». Ce manuscript a été soumis au journal Ore Geology Reviews pour le

volume spécial basé sur les contributions du treizième symposium international sur les gisements de Ni-Cu-EGP. Le cinquième chapitre rapporte les conclusions générales de cette thèse de doctorat. Les données utilisées pour chacun des manuscrits sont présentées soit dans le manuscrit lui-même, soit en annexe de cette thèse de doctorat.

1.9 DÉCLARATION DE CONTRIBUTION ORIGINALE

Les résultats présentés dans cette thèse de doctorat sont originaux et ont été soumis à des revues scientifiques en tant que publication originale. Les échantillons ont été collectés lors de campagnes d'échantillonnages antérieures à ce projet doctoral et une base de données était disponible dès le début du projet doctoral. L'auteure de cette thèse de doctorat a réalisé des analyses complémentaires. Les sources des données préliminaires utilisées dans ce projet doctoral ont été citées dans les manuscrits présentés ainsi que les auteurs ayant préalablement publiés des résultats associés à ces données.

1.10 CONTRIBUTION DES COLLABORATEURS

L'auteure principale de cette thèse de doctorat est également l'auteure principale des trois manuscrits soumis. La première auteure a sélectionné des échantillons, a effectué des analyses en laboratoire sur ces échantillons, a réalisé les travaux de modélisation et a rédigé les articles scientifiques présentés dans cette thèse de doctorat. La deuxième auteure, Sarah-Jane Barnes, a assuré la supervision, le financement et la planification de ce projet doctoral ainsi que la révision des articles scientifiques avant leur soumission. Le troisième auteur, Edward W. Sawyer, a co-supervisé le projet de doctorat et a également contribué et guidé la révision des manuscrits avant leur soumission.

1.11 RÉFÉRENCES

Andrews, D., Ripley, E., (1989) Mass transfer and sulfur fixation in the contact aureole of the Duluth Complex, Dunka road Cu-Ni deposit, Minnesota. The Canadian Mineralogist, 27, 293-310.

Baker, D.R., Barnes, S.-J., Simon, G., Bernier, F., (2001) Fluid transport of sulfur and metals between sulfide melt and basaltic melt. The Canadian Mineralogist, 39, 537-546.

Barnes, S.-J., Van Achterbergh, E., Makovicky, E., Chusi, L., (2001) Proton microprobe results for the partitioning of platinum-group elements between monosulfide solid solution and sulfide liquid. South African Journal of Geology, 104, 275.

Barnes, S.-J., Lightfoot, P.C., (2005) Formation of magmatic nickel-sulfide ore deposits and processes affecting their copper and platinum-group elements contents. Economic Geology, 100th Anniversary Volume, 179-213.

Barnes, S.-J., Cox, R., Zientek, M., (2006) Platinum-group element, Gold, Silver and Base Metal distribution in compositionally zoned sulfide droplets from the Medvezky Creek Mine, Noril'sk, Russia. Contributions to Mineralogy and Petrology, 152, 187-200.

Barnes, S.-J., Prichard, H.M., Cox, R.A., Fisher, P.C., Godel, B., (2008) The location of the chalcophile and siderophile elements in platinum-group element ore deposits (a textural, microbeam and whole rock geochemical study): Implications for the formation of the deposits. Chemical Geology, 248, 295-317.

Borisov, A., (2005) Crystallization and stability of noble metal alloys in the magmatic process. Geology of ore deposits, 47, 469-475.

Brenan, J.M., Andrews, D., (2001) High-temperature stability of laurite and Ru–Os–Ir alloy and their role in PGE fractionation in mafic magmas. The Canadian Mineralogist, 39, 341-360.

Campbell, I.H., Naldrett, A.J., (1979) The influence of silicate:sulfide ratios on the geochemistry of magmatic sulfides. Economic Geology, 74, 1503-1506.

Dare, S., Barnes, S.-J., Prichard, H., (2010a) The distribution of platinum group elements (PGE) and other chalcophile elements among sulfides from the Creighton Ni–Cu–PGE sulfide deposit, Sudbury, Canada, and the origin of palladium in pentlandite. Mineralium Deposita, 45, 765-793.

Dare, S., Barnes, S.-J., Prichard, H., Fisher, P., (2010b) The timing and formation of Platinum-Group minerals from the Creighton Ni-Cu-Platinum-Group Element Sulfide Deposit, Sudbury, Canada: Early crystallization of PGE-rich sulfarsenides. Economic Geology, 105, 1071-1096.

Dare, S., Barnes, S.-J., Prichard, H., Fisher, P., (2011) Chalcophile and platinum-group element (PGE) concentrations in the sulfide minerals from the McCreedy East deposit, Sudbury, Canada, and the origin of PGE in pyrite. Mineralium Deposita, 46, 381-407.

Duchesne, L., (2004) Fusion partielle et microstructures associées dans l'auréole de contact du complexe igné de Duluth, Minnesota. Mémoire de maîtrise, Université du Québec à Chicoutimi.

Ebel, D.S., Naldrett, A.J., (1996) Fractional crystallization of sulfide ore liquids at high temperature. Economic Geology, 91, 607-621.

Farrow, C.E.G., Watkinson, D.H., (1992) Alteration and the role of fluids Ni, Cu and platinium-group elements deposition, Sudbury Igneous Complex contact, Onaping-Levack area, Ontario. Mineral Petrology, 46, 67-83.

Hauck, S.A., Severson, M.J., Zanko, L., Barnes, S.-J., Morton, P., Alminas, H., Foord, E.E., Dahlberg, E.H., (1997) An overview of the geology and oxide, sulfide, and platinum-group element mineralization along the western and northern contacts of the Duluth Complex. Geological Society of America, special paper, 312, 137-185.

Haughton, D.R., Roeder, P.L., Skinner, B.J., (1974) Solubility of sulfur in mafic magmas. Economic Geology, 69, 451-467.

Helmy, H.M., Ballhaus, C., Berndt, J., Bockrath C., Wohlgemuth-Ueberwasser, C., (2007) Formation of Pt, Pd and Ni tellurides: Experiments in sulfide-telluride systems. Contributions to Mineralogy and Petrology, 153, 577-591.

Helz, R.T., (1977) Determination of the P-T dependence of the first appearance of FeS-rich liquid in natural basalts to 20 kb. (abstr.) Transactions American Geophysical Union, EOS, 58, 523.

Holwell, D., McDonald, I., (2010) A review of the behaviour of platinum group elements within natural magmatic sulfide ore systems The importance of semimetals in governing partitioning behaviour. Platinum Metal Review, 54, 26-36.

Huang, W.-L., Williams, R.J., (1980) Melting relations of portions of the system Fe-S-Si-O to 32 kb with implication to the nature of the mantle-core boundary. (abstr.) Lunar and Planetary Science XI, Lunar and Planetary Institute, Houston, 486-488.

Huppert, H.E., Sparks, R.S.J., Turner, J.S., Arndt, N.T., (1984) Emplacement and cooling of komatiite lavas. Nature, 309, 19-22.

Johnson, T.E., Brown, M., White, R.W., (2010) Petrogenetic modelling of strongly residual metapelitic xenoliths within the southern Platreef, Bushveld Complex, South Africa. Journal of Metamorphic Geology, 28, 269-291.

Jugo, P.J., Luth, R.W., Richards, J.P., (2005) An Experimental Study of the Sulfur Content in Basaltic Melts Saturated with Immiscible Sulfide or Sulfate Liquids at 1300°C and 1•0 GPa. Journal of Petrology, 46, 783-798.

Jugo, P.J., (2009) Sulfur content at sulfide saturation in oxidized magmas. Geology, 37, 415-418.

Kullerud, G., Yund, R.A., Moh, G.H., (1969) Phase Relations in the Cu-Fe-S, Cu-Ni-S, and Fe-Ni-S Systems. Magamtic Ore Deposits, a symposium, Economic Geology Monogr, 4, 323-343.

Labotka, T.C., Papike, J.J., Vaniman, D.T. (1981) Petrology of contact metamorphosed argillite from the Rove Formation, Gunflint Trail, Minnesota. American Mineralogist, 66, 70-86.

Lesher, C.M., Arndt, N.T., Groves, D.I., (1984) Genesis of komatiite-associated nickel sulfide deposits at Kambalda, Western Australia: A distal volcanic model. Sulfide deposits in mafic and ultramafic rocks, Institute of Mining and Metallurgy, London, 10 p.

Lesher, C.M., Groves, D.I., (1986) Controls on the Formation of Komatiite-Associated Nickel-Copper Sulfide Deposits. In: Friedrich GH, Genkin AD, Naldrett AJ, Ridge JD, Sillitoe RH, Vokes FM (eds) Geology and Metallogeny of Copper Deposits: Proceedings of the Copper Symposium 27th International Geological Congress Moscow, 1984, vol. Springer Berlin Heidelberg, Berlin, Heidelberg, 43-62.

Lesher C.M., Campbell, I.H., (1993) Geochemica and Fluid Dynamic Modeling of Compositional Variations in Archean Komatiite-Hosted Nickel Sulfide Ores in Western Australia. Economic Geology, 88, 804-816.

Lesher C.M., Burnham, O.M., (1999) Mass balance and mixing in dynamic ore-forming magmatic system. Dynamic processes in magmatic ore deposits and their application in mineral exploration, Geological Associations of Canada Short Course Notes, 13, 413-450.

Lesher, C.M., Burnham, O.M., (2001) Multicomponent elemental and isotopic mixing in Ni–Cu–(PGE) ores at Kambalda, western Australia. The Canadian Mineralogist, 39, 421-446.

Li, C., Barnes, S.-J., Makovicky, E., Rose-Hansen, J., Makovicky, M., (1996) Partitioning of nickel, copper, iridium, rhenium, platinum, and palladium between monosulfide solid solution and sulfide liquid: Effects of composition and temperature, Geochimica et Cosmochimica Acta, 60, 1231-1238.

Li, C., Naldrett, A.J., Coats, C.J.A., Johannessen, P., (1992) Platinum, palladium, gold, copper-rich stringers at the Strathcona Mine, Sudbury; their enrichment by fractionation of a sulfide liquid. Economic Geology, 87, 1584-1598.

Li, C., Ripley, E., (2005) Empirical equations to predict the sulfur content of mafic magmas at sulfide saturation and applications to magmatic sulfide deposits, Mineralium Deposita, 40, 218-230.

Li, C., Ripley, E.M., and Naldrett, A.J., (2009) A new genetic model for the giant Ni-Cu-PGE sulfide deposits associated with the Siberian flood basalts, Economic Geology, 104, 291–301.

Liu, Y., Samaha, N.-T., Baker, D.R., (2007) Sulfur concentration at sulfide saturation (SCSS) in magmatic silicate melts. Geochimica et Cosmochimica Acta, 71, 1783-1799.

Lucente, M.E., Morey, G.B., (1983) Stratigraphy and sedimentology of the Lower Proterozoic Virginia Formation, northern Minnesota, Minnesota Geological Survey, Report of Investigations RI-28, 28 p.

Maier, W., Li, C., De Waal, S.A., (2008) Petrogenesis of contact-style PGE mineralization in the northern lobe of the Bushveld Complex: comparison of data from the farms Rooipoort, Townlands, Drenthe and Nonnenwerth. Mineralium Deposita, 43, 255-280.

Mainwaring, P.R., Naldrett, A., (1977) Country-rock assimilation and the genesis of Cu-Ni sulfides in the Water Hen Intrusion, Duluth Complex, Minnesota. Economic Geology, 72, 1269-1284.

Mavrogenes, J.A., O'Neill, H.S.C., (1999) The relative effects of pressure, temperature and oxygen fugacity on the solubility of sulfide in mafic magmas. Geochimica et Cosmochimica Acta, 63, 1173-1180.

Miller, J.D., Severson, M.J., (2002) dans Miller, J.D., Green, J.C., Severson, M.J., Chandler, V.W., Hauck, S.A., Peterson, D.M., Wahl, T.E., (2002) Geology and mineral potential of the Duluth Complex and related rocks of northeastern Minnesota. Minnesota Geological Survey Report of Investigations, RI-58, 106-143.

Nabil, H., (2003) Genèse des dépôts de Fe-Ti-P associés aux intrusions litées (Exemples : l'intrusion mafique de Sept-Iles, au Québec; complexe de Duluth aux Etats-Unis). Thèse de doctorat, Université du Québec à Chicoutimi, 537 p.

Naldrett, A., (1966) Role of sulphurization in genesis of iron-nickel sulphide deposits of porcupine district Ontario. Canadian Mining and Metallurgical Bulletin, 59, 489.

Naldrett, A., (1969) A portion of the system Fe-S-O between 900 and 1800 °C and its application to sulfide ore magmas. Journal of petrology, 10, 171-201.

Naldrett, A. J. (2011) Fundamentals of magmatic sulfide deposits. Reviews. Economic Geology, 17, 1-50.

Ojakangas, R.W., Morey, G.B., Green, J.C., (2001) The mesoproterozoic midcontinent rift system, Lake Superior Region, USA. Sedimentary Geology, 141, 421-442.

Pang, K.-W., Arndt, N., Svenson, H., Planke, S., Polozov, A., Polteau, S., Iizuka, Y., and Chung, S.-L., (2012) A petrologic, geochemical and Sr-Nd isotopic study on contact metamorphism and degassing of Devonian evaporates in the Noril'sk aureoles, Siberia, Contributions to Mineralogy and Petrology, 165, 683-704.

Peregoedova, A., Barnes, S.-J., Baker, D.R., (2004) The formation of Pt-Ir alloys and Cu-Pd-rich sulfide melts by partial desulfurization of Fe-Ni-Cu sulfides; results of experiments and implications for natural systems. Chemical Geology, 208, 247-264.

Pronost, J., Harris, C., Pin, C., (2008) Relationship between footwall composition, crustal contamination, and fluid–rock interaction in the Platreef, Bushveld Complex, South Africa. Mineralium Deposita, 43, 825-848.

Queffurus, M., Barnes, S.-J., (2014) Selenium and sulfur concentrations in country rocks from the Duluth Complex, Minnesota, USA: Implications for formation of the Cu-Ni-PGE sulfides. Economic Geology, 109, 785-794.

Rao, B.V., Ripley, E. M., (1983) Petrochemical studies of the Dunka Road Cu-Ni deposit, Duluth Complex, Minnesota. Economic Geology, 78, 1222-1238.

Ripley, E.M., (1990) Se/S ratios of the Virginia Formation and Cu-Ni mineralization in the Babbitt area, Duluth Complex, Minnesota. Economic Geology, 85, 1935-1940.

Ripley, E.M., (2014) Ni-Cu-PGE Mineralization in the Partridge River, South Kawishiwi, and Eagle Intrusions: A review of contrasting styles of sulfide-rich occurrences in the Midcontinent Rift System. Economic Geology. 109, 309-324.

Ripley, E.M., Alawi, J.A., (1986) Sulfide mineralogy and chemical evolution of the Babbitt Cu-Ni deposit, Duluth Complex, Minnesota. The Canadian Mineralogist, 24, 347-368.

Ripley, E.M., Alawi, J.A., (1988) Petrogenesis of pelitic xenoliths at the Babbitt Cu-Ni deposit, Duluth Complex, Minnesota, U.S.A. Lithos, 21, 143-159.

Ripley, E.M., Al-Jassar, T.J., (1987) Sulfur and oxygen isotope studies of melt-country rock interaction, Babbitt Cu-Ni deposit, Duluth Complex, Minnesota. Economic Geology, 82, 87-107.

Ripley, E.M., Lambert, D.D., Frick, L.R., (1999) Re-Os, Sm-Nd, and Pb isotopic constraints on mantle and crustal contributions to magmatic sulfide mineralization in the Duluth Complex. Geochimica et Cosmochimica Acta, 62, 3349-3365.

Ripley, E. M., Li, C., (2002) Paragneiss assimilation in the genesis of magmatic Ni-Cu-Co sulfide mineralization at Voisey's Bay, Labrador: δ34S, δ13C, and Se/S evidence. Economic Geology, 97, 1307-1318.

Ripley, E.M., Li, C., (2003) Sulfur isotope exchange and metal enrichment in the formation of magmatic Cu-Ni-(PGE) deposits, Economic Geology, v. 98, p. 635–641.

Ripley, E.M., Li, C., (2013) Sulfide saturation in mafic magmas: Is external sulfur required for magmatic Ni-Cu-(PGE) ore genesis? Economic Geology, 108, 45-58.

Ripley, E.M., Taib, N.I., Chusi, L., Moore, C.H., (2007) Chemical and mineralogical heterogeneity in the basal zone of the Partridge River Intrusion: implications for the origin of Cu–Ni sulfide mineralization in the Duluth Complex, midcontinent rift system. Contributions to Mineralogy and Petrology, 154, 35-54.

Robertson, J., Ripley, E.M., Barnes, S.J., Li, C., (2015) Sulfur liberation from country rocks and incorporation in mafic magmas. Economic Geology, 110, 1111-1123.

Sawyer, E.W., (2014) The inception and growth of leucosomes: microstructure at the start of melt segregation in migmatites. Journal of Metamorphic Geology, 7, 695-712.

Severson, M.J., Hauck, S.A., (1997) Igneous Stratigraphy and Mineralization in the Basal Portion of the Partridge River Intrusion, Duluth Complex, Allen Quadrangle, Minnesota: Duluth, Minnesota, University of Minnesota, Natural Resources Research Institute, Technical Report, NRRI/TR-97/19, 102 p.

Severson, M.J., Hauck, S.A., (2008) Finish logging of Duluth Complex drill core (and a reinterpretation of the geology at the Mesaba (Babbitt) deposit). Duluth, University of Minnesota, Natural Research Institute, Technical Report, NRRI/TR-2008/17, 68 p.

Thériault, R.D., Barnes, S.-J., (1998) Compositional variations in Cu-Ni-PGE sulfides of the Dunka road deposit, Duluth Complex, Minnesota: The importance of combined assimilation and magmatic processes. The Canadian Mineralogist, 36, 869-886.

Thériault, R.D., Barnes, S.-J., Severson, M.J., (1997) The influence of country-rock assimilation and silicate to sulfide ratios (R factor) on the genesis of the Dunka Road Cu – Ni – platinum-group element deposit, Duluth Complex, Minnesota. Canadian Journal of Earth Sciences, 34, 375-389.

Thériault, R.D., Barnes, S.-J., Severson, M.J., (2000) Origin of Cu-Ni-PGE sulfide mineralization in the Partridge River Intrusion, Duluth Complex, Minnesota. Economic Geology, 95, 929-943.

Tracy, R.J., Frost, B.R., (1991) Phase equilibria and thermobarometry of calcareous, ultramafic and mafic rocks, and iron formations. Reviews in Mineralogy and Geochemistry, 26, 207-289.

Wallace, P., Carmichael, I.S.E., (1992) Sulfur in basaltic magmas. Geochimica et Cosmochimica Acta, 56, 1863-1874.

Wendlandt, R.F., (1982) Sulfide saturation of basalt and andesite melts at high pressures and temperatures. American Mineralogist, 67, 877-885.

Williams, C.D., Ripley, E.M., Li, C., (2010) Variations in Os ratios of pyrrhotite as a result of water-rock and magma-rock interaction: Constraints from Virginia Formation-Duluth Complex contact zone. Geochimica et Cosmochimica Acta, 74, 4772-4792.

CHAPITRE 2

THE ROLE OF BLACK SHALES AS A SOURCE OF SULFUR AND SEMIMETALS IN MAGMATIC NICKEL-COPPER DEPOSITS: EXAMPLE FROM THE PARTRIDGE RIVER INTRUSION, DULUTH COMPLEX, MINNESOTA, USA

SAMALENS N.[1], BARNES S.-J. [1], SAWYER E.W.[1]

[1] Université du Québec à Chicoutimi, 555 boulevard de l'Université, Saguenay, QC, G7H 2B1, Canada

ORE GEOLOGY REVIEWS (2017), VOL.81, 173-187

2.1RÉSUMÉ

L'unité basale du Complexe de Duluth (Minnesota, USA) contient des gisements sulfurés de Ni-Cu. Le soufre contenu dans ces derniers provient d'une unité de shales noirs riches en sulfures nommée la *Bedded Pyrrhotite Unit*, unité stratigraphique des roches encaissantes de la Formation de Virginia. Cependant, le mécanisme de transfert du S n'a pas été clairement établi. Nous avons réalisé une étude pétrographique et géochimique des roches de l'auréole de contact et de l'unité basale du Complexe afin de mettre en évidence les modalités de ce transfert.

Dans l'auréole de contact, la *Bedded Pyrrhotite Unit* est composée de shales graphitiques à granulométrie fine avec de fins lits de sulfures composés majoritairement de pyrrhotite et de moins de 1% de chalcopyrite. L'unité basale contient de nombreux xénolithes de roche encaissante de la *Bedded Pyrrhotite Unit* entourés par des norites. Les xénolithes de la *Bedded Pyrrhotite Unit* sont partiellement fondus et les lits de sulfures qu'ils contiennent sont disloqués. Des leucosomes contenant des gouttelettes de sulfure (pyrrhotite, pentlandite, cubanite et chalcopyrite) ont été mis en évidence dans les xénolithes mais également dans le magma entourant ces derniers. Dans les roches mafiques des petites poches de leucosomes contenant des sulfures ont été individualisées. En plus de leur richesse en S les roches de la *Bedded Pyrrhotite Unit* sont également riches en As 38 ppm, Sb 4.1 ppm, Bi 0.6 ppm et Te 0.4 ppm et enregistrent des valeurs élevées pour le rapport $\delta^{34}S$. Une décroissance des valeurs des rapports $\delta^{34}S$, As/S, Bi/S et Sb/S est observée avec la distance depuis les xénolithes. De façon similaire, les valeurs des rapports Ni/S, Cu/S, Se/S et (Éléments du Groupe du Platine)/S sont les plus élevées dans les roches mafiques et augmentent avec la distance depuis les xénolithes.

Notre modèle propose que les gouttelettes de sulfure dérivées des xénolithes de la *Bedded Pyrrhotite Unit* sont entrainées par le liquide fondu silicaté des xénolithes et ainsi transférées au magma mafique. Les gouttelettes de sulfure vont ensuite s'équilibrer avec le magma. Les gouttelettes les plus proches des xénolithes n'auront pas l'opportunité d'interagir avec de grandes quantités de magma et leur composition sera par conséquence similaire à celle des sulfures de la *Bedded Pyrrhotite Unit*, c.à.d. riche en semi-métaux et pauvre en Ni, Cu et EGP. À l'inverse, les gouttelettes de sulfure les plus éloignées des xénolithes peuvent interagir avec de plus grandes quantités de magma et leur composition sera alors proche de celle des sulfures principalement dérivés du magma.

2.2ABSTRACT

The basal unit of the Duluth Complex (Minnesota, USA) contains Ni-Cu sulfide deposits. The S in these is thought to be derived from a sulfide-rich black shale unit known as the Bedded Pyrrhotite Unit, a stratigraphic unit within the Virginia Formation host rocks. However, the mechanism of S transfer has not been clearly established. In order to understand how this transfer occurs we have undertaken petrography and whole rock geochemistry of the rocks from the contact aureole and the basal unit.

In the contact aureole, the Bedded Pyrrhotite Unit consists of a very fine-grained graphitic shales with thin beds of sulfides consisting of pyrrhotite with minor chalcopyrite (<1%). The basal unit contains numerous Bedded Pyrrhotite Unit xenoliths surrounded by norites. The Bedded Pyrrhotite Unit xenoliths are partially melted and the sulfide beds are disrupted. Leucosomes are present and these contain blebs of sulfides consisting of pyrrhotite, pentlandite, cubanite and chalcopyrite. In the mafic rocks surrounding the xenoliths small patches of sulfide-bearing leucosome are found. In addition to being rich in S the Bedded Pyrrhotite Unit is rich in As 38 ppm, Sb 4.1 ppm and Bi 0.6 ppm and Te 0.4 ppm and has high $\delta^{34}S$ values. The $\delta^{34}S$, As/S, Bi/S and Sb/S decrease with distance from the xenoliths. Similarly, the Ni/S, Cu/S, Se/S and (platinum-group elements)/S ratios are higher in the mafic rocks and increase with distance from the xenoliths.

Our model proposes that droplets of sulfide melt derived from the Bedded Pyrrhotite Unit xenoliths were entrained in the anatectic silicate melt of the xenoliths and transferred to the mafic magma. The sulfide droplets equilibrated with the mafic magma. Those close to the xenoliths did not have the opportunity to react with a large quantity of magma, and hence their composition is similar to the sulfides of the Bedded Pyrrhotite Unit, i.e., rich in

semimetals and poor in Ni, Cu and PGE. Farther away from the xenoliths, the sulfide droplets could have reacted with more magma, and the composition of these sulfides approach that of sulfides derived mainly from mafic magma.

Keywords. Duluth Complex; Proterozoic black shales; *in-situ* contamination; partial melting; diffusion; Ni deposits; magmatic sulfides.

2.3 INTRODUCTION

Much of the S in the world's magmatic Ni-Cu-platinum-group element (PGE) deposits is thought to be derived from external sources in the country rocks (Lesher et al., 1984; Ripley and Li, 2013). It is generally thought that S is derived from black shales (Thériault and Barnes, 1998; Lesher and Burnham, 2001). The world famous Noril'sk-Talnakh deposits may be an exception (Grinenko, 1985; Li et al., 2003). Sulfur is not the only element that could be derived from a black shale source. Black shales are enriched in As, Sb, Te and Bi by 1 to 3 orders of magnitude relative to Mid-Ocean Ridge Basalts, picrites and primitive mantle (Table 2.1). These elements are all chalcophile, and therefore contamination of a mafic magma with black shale could produce sulfide melts enriched in these elements compared to sulfide melts formed from mafic magmas. The semimetals may be important in concentrating PGEs within a Ni-Cu-PGE deposit because they are the anions required to form many platinum-group minerals (PGM).

A number of mechanisms for transfer of S from black shales to magma have been proposed: bulk melting of the country rock (Lesher and Burnham, 2001), transfer by gas or hydrothermal fluids (Baker et al., 2001; Ripley et al., 2007; Molnár et al., 2009; Benkó et

al., 2015a, b), and transfer of sulfide droplets during partial melting of black shale xenoliths (Queffurus and Barnes, 2014). The Partridge River Intrusion of the Duluth Complex represents an ideal and well-documented intrusion for studying contamination processes because Ni-Cu sulfide deposits are found in the basal part of the intrusion close to the contact with S-rich black shales of the Virginia Formation (Mainwaring and Naldrett, 1977; Ripley, 1981; Andrews and Ripley, 1989; Thériault et al., 1997; Thériault and Barnes, 1998; Ripley et al., 2007; Severson and Hauck, 2008; Queffurus and Barnes, 2014; Robertson et al., 2015,Fig. 3), and detailed sampling is possible through numerous boreholes across the contact between the basal unit and the country rocks.

The sulfide-rich black shale unit is known as the Bedded Pyrrhotite Unit (Severson, 1994). Based on changes in $\delta^{34}S$ and S/Se values, the Bedded Pyrrhotite Unit has been identified as the source of the sulfur that contaminated the mafic magma (Zanko et al., 1994; Queffurus and Barnes, 2014). We have undertaken a petrographic, mineralogical and whole rock geochemical study of the Bedded Pyrrhotite Unit country rocks, the Bedded Pyrrhotite Unit xenoliths and the enclosing mafic magma with the aim of investigating S and the behaviour of the semimetals during the interaction between the black shales and the mafic magma.

	As (ppm)	Sb (ppm)	Bi (ppm)	Te (ppm)
BPU average – This study	38	4.1	0.6	0.4
SDO-1 average (Henrique-Pinto et al., in press)	62.6	4.11	0.27	0.131
SCHS-1 average (Henrique-Pinto et al., in press)	50.1	0.072	0.102	-
SBC-1 average (Henrique-Pinto et al., in press)	29.4	1.22	0.6	0.184
SH-1 average (Henrique-Pinto et al., in press)	22.5	1.17	1.19	0.198
Median black shale (Ketris and Yudovich, 2009)	30	5	1.1	2
Upper crust average (Hu and Gao, 2008)	5.7	0.75	0.23	0.027
MORB average (Arevalo and McDonough, 2010)	0.11	0.014	0.01	0.005
Picrites average (Dionne-Foster, 2007)	0.45	0.02	0.01	0.02
Primitive mantle average (Lyubetskaya and Korenaga, 2007)	0.05	0.007	0.004	0.008

Table 2.1: Average semimetals contents of the Bedded Pyrrhotite Unit in comparison with average and median values of black shale standards (SDO-1, SCHS-1, SBC-1 and SH-1), black shale, upper crust, MORB, picrites and primitive mantle. Abbreviations: BPU = Bedded Pyrrhotite Unit; MORB = Mid-oceanic ridge basalt; SDO-1 = Devonian Ohio Shale; SCHS-1 = Carbonaceous black shale; SBC-1 = Brush Creek Shale; SH-1 = In-house black shale.

2.4 GEOLOGICAL CONTEXT

The Duluth Complex is a Mesoproterozoic (1100 Ma) mafic complex located in Minnesota, USA. It consists of a number of mafic intrusions (Fig. 2.1) that are associated with the Midcontinent Rift System, and it is related to overlying Keweenawan flood basalts (Severson and Hauck, 1997; Ojakangas et al., 2001; Miller and Severson, 2002). The country rocks range from Paleoproterozoic sedimentary rocks of the Animikie Group in the south to the Archean granite-greenstone in the north (Fig. 2.1).

Magmatic Ni-Cu deposits occur at the bases of two of the intrusions, the Partridge River and the South Kawishiwi. Our study focused on the deposits of the Partridge River Intrusion (Fig. 2.1). The basal unit is composed of the following lithologies: norite, gabbronorite, troctolite and ultramafic rocks (Hauck et al., 1997; Thériault et al., 1997; Miller and Severson, 2002; Severson and Hauck, 2008). Norites correspond to the contaminated part of the magma and are localised in the vicinity of xenoliths in the basal part of the intrusion (Thériault et al., 1997; Queffurus and Barnes, 2014).

The deposits consist of disseminated to massive sulfides. The main minerals present are pyrrhotite, cubanite, chalcopyrite and pentlandite (Thériault and Barnes, 1998; Ripley, 2014). Massive sulfides mainly occur surrounding country rocks xenoliths. Anastomosing veins and veinlets of massive sulfides also occur hosted by the gabbronorites, and in the country rocks close to the contact with the intrusion (Ripley and Alawi, 1986).

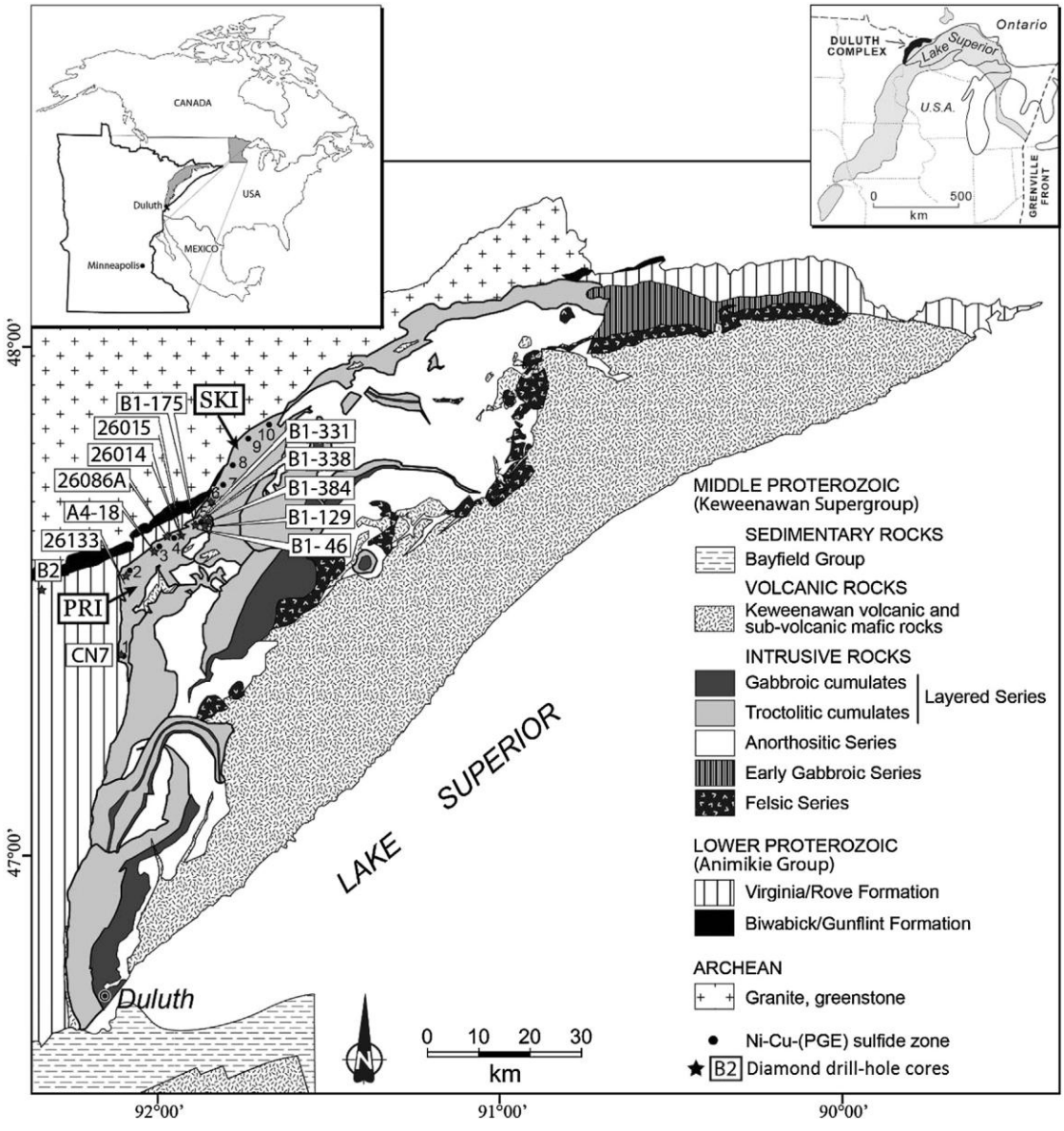

Figure 2.1: Geological and location map of the Duluth Complex (modified from Queffurus and Barnes, 2014; Ojakangas et al., 2001;Miller and Severson, 2002). The right inset shows position of the Duluth Complex in the Midcontinent Rift System. Abbreviations: PRI= Partridge River Intrusion, SKI = South Kawishiwi intrusion. Ni-Cu deposits: 1,Water Hen; 2, Wyman Creek; 3,Wetlegs; 4, NorthMet (Dunka Road); 5, Mesaba (Babbitt); 6, Serpentine; 7, Dunka Pit; 8, Birch Lake; 9, Nokomis; 10. Diamond drill-hole cores are indicated by stars.

The country rocks of the Partridge River Intrusion are Virginia Formation sedimentary rocks of the Animikie Group. The Virginia Formation is composed of carbonate, greywacke, pelite, black shale and siltstone (Lucente and Morey, 1983). Away from the intrusion, the sedimentary rocks are essentially unmetamorphosed and the sulfide present is pyrite (Bonnichsen, 1972; Lucente and Morey, 1983, Fig. 2A; Queffurus and Barnes, 2014). However, close to the intrusion, the sedimentary rocks of the Virginia Formation have undergone contact metamorphism at temperatures greater than 800°C, and formed diatexite migmatites close to the contact with the mafic magma (Labotka et al., 1981; Tracy and Frost, 1991; Sawyer, 2014).

One unit of particular interest is the Bedded Pyrrhotite Unit consisting of sulfide-rich black shales in the Virginia Formation and believed to have been deposited in a restricted anoxic basin (Hauck et al., 1997). The Bedded Pyrrhotite Unit is mostly present close to the contact with the Duluth Complex (Severson and Hauck, 2008). This unit is approximately 200 m thick, but is sporadically distributed. The basal unit of the Partridge River Intrusion (Unit I) contains numerous xenoliths of the Bedded Pyrrhotite Unit and the Virginia Formation (Ripley and Alawi, 1988; Thériault et al., 2000; Severson and Hauck, 2008; Queffurus and Barnes, 2014).

2.5 METHODOLOGY

Thirty-five samples were selected from diamond drill-hole cores that intersected the contact between the Virginia Formation and Partridge River Intrusion at the NorthMet, Mesaba, and Wetlegs deposits (Fig. 2.1 and Appendix 1). Bedded Pyrrhotite Unit samples from the contact aureole come from boreholes AA-18 and A4-15. Xenoliths of the Bedded

Pyrrhotite Unit, plus norites and gabbronorites, were collected from the NorthMet and Mesaba deposits (Fig. 2.1 and Appendix 1). Data were combined with results from previous studies for a total database of 126 samples (Thériault et al., 1997; Thériault and Barnes, 1998; Thériault et al., 2000; Duchesne, 2004; Queffurus and Barnes, 2014).

Polished sections of each sample were obtained and petrographic observations were made, taking particular note of the sulfide mineralogy and textural changes between samples from the contact aureole, the xenoliths, and the norites.

Sulfur, Se, PGEs, and semimetals were determined at LabMaTer, Université du Québec à Chicoutimi (UQAC). Sulfur concentrations were determined using a HORIBA EMIA-220V infrared and combustion S and C analyser using the method of Bédard et al. (2008). Platinum-group elements were determined by NiS-fire assay preconcentration followed by Te-co-precipitations and ICP-MS analysis. In addition, five samples were analysed by isotope dilution using the method of Savard et al. (2010). The semimetals in the black shales were determined using a new analytical protocol specially designed for black shales using an Agilent 7700X Series ICP-MS (Henrique-Pinto et al., in press).

Major oxides and trace elements were determined at Activation Laboratories Ltd (Actlabs), Ontario, Canada by Fusion ICP-MS (Method WRA42B). Sulfur isotopes were determined at the Environmental Isotope Laboratory (University of Waterloo, ON, Canada) using Micromass IsoChrom elemental analyzer-isotope ratio mass spectrometer (EA-IRMS) with V-CDT as internal standard. Results for the certified reference materials are presented in Appendices 3 and 5.

2.6 RESULTS

2.6.1 PETROGRAPHY

The mineralogy and form of the sulfides occurring within the contact aureole differ from those in the xenoliths. In samples of the Bedded Pyrrhotite Unit from the contact aureole partial melting occurred (Duchesne, 2004; Sawyer, 2014), and the rocks close to the contact with the intrusion are now diatexite migmatites with thin pyrrhotite beds (~0.5 to 3 mm thick) disrupted by a silicate anatectic melt network (Fig. 2.2a) that is now pseudomorphed by quartz, plagioclase and K-feldspar**.** The beds consist almost exclusively of pyrrhotite with rare (<1%) chalcopyrite intergrowths (Fig. 2.2b), but no pentlandite or cubanite.

In contrast, in the xenoliths the sulfide assemblage contain less pyrrhotite (~70 modal%), and more chalcopyrite, cubanite, and pentlandite (Fig. 2.2c). Angular shaped sulfide patches with low interfacial angles with the silicate phases, together with sulfide microveinlets that fill space between silicate grains, occur at the margins of sulfide beds (Fig. 2.2d). There is also a variation in the proportion of sulfides within the xenoliths. In meter-sized xenoliths, the sulfide assemblages at the cores consists largely of pyrrhotite (~90 modal%), with some chalcopyrite and cubanite (~10 modal%), and little or no pentlandite (<1 modal%). The sulfide assemblage at the margins contain a large proportion of chalcopyrite and cubanite (up to 30 modal%), and some pentlandite (~5 modal%).

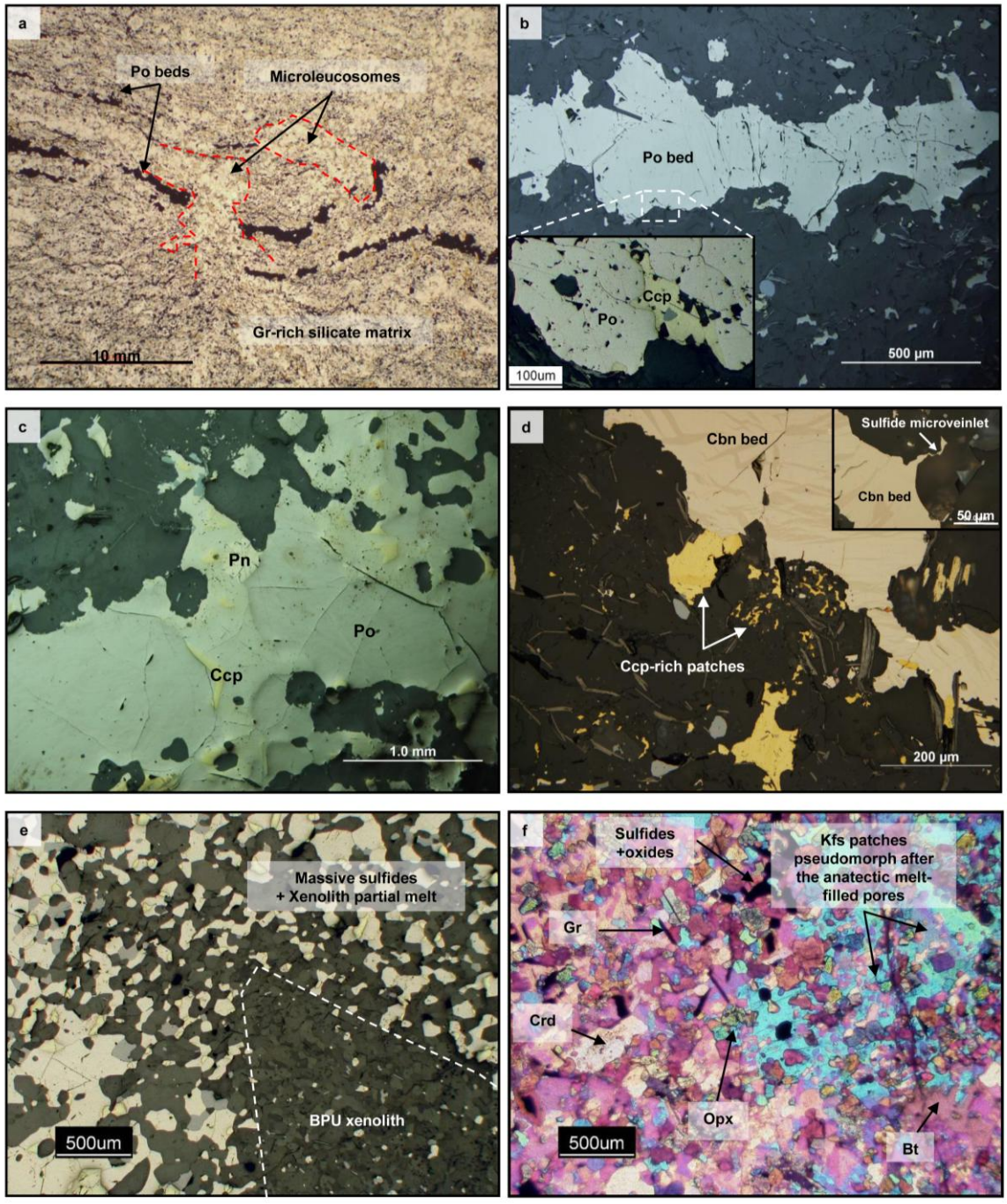
a
Po beds
Microleucosomes
Gr-rich silicate matrix
10 mm
b
Po bed
Ccp
Po
100um
500 µm
c
Pn
Po
Ccp
1.0 mm
d
Cbn bed
Sulfide microveinlet
Cbn bed
50 µm
Ccp-rich patches
200 µm
e
Massive sulfides
+ Xenolith partial melt
BPU xenolith
500um
f
Sulfides
+oxides
Kfs patches
pseudomorph after
the anatectic melt-
filled pores
Gr
Crd
Opx
Bt
500um

Figure 2.2: Photomicrographs of Bedded Pyrrhotite Unit (BPU) sulfide and silicate textures from the contact aureole and inside the intrusion. a) Sulfide beds crosscut by anatectic melt in partially molten BPU from the contact aureole. b) Pyrrhotite bed in BPU metamorphosed from the contact aureole. Inset shows details for chalcopyrite grain in pyrrhotite bed. Notice that pentlandite and cubanite are absent of BPU country rocks. c) Sulfide bed in BPU xenolith within the intrusion. d) Delaminated sulfide bed in BPU xenolith. Chalcopyrite-rich patches close to the sulfide bed and sulfide microveinlets. Low angle interfaces occurs between sulfides and silicates. e) Massive sulfides surrounding BPU xenolith within the intrusion. f) Silicate mineralogical assemblage in a partially melted BPU xenolith. Quartz plate is added to better identify the inclusions of former anatectic melt. Abbreviations (Whitney and Evans, 2010): Silicates: Bt = Biotite; Opx = Orthopyroxene; Crd = Cordierite; Pl = Plagioclase; Kfs = K-Feldspar; Qtz = Quartz. Sulfides:Ccp = Chalcopyrite; Cbn = Cubanite; Po = Pyrrhotite; Pn = Pentlandite. Gr = Graphite.

In some cases pyrrhotite-rich massive sulfides occur mixed with xenolith anatectic melt in a narrow zone (~5cm) at the edge of the Bedded Pyrrhotite Unit xenoliths (Fig. 2.2e). The sulfide assemblage consists of approximately equal amounts of pentlandite and chalcopyrite (~ 5 to 10 modal% of each), with the balance consisting of pyrrhotite.

The silicate portions of the Bedded Pyrrhotite Unit xenoliths have undergone partial melting. The mineralogical assemblage in the silicate portion of the Bedded Pyrrhotite Unit xenoliths is orthopyroxene + cordierite + biotite + plagioclase + melt +/- K-feldspar, graphite and ilmenite (Fig. 2.2f). Former melt pockets are composed of large (~500µm) K-feldspar and quartz grains with plagioclase, orthopyroxene, and less commonly cordierite inclusions. The melt pockets occur as films and interconnected networks, i.e., microleucosomes, in the xenoliths of the Bedded Pyrrhotite Unit. The xenolith mineralogical assemblage is consistent with those of the migmatites from the contact aureole that recorded temperatures hotter than 800°C (Sawyer, 2014).

Sulfide patches, which consist of an intergrowth of the sulfide minerals, commonly occur within the patches of former anatectic melt in the Bedded Pyrrhotite Unit xenoliths (Fig. 2.3a, b). The rounded shapes of sulfide patches in anatectic melt contrast with the angular shape of sulfides that occur in the matrix of the Bedded Pyrrhotite Unit xenoliths.

In addition, the zones (~5cm) around the xenoliths contains large amounts of anatectic melt (up to 50 modal %), and in some samples pyrrhotite-rich massive sulfides. These zones consist of xenolith anatectic melt mixed with the mafic magma (Fig. 2.3c, e). Relics of former anatectic melt consists of quartz-rich patches (~mm) and films (less than 100µm). Sulfide droplets (~50-200µm) are present in the anatectic melt (Fig. 2.3d, f).

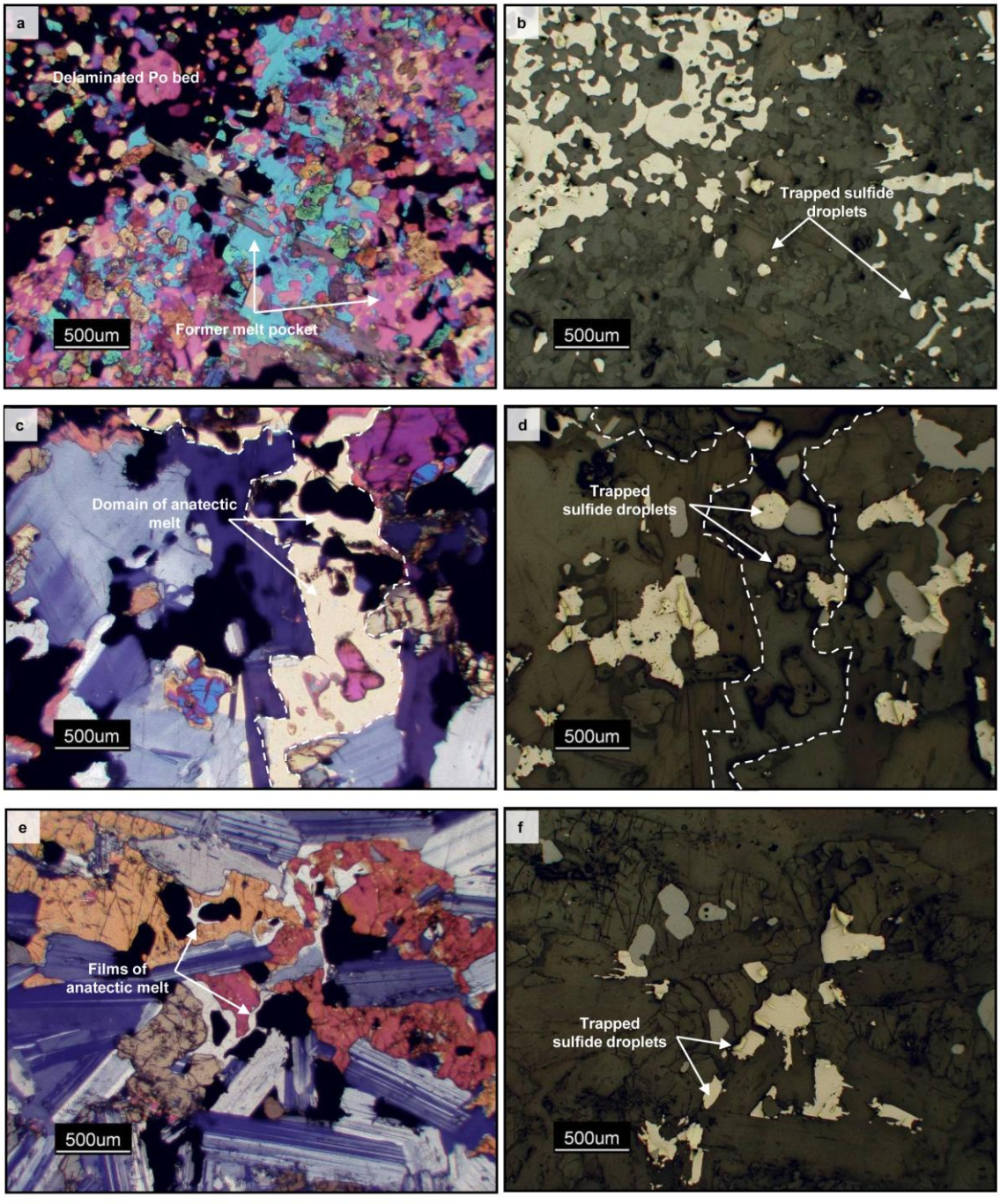
a
Delaminated Po bed
500um
Former melt pocket
b
Trapped sulfide droplets
500um
c
Domain of anatectic melt
500um
d
Trapped sulfide droplets
500um
e
Films of anatectic melt
500um
f
Trapped sulfide droplets
500um

Figure 2.3: Photomicrographs of partial melting textures of Bedded Pyrrhotite Unit (BPU) xenoliths and surrounding zones. a) Detached pyrrhotite bed in BPU xenoliths in contact with melt filled space between the grains in BPU xenolith. Quartz plate is added to better show anatectic melt pockets. b) Sulfide droplets in pockets of anatectic melt pockets in same area of the photomicrograph a). c) Anatectic melt patches with trapped sulfide droplets in the anatectic melt-rich zone surrounding BPU xenolith. d) Rounded sulfide droplets trapped in xenolith anatectic melt patches from same area as the photomicrograph c). e) Films of anatectic melt that contained sulfide droplets in zones surrounding the BPU xenolith. f) Details of sulfide droplets trapped in small pockets of anatectic melt, same area than photomicrograph e). Abbreviation: BPU = Bedded Pyrrhotite Unit.

2.6.2 GEOCHEMISTRY

2.6.2.1 CHALCOPHILE ELEMENTS

The S content of the Bedded Pyrrhotite Unit from the contact aureole and the xenoliths ranges from ~ 0.5 to 10 % S. The $\delta^{34}S$ values vary from 16 to 20‰ in the contact aureole, and from 9 to 18‰ in the xenoliths (Fig. 2.4a). Massive sulfides contain 16 to 35 % S, and the $\delta^{34}S$ values range from 8 to 16‰, similar to the xenoliths. Most norites and gabbronorites are poorer in S, containing ~0.01 to 8.35% S; the $\delta^{34}S$ values are more depleted, ranging from 1.6 to ~15‰ (Fig. 2.4a).

The metals are plotted versus S in order to examine whether they are hosted by sulfide minerals. Taking all the rock types together there is a broad correlation between the metals and S (Figs. 2.4 and 2.5). The mafic rocks are the most enriched in metals for a given S content, the xenoliths have an intermediate content, and the contact aureole rocks record the lowest metal contents (Figs. 2.4 b-d and 2.5). The massive sulfides are richer in Ni and Co than the other rock types, and they lie along the extension of the trends for the mafic rocks. In contrast the massive sulfide samples contain more Cu than most, but not all, samples from other rock types.

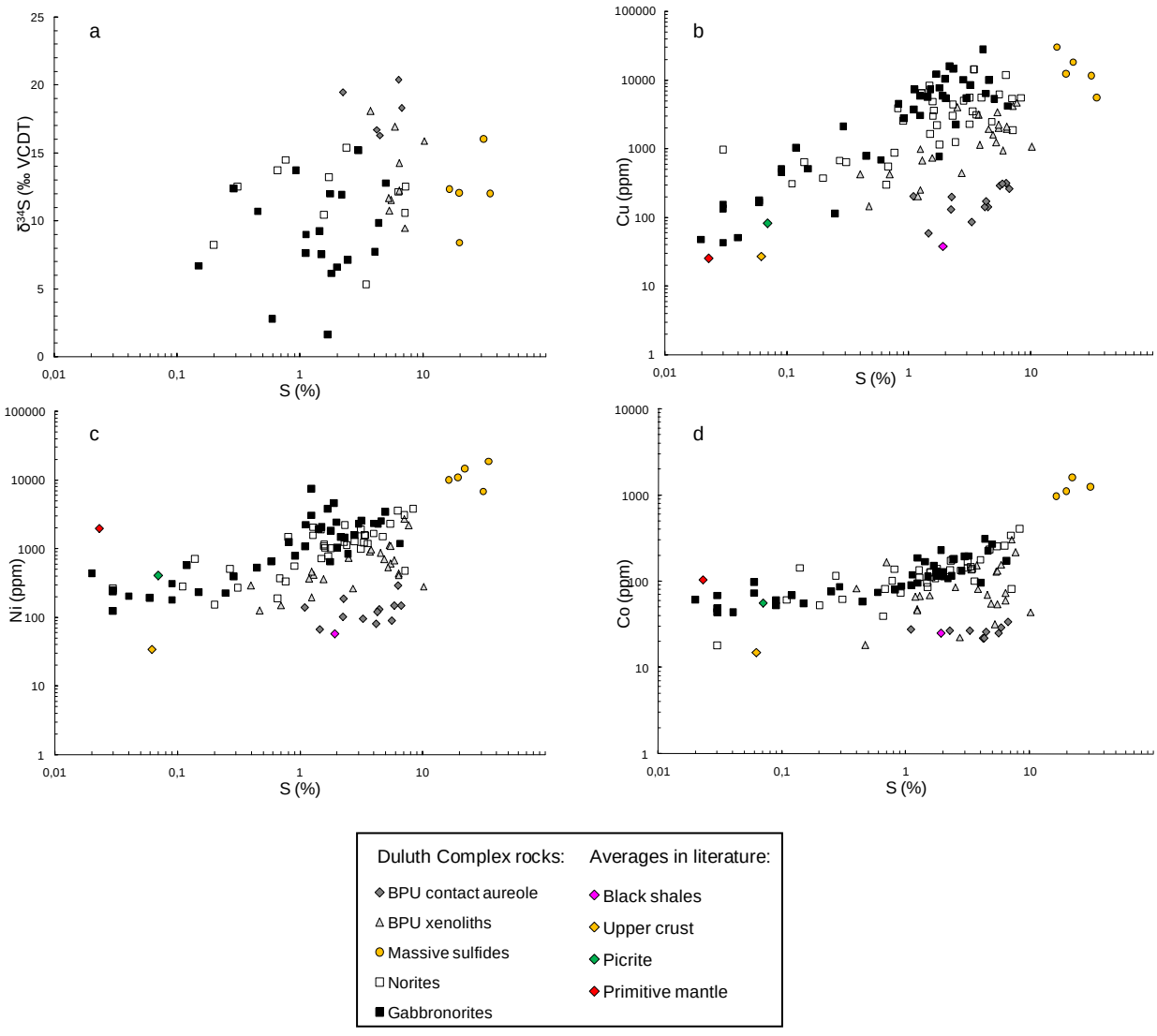

Figure 2.4: Plots of (a) $\delta^{34}S$, (b) Cu, (c) Ni and (d) Co vs. S. Isotopic ratio $\delta^{34}S$ of mantle is comprised between 0 and 1‰. Averages of black shales, upper crust, picrites, and primitive mantle are shown for reference (Dionne-Foster, 2007; Lyubetskaya and Korenaga, 2007; Hu and Gao, 2008; Henrique-Pinto et al., in press). Abbreviation:

Despite having similar S values, the Bedded Pyrrhotite Unit from the contact aureole has lower concentrations of chalcophile elements than the Bedded Pyrrhotite Unit xenoliths (Figs. 2.4b-d and 2.5). For example, the Cu content of rocks from the contact aureole is ~60 to 300 ppm, whereas the xenoliths contain ~150 to 4700 ppm. These observations are consistent with the petrographic observation that more chalcopyrite and pentlandite are observed in the Bedded Pyrrhotite Unit xenoliths than in the Bedded Pyrrhotite Unit rocks from the contact aureole.

Platinum-group elements and Ag also show broad correlations with S (Fig. 2.5a-d). The Bedded Pyrrhotite Unit rocks from the contact aureole have the lowest concentrations of platinum-group elements for a given S content, and the mafic rocks have the highest concentrations. The massive sulfides have greater Os, Ir, Ru and Rh concentrations than the other rocks types and the massive sulfides lie along the extension of the mafic rock trends (Ir and Rh shown in Fig. 2.5b, c). In contrast, the massive sulfides have contents similar in Pd, Pt, Au, and Ag to the S-rich xenoliths and mafic rocks (Pd and Ag shown in Fig. 2.5a, d).

The Bedded Pyrrhotite Unit rocks contain between 5 and 200 ppm As, similar to black shale averages from literature (Fig. 2.6a and Table 2.1). The mafic rocks contain less As than the Bedded Pyrrhotite Unit rocks, i.e., between 0.1 and 50 ppm, whereas the massive sulfides contain between 25 and 175 ppm, similar to the Bedded Pyrrhotite Unit. A broad correlation between As and S is shown for all the rock types. In general, the Bedded Pyrrhotite Unit rocks are richer in As than the mafic rocks for the same S content, and the Bedded Pyrrhotite Unit xenoliths appear to be particularly enriched in As.

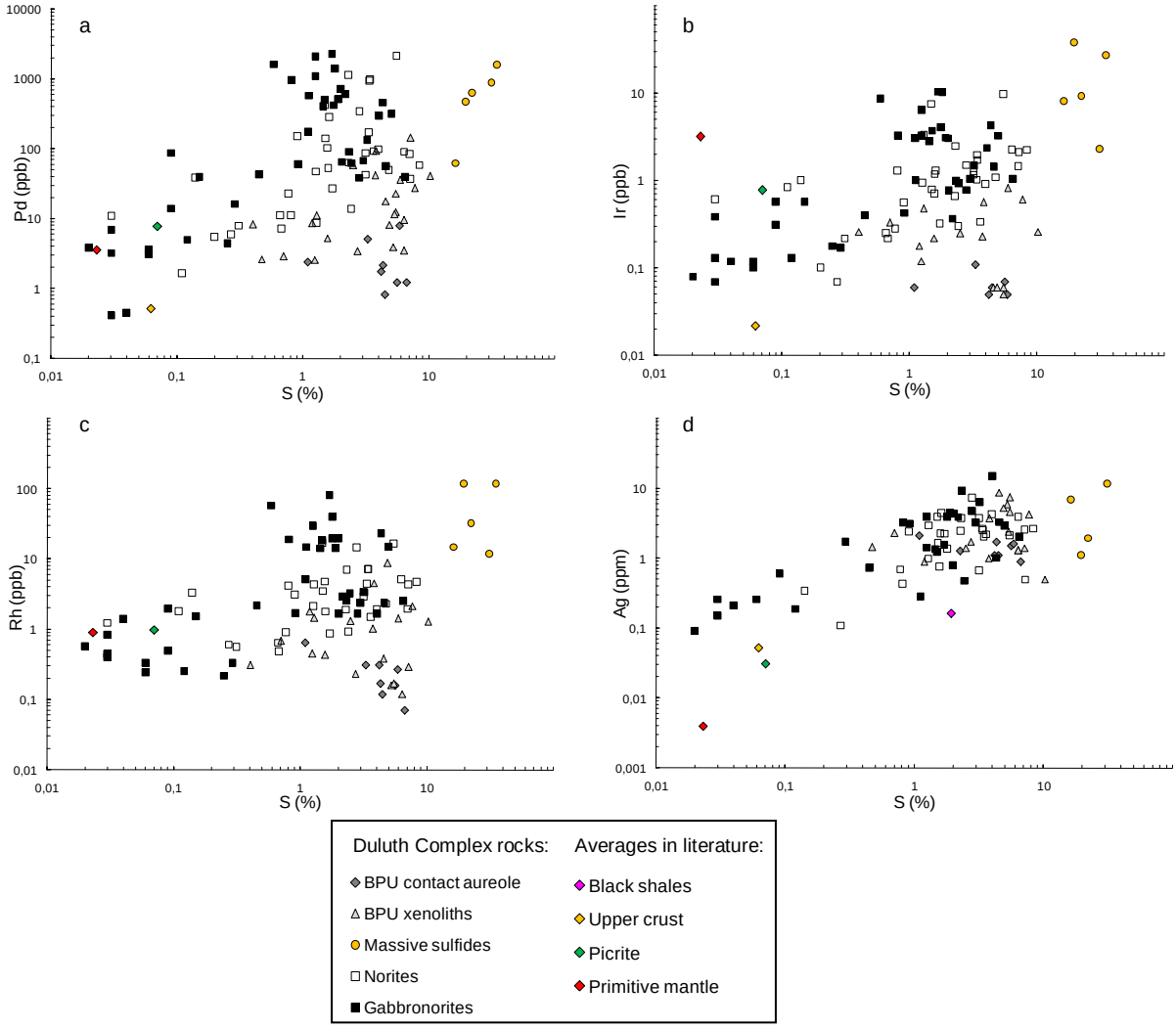

Figure 2.5: Trace metals (a) Pd, (b) Ir, (c) Rh and (d) Ag vs. S for all rocks. Averages of black shales, upper crust, picrites, and primitive mantle are shown for reference (Dionne-Foster, 2007; Lyubetskaya and Korenaga, 2007; Hu and Gao, 2008; Henrique-Pinto et al., in press). Abbreviation: BPU = Bedded Pyrrhotite Unit.

The Bedded Pyrrhotite Unit rocks contain between 0.2 and ~10 ppm Sb, similar to black shale averages from the literature (Fig. 2.6b and Table 2.1). The mafic rocks record between ~0.05 and 4 ppm Sb, and the massive sulfides contain ~0.1 to 2 ppm Sb. There is no obvious correlation between Sb and S for the sample set as whole, but the norites show a moderate correlation.

The Bedded Pyrrhotite Unit rocks contain ~0.1 to 2 ppm Bi, and ~0.07 to 0.6 ppm Te, similar to black shale averages from literature (Fig. 2.6c, d, and Table 2.1). Mafic rocks contain ~0.1 to 5 ppm Bi and ~0.3 to 2 ppm Te. Mafic rocks contain higher Te contents for a given S content than the Bedded Pyrrhotite Unit rocks. The massive sulfides lie along the extension of the trend of the Bedded Pyrrhotite Unit.

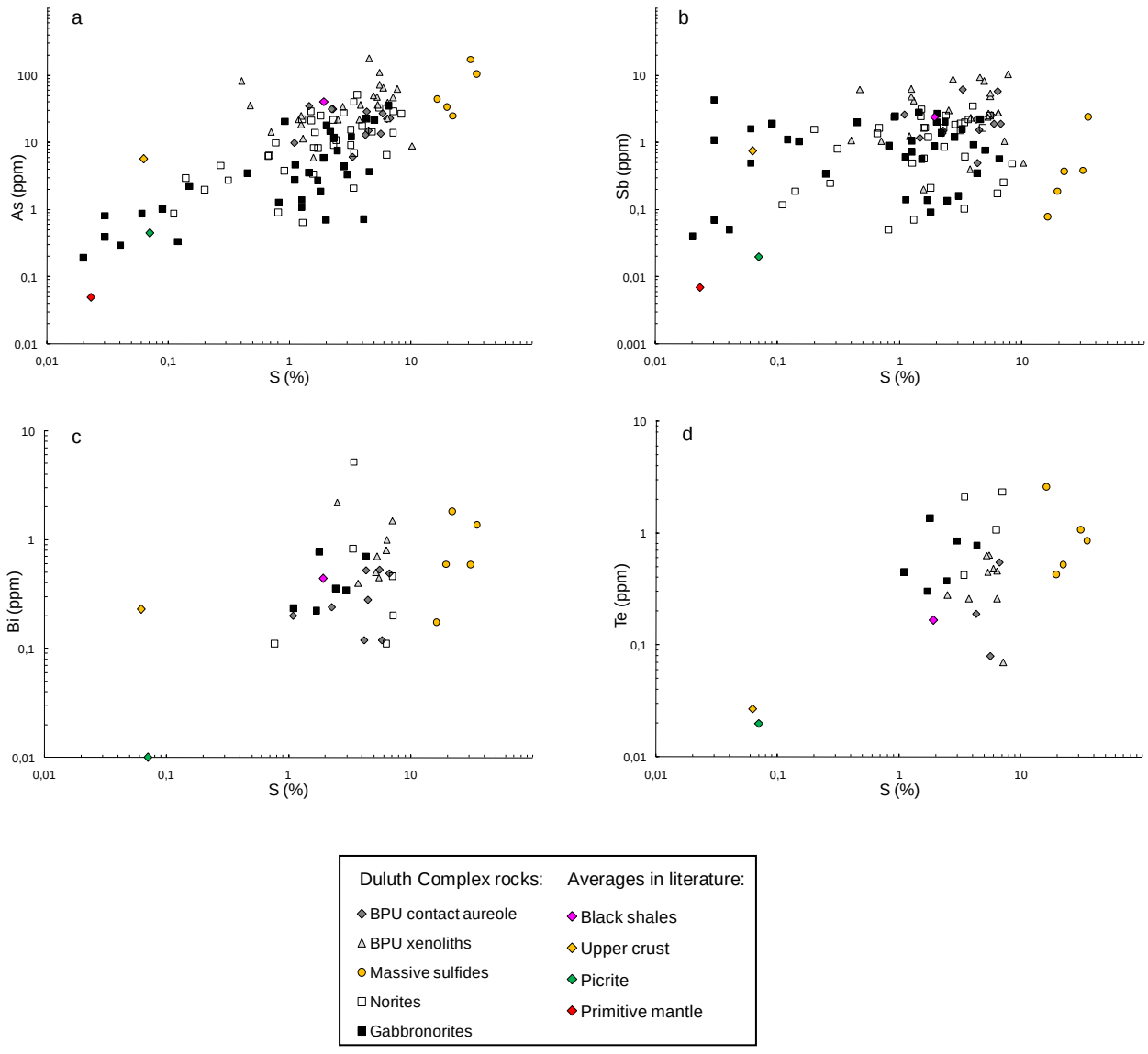

Figure 2.6: Semimetals (a) As, (b) Sb, (c) Bi and (d) Te vs. S for all rocks. Averages of black shales, upper crust, picrites, and primitive mantle are shown for reference (Dionne-Foster, 2007; Lyubetskaya and Korenaga, 2007; Hu and Gao, 2008; Henrique-Pinto et al., in press). Abbreviation: BPU = Bedded Pyrrhotite Unit.

2.6.2.2 NORMALIZATION TO 100% SULFIDES

In order to compare the composition of the sulfide component in each rock type the composition of the sulfide component has been calculated from the averages for the rocks containing more than 0.3 wt% S (Table 2.2). Sulfides from the Bedded Pyrrhotite Unit from the contact aureole contain the lowest Ni and Cu contents at 0.14 and 0.18 wt %, respectively, whereas the Bedded Pyrrhotite Unit xenolith sulfides have a higher Ni and Cu contents 0.75 and 1.7 wt %, respectively. The amount of Ni and Cu in the norite is greater than in the xenolith sulfides, and the gabbronorite contains the highest Ni and Cu contents at 4.5 and 13 wt % respectively. These calculated compositions are in agreement with the observations that the contact aureole does not contain pentlandite and only a little chalcopyrite, the xenolith sulfides contain some pentlandite and chalcopyrite, and the gabbronorite sulfides have the greatest concentrations of pentlandite and chalcopyrite.

Most of the other chalcophile elements (Co to Se on Fig. 2.7, Table 2.2) follow the same order of enrichment with the sulfides from the contact aureole having the lowest concentrations and the gabbronorite having the highest concentrations. In contrast, the elements from Bi to Mo show variable degrees of enrichment. Arsenic and Sb concentrations are the highest in the Bedded Pyrrhotite Unit xenoliths, whereas they are similar for the other rock types. Lead and Bi show similar concentrations in the xenoliths and the norites.

	Mo	As	Sb	Pb	Bi	Se	Ag	Cu	Au	Te	Pd	Pt	Rh	Ru	Ir	Os	Ni	Co
	ppm	ppm	ppm	ppm	ppm	ppm	ppm	ppm	ppb	ppm	ppb	ppb	ppb	ppb	ppb	ppb	ppm	ppm
BPU c.a. (n = 11)	197	273	18	221	3	24	11	1842	40	2	17	43	2	1	0.4	2	1381	217
BPU xenoliths (n = 26)	128	540	72	165	8	20	40	16,698	669	3	240	149	19	58	4	9	7468	1322
Massive sulfides (n = 6)	52	105	1	13	1	40	9	28,163	1982	2	960	60	89	54	27	7	18,951	2091
Norites (n = 32)	288	255	30	275	12	43	41	71,849	3119	11	3296	1722	74	97	27	23	22,826	2596
Gabbronorites (n = 27)	n.d.	147	28	n.d.	7	80	61	128,300	12,675	12	15,906	3729	452	337	80	43	44,577	2872

Table 2.2: Average values of chalcophile elements in the Partridge River Intrusion and the contact aureole rocks, recalculated to 100% sulfides. Abbreviations: BPU = Bedded Pyrrhotite Unit; c.a. = contact aureole; n.d. = not determined.

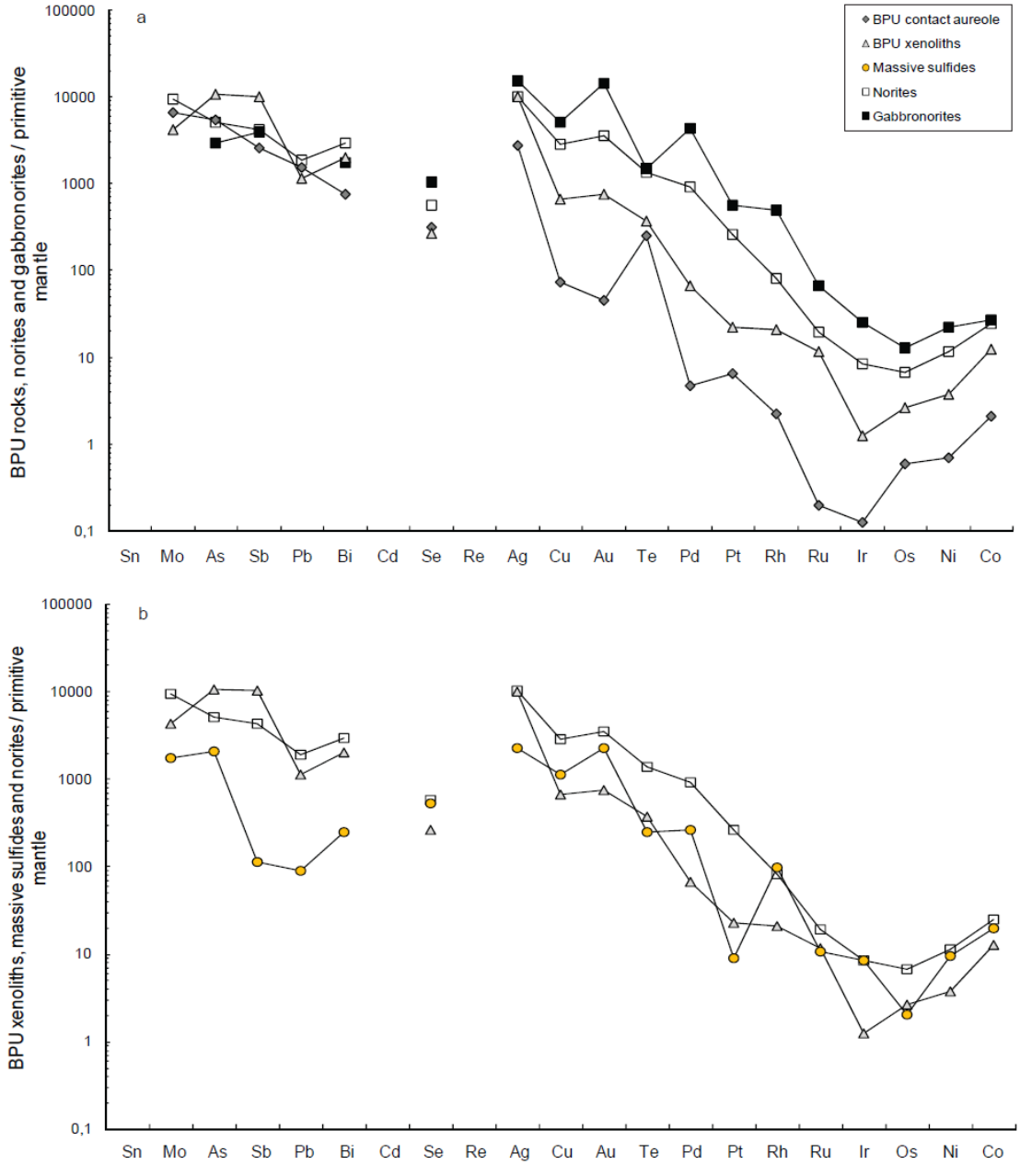
a
BPU contact aureole
BPU xenoliths
Massive sulfides
Norites
Gabbronorites
BPU rocks, norites and gabbronorites / primitive mantle
100000
10000
1000
100
10
1
0,1
Sn Mo As Sb Pb Bi Cd Se Re Ag Cu Au Te Pd Pt Rh Ru Ir Os Ni Co
b
BPU xenoliths, massive sulfides and norites / primitive mantle
100000
10000
1000
100
10
1
0,1
Sn Mo As Sb Pb Bi Cd Se Re Ag Cu Au Te Pd Pt Rh Ru Ir Os Ni Co

Figure 2.7: Mantle-normalized chalcophile elements recalculated to 100% sulfides and plotted in order of compatibility with picrite mantle (Barnes, 2016) of (a) BPU rocks, norites and gabbronorites and (b) massive sulfides. (a) Note that the concentrations of the elements from Co to Se increase from the contact aureole rocks to the norites through the BPU xenoliths with the highest concentrations in gabbronorites. Arsenic and Sb concentrations are the highest in the xenolith-hosted sulfides whereas the other sulfides from the other rocks types contain similarlevelsto each other. Lead concentrations are similar in all rock types. (b) Note that the massive sulfides contain similar concentrations of Co, Ni, Ir, Ru and Rh to the norite hosted sulfides but are depleted in most other chalcophile elements. In addition the massive sulfides have negative Pt anomalies. Abbreviation: BPU = Bedded Pyrrhotite Unit.

The overall shape of the mantle normalized patterns from all four rocks types is similar, with a steady increase from Co through the PGE to Ag (Fig. 2.7a) with Co/Ag of approximately 300 to 500. From Ag onwards the patterns tend to be approximately flat. Exceptions to these general trends are that the Bedded Pyrrhotite Unit from the contact aureole and the gabbronorite patterns have positive and negative Te anomalies, respectively.

The massive sulfides contain similar amounts of Co, Ni, Ir, Ru, and Rh to the norite sulfides, but they are depleted in most of the other chalcophile elements (Fig. 2.7b and Table 2.2). The mantle normalized concentrations increase from Co to Ag, but the pattern is not as steep as for the other sulfides, with a Co/Ag ratio of ~60 versus greater than 250 for the sulfides hosted by other rock types. The massive sulfides mantle normalized pattern show large negative Pt anomaly (Fig. 2.7b).

2.6.2.3 CHANGE IN SULFIDE COMPOSITION WITH DISTANCE FROM THE BEDDED PYRRHOTITE UNIT XENOLITHS

Queffurus and Barnes (2014) found that the sulfides close to the Bedded Pyrrhotite Unit xenoliths are poorer in Se than those close to the xenoliths. Thériault and Barnes (1997) found that there are more Sb- and As-bearing minerals present in the rocks close to the xenoliths. Our current more detailed sampling shows that As and Sb contents of norite and gabbronorite-hosted sulfides decrease with distance from the Bedded Pyrrhotite Unit xenoliths in the basal Unit I (Fig. 2.8a, b) whereas for most of the other elements the content increases (Pd and Ir shown in Fig. 2.8c, d).

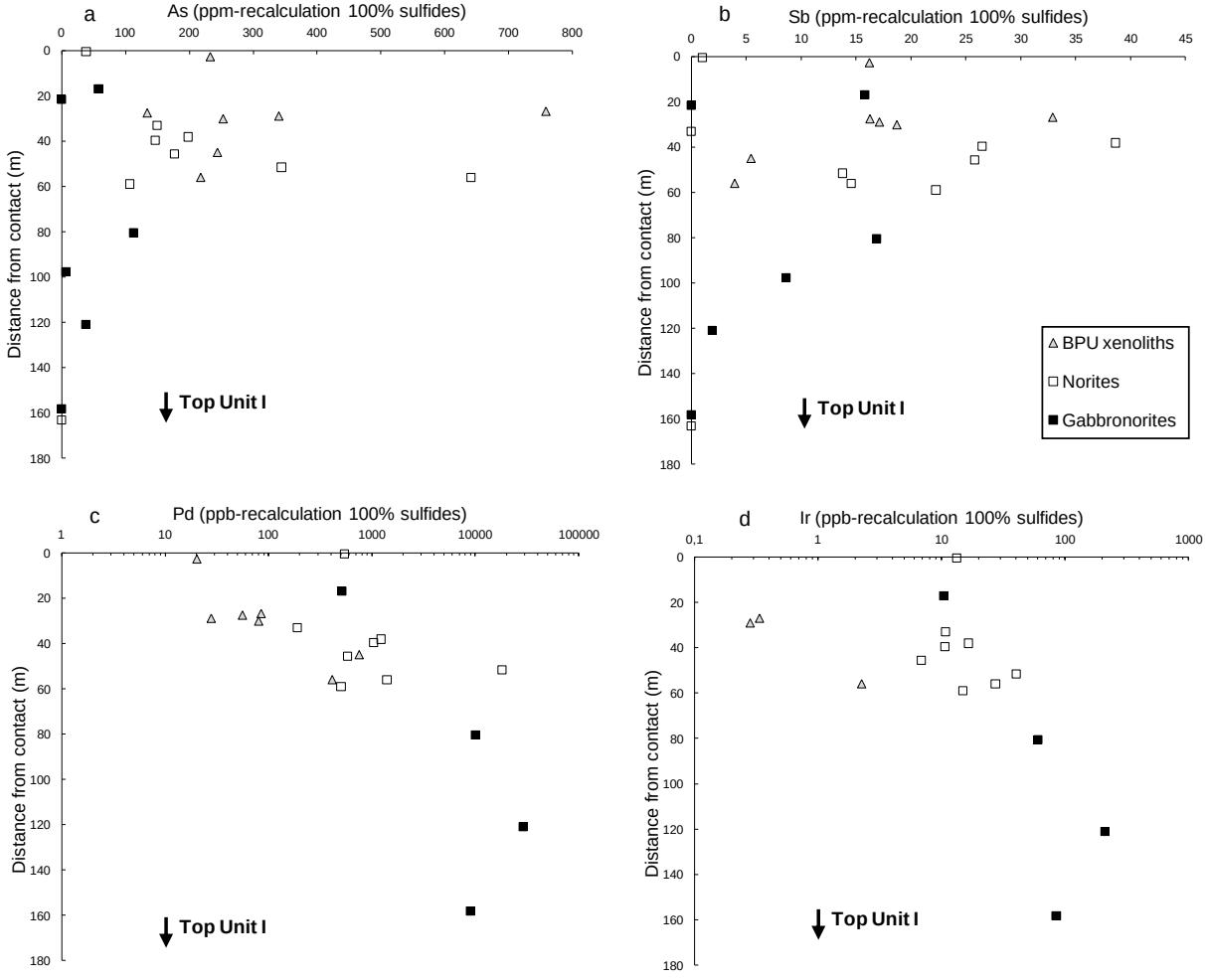

Figure 2.8: Variations of semimetals and PGE contents, a) As, b) Sb, c) Pd and d) Ir in 100% sulfides with distance from contact in the B1-384 borehole, Mesaba deposit. Contact between Virginia Formation sedimentary rocks and mafic magma corresponds to distance zero. Arsenic, Sb, Pd and Ir values are plotted for rocks in the basal unit of the Partridge River Intrusion, i.e. Unit I. Semimetals contents of sulfides decrease with distance from the Bedded Pyrrhotite Unit xenoliths whereas Pd and Ir contents of the norite and gabbronorite-hosted sulfides increase with distance from xenoliths. Abbreviation: BPU = Bedded Pyrrhotite Unit.

2.7 DISCUSSION

2.7.1 ROLE OF PARTIAL MELTING IN CONTAMINATION PROCESSES

Based on decreases in S/Se ratios and in $\delta^{34}S$ values, and the increase in (Pt+Pd)/S ratios from the Bedded Pyrrhotite Unit xenoliths into the norite and gabbronorite of the Unit I, Queffurus and Barnes (2014) argued that S was added to the mafic magma by partial melts of the Bedded Pyrrhotite Unit carrying sulfide droplets. Our petrographic observations support this model.

Metamorphosed Bedded Pyrrhotite Unit in the contact aureole, close to the contact with the intrusion, records temperatures of 800 to 870°C (Sawyer, 2014). Xenoliths of the Bedded Pyrrhotite Unit would have experienced even hotter temperatures as they were surrounded by mafic magma (~1100-1200°C; typical values for basaltic magma). Petrological features in the Bedded Pyrrhotite Unit xenoliths show pockets and pores of former anatectic melt pseudomorphed by large grains of K-feldspar and quartz that contain inclusions of orthopyroxene, plagioclase and cordierite. These features suggest that xenoliths of the Bedded Pyrrhotite Unit reached temperature of at least 800 to ~950°C in the granulite facies (White et al., 2003; Grant, 2009; Chu and Ague, 2013).

We interpret the rounded sulfide blebs found in the patches of former anatectic melt in the Bedded Pyrrhotite Unit xenoliths, and in the anatectic patches in the norite, as globules of a sulfide melt. We suggest that small droplets of sulfide melt were carried into the mafic magma by the silicate anatectic melt that was expelled from xenoliths of the Bedded Pyrrhotite Unit and in the process transferred S and semimetals to the mafic magma. Partial melting of sulfide minerals occurred in xenoliths of the Bedded Pyrrhotite Unit. The disrupted sulfide beds in the Bedded Pyrrhotite Unit xenoliths (Fig. 2.2d of this study; Fig.

2 of Queffurus and Barnes, 2014) reveal microstructures typical of sulfide partial melting, i.e., low interfacial angles between sulfide and silicate phases, and sulfide microveinlets that fill space between silicate grains (Frost et al., 2002; Tomkins et al., 2007). It might be thought that the melting temperature of pyrrhotite is too high (1190°C) for it to have melted. However, the presence of C, sulfosalts, and tellurides lowers the melting temperature of sulfides (Dasgupta et al., 2009, Tomkins et al., 2007), and thus the sedimentary sulfides could have melted.

2.7.2 COMPOSITION OF SULFIDE DROPLETS AND MASSIVE SULFIDES

The composition of the sulfide droplets is expected to change from essentially sedimentary to igneous as they equilibrated with the mafic magma. Queffurus and Barnes (2014) modeled the changes in $\delta^{34}S$, S/Se, and (Pt+Pd)/S using equations 5 and 8 of Lesher and Burnham (2001):

$$C_s = [(C_iR+C_{ss})D^{sul/sil}]/(R+D^{sul/sil})$$

$$I_s=\{I_iC_i[R/(1+R)]+I_{ss}C_{ss}[1/(1+R)]\}/\{C_i[R/(1+R)]+C_{ss}[1/(1+R)]\}$$

where C_s = concentration in the sulfide after equilibration; C_i=concentration of the element in the mafic magma; C_{ss}= concentration of the element in the sedimentary sulfides; R= ratio of silicate liquid to sulfide liquid; $D^{sul/sil}$ = partition coefficient between sulfide and silicate liquid; I_s= isotopic ratio in the sulfides after equilibration; I_i= isotopic ratio of mafic magma before contamination; and I_{ss}= isotopic ratio of the sedimentary sulfides.

A critical variable in these equations is the ratio of sulfide to silicate liquid. They found for the norites close to the xenoliths R-factors as low of 25 were required to model

the sulfide composition, whereas for sulfides from the gabbronorite R-factors were up to 6000. We have applied this approach to our larger data sets (Table 2.3).

On the plot $\delta^{34}S$ vs. Cu in 100% sulfides, a progressive decrease of $\delta^{34}S$ occurs from the Bedded Pyrrhotite Unit xenoliths to the mafic magma with intermediate values for norites (Fig. 2.9a). Massive sulfides and norite-hosted sulfides close to xenoliths of the Bedded Pyrrhotite Unit plot at low R-factors (50), whereas most of gabbronorite-hosted sulfides require an R-factor greater than 500 (Fig. 2.9a).

Nickel, Cu, Co, and trace metals concentrations are highest in gabbronorite-hosted sulfides and lowest in sulfides from the Bedded Pyrrhotite Unit xenoliths; intermediate values occur in the norite-hosted sulfides (only Pd vs. Cu is shown in Fig. 2.9b). Thériault et al., (1997) proposed that the metal contents of norite and gabbronorite-hosted sulfides result from variations in the degree of magma contamination and R-factor. Modeling of sulfide composition after equilibration of Bedded Pyrrhotite Unit sulfides with the mafic magma is illustrated in figure 2.9b for Pd. The plot of Pd vs. Cu shows that massive sulfides and norite-hosted sulfides close to xenoliths of the Bedded Pyrrhotite Unit plot at R-factor values of 50 and 500 whereas most of the gabbronorite-hosted sulfides require higher R-factors (>500). Most of the other metals show similar results.

R factor:	As (ppm)	As (ppm)	Sb (ppm)	Sb (ppm)	Bi (ppm)	Te (ppm)	Cu (ppm)	Pd (ppb)	$\delta^{34}S$ (‰)
0	837.00	837.00	73.00	73.00	3.00	3.00	17621	263.0	13.40
2	832.35	698.25	72.56	60.87	3.01	3.04	17903	278.8	13.37
4	827.76	599.14	72.12	52.20	3.03	3.08	18185	294.5	13.34
10	814.35	420.75	70.84	36.60	3.07	3.19	19026	341.8	13.24
50	736.71	143.25	63.43	12.33	3.33	3.96	24508	656.6	12.63
500	398.25	20.82	31.13	1.63	5.33	11.70	74097	4179.8	8.48
1000	297.00	12.74	21.46	0.92	6.50	18.82	111747	8053.5	6.35
2000	226.57	8.64	14.74	0.56	7.67	29.77	158811	15674.7	4.41
3200	195.17	7.09	11.74	0.43	8.33	39.16	191393	24604.2	3.38
6400	166.43	5.80	9.00	0.31	9.05	54.08	232767	47329.4	2.32
Concentrations in sedimentary sulfides	837	837	73	73	3	3	17621	263	–
Concentrations in silicate magma	0.45	0.45	0.02	0.02	0.01	0.02	150	7.88	–
Dsulfide/silicate	300	10	300	10	1000	4500	2000	90000	–
Temperature (°C)	900	1100	900	1100	–	–	–	–	–
$\delta^{34}S$ magma	–	–	–	–	–	–	–	–	1
$\delta^{34}S$ sediments	–	–	–	–	–	–	–	–	13.4

Table 2.3: Results of modeling the compositions of sulfides. Calculations are based on Eq. (5) in Lesher and Burnham (2001). Grey section corresponds to final concentrations of elements in the sulfide magma after modeling. Values for model calculations are concentrations of elements in the sedimentary sulfides, i.e. average of the BPU xenolith concentrations; concentrations of elements in silicate magma, i.e. average of picrite concentrations (Dionne-Foster, 2007) and partition coefficients between sulfide and silicate melts (Li and Audétat, 2012; Kiseeva and Wood, 2013; Patten et al., 2013; Brenan, 2015; Li and Audétat, 2015; Liu and Brenan, 2015). Abbreviations: BPU = Bedded Pyrrhotite Unit.

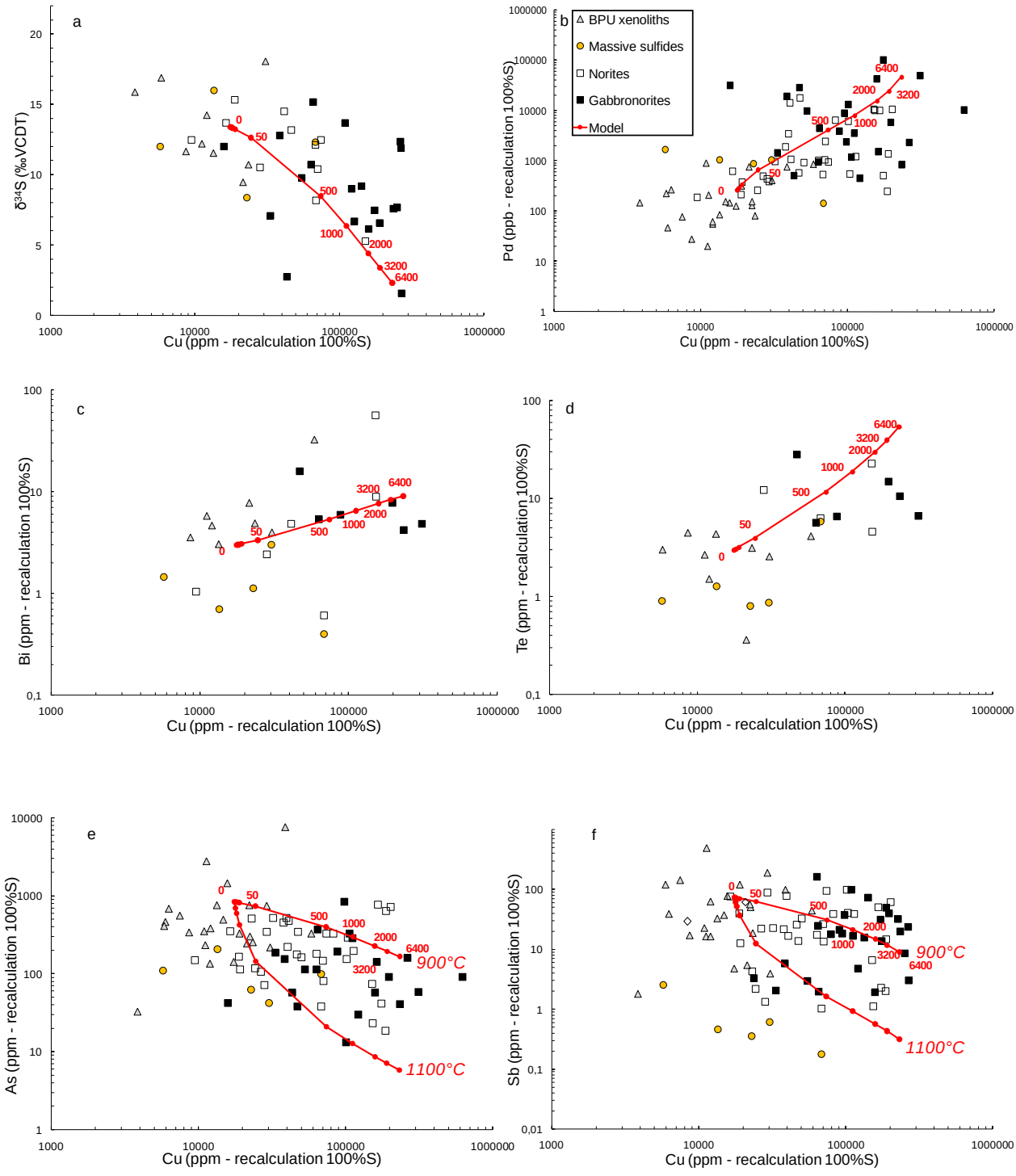
a
δ34S (‰VCDT)
Cu (ppm - recalculation 100%S)
b
BPU xenoliths
Massive sulfides
Norites
Gabbronorites
Model
Pd (ppb - recalculation 100%S)
c
Bi (ppm - recalculation 100%S)
d
Te (ppm - recalculation 100%S)
e
As (ppm - recalculation 100%S)
900°C
1100°C
f
Sb (ppm - recalculation 100%S)

Figure 2.9: Plots of Cu vs. a) $\delta^{34}S$, b) Pd, c) Bi, d) Te, e) As and f) Sb in 100% sulfides of rocks within the intrusion and results of the modeling. Red line represents interaction model from calculation based on equations of Lesher and Burnham, 2001. Numbers along the line represent different R factor values. Models for As and Sb are plotted for partition coefficients at 900°C and 1000°C. Abbreviation: BPU = Bedded Pyrrhotite Unit.

The results for the semimetals are more complex. Despite the fact that the Bedded Pyrrhotite Unit xenoliths are rich in Bi and Te, the sulfide component of the norite is richer in Bi and Te than the xenolith sulfides (Fig. 2.9c, d). Modeling shows that the concentrations of these elements rise in the sulfides as the R-factor increases, i.e., as the sulfide interacts with more mafic magma. This counter-intuitive result occurs because of the high partition coefficients for these elements into the sulfide liquid (Li and Audétat, 2015; Brenan, 2015). Although the mafic magma has low Bi and Te contents compared with the Bedded Pyrrhotite Unit xenoliths, the high partition coefficients of these elements into sulfides, combined with the high R-factor, results in the sulfide droplets from the Bedded Pyrrhotite Unit xenoliths collecting a large quantity of these elements (Fig. 2.9c, d).

In contrast, the Bedded Pyrrhotite Unit xenolith-hosted sulfides are richer in As and Sb than the norite or gabbronorite-hosted sulfides (Fig. 2.9e, f). Modeling of the sulfide compositions indicates that the concentrations of these elements decrease as the sedimentary sulfide interacts with the magma, but the observed sulfide compositions cover a wide range rather than a single trend (Fig. 2.9e, f). Possibly this wide range of results is due to the extreme sensitivity of the partition coefficients to fO_2 and temperature (Li and Audétat, 2015). At relatively cooler temperatures (900°C) in the xenolith, the partition coefficients would have been high (100-300), whereas at hotter temperatures (1100°C) in the mafic magma, the partition coefficients would have been lower (1-10). Consequently, the effect of higher R-factor in the mafic magma was offset by the lower partition coefficient in the mafic magma.

Thériault and Barnes (1998) show based on petrographic and geochemical observations that massive sulfides surrounding the xenoliths have undergone fractional crystallization. The massive sulfides in our current study are depleted in most of the chalcophile elements relative to Co, Ni, Ir, Ru, and Rh. This type of depletion is commonly observed in monosulfide-solid solution cumulates (Barnes et al., 1997). Given the position of the massive sulfides as narrow rims around the xenoliths; our interpretation is that they represent residual monosulfide-solid solution.

The sulfides hosted by the Bedded Pyrrhotite Unit from the contact aureole show similar chalcophile mantle-normalized patterns to the sulfides in the Bedded Pyrrhotite Unit xenoliths, but are depleted in all the chalcophile elements, except Se, relative to the sulfides in the xenoliths. It is possible that the contact aureole black shales initially had a slightly different composition to the xenoliths, but field observations suggest that they are the same unit. Another possibility is that the xenoliths have preferentially lost S and thus the recalculated sulfide compositions are too high. We do not think that this occurred because the xenolith and the contact aureole rocks contain on average similar amounts of S (~4%), and the xenolith sulfides are 3 to 10 times richer in most elements than the contact aureole sulfides, thus the xenoliths would have to have lost 66 %, or more, of their S. In other words, for elements such as Pd and Ni, which are strongly enriched, the xenoliths would have originally contained 24 to 40 % S. Therefore, we argue that the sulfides in the xenoliths have been enriched in chalcophile metals by diffusion of the elements from the mafic magma to the xenolith sulfides prior to the transfer of the sulfide droplets to the mafic magma. The reason for this diffusion was the chemical potential difference between

the sulfide droplet in the anatectic melt in the xenolith and the chalcophile elements in the mafic magma.

2.7.3 PROPOSED MODEL FOR S AND SEMIMETALS CONTAMINATION OF THE MAFIC MAGMA

Based on petrological and geochemical observations, a synthesis model is proposed in Figure 2.10 to explain S and semimetals contamination of the mafic magma from xenoliths of the Bedded Pyrrhotite Unit:

1) Xenoliths of the Bedded Pyrrhotite Unit isolated in the gabbronorite magma of the basal unit, undergo partial melting at temperatures of ~900°C (Fig. 2.10a). Sulfide layers in the xenoliths undergo partial melting and sulfide droplets are incorporated in pockets of anatectic silicate melt. Simultaneously, diffusion of Ni, Cu, and trace metals may occur from the surrounding mafic magma into the xenoliths of the Bedded Pyrrhotite Unit.
2) Rounded droplets of sulfides in the anatectic silicate melt are transferred to the mafic magma (Fig. 2.10a). As a result, norites close to the xenoliths are enriched in semimetals. After dissolution of the silicate anatectic melt in the mafic magma, the entrained sulfide droplets interact and equilibrate with the mafic magma. This results in a minor metal enrichment of the sulfide droplets because of the low R-factor calculated for norite close to xenoliths of the Bedded Pyrrhotite Unit. Dissolution of sulfide droplets in the mafic magma leads to S contamination of the mafic magma as shown by Queffurus and Barnes (2014), with progressive decrease of $\delta^{34}S$ values from the Bedded Pyrrhotite Unit xenoliths to the mafic magma.

3) As the degree of partial melting increases, connectivity between pores and pockets of melt is established and large volumes of silicate anatectic melt are segregated to the mafic magma leaving the xenoliths with residual bulk compositions (Fig. 2.10b). As a consequence, numerous sulfide droplets trapped in the silicate anatectic melt are also transferred to the mafic magma and norites close to the xenoliths record enrichment in semimetals. Accumulation of these sulfide droplets close to xenoliths could result in the formation of massive sulfide. These massive sulfides are poor in metals because there is no interaction between these sulfides and the mafic magma. Massive sulfides may undergo fractional crystallization and as a result they represent a monosulfide-solid solution cumulate, as was suggested by Thériault and Barnes (1998).

4) Movement of the magma, perhaps driven by a new injection of magma or by seismic shaking in the partially molten system, allows bulk flow and hence transport of the sulfides away from the xenoliths, and this results in a larger-scale contamination of the mafic magma by S and semimetals (Fig. 2.10c). Hence, platinum-group minerals are found in sulfides from gabbronorites within the basal Unit I (McSwiggen, 1999; Severson and Hauck, 2003; Table 6a; Cervin, 2011). Enriched metal contents are recorded in sulfides away from the xenoliths, because of the interaction of the entrained sulfides with large volumes of magma, i.e., high R-factor.

a) Xenolith partial melting

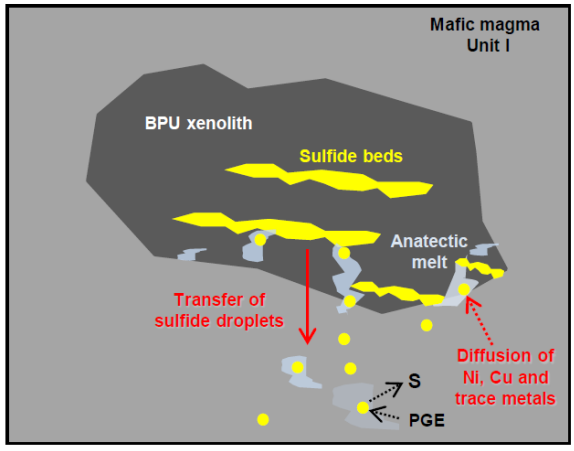

b) Increase of partial melting degree

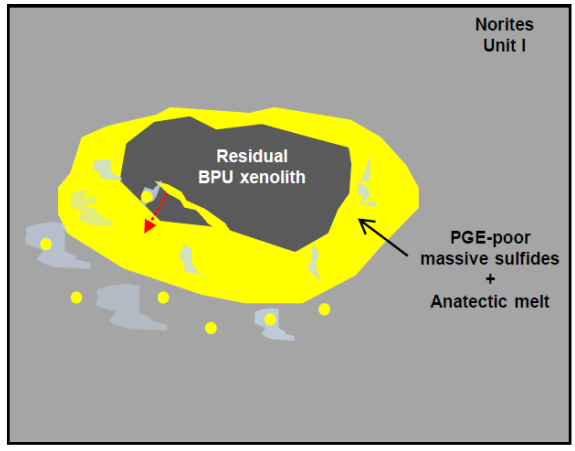

c) Magma disturbance

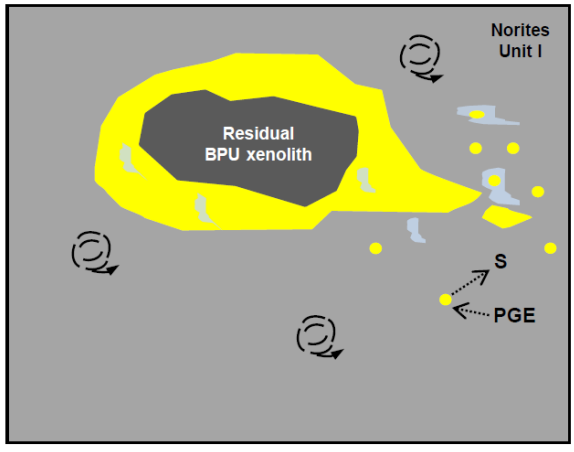

Figure 2.10: Proposed model for S and semimetals contamination of the mafic magma. a) Partial melting of Bedded Pyrrhotite Unit xenoliths in the magma. Sulfides are transferred to the mafic magma via the anatectic silicate melt. This transfer leads to S and semimetals contamination of the mafic magma. In addition, diffusive transfer of Ni, Cu and trace metals from the mafic magma to the Bedded Pyrrhotite Unit xenolith occurs. Low R factor are recorded in the mafic magma. b) Massive sulfide accumulation after increase in the degree of partial melting. Massive sulfides are PGE-poor because of lack of interaction with the magma. c) Magma disturbance, i.e. new injection of magma or possibly related to seismic fault activity, results in sulfide transportation. Platinum-group element enrichment of sulfide droplets occurs because of high R-factor of the mafic magma. Large-scale sulfur and semimetals contamination of the mafic magma occurs in the basal unit. Hence, platinum-group minerals are present in gabbronorites in the whole basal unit I. Abbreviations: BPU=Bedded Pyrrhotite Unit; PGE=Platinum-group elements.

2.8 CONCLUSIONS

Sulfur and semimetals contamination of the mafic magma occurs by the transfer of sulfide droplets in a mobile, silicate partial melt of the Bedded Pyrrhotite Unit xenoliths to the mafic magma. This conclusion is supported by:

1) Petrological observations of sulfide droplets trapped within former anatectic melt of the xenoliths of the Bedded Pyrrhotite Unit in the xenolith margins and surrounding the Bedded Pyrrhotite Unit xenoliths. We suggest that small droplets of sulfide melt were carried into the mafic magma by anatectic melt that was segregated from the Bedded Pyrrhotite Unit xenoliths.
2) Geochemical study which shows that a progressive decrease of $\delta^{34}S$ values from the Bedded Pyrrhotite Unit xenoliths to the mafic magma together with a progressive decrease of the semimetals content of norite- and gabbronorite-hosted sulfides occurs with distance from the Bedded Pyrrhotite Unit xenoliths in the basal Unit I.
3) Modeling of the composition of sulfides shows that the semimetals content of sulfides in the magma results from their equilibration after transfer to the mafic magma and depends on R-factor, i.e., interaction rate of sulfides with the mafic magma, and partition coefficients for these elements into the sulfide liquid.

In addition, petrographic and geochemical observations show that higher proportions of pentlandite and chalcopyrite occurs in the Bedded Pyrrhotite Unit xenoliths than in the Bedded Pyrrhotite Unit from the contact aureole, and that sulfides in the Bedded Pyrrhotite Unit from the contact aureole are depleted in Ni, Cu, and trace metals relative to the Bedded Pyrrhotite Unit xenolith-hosted sulfides. We propose that these elements diffused

from the mafic magma to the Bedded Pyrrhotite Unit xenolith-hosted sulfides at temperatures in excess of 900°C.

2.9 ACKNOWLEDGMENTS

This work was funded by a Natural Science and Engineering Research Council of Canada Discovery Grant to SJB (17313) and a Canada Research Chair program grant to SJB (215503). We thank Mark Severson for providing some samples of the Bedded Pyrrhotite Unit from the contact aureole. Sadia Medhi and Dany Savard from LabMaTer are thanked to help in carrying out analyses. We would like to thank Dr. Valentina Taranovic and an anonymous reviewer for helping us improve the clarity of our arguments. Dr. Franco Pirajno, Dr. Timothy Horscroft and Dr. Jeffrey Mauk are also thanked for their editorial handling and for inviting this paper.

2.10 REFERENCES

Andrews, D., Ripley, E., (1989) Mass transfer and sulfur fixation in the contact aureole of the Duluth Complex, Dunka road Cu-Ni deposit, Minnesota. Can. Mineral. 27, 293-310.

Arevalo, Jr.R., McDonough, W.F., (2010) Chemical variations and regional diversity observed in MORB. Chem. Geol. 271, 70-85.

Baker, D.R., Barnes, S.-J., Simon, G., Bernier, F., (2001) Fluid transport of sulfur and metals between sulfide melt and basaltic melt. Can. Mineral. 39, 537-546.

Barnes, S.-J., Makovicky, E., Makovicky, M., Rose-Hansen, J., Karup-Moller, S., (1997) Partition coefficients for Ni, Cu, Pd, Pt, Rh, and Ir between monosulfide solid

solution and sulfide liquid and the formation of compositionally zoned Ni – Cu sulfide bodies by fractional crystallization of sulfide liquid. Can. J. Earth Sci. 34, 366-374.

Barnes, S.-J., (2016) Chalcophile elements. Encyclopedia of Geochemistry. Ed. W.M. White.In press.

Bédard, L.P., Savard, D., Barnes, S.-J., (2008) Total sulfur concentration in geological reference materials by elemental infrared analyser. Geostand. Geoanal. Res. 32, 203-208.

Benkó, Z., Mogessie, A., Molnár, F., Krenn, K., Poulson, S.R., Hauck, S.A., Severson, M.J., Arehart, G.B., (2015a) Hydrothermal alteration and Cu–Ni–PGE mobilization in the charnockitic rocks of the footwall of the South Kawishiwi intrusion, Duluth Complex, USA. Ore Geol Rev. 67, 170-188.

Benkó, Z., Mogessie, A., Molnár, F., Severson, M.J., Hauck, S.A., Raič, S., (2015b) Partial Melting Processes and Cu-Ni-PGE Mineralization in the Footwall of the South Kawishiwi Intrusion at the Spruce Road Deposit, Duluth Complex, Minnesota.Econ.Geol. 110, 1269-1293.

Bonnichsen, W., (1972) Sulfide minerals in the Duluth Complex. In Sims, P. K., and Morey, G. W., eds., Geology of Minnesota: A centennial volume: Minn. Geol. Survey.pp. 388-393.

Brenan, J.M., (2015) Se–Te fractionation by sulfide–silicate melt partitioning: Implications for the composition of mantle-derived magmas and their melting residues. Earth Planet. Sci. Lett. 422, 45-57.

Cervin, D.O., (2011) Characterization of precious metal mineral occurrences in the NorthMet deposit of the Partridge River Intrusion, Duluth complex, Minnesota, USA: Unpublished. M.Sc. thesis, University of Minnesota, 155 p.

Chu, X., Ague, J.J., (2013) Phase equilibria for graphitic metapelite including solution of CO_2 in melt and cordierite: implications for dehydration, partial melting and graphite precipitation. J. Metamorph. Geol. 31, 843-862.

Dasgupta, R., Buono, A., Whelan, G., Walker, D., (2009) High-pressure melting relations in Fe–C–S systems: Implications for formation, evolution, and structure of metallic cores in planetary bodies. Geochim. Cosmochim. Acta. 73, 6678-6691.

Dionne-Foster, C., (2007) Géologie et indices de Ni-Cu-EGP de la zone Frontier dans la ceinture de Cape Smith, Nouveau Québec: Unpublished. M.Sc. thesis, Université du Québec à Chicoutimi, 320 p.

Duchesne, L., (2004) Fusion partielle et microstructures associées dans l'auréole de contact du complexe igné de Duluth, Minnesota: Unpublished. M.Sc. thesis, Université du Québec à Chicoutimi, 217 p.

Frost, B.R., Mavrogenes, J.A., Tomkins, A.G., (2002) Partial melting of sulfide or deposits during medium- and high-grade metamorphism. Can. Mineral.40, 1-18.

Grant, J.A., (2009) Thermocalc and experimental modeling of melting of pelite, Morton Pass, Wyoming. J. Metamorph. Geol. 27, 571-578.

Grinenko, L.N., (1985) Sources of sulfur of the nickeliferous and barren gabbro-dolerite intrusions of the northwest Siberian platform. Int Geol Rev. 28, 695-708.

Hauck, S.A., Severson, M.J., Zanko, L., Barnes, S.-J., Morton, P., Alminas, H., Foord, E.E., Dahlberg, E.H., (1997) An overview of the geology and oxide, sulfide, and

platinum-group element mineralization along the western and northern contacts of the Duluth Complex. Geol Soc Am, special paper. 312, 137–185.

Henrique-Pinto, R., Barnes, S.-J., Savard, D., Mehdi, S., (2016) Quantification of metals and semimetals in carbon-rich rocks: A new sequential protocol including extraction from humic substances. Geostand. Geoanal. Res. doi: 10.1111/j.1751-908X.2015.00340.x (in press).

Hu, Z., Gao, S., (2008) Upper crustal abundances of trace elements: A revision and update. Chem. Geol. 253, 205-221.

Ketris, M.P., Yudovich, Y.E., (2009) Estimations of Clarkes for Carbonaceous biolithes: World averages for trace element contents in black shales and coals. Int J Coal Geol. 78, 135-148.

Kiseeva, E.S., Wood, B.J., (2013) A simple model for chalcophile element partitioning between sulfide and silicate liquids with geochemical applications. Earth Planet. Sci. Lett. 383, 68-81.

Labotka, T.C., Papike, J.J., Vaniman, D.T. (1981) Petrology of contact metamorphosed argillite from the Rove Formation, Gunflint Trail, Minnesota. Am. Mineral. 66, 70-86.

Lesher, C.M., Arndt, N.T, Groves, D.I., (1984) Genesis of komatiite-associated nickel sulfide deposits at Kambalda, Western Australia: A distal volcanic model. Sulfide deposits in mafic and ultramafic rocks, Institute of Mining and Metallurgy, London, 10 p.

Lesher, C.M., Burnham, O.M., (2001) Multicomponent elemental and isotopic mixing in Ni–Cu–(PGE) ores at Kambalda, western Australia. Can. Mineral. 39, 421-446.

Li, C., Ripley, E.M., Naldrett, A.J., (2003) Compositional variation of olivine and sulfur isotopes in the Noril'sk and Talnakh intrusions, Siberia: Implications for ore-forming processes in dynamic magma conduits. Econ. Geol. 98, 69-86.

Li, Y., Audétat, A., (2012) Partitioning of V, Mn, Co, Ni, Cu, Zn, As, Mo, Ag, Sn, Sb, W, Au, Pb, and Bi between sulfide phases and hydrous basanite melt at upper mantle conditions. Earth Planet. Sci. Lett. 355, 327-340.

Li, Y., Audétat, A., (2015) Effects of temperature, silicate melt composition, and oxygen fugacity on the partitioning of V, Mn, Co, Ni, Cu, Zn, As, Mo, Ag, Sn, Sb, W, Au, Pb, and Bi between sulfide phases and silicate melt. Geochim. Cosmochim. Acta. 162, 25-45.

Liu, Y., Brenan, J., (2015) Partitioning of platinum-group elements (PGE) and chalcogens (Se, Te, As, Sb, Bi) between monosulfide-solid solution (MSS), intermediate solid solution (ISS) and sulfide liquid at controlled fO_2–fS_2 conditions. Geochim. Cosmochim. Acta. 159, 139-161.

Lucente, M.E., Morey, G.B., (1983) Stratigraphy and sedimentology of the Lower Proterozoic Virginia Formation, northern Minnesota. Minnesota Geological Survey, Report of Investigations RI-28, 28 p.

Lyubetskaya, T., Korenaga, J., (2007) Chemical composition of Earth's primitive mantle and its variance: 1. Method and results. J. Geophys. Res.: Solid Earth. 112, 1-21.

Mainwaring, P.R., Naldrett, A., (1977) Country-rock assimilation and the genesis of Cu-Ni sulfides in the Water Hen Intrusion, Duluth Complex, Minnesota. Econ. Geol. 72, 1269-1284.

McSwiggen, P.L., (1999) Platinum-palladium group minerals, gold, silver, and cobalt in the Minnamax copper-nickel sulfide deposit, Duluth Complex, northeastern Minnesota. Minnesota Geological Survey, Report of Investigations RI-54, 29 p.

Miller, J.D., Jr., and Severson, M.J., (2002) Geology of the Duluth Complex: geology and mineral potential of the Duluth Complex and related rocks of northeastern Minnesota: Minnesota Geological Survey, Report of Investigations RI-58, 207p.

Molnár, F., Arehart, G.B., Poulson, S., Hauck, S., (2009) Sulfur isotope constraints for a dynamic magmatic sulfide ore deposition model in the sill-like South Kawishiwi Intrusion of the Duluth Complex, Minnesota. Geol. Soc. America., Annual Meeting, Portland, OR. Abstr. Vol. 41, 25 p.

Ojakangas, R.W., Morey, G.B., Green, J.C., (2001) The Mesoproterozoic midcontinent rift system, Lake Superior Region, USA.Sediment. Geol. 141–142, 421-442.

Patten, C., Barnes, S.-J., Mathez, E.A., Jenner, F.E., (2013) Partition coefficients of chalcophile elements between sulfide and silicate melts and the early crystallization history of sulfide liquid: LA-ICP-MS analysis of MORB sulfide droplets. Chem. Geol. 358, 170-188.

Queffurus, M., Barnes, S.-J., (2014) Selenium and sulfur concentrations in country rocks from the Duluth Complex, Minnesota, USA: Implications for formation of the Cu-Ni-PGE sulfides. Econ. Geol. 109, 785-794.

Ripley, E.M., (1981) Sulfur isotopic studies of the Dunka road Cu-Ni deposit, Duluth Complex, Minnesota. Econ. Geol. 76, 610-620.

Ripley, E.M., Alawi, J.A., (1986) Sulfide mineralogy and chemical evolution of the Babbitt Cu-Ni deposit, Duluth Complex, Minnesota. Can. Mineral. 24, 347-368.

Ripley, E.M., Alawi, J.A., (1988) Petrogenesis of pelitic xenoliths at the Babbitt Cu-Ni deposit, Duluth Complex, Minnesota, U.S.A. Lithos. 21, 143-159.

Ripley, E.M., Taib, N.I., Chusi, L., Moore, C.H., (2007) Chemical and mineralogical heterogeneity in the basal zone of the Partridge River Intrusion: implications for the origin of Cu–Ni sulfide mineralization in the Duluth Complex, Midcontinent Rift System. Contrib. Mineral. Petrol. 154, 35-54.

Ripley, E.M., Li, C., (2013) Sulfide saturation in mafic magmas: Is external sulfur required for magmatic Ni-Cu-(PGE) ore genesis? Econ. Geol. 108, 45-58.

Ripley, E.M., (2014) Ni-Cu-PGE Mineralization in the Partridge River, South Kawishiwi, and Eagle Intrusions: A review of contrasting styles of sulfide-rich occurrences in the Midcontinent Rift System. Econ. Geol. 109, 309-324.

Robertson, J., Ripley, E.M., Barnes, S.J., Li, C., (2015) Sulfur liberation from country rocks and incorporation in mafic magmas. Econ. Geol. 110, 1111-1123.

Savard, D., Barnes, S.-J., Meisel, T., (2010) Comparison between Nickel-Sulfur Fire Assay Te Co-precipitation and Isotope Dilution with High-Pressure Asher Acid Digestion for the Determination of Platinum-Group Elements, Rhenium and Gold. Geostand. Geoanal. Res. 34, 281-291.

Sawyer, E.W., (2014) The inception and growth of leucosomes: microstructure at the start of melt segregation in migmatites. J. Metamorph. Geol. 7, 695-712.

Severson, M.J., (1994) Igneous stratigraphy of the South Kawishiwi intrusion, Duluth Complex, northeastern Minnesota: Duluth, University of Minnesota, Natural Resources Research Institute, Technical Report, NRRI/TR-93/34, 210 p.

Severson, M.J., Hauck, S.A., (1997) Igneous Stratigraphy and Mineralization in the Basal Portion of the Partridge River Intrusion, Duluth Complex, Allen Quadrangle, Minnesota: Duluth, Minnesota, University of Minnesota, Natural Resources Research Institute, Technical Report, NRRI/TR-97/19, 102 p.

Severson, M.J., Hauck, S.A., (2003) Platinum group elements (PGEs) and platinum group minerals (PGMs) in the Duluth Complex: Duluth, Minnesota, University of Minnesota, Natural Resources Research Institute, Technical Report, NRRI/TR-2003/37, 312 p.

Severson, M.J., Hauck, S.A., (2008) Finish Logging of Duluth Complex Drill Core (And a Reinterpretation of the Geology at the Mesaba (Babbitt) deposit): Duluth, University of Minnesota, Natural Resources Research Institute, Technical Report, NRRI/TR-2008/17, 68 p.

Thériault, R.D., Barnes, S.-J., Severson, M.J., (1997) The influence of country-rock assimilation and silicate to sulfide ratios (R-factor) on the genesis of the Dunka Road Cu – Ni – platinum-group element deposit, Duluth Complex, Minnesota. Can. J. Earth Sci. 34, 375-389.

Thériault, R.D., Barnes, S.-J., (1998) Compositional variations in Cu-Ni-PGE sulfides of the Dunka road deposit, Duluth Complex, Minnesota: The importance of combined assimilation and magmatic processes. Can. Mineral. 36, 869-886.

Thériault, R.D., Barnes, S.-J., Severson, M.J., (2000) Origin of Cu-Ni-PGE Sulfide Mineralization in the Partridge River Intrusion, Duluth Complex, Minnesota. Econ. Geol. 95, 929-943.

Tomkins, A.G., Pattison, D.R.M., Frost, B.R., (2007) On the initiation of metamorphic sulfide anatexis. J. Petrol. 48, 511-535.

Tracy, R.J., Frost, B.R., (1991) Phase equilibria and thermobarometry of calcareous, ultramafic and mafic rocks, and iron formations. Rev. Mineral. Geochem. 26, 207-289.

White, R.W., Powell, R., Clarke, G.L., (2003) Prograde metamorphic assemblage evolution during partial melting of metasedimentary rocks at low pressures: Migmatites from Mt Stafford, Central Australia. J. Petrol. 44, 1937-1960.

Whitney, D.L., Evans, B.W., (2010) Abbreviations for names of rock-forming minerals. Am. Mineral. 95, 185-187.

Zanko, L.M., Severson, M.J., Ripley, E.M., (1994) Geology and mineralization of the Serpentine copper-nickel deposit, Duluth Complex, Minnesota: Duluth, Minnesota, University of Minnesota, Natural Resources Research Institute, Technical Report, NRRI/TR-93/52, 90 p.

Remarques additionnelles suite aux commentaires du jury sur le Chapitre 2:

- Le terme *contamination* employé dans ce chapitre, ainsi que les chapitres suivants, couvre une large gamme de processus. La terminologie *assimilation* conviendrait davantage dans cette étude: l'assimilation de liquide sulfuré dans le magma depuis les xénolithes de roches encaissantes lors de la fusion partielle de ces xénolithes.

- La terminologie *leucosome* est employée pour désigner l'accumulation de produit de fusion partielle formé suite à la fusion partielle des shales noirs. Le terme *xenomelt* pourrait être employé pour désigner les produits de fusion partielle résultant de la fusion partielle de ces roches.

- Le S nécessaire à la formation de gisements de Ni-Cu-EGP est dérivé de shales noirs dans le cas du Complexe de Duluth, des gisements de Raglan et de Pechenga à l'inverse des gisements de Kambalda, Norils'k, Sudbury et Thompson.

- Lesher et Burnham (2001) propose un modèle de fusion partielle de xénolithes de roches encaissantes et le transfert de S depuis ces xenolithes via la libération dans le magma d'un *xenomelt* sulfuré. Le transfert de gouttelettes de sulfures au magma lors de la fusion de xénolithes de shales noirs a été également proposé par Lesher et Campbell (1993) et Lesher et Burnham (2001).

- La modalité de transfert de S au magma depuis les roches encaissantes par une phase fluide riche en H_2S fut proposée par Naldrett (1966) et d'autres auteurs avant le modèle expérimental proposé Baker et al. (2001).

- La *Bedded Pyrrhotite Unit* serait formée suite au métamorphisme de shales noirs riches en S dans l'auréole de contact du Complexe de Duluth (Severson, 1994).

- Les sulfures « massifs » présents dans les roches mafiques autour des xénolithes sont en réalité des sulfures semi-massifs en fonction des proportions de sulfures de ces échantillons, c.à-.d., 50% de sulfures. Ces sulfures sont appauvris en la plupart des semi-métaux en comparaison avec les sulfures disséminés dans les roches mafiques. L'accumulation de sulfures massifs autour des xénolithes est un processus progressif et dépendant des taux d'assimilation des xénolithes dans le magma. En addition des cumulats de type *mss* obervés autour des xénolithes, des sulfures riches en Cu ont également été observés autour des xénolithes de la *Bedded Pyrrhotite Unit* (Queffurus et Barnes, 2014; Figure 2E).

- Les calculs de normalisation des analyses à 100% sulfures ont été réalisés à partir de l'équation (1) dans Barnes et Lightfoot (2005).

- Les équations 5 et 8 de Lesher et Burnham (2001) ont été utilisées pour modéliser la composition des sulfures dans ce chapitre.

- La fusion partielle des sulfures dans les xénolithes a été discutée dans ce chapitre. L'évidence majeure d'une fusion partielle des sulfures dans les xénolithes est la présence de microveines de sulfures remplissant l'espace entre les phases silicatées. Les valeurs des angles interfaciaux entre les phases silicatées et sulfurées sont variables, c.à-.d., angles interfaciaux faibles si le produit de fusion partielle n'est pas en contact avec le liquide sulfuré et grands si le produit de fusion partielle et le liquide sulfuré sont en contact.

- Le S est sous forme dissoute dans le magma dans les stades précoces de contamination du magma, c-à.-d., avant le stade de saturation en sulfures du magma.

- Dans la représentation schématique de la Figure 2.10 C, la flèche représentant la libération de S dans le magma dans ce schéma n'illustre pas une dissolution du S dans le magma car le magma est saturé en sulfures à cette étape du modèle.

- Des éléments majeurs tels que SiO_2, Al_2O_3, K_2O, Na_2O sont également transférés depuis les xénolithes dans le magma mafique (Ripley et Alawi, 1988).

- Les gabbrononrites sont plus distales par rapport aux xénolithes que les norites, tel que décrit par Thériault et al. (2000) et Queffurus et Barnes (2004).

- Les shales noirs les moins métamorphisés, i.e. les échantillons disponibles les plus éloignés du contact avec le Complexe de Duluth, sont composés de lits de pyrite et de pyrrhotite, ainsi que de grains de chalcopyrite.

CHAPITRE 3

MODELING THE PARTIAL MELTING OF SULFUR-RICH BLACK SHALE XENOLITHS IN THE DULUTH COMPLEX, MINNESOTA, U.S.A.

SAMALENS N.[1], BARNES S.-J. [1], SAWYER E.W.[1]

[1] Université du Québec à Chicoutimi, 555 boulevard de l'Université, Saguenay, QC, G7H 2B1, Canada

JOURNAL OF METAMORPHIC GEOLOGY, ACCEPTED JANUARY 22, 2017

3.1RÉSUMÉ

Le soufre (S) présent dans de nombreux gisements de Ni-Cu-Éléments du groupe du platine (EGP) est principalement dérivé de roches sédimentaires riches en S. Cependant, le ou les mécanisme(s) permettant le transfert du S au magma mafique n'ont pas été clairement mis en évidence. Le Complexe de Duluth, situé au Minnesota, contient de nombreux gisements sulfurés magmatiques de Ni-Cu et le S provient d'une unité de shales noirs nommée la *Bedded Pyrrhotite Unit*. Cette unité est présente dans l'auréole de contact et sous forme de xénolithes dans la zone basale du Complexe. Nous avons mené une étude pétrographique et géochimique, ainsi que des calculs des minéraux à l'équilibre dans le système NCKFMASHMT dans le but de vérifier si les températures des xénolithes sont suffisamment hautes pour que leur sulfures qu'ils contiennent soient fondus, et ainsi permettent la contamination du magma.

Les assemblages minéralogiques des roches de l'unité *Bedded Pyrrhotite Unit* varient entre l'auréole de contact et les xénolithes. Les roches de la *Bedded Pyrrhotite Unit* dans l'auréole de contact sont peu résiduelles et ont pour assemblage minéralogique: cordiérite + plagioclase + feldspath potassique + quartz + produit de fusion partielle silicaté (cristallisé sous forme de quartz + plagioclase + feldspath potassique + biotite) + sillimanite + graphite + sulfures +/- rutile, alors que les roches de la *Bedded Pyrrhotite Unit* les plus résiduelles sont des xénolithes dépourvus de quartz et de feldspath potassique avec pour assemblage: cordiérite + orthopyroxene + produit de fusion partielle silicaté (quartz + feldspath potassique + plagioclase + biotite + orthopyroxene) + sulfures + spinelle.

Des pseudosections ont été calculées pour les roches de la *Bedded Pyrrhotite Unit* dans le but de déterminer les températures du pic de métamorphisme. Les xénolithes enregistrent des températures comprises entre ~800 à 1000°C. Cette gamme thermique est en partie dépendante de la taille des xénolithes avec les plus basses températures enregistrées à l'intérieur des xénolithes les plus grands. En revanche, les températures maximales des roches de l'auréole de contact sont d'environ ~870°C. Les résultats de la modélisation géochimique indique que les roches de la *Bedded Pyrrhotite Unit* dans l'auréole de contact et le centre des xénolithes de grande taille contiennent une grande quantité de produit de fusion partielle alors que les xénolithes les plus résiduels ont perdus plus de 50% de produit de fusion partielle. Des poches de produit de fusion partielle des xénolithes (quartz + feldspath potassique + plagioclase +/- biotite, orthopyroxene) ont été identifiés par une étude pétrographique dans les xénolithes et dans le faciès noritique entourant les xénolithes. De plus, des gouttelettes de sulfures composées de pyrrhotite, chalcopyrite et de faibles quantités de pentlandite ont été observées dans ces poches de produit de fusion partielle. Les températures calculées pour les xénolithes sont suffisamment élevées pour permettre la fusion des minéraux sulfurés initiaux des xénolithes de la *Bedded Pyrrhotite Unit* (pyrrhotite et chalcopyrite) et ainsi autoriser leur transport par le produit de fusion partielle sous forme de liquide sulfuré depuis les xénolithes vers le magma mafique.

3.2ABSTRACT

The sulfur (S) that occurs in many magmatic Ni-Cu-platinum-group element (PGE) deposits is thought to have been derived from S-rich sedimentary country rock. However, the mechanism(s) of how this S is transferred to the mafic magma has not been clearly established. The Duluth Complex, Minnesota, contains numerous magmatic Ni-Cu sulfide deposits and the source of the S for these is thought to be black shales of the Bedded Pyrrhotite Unit. The Bedded Pyrrhotite Unit occurs in the contact aureole and as xenoliths in the basal zone of the Complex. We have carried out petrographic and geochemical study along with mineral equilibria calculations in the NCKFMASHMT system of rocks from both settings in order to investigate whether temperatures were sufficiently high that the sulfide minerals melted and may have been how the mafic magma was contaminated.

The mineral assemblage in the Bedded Pyrrhotite Unit shows systematic changes between the contact aureole and the xenoliths. The Bedded Pyrrhotite Unit in the contact aureole is less residual and has the assemblage: cordierite + plagioclase + K-feldspar + quartz + silicate melt (crystallized to quartz + plagioclase + K-feldspar + biotite) + sillimanite + graphite + sulfides +/- rutile, whereas the most residual Bedded Pyrrhotite Unit rocks are xenoliths that are quartz- and K-feldspar-absent and contain: cordierite + orthopyroxene + silicate melt (quartz + K-feldspar + plagioclase + biotite + orthopyroxene) + sulfides + spinel. Pseudosections were calculated for the Bedded Pyrrhotite Unit in order to determine peak metamorphic temperatures. Xenoliths record temperatures that range from ~800 to 1000°C, in part this range is a function of the size of xenolith; the interiors of the largest record the lowest temperatures. In contrast, the maximum temperature attained in the contact aureole rocks studied was ~870°C. Geochemical modeling indicates that the

Bedded Pyrrhotite Unit from the contact aureole and the center of large xenoliths of the Bedded Pyrrhotite Unit contain similar and significant amounts of melt, whereas the most residual of the xenoliths have lost more than 50% silicate melt. Petrographic study shows patches of the anatectic melt product (quartz + K-feldspar + plagioclase +/- biotite, orthopyroxene) both within the xenolith and in the norite surrounding the xenoliths. Sulfide droplets consisting of pyrrhotite, chalcopyrite and minor pentlandite occur within these patches. The calculated temperatures from the xenoliths are sufficiently high for the original sulfide minerals (pyrrhotite and chalcopyrite) in Bedded Pyrrhotite Unit to have melted and be transported by the silicate anatectic melt from the xenolith into the mafic magma as a sulfide melt.

Keywords: Duluth Complex, partial melting, black shale, xenoliths, thermodynamic modeling

3.3 INTRODUCTION

Partial melting and assimilation of sedimentary country-rocks into intrusive magmas is a well-documented process (Bowen, 1922; Gribble and O'Hara, 1967; Ripley and Alawi, 1988; McLeod and Sparks, 1998; Preston et al., 1999; Chesley et al., 2002; Beard et al., 2005; Markl, 2005; Clarke, 2007; Erdmann et al., 2007; Clarke et al., 2009; Shaw, 2009; Díaz-Alvarado et al., 2011; Hiebert et al., 2013; Dorfler et al., 2015; Robertson et al., 2015). In addition to having fundamental implications for the evolution of the continental crust, these processes are thought to be important in the formation of the World's magmatic Ni-Cu-platinum-group element (PGE) deposits because much of the S in these deposits is thought to be derived from the country rocks (Lesher et al., 1984; Ripley and Li, 2013).

A number of mechanisms have been proposed for the transfer of S from country rocks to the mafic magma and these include vapor transport, partial melting and bulk melting (Naldrett, 1966; Huppert, 1984; Lesher et al., 1984; Baker et al., 2001; Lesher and Burnham, 2001; Queffurus and Barnes, 2014). Numerous studies have made the connexion between melting of country rocks and the formation of economic deposits with S-rich black shales being suggested as a particularly suitable source of S (Ripley and Alawi, 1988; Thériault et al., 1997; Thériault and Barnes, 1998; Amelin et al., 2000; Li and Naldrett, 2000; Ripley et al., 2000; Johnson et al., 2010; Queffurus and Barnes, 2014; Robertson et al., 2015). The P-T conditions of melting, the degree of partial melting as well as the nature and composition of the protolith are critical parameters in these models. The study of *in-situ* partial melting in xenoliths caught in the magma may thus provide direct evidence of the conditions under which the magma was contaminated.

The Duluth Complex represents an ideal and well-documented intrusion for studying contamination processes (Mainwaring and Naldrett, 1977; Ripley, 1981; Andrews and Ripley, 1989; Thériault et al., 1997; Thériault and Barnes, 1998; Ripley et al., 2007; Severson and Hauck, 2008; Queffurus and Barnes, 2014; Robertson et al., 2015). In the Partridge River Intrusion, Ni-Cu sulfide deposits occur in the basal part close to the contact with S-rich black shales of the Virginia Formation known as the Bedded Pyrrhotite Unit (Severson, 1994). In addition, xenoliths of the Bedded Pyrrhotite Unit with patches of sulfide minerals surrounding them occur in the basal part of the intrusion (Severson and Hauck, 2008; Queffurus and Barnes, 2014, Fig. 2).

We have undertaken a petrographic and geochemical study to investigate partial melting processes in the contact aureole and the xenoliths of the Bedded Pyrrhotite Unit. Thermodynamic modeling (Spear et al., 1999; Holland and Powell, 2001; White et al., 2001; White et al., 2007; Álvarez-Valero and Kriegsman, 2010; Álvarez-Valero and Waters, 2010; Johnson et al., 2010) allows us to establish the metamorphic temperature conditions in both the aureole and the xenoliths. The modeling indicates that temperatures were high enough to produce partial melting in both the xenoliths and the aureole. However, petrographic observations and whole rock compositions show that partial melt has not been removed from the aureole rocks, whereas it has been removed from the xenoliths.

3.4 GEOLOGICAL CONTEXT

The Duluth Complex is a Keweenawan-age (1100 Ma) mafic complex located in Minnesota, USA. The Complex is composed of several mafic intrusions related to a mantle plume that was located beneath the Midcontinent-rift system (Ojakangas et al., 2001).

The Duluth Complex is divided into two main mafic intrusions: the Partridge River Intrusion and the South Kawishiwi Intrusion (Fig. 3.1). The present study is focused on the Partridge River Intrusion. The basal unit, also called Unit I, of the Partridge River Intrusion contains abundant xenoliths of the host-rocks and most of the sulfide mineralization (Severson and Hauck, 1994). This basal unit is composed of the following lithologies: norite, gabbronorite, troctolite and ultramafic rocks (Hauck et al., 1997; Thériault et al., 1997; Miller et al., 2002; Severson and Hauck, 2008). A prominent metamorphic aureole up to several metres wide is developed in the country rocks close to the contact with the intrusion (French, 1968; Morey et al., 1972; Labotka et al., 1981; Sawyer, 2014).

The western side of the Duluth Complex is intruded into Archean and Paleoproterozic rocks (Fig. 3.1). The Paleoproterozoic Animikie Group sedimentary rocks are divided into two units, the Virginia Formation and the Biwabik Formation. The Biwabik Formation consists of banded iron formation and carbonates. The Virginia Formation consists of carbonates, greywackes, pelites, black shales and siltstones (Lucente and Morey, 1983). A few kilometers away from the intrusion the sediments are essentially unmetamorphosed (Bonnichsen, 1972; Lucente and Morey, 1983). The black shales are of particular interest because they contain sulfides. The unmetamorphosed black shales are dark, fine-grained (grain size ~10µm) rocks with clay minerals, organic matter, quartz, plagioclase and ilmenite (Lucente and Morey, 1983; Andrews and Ripley, 1989).

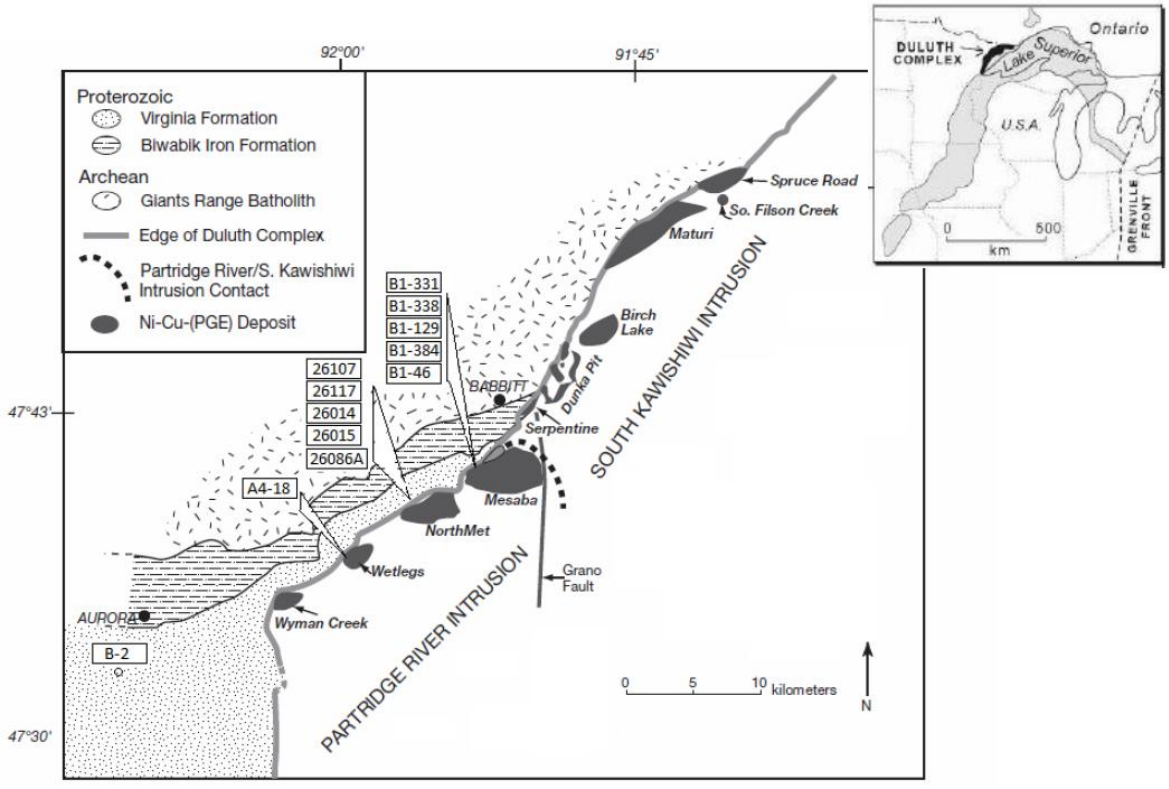

Figure 3.1: Geological and location map of the Duluth Complex (modified from Ojakangas et al., 2001; Queffurus and Barnes, 2014; Ripley, 2014). The location of sampled diamond drill-hole cores are shown in the map.

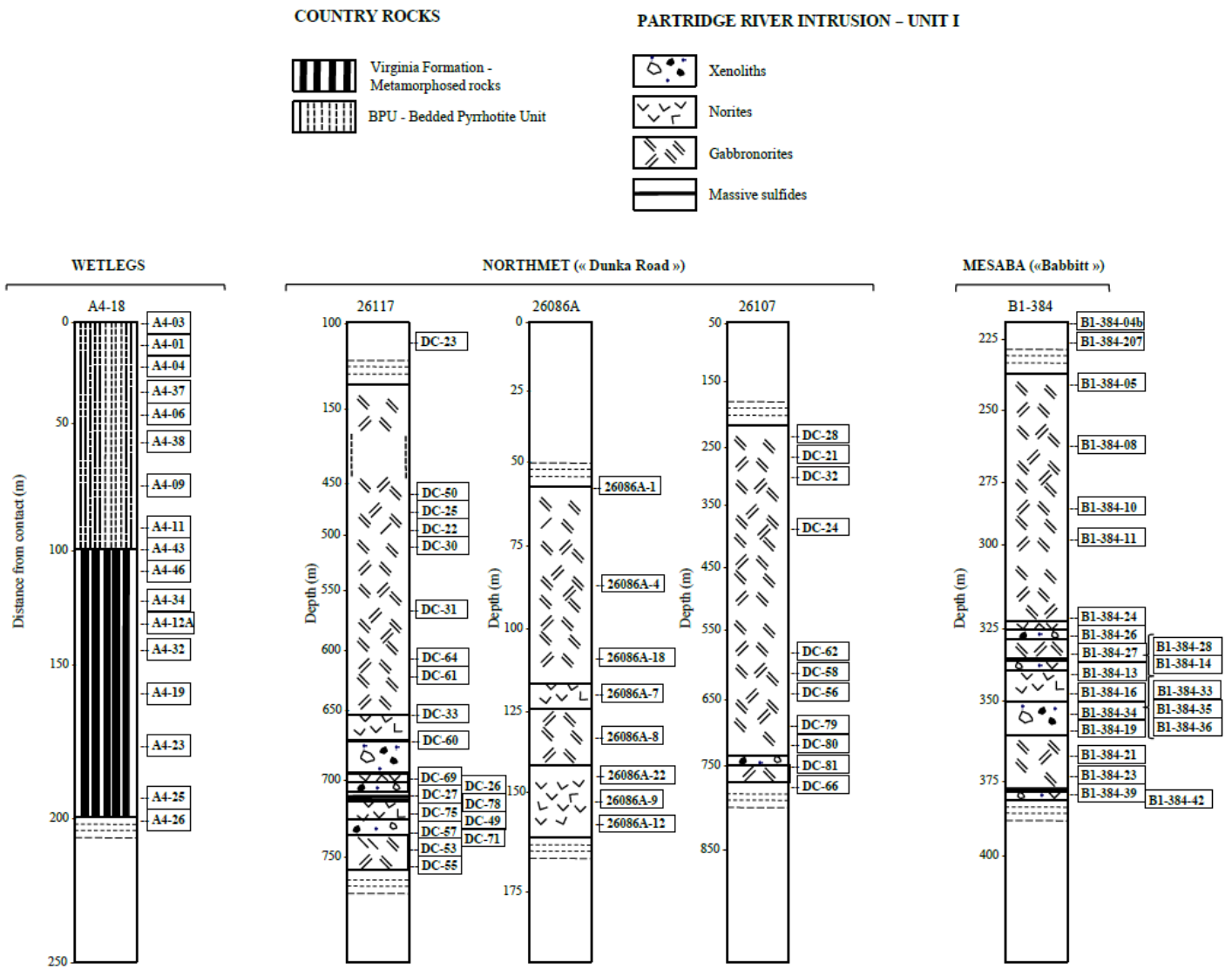
COUNTRY ROCKS
Virginia Formation - Metamorphosed rocks
BPU - Bedded Pyrrhotite Unit
PARTRIDGE RIVER INTRUSION – UNIT I
Xenoliths
Norites
Gabbronorites
Massive sulfides
WETLEGS
A4-18
Distance from contact (m)
A4-03
A4-01
A4-04
A4-37
A4-06
A4-38
A4-09
A4-11
A4-43
A4-46
A4-34
A4-12A
A4-32
A4-19
A4-23
A4-25
A4-26
NORTHMET (« Dunka Road »)
26117
Depth (m)
DC-23
DC-50
DC-25
DC-22
DC-30
DC-31
DC-64
DC-61
DC-33
DC-60
DC-69
DC-27
DC-75
DC-57
DC-53
DC-55
DC-26
DC-78
DC-49
DC-71
26086A
26086A-1
26086A-4
26086A-18
26086A-7
26086A-8
26086A-22
26086A-9
26086A-12
26107
DC-28
DC-21
DC-32
DC-24
DC-62
DC-58
DC-56
DC-79
DC-80
DC-81
DC-66
MESABA («Babbitt »)
B1-384
B1-384-04b
B1-384-207
B1-384-05
B1-384-08
B1-384-10
B1-384-11
B1-384-24
B1-384-26
B1-384-27
B1-384-13
B1-384-16
B1-384-34
B1-384-19
B1-384-21
B1-384-23
B1-384-39
B1-384-28
B1-384-14
B1-384-33
B1-384-35
B1-384-36
B1-384-42

Figure 3.2: Stratigraphic position of the samples in the borehole sections of the Virginia Formation country-rocks and the basal part (Unit I) of the Partridge River Intrusion (modified from Queffurus and Barnes, 2014; Samalens et al., 2017). The few samples taken from boreholes26014, 26015, B1-46, B1-129, B1-331, B1-338, B-2 and LTV mine are not indicated.

In the contact aureole all of the different types of sedimentary rocks are present. Pelitic and semipelitic sediments closest to the Duluth Complex became diatexite migmatites and have experienced temperatures greater than 800°C (maximum ~870°C) (Labotka et al., 1981; Tracy and Frost, 1991; Sawyer, 2014). Pressure has been estimated at between ~ 2 and 2.5 kbars at the time of intrusion (Labotka et al., 1981; Andrews and Ripley, 1989).

The black shale is represented by the Bedded Pyrrhotite Unit and is approximately 200 m thick, but has a sporadic distribution (Severson and Hack, 2008). Xenoliths of the Bedded Pyrrhotite Unit occur in the basal unit of the Partridge River Intrusion and range in size from few centimeters to meter-scale. Based on the S-rich nature of the Bedded Pyrrhotite Unit, the presence of abundant xenoliths in the basal unit of the intrusion, S isotopic composition and S/Se ratios, the source of the S in the Ni-Cu-PGE mineralization is interpreted to come from the Bedded Pyrrhotite Unit (Ripley and Alawi, 1988; Severson et al., 1996; Thériault et al., 1997; Arcuri et al., 1998; Queffurus and Barnes, 2014; Samalens et al., 2017).

3.5 METHODOLOGY

In order to estimate the changes in xenolith petrography and compositions from their original petrography and composition five representative samples of black shale from outside the aureole, nine representative samples of the Bedded Pyrrhotite Unit from within the aureole and nineteen representative samples of xenoliths of Bedded Pyrrhotite Unit were selected. In addition eight leucosomes from the Bedded Pyrrhotite Unit and norites and gabbronorites from immediately around the xenoliths were selected. The location of the samples is shown in Figures 3.1 and 3.2 and Appendix 1.

Petrographic observations of the Bedded Pyrrhotite Unit and magmatic rocks from the basal Unit I, were made taking particular note of the mineral assemblages and textures associated with partial melting. Twenty thin sections that cover the interior and margins of Bedded Pyrrhotite Unit xenoliths and their interaction with the mafic magma were examined in detail.

Electron probe microanalyses of plagioclase, K-feldspar, biotite and pyroxene from 6 samples of xenoliths and mafic rocks surrounding the xenoliths were carried out at Laval University (Laboratoire de microanalyse) by wavelength dispersive X-ray emission spectrometry (WD-XRES) using the CAMECA SX-100 electron probe microanalyses. Silicates and oxides standards provided by ASTIMEX and PandH developments were used for microprobe calibration. Microprobe data are provided in Tables 3.1 and 3.5.

Thirteen new whole rock analyses were added to our existing data base of whole rock analyses of the Bedded Pyrrhotite Unit and mafic rocks immediately around the xenoliths (Thériault et al., 1997; Duchesne, 2004; Queffurus and Barnes, 2014). Major oxides and trace elements were determined at Activation Laboratories Ltd (Actlabs), Ontario, Canada by Fusion ICP-MS (Method WRA42B). Results are presented in Tables 3.2, 3.3 and Appendix 4. For the new analyses major oxides and trace elements were determined at Activation Laboratories Ltd. (Actlabs), Ontario, Canada by Fusion ICP-MS (protocol WRA42B); values obtained for the reference materials are given in Appendix 5.

Details of the calculation of phase equilibria and the construction of pseudosections in order to constrain the metamorphic temperatures reached by the xenoliths will be discussed later in the text.

3.6 PETROGRAPHY

3.6.1 BEDDED PYRRHOTITE UNIT IN THE CONTACT AUREOLE

The rocks of the Bedded Pyrrhotite Unit in the contact aureole are meta-argillites that are composed of feldspar (~30 modal % plagioclase and ~15 modal % K-feldspar), quartz (<10 modal %), micas (<10 modal %), cordierite (~40 modal %), sillimanite (<5 modal %) and opaque minerals (~5 modal %) (Fig. 3.3a); modal proportions of minerals were obtained by visual estimation.

The Bedded Pyrrhotite Unit in the inner part of the contact aureole at the Duluth Complex has undergone partial melting (Sawyer, 2014) and microstructural evidence for partial melting is widely preserved in the contact aureole (Fig. 3.3). Quartz and feldspar occur as mineral films and cupsoid-shaped grains that fill the spaces between rounded grains of feldspar ~100µm (Fig. 3.3b). The quartz and feldspar films are interpreted as anatectic melt and melt-filled pore space, whereas the polygonal and rounded feldspar and quartz are interpreted as the prograde microstructure in the reactant mineral assemblage. In addition, quartzo-feldspathic veinlets that are filled by feldspar and quartz of larger grain size than the matrix (Fig. 3.3c) are interpreted as leucosomes: generally these crosscut the primary structures. Mica, mostly biotite or phlogopite, but also muscovite, occur as porphyroblasts ~100 to 200µm (Fig. 3.3a,d). Relics and subeuhedral grains of aluminosilicate (sillimanite, or sillimanite replaced by mullite) occurs (Fig. 3.3a,d) in some samples. The common mineral assemblage of the Bedded Pyrrhotite Unit in the contact aureole is cordierite + plagioclase + K-feldspar + quartz + muscovite + biotite/phlogopite + sillimanite + melt (now represented by quartz + plagioclase + K-feldspar) + graphite + sulfides +/- rutile. Graphite can be abundant (higher than 20 modal %).

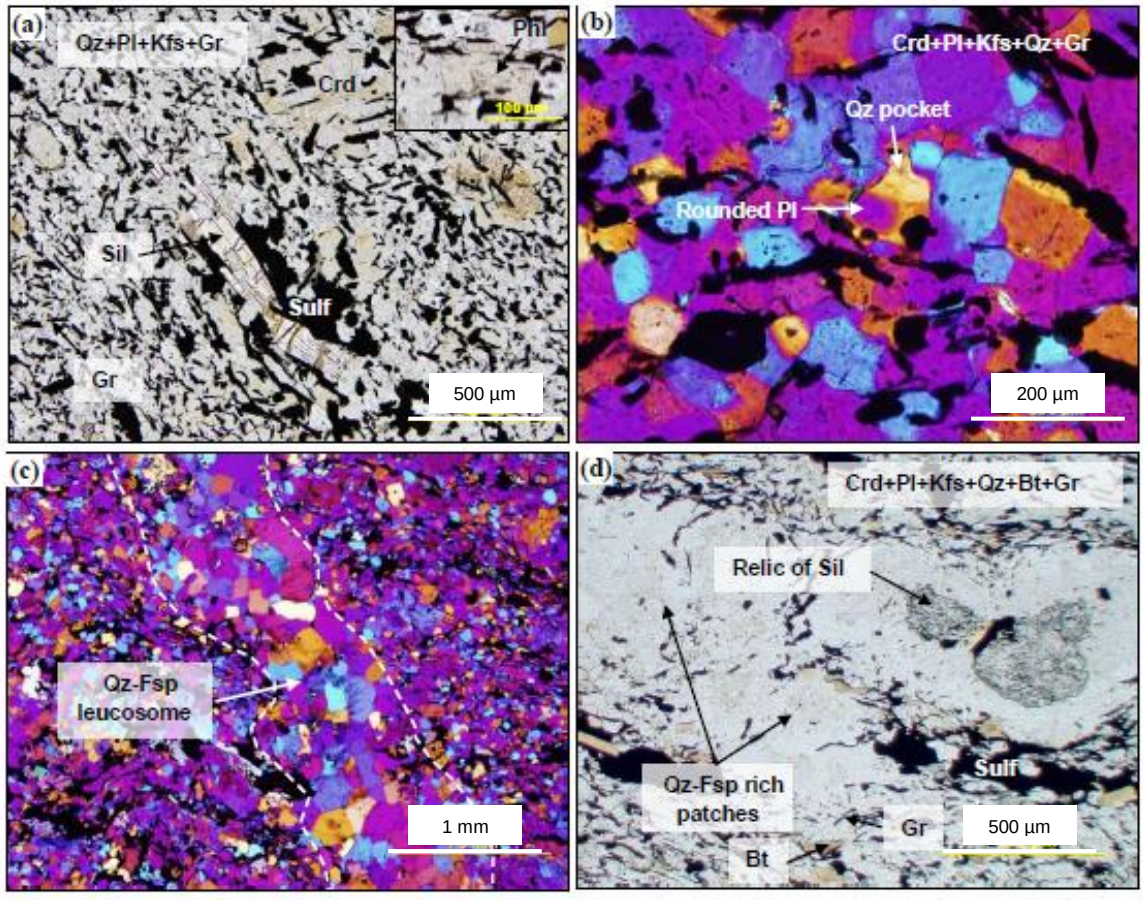

Figure 3.3: Photomicrographs of the Bedded Pyrrhotite Unit (BPU) from the contact aureole. (a) Sillimanite grain in a quartz, feldspar, cordierite and graphite matrix. Inset shows details of a phlogopite grain from the matrix. (b) Quartz-filled former anatectic melt pocket; note the flakes of graphite. (c) Quartzo-feldspathic veinlet (leucosome). The quartz plate has been added in photomicrographs B and C to better identify the inclusions of former anatectic melt. (d) Relic grain of sillimanite and quartzo-feldspatic patches in a cordierite, feldspar, quartz, biotite and graphite matrix. Abbreviations (Whitney and Evans, 2010): Bt = Biotite; Opx = Orthopyroxene; Crd = Cordierite; Pl = Plagioclase; Kfs = K-feldspar; Qz = Quartz; Sil = Sillimanite; Gr = Graphite; Phl = Phlogopite; Fsp = Feldspar (undifferentiated); Sulf = Sulfide.

3.6.2 BEDDED PYRRHOTITE UNIT XENOLITHS

Xenoliths of the Bedded Pyrrhotite Unit consist of a fine to medium-grained feldspar + biotite + cordierite + orthopyroxene silicate matrix with numerous sulfide beds (Queffurus and Barnes, 2014, Fig. 2E; Samalens et al., 2017). All xenoliths of the Bedded Pyrrhotite Unit in the Mesaba and the NorthMet deposits show microstructural evidence that partial melting occurred. However, microstructures and parageneses in the xenoliths from the Mesaba deposit differ from those at the NorthMet deposit.

3.6.2.1 BPU XENOLITHS IN THE MESABA DEPOSIT

Xenoliths of the Bedded Pyrrhotite Unit range in size from a few centimeters to meter scale in the Mesaba deposit. Macroscopic (centimeter-size) quartzo-feldspathic veins and patches occur in all the xenoliths and are interpreted as evidence of *in situ* partial melting of the xenoliths and segregation of the melt into in-source leucosomes (Fig. 3.4a).

There is abundant microstructural evidence that partial melting occurred in the xenoliths at the Mesaba deposit. Quartz, feldspar and cordierite occur as anhedral patches that are of larger size than the matrix minerals and as thin mineral films filling space between the grains. The former are interpreted as melt-filled pores, or pockets (Harte et al., 1991; Sawyer, 2001) and the latter as former melt-bearing grain boundaries (Fig. 3.4b, c). Orthopyroxene occurs in some samples as irregular grains (~50µm) that fill space between the matrix grains (Fig. 3.4b), or occur as small inclusions (<20µm) in large feldspar and cordierite grains (Fig. 3.4c); these grains are interpreted as the result of peritectic reaction. Biotite occurs as small rounded inclusions within feldspar and cordierite grains, or as large irregular-shaped porphyroblasts (>200µm) (Fig. 3.4d) that appear to fill space between

minerals. One sample that is a part of a meter-size xenolith, contains relics of an aluminosilicate, presumably, mullite based on the petrographic observations (Fig. 3.4e). The common mineral assemblage in xenoliths of the Bedded Pyrrhotite Unit at the Mesaba deposit is orthopyroxene + cordierite + biotite + plagioclase + melt (now represented by quartz + plagioclase + K-feldspar) + ilmenite + sulfides +/- graphite +/- sillimanite/mullite.

In addition to the small patches of former silicate melt, some xenoliths of the Bedded Pyrrhotite Unit at the Mesaba deposit contain larger quartzo-feldspathic aggregates, or veins. Typically these comprise large (>500µm) equant, but irregularly-shaped porphyroblasts of quartz and feldspar, some of which contain quartz-plagioclase intergrowths (Fig. 3.4f), possibly granophyre. These aggregates are interpreted to represent larger pockets of melt, or leucosomes.

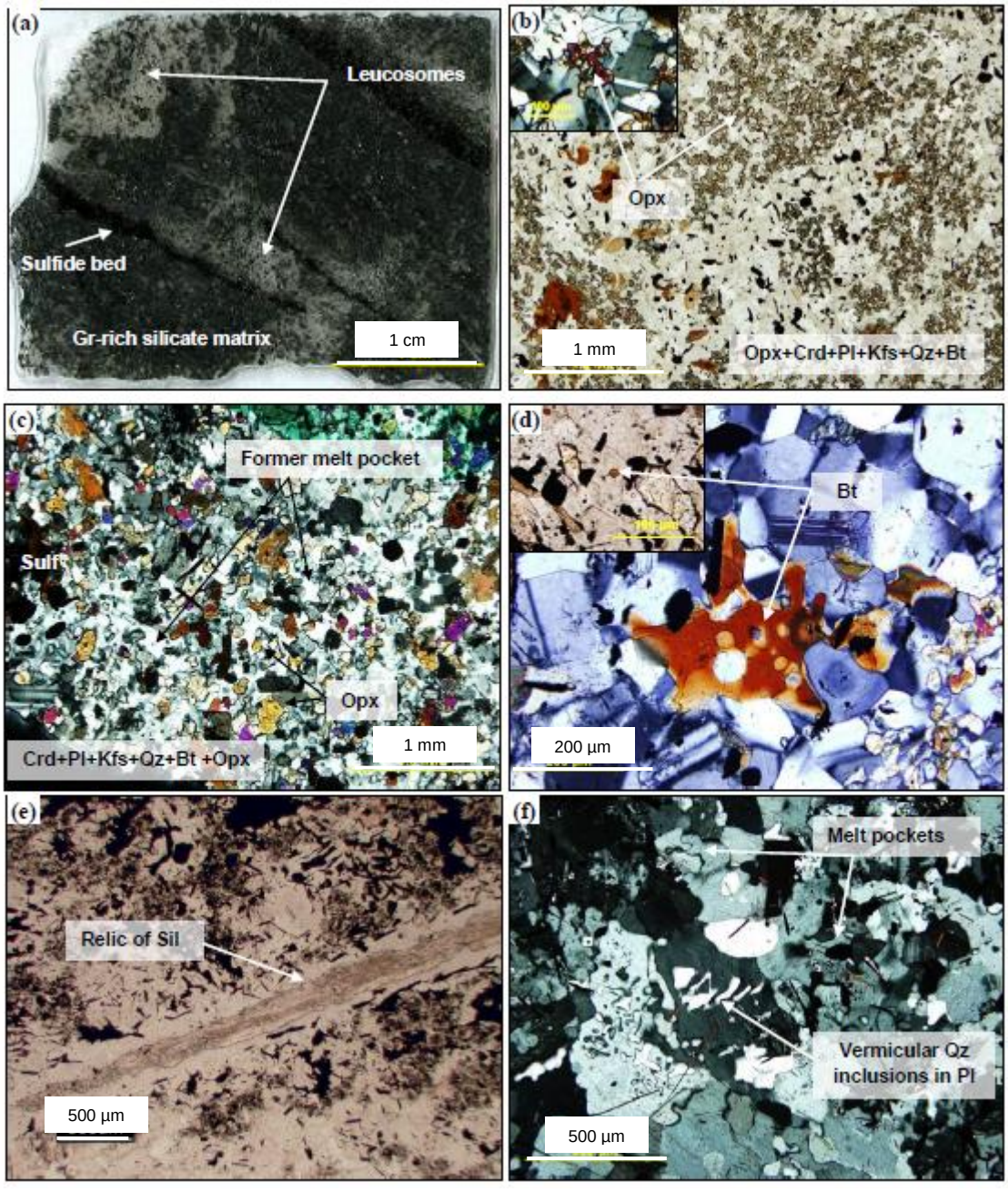
(a)
Leucosomes
Sulfide bed
Gr-rich silicate matrix
1 cm
(b)
Opx
1 mm
Opx+Crd+Pl+Kfs+Qz+Bt
(c)
Former melt pocket
Opx
1 mm
Crd+Pl+Kfs+Qz+Bt +Opx
(d)
Bt
200 µm
(e)
Relic of Sil
500 µm
(f)
Melt pockets
Vermicular Qz inclusions in Pl
500 µm

Figure 3.4: Photomicrographs from xenoliths of Bedded Pyrrhotite Unit (BPU) at the Mesaba deposit. (a) Macroscopic leucosomes in partially molten BPU xenoliths. (b) Opx-rich Bedded Pyrrhotite Unit xenolith. Inset shows details of irregular shape orthopyroxene grains from the matrix. (c) Former anatectic melt pockets with orthopyroxene inclusions. (d) Irregular-shaped biotite grain in the matrix and a rounded biotite inclusion in feldspar (inset). (e) Relic of sillimanite grain. (f) Former pockets of anatectic melt (leucosome) in a BPU xenolith. Note the elongate quartz inclusions in plagioclase.

3.6.2.2 BPU XENOLITHS IN THE NORTHMET DEPOSIT

Xenoliths of the Bedded Pyrrhotite Unit in the NorthMet deposit are no more than a few centimeters in size and contain abundant microstructural evidence of partial melting. Large equant feldspar and cordierite grains (>1mm) have cupsoid boundaries and occur as patches in the xenoliths (Fig. 3.5a-c). These minerals are interpreted to have crystallized from small pockets, or pores, of anatectic melt scattered in a matrix of largely residual and peritectic phases. The crystals of feldspar and cordierite that form patches commonly contain tiny inclusions of quartz (Fig. 3.5a). Orthopyroxene occurs as small inclusions (<50µm) within the feldspar and cordierite patches (Fig. 3.5b), or as irregular grains (~100µm) that occupy the space between the feldspar and cordierite grains (Fig. 3.5c). Biotite forms large irregular-shaped porphyroblasts (>1mm) that fill the space between the grains; these are also interpreted to have crystallized from pockets of anatectic melt (Fig. 3.5b) in the residual matrix. Rarely, small inclusions of spinel (< 5 modal %) occur in the feldspar (Fig. 3.5d). The common mineral assemblage is cordierite + orthopyroxene + melt (quartz + K-feldspar + plagioclase + biotite + orthopyroxene) +/- graphite +/- spinel + ilmenite + sulfides. Thus, these assemblages were quartz + K-feldspar + biotite- absent at the peak metamorphic temperature. Xenoliths at the NorthMet deposit have low abundance of graphite and oxides (< 5 modal %).

At the NorthMet deposit centimetric leucocratic layers are commonly occur between xenoliths of the Bedded Pyrrhotite Unit and the surrounding mafic rocks (Fig. 3.5e, f); they form a rind. The common mineral assemblage of these layers is plagioclase + orthopyroxene + quartz +/- K-feldspar. Plagioclase occur as large irregular grains (>500µm) that form patches with quartz and K-feldspar; the patches occupy the space

between the grains (Fig. 3.5e). Quartz+feldspar-rich patches are interpreted as crystallized products after large pockets of melt, or, as leucosomes (Fig. 3.5e). Orthopyroxene occurs as inclusions (<100µm) in plagioclase grains and as irregular grains (~500µm) which are typically oriented into a band-like structure (Fig. 3.5e, f). Leucocratic host material also contains some sulfide minerals (Fig. 3.5f). An orthopyroxene-rich selvedge is commonly present at the margins of the xenolith close to the leucocratic layer (Fig. 3.5e).

3.6.3 MAFIC MAGMA

The groundmass of norites and gabbronorites around the xenoliths contains tabular subeuhedral plagioclase grains (~1mm) and large orthopyroxene grains (>500µm) (Fig. 3.6). In addition, K-feldspar, plagioclase and quartz occur as patches and films that filled space between the grains and these are interpreted to represent pockets of anatectic melt, or leucosomes between magmatic primocrysts that crystallized from the mafic magma (Fig. 3.6). Small rounded grains of orthopyroxene (<300µm) are included in these anatectic melt pockets or leucosomes.

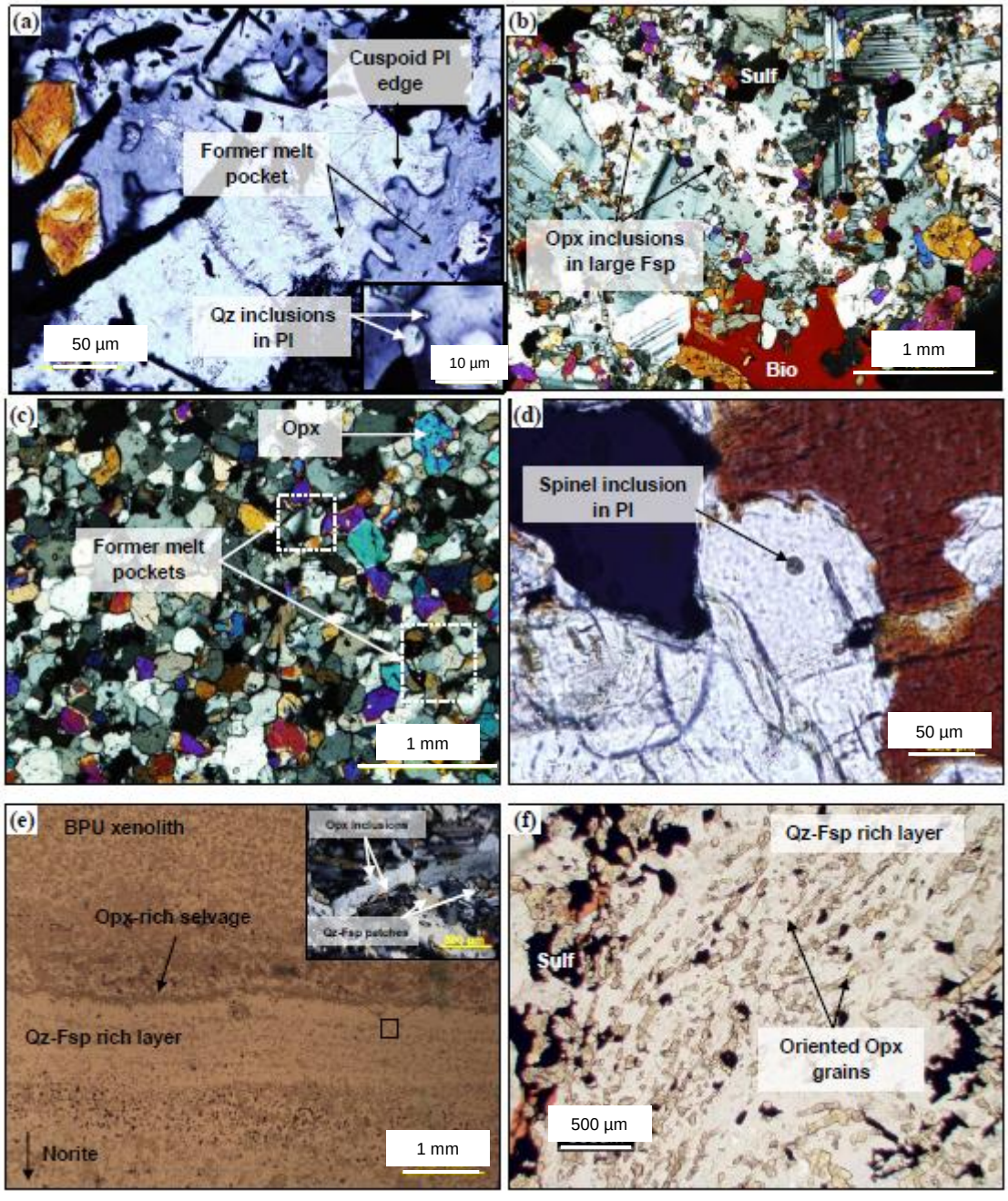
(a)
Cuspoid Pl edge
Former melt pocket
Qz inclusions in Pl
50 µm
10 µm
(b)
Sulf
Opx inclusions in large Fsp
Bio
1 mm
(c)
Opx
Former melt pockets
1 mm
(d)
Spinel inclusion in Pl
50 µm
(e)
BPU xenolith
Opx-rich selvage
Qz-Fsp rich layer
Norite
1 mm
(f)
Qz-Fsp rich layer
Sulf
Oriented Opx grains
500 µm

Figure 3.5: Photomicrographs from xenoliths of the Bedded Pyrrhotite Unit (BPU) at the NorthMet deposit. (a) Textural evidence for the former presence of anatectic melt. Inset shows quartz inclusions in a plagioclase grain. (b) Large feldspar patches with orthopyroxene inclusions, interpreted as patches of anatectic melt. (c) Former pocket of melt in an Opx + Crd + Pl + Kfs + Qz matrix. (d) Green spinel inclusion (hercynite) in plagioclase. (e) Macroscopic image of a leucocratic layer between a xenolith of the BPU and the mafic rocks. Inset shows microscopic details of plagioclase, quartz and orthopyroxene grains from the leucocratic layer. (f) Oriented orthopyroxene grains in the quartz-feldspar-rich layer surrounding the xenolith. Note the low abundance of graphite in the xenoliths.

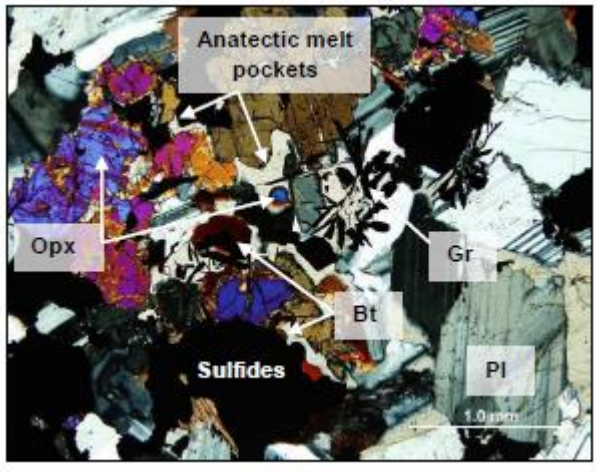

Figure 3.6: Photomicrograph of norite from the basal Unit I at the Mesaba deposit. Norites contain pockets of former anatectic melt or leucosomes in the basal Unit I.

3.7 GEOCHEMICAL STUDY

3.7.1 MINERAL CHEMISTRY

3.7.1.1 FELDSPARS

The compositions of plagioclase from the Bedded Pyrrhotite Unit in the contact aureole are different from those in the xenoliths (Fig. 3.7a and Table 3.1). Plagioclase compositions in the contact aureole range An_{25-38}, and although plagioclase compositions from the xenoliths overlap those from the contact aureole, they extend to higher anorthite contents ($\sim An_{31-62}$). There is a progressive increase in the anorthite content of plagioclase in the mafic rocks with distance from the xenoliths; compositions change from $\sim An_{40-60}$ in the mixed zone close the xenoliths to An_{55-85} in the norites and gabbronorites. Plagioclases in the zone immediately surrounding the xenoliths, which correspond to first few centimeters of magma from the xenolith, have intermediate values. These relationships suggest that there is a zone of chemical interaction between the xenolith and its hosting mafic magma. Similar composition-spatial variation trends for plagioclase are observed at the Mesaba and NorthMet deposits (Fig. 3.7a).

Potassium feldspar has only been analyzed in the Bedded Pyrrhotite Unit from the contact aureole and in the Bedded Pyrrhotite Unit xenoliths at the Mesaba deposit. Potassium feldspars in the Bedded Pyrrhotite Unit from the contact aureole have similar orthoclase component ($\sim Or_{68-89}$) to those from xenoliths of the Bedded Pyrrhotite Unit at the Mesaba deposit (Fig. 3.7a and Table 3.1).

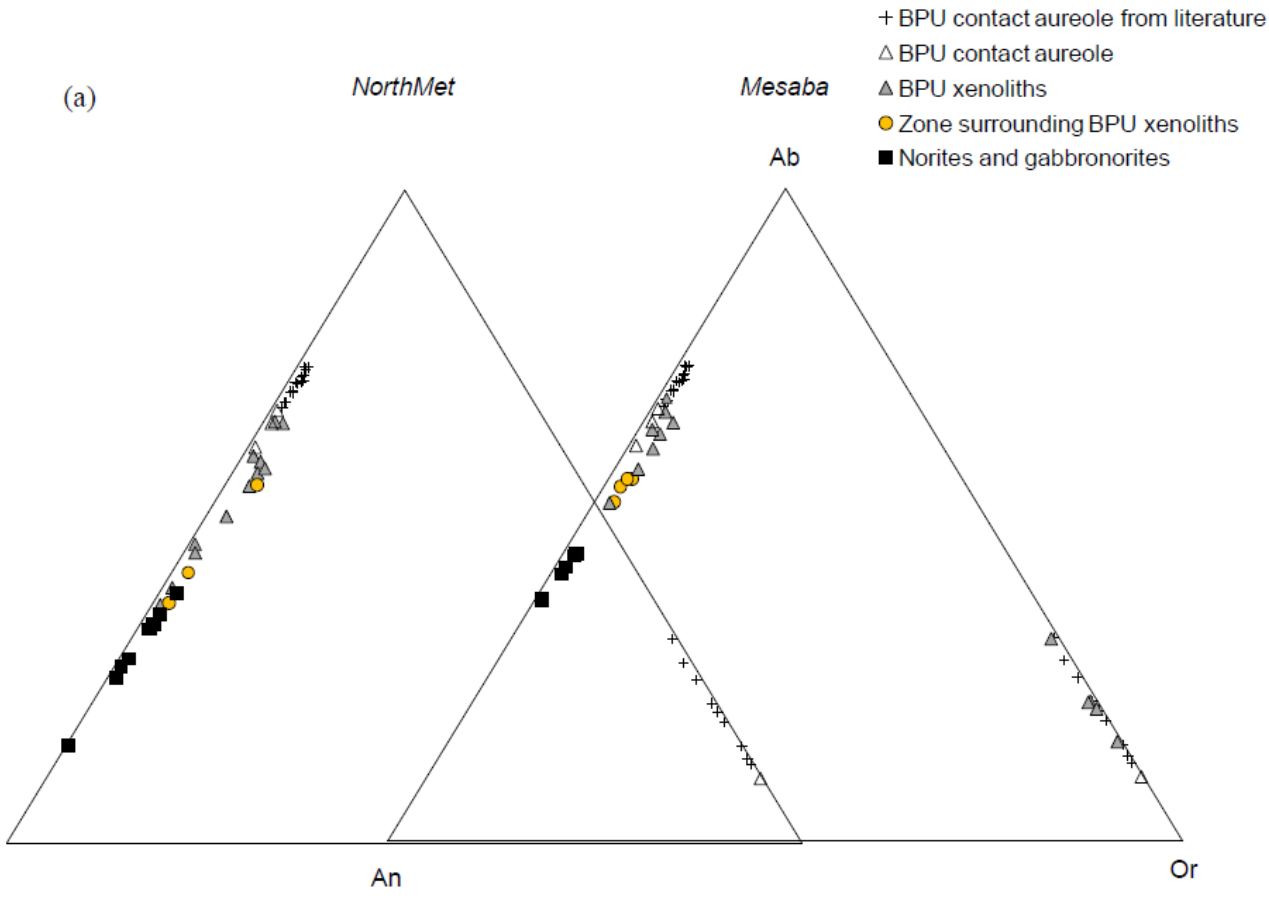
(a)
NorthMet
Mesaba
Ab
An
Or
BPU contact aureole from literature
BPU contact aureole
BPU xenoliths
Zone surrounding BPU xenoliths
Norites and gabbronorites

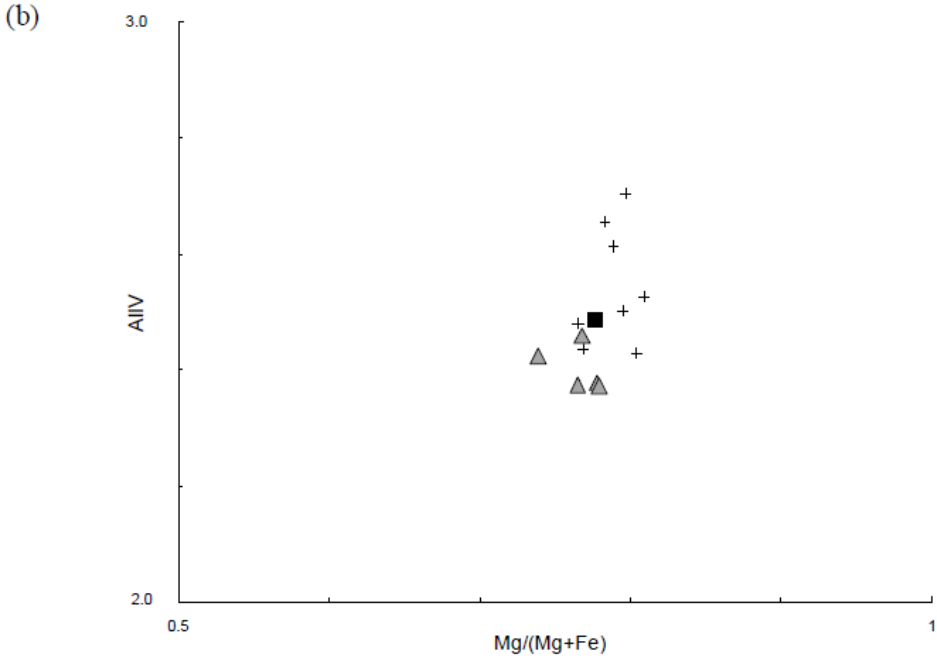
(b)
3.0
2.0
AlIV
0.5
1
Mg/(Mg+Fe)

Figure 3.7: Ternary diagram of albite (Ab), anorthite (An) and orthoclase (Or) content in feldspar (a) and plot of Mg# vs. Al^{IV} content of biotite from microprobe analyses of Bedded Pyrrhotite Unit (BPU) from the contact aureole, BPU xenoliths and mafic magma (b). Zones surrounding the xenoliths correspond to first few centimeters of magma from the xenolith. Feldspar and biotite compositions of BPU from the contact aureole from literature are from the Duchesne (2004) database.

Feldspars

Deposit	Sample	Rock type	wt% SiO_2	TiO_2	Al_2O3	MgO	CaO	MnO	FeO	SrO	BaO	Na_2O	K_2O	Total	a.p.f.u Si	Ti	Al	Mg	Ca	Mn	Fe	Sr	Ba	Na	K	Ab	An	Orth
Mesaba	B1-384-39	BPU xenolith	64,13	0,00	18,65	0,01	0,16	0,00	0,01	0,00	0,50	2,42	13,13	99,00	2,98	0,00	1,02	0,00	0,01	0,00	0,00	0,00	0,01	0,22	0,78	21,7	0,8	77,5
Mesaba	B1-384-39	BPU xenolith	64,56	0,09	18,83	0,01	0,23	0,00	0,05	0,00	0,60	2,39	13,14	99,89	2,97	0,00	1,02	0,00	0,01	0,00	0,00	0,00	0,01	0,21	0,77	21,4	1,2	77,4
Mesaba	B1-384-39	BPU xenolith	64,64	0,00	18,93	0,01	0,21	0,00	0,02	0,00	0,51	3,46	11,44	99,21	2,98	0,00	1,03	0,00	0,01	0,00	0,00	0,00	0,01	0,31	0,67	31,1	1,0	67,9
Mesaba	B1-384-39	BPU xenolith	64,17	0,01	18,16	0,05	0,10	0,00	0,49	0,00	0,44	1,68	13,91	99,01	2,99	0,00	1,00	0,00	0,01	0,00	0,02	0,00	0,01	0,15	0,83	15,4	0,5	84,1
Mesaba	B1-384-39	BPU xenolith	64,78	0,02	18,71	0,01	0,13	0,00	0,08	0,00	0,49	2,30	13,53	100,04	2,98	0,00	1,01	0,00	0,01	0,00	0,00	0,00	0,01	0,21	0,79	20,4	0,6	79,0
Mesaba	B1-384-39	BPU xenolith	60,28	0,03	24,47	0,00	6,50	0,00	0,14	0,07	0,01	7,96	0,18	99,63	2,70	0,00	1,29	0,00	0,31	0,00	0,01	0,00	0,00	0,69	0,01	68,2	30,8	1,0
Mesaba	B1-384-14	BPU xenolith	58,67	0,04	25,28	0,01	7,65	0,00	0,11	0,08	0,01	7,02	0,56	99,41	2,64	0,00	1,34	0,00	0,37	0,00	0,00	0,00	0,00	0,61	0,03	60,5	36,4	3,2
Mesaba	B1-384-14	BPU xenolith	56,53	0,05	27,10	0,01	9,60	0,00	0,00	0,10	0,07	6,01	0,33	99,80	2,55	0,00	1,44	0,00	0,46	0,00	0,00	0,00	0,00	0,53	0,02	52,1	46,0	1,9
Mesaba	B1-384-14	BPU xenolith	59,62	0,00	25,09	0,00	7,15	0,05	0,02	0,06	0,02	7,21	0,52	99,74	2,67	0,00	1,32	0,00	0,34	0,00	0,00	0,00	0,00	0,63	0,03	62,7	34,4	2,9
Mesaba	B1-384-14	BPU xenolith	59,76	0,05	24,22	0,01	6,62	0,00	0,04	0,08	0,00	7,40	0,63	98,81	2,70	0,00	1,29	0,00	0,32	0,00	0,00	0,00	0,00	0,65	0,04	64,5	31,8	3,7
Mesaba	B1-384-14	BPU xenolith	59,31	0,02	24,55	0,02	6,69	0,00	0,52	0,01	0,09	7,63	0,33	99,17	2,68	0,00	1,31	0,00	0,32	0,00	0,02	0,00	0,00	0,67	0,02	66,1	32,0	1,9
Mesaba	B1-384-14	BPU xenolith	58,88	0,03	25,26	0,00	7,37	0,04	0,04	0,13	0,01	7,37	0,28	99,41	2,65	0,00	1,34	0,00	0,36	0,00	0,00	0,00	0,00	0,64	0,02	63,4	35,0	1,6
Mesaba	B1-384-14	BPU xenolith	57,73	0,05	25,76	0,01	8,27	0,00	0,09	0,09	0,03	6,58	0,50	99,11	2,61	0,00	1,37	0,00	0,40	0,00	0,00	0,00	0,00	0,58	0,03	57,3	39,8	2,9
Mesaba	B1-384-13	Norite	53,36	0,03	28,81	0,01	11,79	0,00	0,15	0,07	0,02	4,84	0,22	99,30	2,44	0,00	1,55	0,00	0,58	0,00	0,01	0,00	0,00	0,43	0,01	42,1	56,6	1,3
Mesaba	B1-384-13	Norite	54,35	0,02	28,76	0,02	11,33	0,00	0,30	0,09	0,03	5,03	0,26	100,19	2,46	0,00	1,53	0,00	0,55	0,00	0,01	0,00	0,00	0,44	0,02	43,9	54,6	1,5
Mesaba	B1-384-13	Norite	54,39	0,04	28,05	0,03	11,38	0,04	0,10	0,11	0,00	5,14	0,27	99,54	2,47	0,00	1,50	0,00	0,55	0,00	0,00	0,00	0,00	0,45	0,02	44,3	54,2	1,6
Mesaba	B1-384-13	Norite	53,50	0,04	29,05	0,02	11,96	0,00	0,13	0,05	0,04	4,71	0,24	99,74	2,43	0,00	1,56	0,00	0,58	0,00	0,01	0,00	0,00	0,42	0,01	41,0	57,6	1,4
Mesaba	B1-384-13	Norite	52,52	0,11	30,07	0,02	13,12	0,00	0,20	0,03	0,00	4,33	0,14	100,54	2,38	0,00	1,60	0,00	0,64	0,00	0,01	0,00	0,00	0,38	0,01	37,1	62,1	0,8
NorthMet	DC-30	Gabbronorite	50,33	0,05	31,00	0,04	14,71	0,00	0,23	0,01	0,00	3,26	0,22	99,86	2,30	0,00	1,67	0,00	0,72	0,00	0,01	0,00	0,00	0,29	0,01	28,3	70,5	1,3
NorthMet	DC-30	Gabbronorite	49,50	0,09	31,67	0,04	15,21	0,00	0,24	0,08	0,03	2,91	0,18	99,94	2,27	0,00	1,71	0,00	0,75	0,00	0,01	0,00	0,00	0,26	0,01	25,4	73,5	1,1
NorthMet	DC-30	Gabbronorite	51,94	0,00	30,31	0,04	13,57	0,01	0,23	0,00	0,00	3,89	0,29	100,28	2,36	0,00	1,62	0,00	0,66	0,00	0,01	0,00	0,00	0,34	0,02	33,6	64,7	1,7
NorthMet	DC-30	Gabbronorite	46,43	0,00	33,91	0,01	17,66	0,03	0,30	0,06	0,00	1,72	0,05	100,17	2,14	0,00	1,84	0,00	0,87	0,00	0,01	0,00	0,00	0,15	0,00	15,0	84,7	0,3
NorthMet	DC-30	Gabbronorite	51,49	0,02	30,12	0,05	13,67	0,00	0,26	0,13	0,00	3,78	0,25	99,77	2,35	0,00	1,62	0,00	0,67	0,00	0,01	0,00	0,00	0,34	0,02	32,9	65,7	1,5
NorthMet	DC-30	Gabbronorite	49,65	0,01	31,63	0,06	15,09	0,00	0,30	0,01	0,00	3,14	0,16	100,04	2,27	0,00	1,71	0,00	0,74	0,00	0,01	0,00	0,00	0,28	0,01	27,1	72,1	0,9
NorthMet	DC-30	Gabbronorite	52,59	0,01	30,35	0,03	13,19	0,03	0,21	0,08	0,00	4,03	0,30	100,83	2,37	0,00	1,61	0,00	0,64	0,00	0,01	0,00	0,00	0,35	0,02	35,0	63,3	1,7
NorthMet	DC-30	Gabbronorite	53,21	0,00	29,31	0,04	12,41	0,03	0,23	0,04	0,00	4,44	0,38	100,08	2,41	0,00	1,57	0,00	0,60	0,00	0,01	0,00	0,00	0,39	0,02	38,5	59,4	2,2
NorthMet	DC-70	BPU c.a.	58,07	0,00	26,21	0,01	8,04	0,00	0,08	0,12	0,00	7,07	0,14	99,75	2,61	0,00	1,39	0,00	0,39	0,00	0,00	0,00	0,00	0,62	0,01	60,9	38,3	0,8
NorthMet	DC-70	BPU c.a.	59,37	0,00	25,53	0,00	6,88	0,00	0,06	0,08	0,00	7,75	0,13	99,79	2,65	0,00	1,35	0,00	0,33	0,00	0,00	0,00	0,00	0,67	0,01	66,6	32,7	0,7
NorthMet	DC-70	BPU c.a.	59,16	0,00	25,50	0,01	7,30	0,04	0,13	0,05	0,02	7,57	0,18	99,96	2,65	0,00	1,34	0,00	0,35	0,00	0,01	0,00	0,00	0,66	0,01	64,6	34,4	1,0
NorthMet	DC-70	BPU c.a.	64,21	0,00	18,55	0,01	0,04	0,00	0,10	0,00	0,31	1,07	14,76	99,05	2,99	0,00	1,02	0,00	0,00	0,00	0,00	0,00	0,01	0,10	0,88	9,9	0,2	89,8
NorthMet	DC-71	BPU xenolith	58,30	0,03	26,04	0,00	8,41	0,02	0,08	0,10	0,00	7,07	0,23	100,28	2,61	0,00	1,37	0,00	0,40	0,00	0,00	0,00	0,00	0,61	0,01	59,6	39,2	1,3
NorthMet	DC-71	BPU xenolith	59,71	0,03	24,82	0,01	6,97	0,00	0,07	0,02	0,03	7,57	0,44	99,66	2,68	0,00	1,31	0,00	0,34	0,00	0,00	0,00	0,00	0,66	0,03	64,6	32,9	2,5
NorthMet	DC-71	BPU xenolith	59,51	0,00	25,45	0,00	7,10	0,00	0,08	0,06	0,00	7,52	0,23	99,96	2,66	0,00	1,34	0,00	0,34	0,00	0,00	0,00	0,00	0,65	0,01	64,9	33,8	1,3
NorthMet	DC-71	BPU xenolith	54,46	0,14	28,54	0,02	11,24	0,00	0,11	0,06	0,03	5,36	0,13	100,08	2,46	0,01	1,52	0,00	0,54	0,00	0,00	0,00	0,00	0,47	0,01	46,0	53,3	0,7
NorthMet	DC-71	BPU xenolith	54,55	0,00	28,87	0,02	11,39	0,07	0,02	0,12	0,01	5,20	0,25	100,48	2,46	0,00	1,53	0,00	0,55	0,00	0,00	0,00	0,00	0,45	0,01	44,6	54,0	1,4
NorthMet	DC-71	BPU xenolith	53,19	0,04	29,80	0,01	12,63	0,03	0,04	0,06	0,03	4,60	0,21	100,64	2,40	0,00	1,58	0,00	0,61	0,00	0,00	0,00	0,00	0,40	0,01	39,3	59,6	1,2
NorthMet	DC-71	BPU xenolith	52,56	0,08	30,05	0,01	13,09	0,00	0,09	0,03	0,01	4,26	0,18	100,36	2,38	0,00	1,60	0,00	0,64	0,00	0,00	0,00	0,00	0,37	0,01	36,7	62,3	1,0
NorthMet	DC-71	BPU xenolith	58,54	0,13	26,00	0,00	8,15	0,02	0,04	0,12	0,06	6,82	0,45	100,34	2,62	0,00	1,37	0,00	0,39	0,00	0,00	0,00	0,00	0,59	0,03	58,7	38,7	2,6
NorthMet	DC-71	BPU xenolith	56,08	0,02	27,28	0,01	9,82	0,03	0,05	0,11	0,01	5,77	0,43	99,60	2,54	0,00	1,45	0,00	0,48	0,00	0,00	0,00	0,00	0,51	0,03	50,3	47,2	2,5
NorthMet	DC-71	BPU xenolith	57,90	0,00	25,76	0,01	8,39	0,02	0,06	0,14	0,05	6,61	0,54	99,47	2,61	0,00	1,37	0,00	0,41	0,00	0,00	0,00	0,00	0,58	0,03	56,9	40,0	3,1
NorthMet	DC-71	BPU xenolith	57,08	0,12	26,48	0,01	8,88	0,00	0,03	0,10	0,04	6,41	0,54	99,69	2,58	0,00	1,41	0,00	0,43	0,00	0,00	0,00	0,00	0,56	0,03	54,9	42,0	3,0
NorthMet	DC-71	BPU xenolith	57,87	0,06	25,62	0,01	8,12	0,00	0,01	0,13	0,03	6,69	0,64	99,17	2,62	0,00	1,37	0,00	0,39	0,00	0,00	0,00	0,00	0,59	0,04	57,7	38,7	3,6
NorthMet	DC-71	Mixing zone	57,68	0,04	26,39	0,01	8,65	0,10	0,06	0,06	0,07	6,42	0,70	100,16	2,59	0,00	1,40	0,00	0,42	0,00	0,00	0,00	0,00	0,56	0,04	55,1	41,0	3,9
NorthMet	DC-71	Mixing zone	53,70	0,01	28,85	0,02	11,77	0,00	0,06	0,06	0,00	4,79	0,35	99,61	2,44	0,00	1,55	0,00	0,57	0,00	0,00	0,00	0,00	0,42	0,02	41,6	56,5	2,0
NorthMet	DC-71	Mixing zone	52,76	0,10	29,48	0,01	12,76	0,03	0,04	0,01	0,00	4,25	0,33	99,76	2,40	0,00	1,58	0,00	0,62	0,00	0,00	0,00	0,00	0,38	0,02	36,9	61,2	1,9

Biotites

Deposit	Sample	Rock type	wt% SiO_2	TiO_2	Al_2O_3	Cr_2O3	MgO	CaO	MnO	FeO	NiO	Na_2O	K_2O	H_2O	F	Cl	Total	a.p.f.u. Si	Ti	Al IV	Cr	Mg	Ca	Mn	Fe	Ni	Na	K	Mg#	XTi
Mesaba	B1-384-14	BPU xenolith	38,53	4,96	13,76	0,21	17,85	0,02	0,06	9,79	0,00	0,10	9,78	3,44	1,32	0,13	99,93	5,64	0,55	2,37	0,02	3,90	0,00	0,01	1,20	0,00	0,03	1,83	76,5	6,8
Mesaba	B1-384-14	BPU xenolith	38,22	5,04	13,96	0,29	16,77	0,01	0,02	10,57	0,05	0,10	9,74	3,58	1,01	0,06	99,41	5,63	0,56	2,42	0,03	3,69	0,00	0,00	1,30	0,01	0,03	1,83	73,9	7,0
Mesaba	B1-384-14	BPU xenolith	38,53	4,64	13,75	0,29	18,20	0,01	0,04	9,28	0,04	0,06	9,58	3,41	1,40	0,04	99,29	5,66	0,51	2,38	0,03	3,98	0,00	0,01	1,14	0,01	0,02	1,80	77,8	6,4
Mesaba	B1-384-14	BPU xenolith	38,07	4,44	13,52	0,14	18,19	0,00	0,04	9,19	0,04	0,14	9,23	3,28	1,54	0,08	97,91	5,67	0,50	2,37	0,02	4,04	0,00	0,01	1,14	0,01	0,04	1,75	77,9	6,2
NorthMet	DC-71	BPU xenolith	37,95	5,70	14,22	0,45	17,21	0,00	0,03	9,27	0,00	0,08	9,78	3,33	1,57	0,05	99,62	5,57	0,63	2,46	0,05	3,77	0,00	0,00	1,14	0,00	0,02	1,83	76,8	7,9
NorthMet	DC-30	Gabbronorite	38,42	4,32	14,49	0,06	18,60	0,00	0,05	9,56	0,04	0,11	9,61	3,67	0,86	0,15	99,95	5,60	0,47	2,49	0,01	4,04	0,00	0,01	1,17	0,01	0,03	1,79	77,6	5,8

Table 3.1: EPMA of feldspars and biotites. Abbreviations: BPU=Bedded Pyrrhotite Unit; c.a.=contact aureole. Formula: XTi(Biotite) = Ti/(Al+Ti+Mg+Fe+Mn).

3.7.1.2 BIOTITE

Biotite has a similar compositional range in all rock types with Mg# ~0.7 (Mg# = [Mg/(Mg+Fe)]), low Ti (~ 5 wt %) and Ti_{Bt} ~0.07 (Ti_{Bt}=[Ti/(Ti+Al+Mg+Fe+Mn)]) (Fig. 3.7b and Table 3.1). The compositional ranges of the biotites do not allow meaningful discrimination between the deposits or rock types, except for Al^{IV}, which appears to be higher for biotite in the contact aureole (2.4-2.7 a.p.f.u) than from the xenoliths of Bedded Pyrrhotite Unit (2.3-2.4 a.p.f.u) and the gabbronorites (2.5 a.p.f.u).

3.7.2 WHOLE ROCK COMPOSITIONS

The composition of the average Bedded Pyrrhotite Unit from outside the contact aureole is similar to that of the Bedded Pyrrhotite Unit in the contact aureole with SiO_2 in the 62 to 68 wt % range (Fig. 3.8 and Table 3.2). In contrast, the xenoliths show a much wider range in SiO_2 contents from 44 to 64 wt %. Samples from the interior of a meter-sized xenolith of Bedded Pyrrhotite Unit from the Mesaba deposit have very similar major element contents to the Bedded Pyrrhotite Unit in the contact aureole (Fig 3.8 and Appendix 4). Several xenoliths of the Bedded Pyrrhotite Unit from the Mesaba deposit have low SiO_2 contents (52 to 56 wt %), but none are as low as the NorthMet xenoliths where several samples are in the range 44 to 50 wt %.

Samples from the Bedded Pyrrhotite Unit outside the contact aureole, the Bedded Pyrrhotite Unit in the contact aureole, the xenoliths of Bedded Pyrrhotite Unit and their associated leucosomes define linear geochemical trends for most of the major elements on Harker diagrams (Fig. 3.8). The compatible elements, Al_2O_3 and ($MgO+FeO+TiO_2$) show negative correlations with SiO_2 (Fig. 3.8a, b), whereas K_2O shows a positive correlation

with SiO_2 (Fig. 3.8c). Both Na_2O and CaO increase with falling SiO_2 until ~ 50 wt % but then fall abruptly (Fig. 3.8d, e). In summary, the xenoliths with the lowest SiO_2 have the highest Al_2O_3 and ($MgO+FeO+TiO_2$), but lowest K_2O, Na_2O and CaO contents.

Considering their mineral assemblages and major element chemistry the samples with low SiO_2 are interpreted as the most residual rocks. The Bedded Pyrrhotite Unit black shales from outside the contact aureole have compositions that lie between the xenoliths and their associated leucosomes, this relationship is consistent with these black shales being the protolith of the xenoliths.

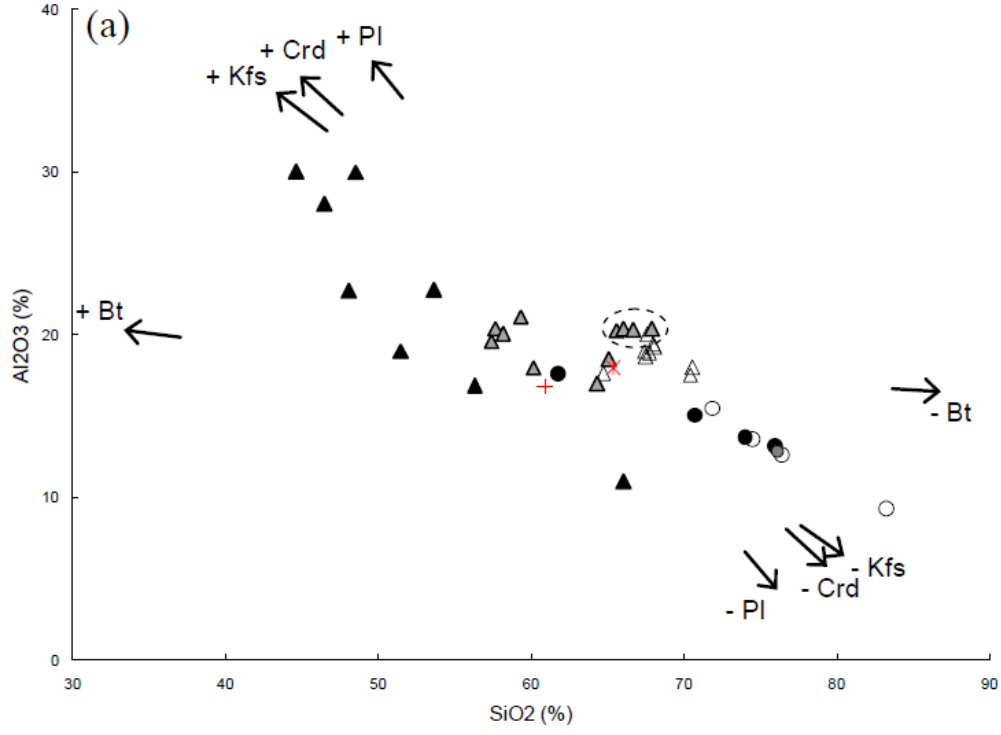
(a)
+ Crd
+ Pl
+ Kfs
+ Bt
- Bt
- Kfs
- Crd
- Pl
Al2O3 (%)
SiO2 (%)
0
10
20
30
40
30
40
50
60
70
80
90

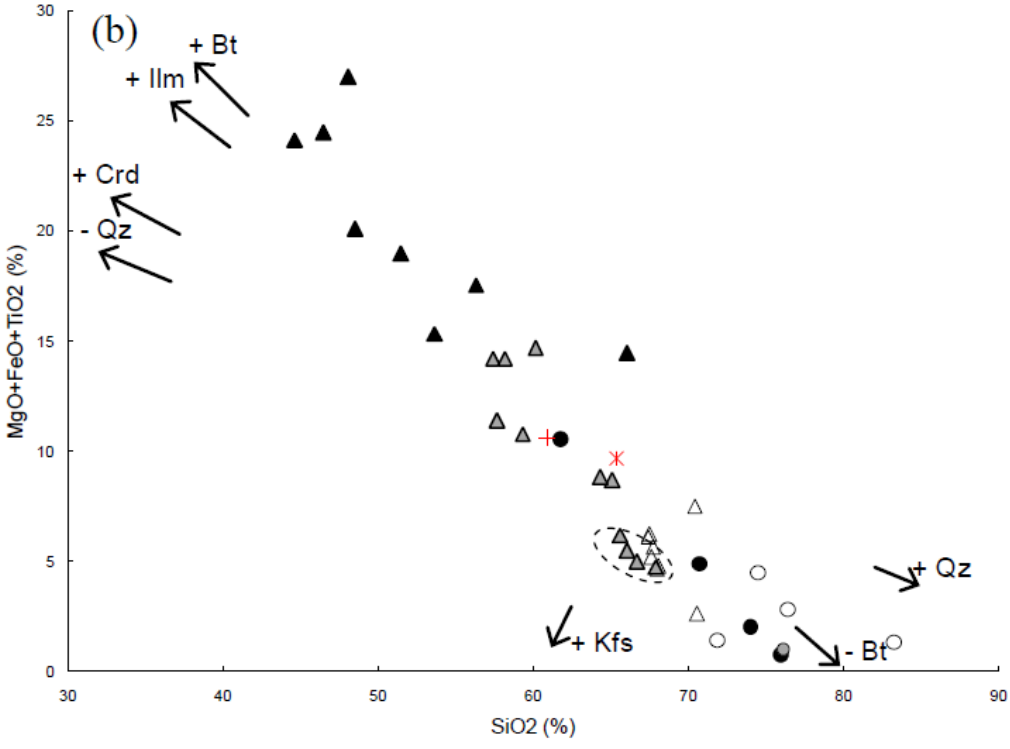
(b)
+ Bt
+ Ilm
+ Crd
- Qz
+ Qz
+ Kfs
- Bt
MgO+FeO+TiO2 (%)
SiO2 (%)
0
5
10
15
20
25
30
30
40
50
60
70
80
90

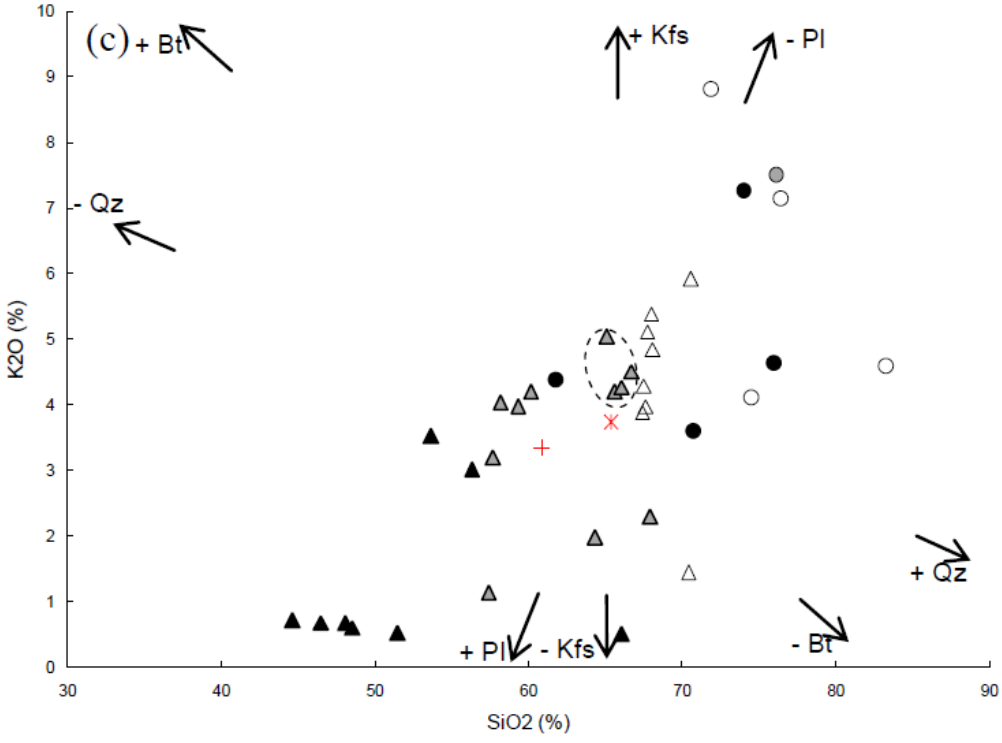
(c)
+ Bt
+ Kfs
- Pl
- Qz
+ Qz
+ Pl
- Kfs
- Bt
K2O (%)
SiO2 (%)

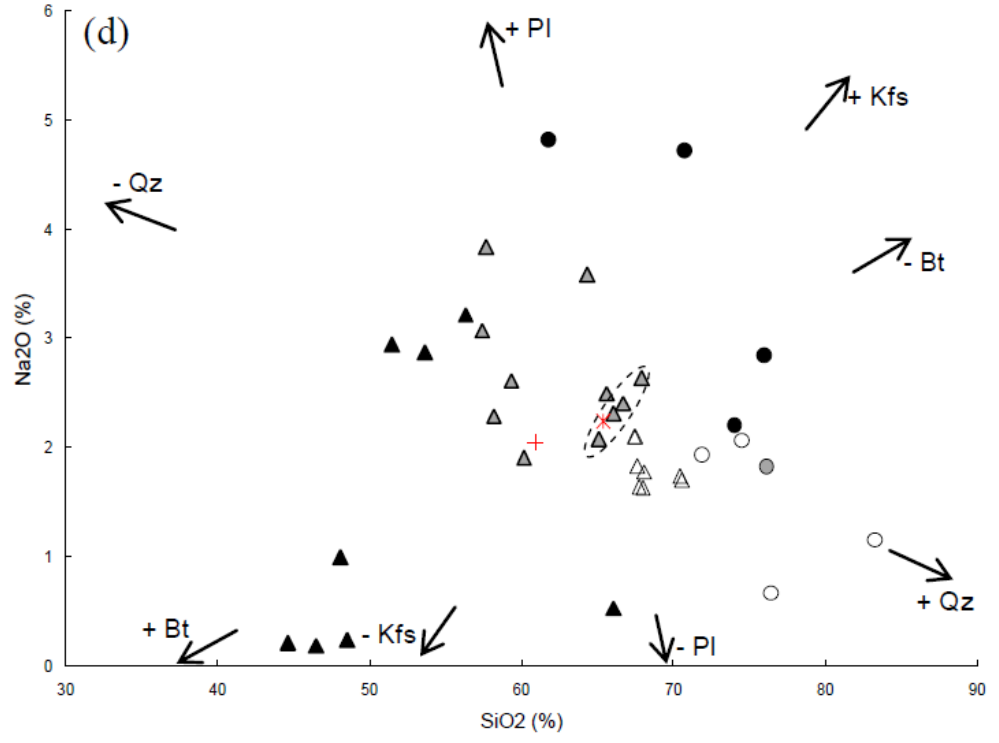
(d)
+ Pl
+ Kfs
- Qz
- Bt
+ Qz
+ Bt
- Kfs
- Pl
Na2O (%)
SiO2 (%)

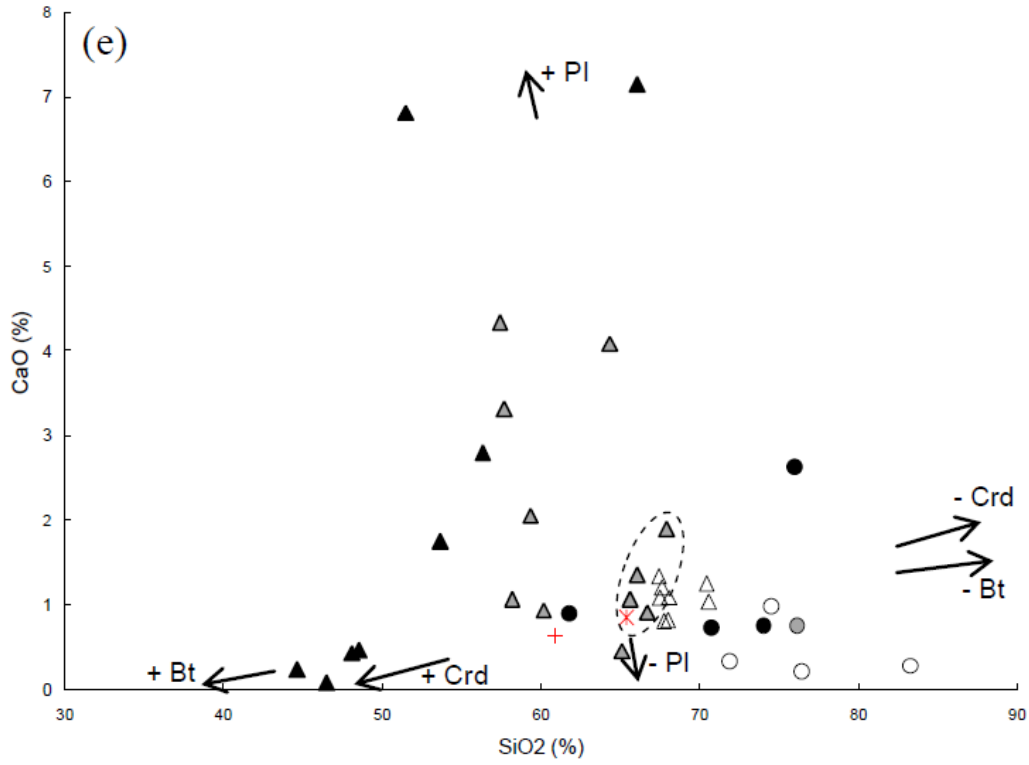

△ BPU contact aureole

▲ BPU xenoliths Mesaba

▲ BPU xenoliths NorthMet

○ Leucosomes BPU contact aureole

● Leucosomes Mesaba

● Leucosomes NorthMet

✳ Average BPU outside contact aureole (S>1%)

+ Average black shales outside contact aureole from literature

Figure 3.8: Plots of (a) Al_2O_3, (b) MgO+FeO+TiO2, (c) K_2O, (d) Na_2O and (e) CaO vs. SiO_2 for Bedded Pyrrhotite Unit (BPU) from the contact aureole, BPU xenoliths and associated leucosomes (Harker diagrams). Positive correlations occur for (a) Al_2O_3, (b) $MgO+FeO+TiO_2$ and (c) K_2O vs. SiO_2. Meter-size BPU xenoliths from the Mesaba deposit are delimited by dotted circles in graphs. Averages of black shales outside contact aureole from the literature are from Rao and Ripley (1983).

Rock type	n	SiO_2(%)	TiO_2 (%)	Al_2O_3(%)	FeO (%)	MnO (%)	MgO (%)	CaO (%)	Na_2O (%)	K_2O (%)	P_2O_5 (%)
BS outside c.a. (S>1%)	5	65,34	0,98	17,93	5,57	0,04	3,12	0,84	2,24	3,73	0,19
BPU c.a	9	67,99	0,85	18,71	2,10	0,04	2,94	1,02	1,82	4,40	0,12
BPU xenoliths Mesaba	11	62,58	0,80	19,62	4,57	0,06	4,09	1,95	2,66	3,53	0,13
BPU xenoliths NorthMet	8	51,89	0,94	22,55	11,21	0,12	8,10	2,47	1,40	1,28	0,07
BPU leucosomes	8	73,55	0,28	13,81	1,82	0,02	1,20	0,91	2,70	5,61	0,11

Table 3.2: Averages of whole rock data for the Bedded Pyrrhotite Unit (wt %). Sulfide component has been removed and renormalized. Abbreviations: BPU =Bedded Pyrrhotite Unit; c.a. = contact aureole, BS = black shale.

3.7.3 TRACE ELEMENTS COMPOSITIONS

When normalized to the primitive mantle composition (Fig. 3.9a) the Bedded Pyrrhotite Unit from outside the contact aureole shows strong positive anomalies for U, K and Pb, negative anomalies for Ti and Sr and flatter pattern for the High Field Strength Elements (HFSE), i.e. Nb, Ta, Ti, Zr, Hf, Th. This pattern and its anomalies are very similar to those shown by the average of black shales (Fig. 3.9a) from Ketris and Yudovich (2009), although the Bedded Pyrrhotite Unit is slightly richer in Pb and poorer in Sr. However, it is possible that our estimate of Sr is too low, since Sr was determined on only two samples.

In order to study the fingerprint of partial melting processes on the variation of trace element content, the compositions of the Bedded Pyrrhotite Unit from the contact aureole and from the xenoliths (including their associated leucosomes) are normalized to the average of the Bedded Pyrrhotite Unit from outside the contact aureole, the probable protolith, which are the least metamorphosed black shale samples and so have not experienced the compositional changes related to high-grade metamorphism and anatexis (Table 3.3).

The trace element contents of the Bedded Pyrrhotite Unit from the contact aureole and their leucosomes are shown normalized to the average of the Bedded Pyrrhotite Unit from outside the contact aureole on Figure 3.9b. The median Bedded Pyrrhotite Unit from the contact aureole has quite similar trace element contents as the average of the Bedded Pyrrhotite Unit from outside the contact aureole, except for the enrichment in Sr and U in these samples. This similarity in the trace element contents suggests that they have not lost a significant melt fraction. Numerous anatectic melt pockets and leucosomes are observed

within rocks in the contact aureole, from this Sawyer (2014) concluded that these rocks have not lost significant melt fraction. Leucosomes from the contact aureole are depleted in most of the elements except U and K in comparison with the Bedded Pyrrhotite Unit from outside the contact aureole. The positive K and Eu anomalies in the median of Bedded Pyrrhotite Unit leucosomes from the contact aureole are interpreted to result from the presence of abundant, possibly cumulate, feldspar in these samples (Fig. 3.9b). Leucosomes from the contact aureole have similar rare earth element (REE) contents to the average of silicate glasses in partially melted metapelitic enclaves from south east of Spain (Acosta-vigil et al., 2010).

The plots (Figs. 3.9c, d) show the trace element and rare earth element (REE) contents of xenoliths of Bedded Pyrrhotite Unit and their associated leucosomes from Mesaba and NorthMet normalized to the average of the Bedded Pyrrhotite Unit from outside the contact aureole. At the Mesaba deposit xenoliths of the Bedded Pyrrhotite have trace element patterns that are generally slightly depleted in Eu, Pb, K, Rb, Ba (i.e. Large Ion Lithophile Elements), Ta, Ti, Zr, Hf, Th (i.e. High Field Strength Elements) and Light Rare Earth Elements (LREE) relative to the proposed protolith, but are slightly enriched in Heavy Rare Earth Elements (HREE) and strongly enriched in Nb and Sr. In contrast, the leucosomes are more depleted in most of the elements except for Sr, K, Nb and Rb (Fig. 3.9c). The positive Rb and K anomalies are interpreted to result of the presence of cumulate feldspar in the leucosomes. However, Sr is greatly enriched in both the xenolith and leucosome relative to the Bedded Pyrrhotite Unit from outside the aureole; hence the black shale from which the xenoliths and melt came from at Mesaba was more enriched in Sr than our choice of protolith, or Sr was added to the xenolith from the mafic magma. The

complementarity of the two trace element patterns like the major elements, suggests that the xenoliths represent slightly melt-depleted residual material and the leucosomes represent the crystallized product of the partial melt from the xenoliths. Rare earth element (REE) contents of leucosomes from the Mesaba deposit are similar to the average of similar bulk compositions from literature (Acosta-vigil et al., 2010).

As mentioned previously the NorthMet xenoliths are poorer in SiO_2 but richer in FeO, MgO and TiO_2 than the Mesaba xenoliths. They also have lower abundances of all trace elements (except Sr) including the HREE relative to the proposed protolith (Table 3.3 and Fig. 3.9d). Thus, all the trace elements (except Sr) were lost and their abundance is typically <0.5 that of the Bedded Pyrrhotite Unit from outside the contact. However the strong positive Sr and Eu anomalies likely related to the presence residual plagioclase in the xenoliths and the positive anomalies for Ti, Nb and Ta probably related to the presence of residual ilmenite (Fig. 3.9d).

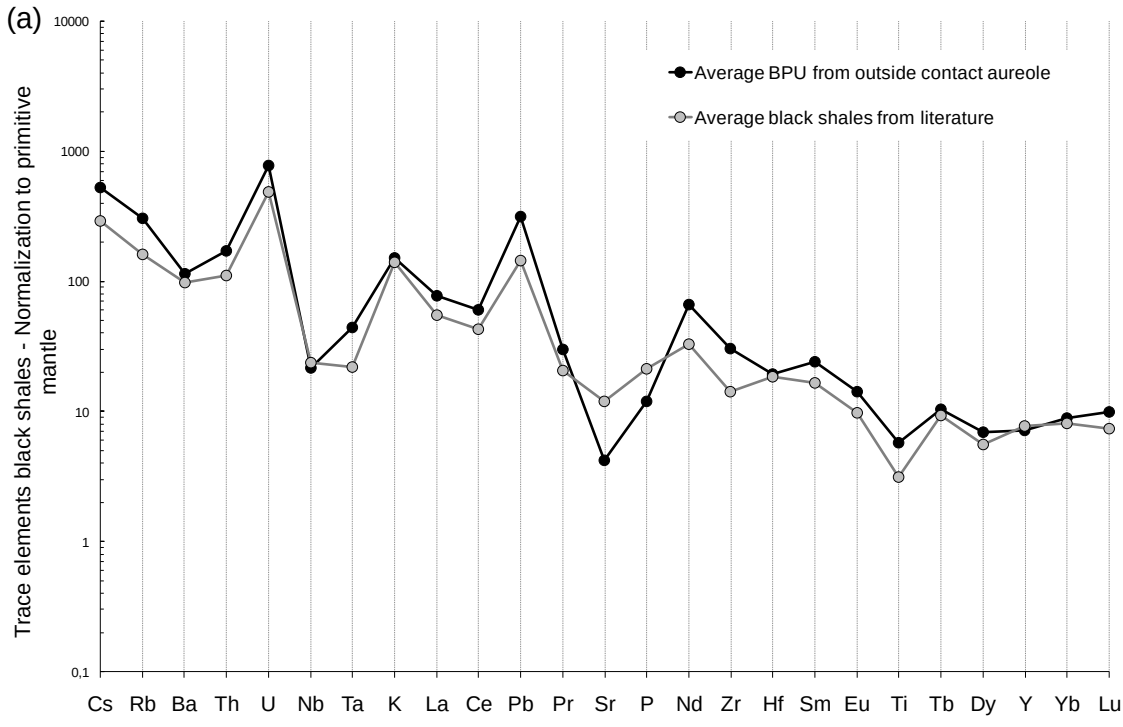
(a)
Trace elements black shales - Normalization to primitive mantle
10000
1000
100
10
1
0,1
Average BPU from outside contact aureole
Average black shales from literature
Cs Rb Ba Th U Nb Ta K La Ce Pb Pr Sr P Nd Zr Hf Sm Eu Ti Tb Dy Y Yb Lu

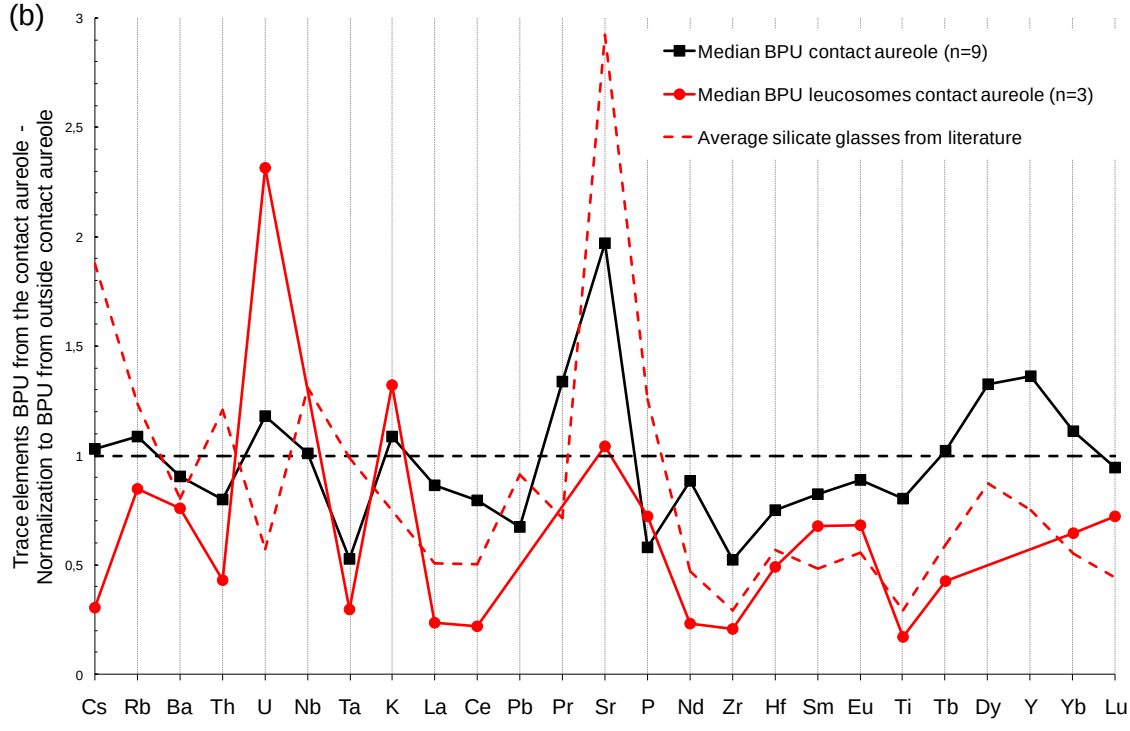
(b)
Trace elements BPU from the contact aureole - Normalization to BPU from outside contact aureole
3
2,5
2
1,5
1
0,5
0
Median BPU contact aureole (n=9)
Median BPU leucosomes contact aureole (n=3)
Average silicate glasses from literature
Cs Rb Ba Th U Nb Ta K La Ce Pb Pr Sr P Nd Zr Hf Sm Eu Ti Tb Dy Y Yb Lu

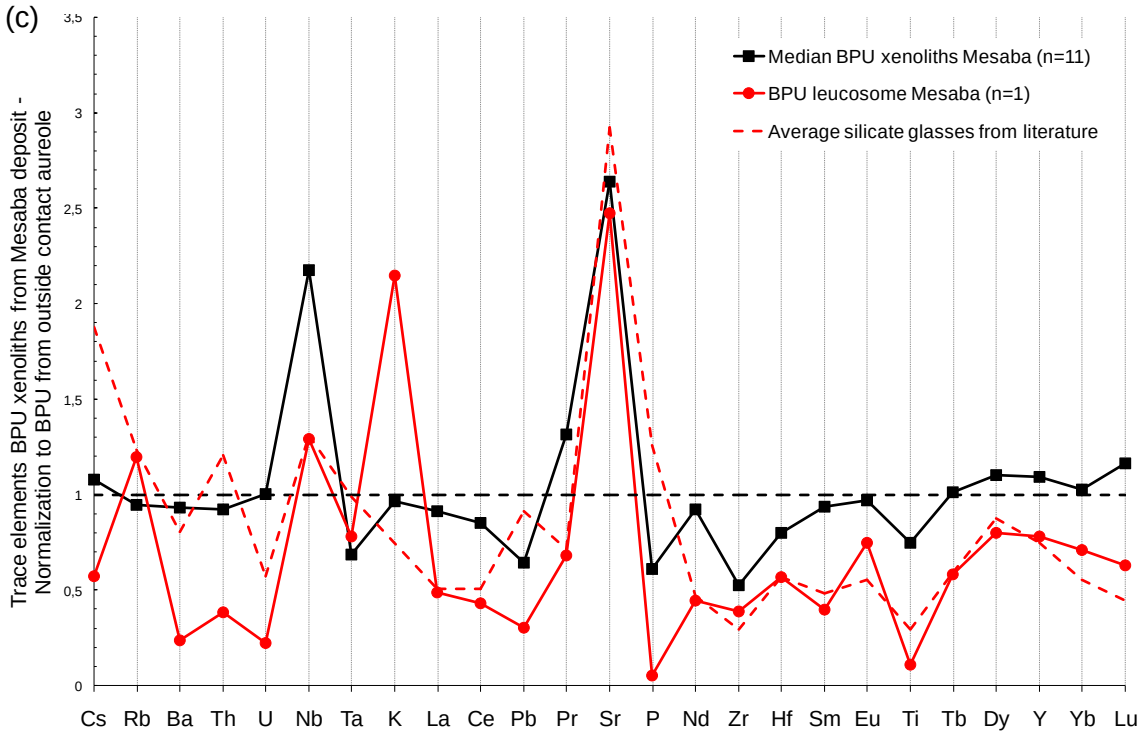
(c)
Trace elements BPU xenoliths from Mesaba deposit - Normalization to BPU from outside contact aureole
Median BPU xenoliths Mesaba (n=11)
BPU leucosome Mesaba (n=1)
Average silicate glasses from literature
3,5
3
2,5
2
1,5
1
0,5
0
Cs Rb Ba Th U Nb Ta K La Ce Pb Pr Sr P Nd Zr Hf Sm Eu Ti Tb Dy Y Yb Lu

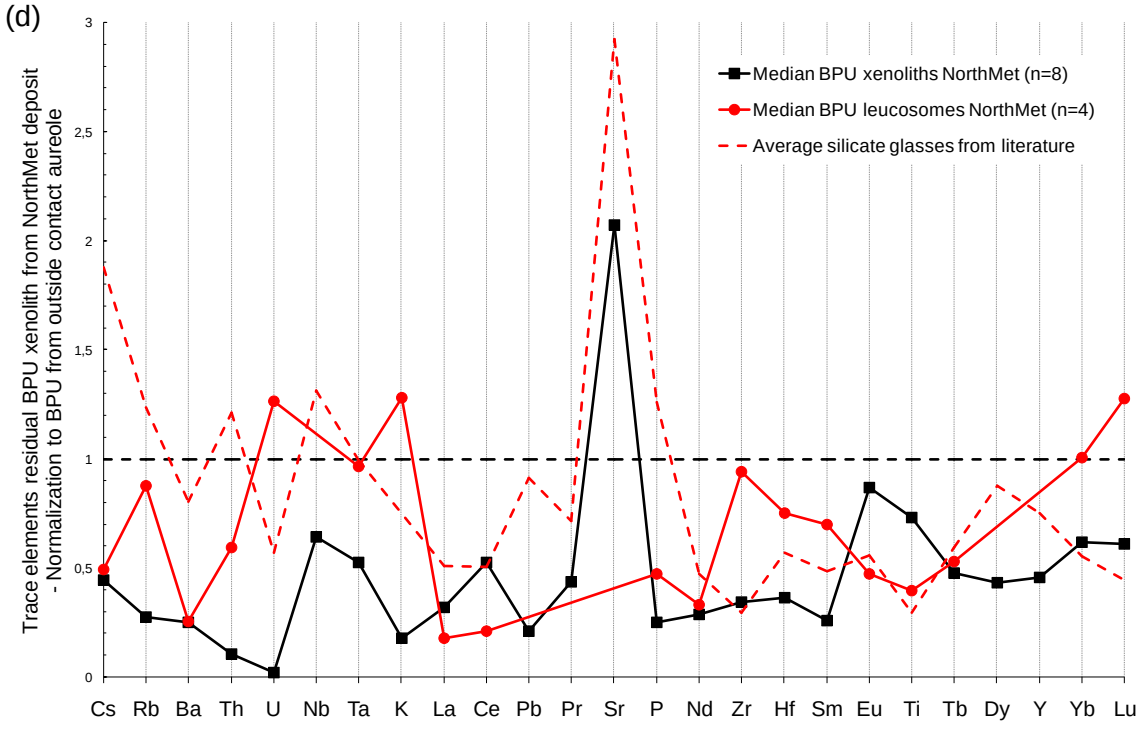
(d)
Trace elements residual BPU xenolith from NorthMet deposit - Normalization to BPU from outside contact aureole
Median BPU xenoliths NorthMet (n=8)
Median BPU leucosomes NorthMet (n=4)
Average silicate glasses from literature
3
2,5
2
1,5
1
0,5
0
Cs Rb Ba Th U Nb Ta K La Ce Pb Pr Sr P Nd Zr Hf Sm Eu Ti Tb Dy Y Yb Lu

Figure 3.9: Trace elements contents of the Bedded Pyrrhotite Unit (BPU), BPU and leucosomes from the contact aureole (b) and BPU xenoliths and leucosomes from Mesaba (c) and NorthMet deposits (d) normalized to BPU sample from outside the contact aureole (a). Average of trace elements contents of black shales are from the Ketris and Yudovich (2009) compilation. Primitive mantle values for the normalization are from Lyubetskaya and Korenaga (2007). Averages of trace elements contents of silicate glasses are extracted from Acosta-Vigil et al. (2010).

		ppm																					
Rock type	**n**	**Ba**	**Ce**	**Cs**	**Dy**	**Eu**	**Hf**	**La**	**Lu**	**Nb**	**Nd**	**Pb**	**Pr**	**Rb**	**Sm**	**Sr**	**Ta**	**Tb**	**Th**	**U**	**Y**	**Yb**	**Zr**
BPU outside c.a.	5	582	80,9	8,52	3,77	1,74	4,38	39,3	0,54	9,9	36,0	45,9	6,15	139	7,85	67	1,41	0,84	10,74	13,46	24,0	3,07	258
BPU c.a	9	498	63,5	9,48	5,0	1,54	3,30	33,3	0,50	10,0	31,6	31,0	8,23	159	6,46	132	0,73	0,84	8,32	16,50	32,7	3,40	134
BPU leucosomes c.a.	3	442	18,0	2,61	-	1,19	2,16	9,4	0,39	-	8,4	-	-	118	5,33	70	0,42	0,36	4,62	31,19	-	1,99	54
BPU xenoliths Mesaba	11	545	69,2	9,22	4,16	1,69	3,50	36,0	0,63	21,6	33,3	29,7	8,10	132	7,37	177	0,97	0,85	9,95	13,50	26,3	3,15	136
BPU leucosomes Mesaba	1	140	35,0	4,90	3,03	1,30	2,50	19,2	0,34	12,8	16,0	14,0	4,19	167	3,13	166	1,10	0,49	4,15	3,05	18,8	2,19	101
BPU xenoliths NorthMet	8	147	42,4	3,78	1,64	1,51	1,60	12,6	0,33	6,4	10,4	9,6	2,68	39	2,03	139	0,74	0,40	1,12	0,29	10,95	1,91	89
BPU leucosomes NorthMet	4	149	17,1	4,21	-	0,83	3,29	7,0	0,69	-	11,9	-	-	122	5,49	-	1,36	0,45	6,40	17,02	-	3,10	243

Table 3.3: Average and medians of the Bedded Pyrrhotite Unit from outside the contact aureole, the Bedded Pyrrhotite Unit from the contact aureole, the Bedded Pyrrhotite Unit xenoliths and leucosomes. Abbreviations: BPU =Bedded Pyrrhotite Unit; BS = black shale, c.a. =contact aureole.

3.8 MINERAL EQUILIBRIA MODELING

Mineral equilibria calculations were made in the NCKFMASHMnT (Na_2O–CaO–K_2O–FeO–MgO–Al_2O_3–SiO_2–H_2O–MnO-TiO_2) system using Perple_X 07 software (Connolly, 2005; Connolly, 2009) with the Holland and Powell (1998) database. The water content of the system is unknown, but based on the occurrence of hydrate minerals and the dehydration melting reactions proposed for the metasediments in the contact aureole at the Duluth Complex by Sawyer (2014), the system cannot have had H_2O as a phase. Thus, the H_2O content was fixed such that the parageneses in the T-X(H_2O) diagrams were water-undersaturated (~ 0.1 mol, or ~2 wt %) (Appendix 7). The models for solid solutions used are: biotite (Tajčmanová et al., 2009); melt (Holland and Powell, 2001; White et al., 2001); cordierite (Berman and Aranovich, 1996); plagioclase (Newton et al., 1980); K-feldspar (Waldbaum and Thompson, 1968); ilmenite (White et al., 2000); orthopyroxene (Holland and Powell, 1996) and white mica (Coggan and Holland, 2002). Phase abbreviations used on the pseudosections are: Bt = biotite; Crd = cordierite; Hc= hercynite; Ilm = ilmenite; Kfs = alkali feldspar; Ms = muscovite; Opx = orthopyroxene; Pl = plagioclase; Qz = quartz; Rt = rutile; Sil = sillimanite; Spr = Sapphirine (Whitney and Evans, 2010).

The bulk compositions of the residual xenoliths used for calculating the pseudosections are reported in Table 3.4. The temperatures attained by the xenoliths were deduced by selecting the paragenesis from the pseudosections most compatible with the petrographic observations and with the observed composition (Tables 3.1 and 3.5) and proportion of minerals; i.e. isopleths and modes.

				wt%									
Figure n°	**Samples**	**Rock type**	**Deposit**	**SiO_2**	**TiO_2**	**Al_2O_3**	**FeO**	**MnO**	**MgO**	**CaO**	**Na_2O**	**K_2O**	**H_2O**
10	A4-18-09	BPU c.a.	Wetlegs	69,16	0,67	17,64	0,12	0,02	1,78	1,01	1,67	5,80	2,13
11	B1-384-34	BPU xenolith	Mesaba	64,75	0,88	19,94	1,29	0,04	3,20	1,33	2,27	4,19	2,13
11	B1-384-14	BPU xenolith	Mesaba	56,45	0,80	19,96	5,13	0,12	5,23	3,25	3,76	3,13	2,18
12	DC-71	BPU xenolith	NorthMet	52,49	0,82	22,29	8,27	0,07	5,91	1,71	2,81	3,45	2,16
12	DC-69	BPU xenolith	NorthMet	44,17	0,67	29,73	12,84	0,06	10,38	0,23	0,21	0,71	1,01
14-15	BS protolith	BS outside c.a.	-	64,19	0,96	17,61	5,47	0,04	3,07	0,83	2,21	3,66	1,96

Table 3.4: Normalized NCKFMASHMnT composition used in the pseudosection calculations. Abbreviations: BPU=Bedded Pyrrhotite Unit; c.a.=contact aureole, BS= black shale.

	Deposit	Sample	Rock type	wt%											a.p.f.u.											
				SiO_2	TiO_2	Al_2O_3	Cr_2O_3	MgO	CaO	MnO	FeO	NiO	Na_2O	K_2O	Total	Si	Ti	Al	Cr	Mg	Ca	Mn	Fe	Na	En (%)	Fs (%)
Pyroxenes	Mesaba	B1-384-14	BPU xenolith	53,20	0,13	0,85	0,06	22,43	0,25	0,56	22,36	0,00	0,00	0,01	99,83	1,98	0,00	0,04	0,00	1,25	0,01	0,02	0,70	0,00	63,80	35,69
	Mesaba	B1-384-14	BPU xenolith	53,70	0,08	1,17	0,10	25,36	0,29	0,59	17,72	0,00	0,10	0,01	99,12	1,97	0,00	0,05	0,00	1,39	0,01	0,02	0,55	0,01	71,38	28,01
	Mesaba	B1-384-14	BPU xenolith	51,37	2,77	0,97	0,11	24,55	0,25	0,64	19,07	0,01	0,01	0,00	99,77	1,90	0,08	0,04	0,00	1,35	0,01	0,02	0,59	0,00	69,29	30,19
	Mesaba	B1-384-39	BPU xenolith	51,05	0,13	0,78	0,04	13,13	0,48	0,56	35,02	0,00	0,14	0,00	101,33	1,95	0,00	0,04	0,00	0,79	0,02	0,02	1,19	0,01	39,36	59,59
	Mesaba	B1-384-39	BPU xenolith	50,31	0,19	0,68	0,08	12,96	0,49	0,61	34,44	0,00	0,01	0,00	99,78	1,96	0,01	0,03	0,00	0,79	0,02	0,02	1,19	0,00	39,44	59,46
	Mesaba	B1-384-39	BPU xenolith	50,66	0,16	0,63	0,09	12,94	0,51	0,57	34,76	0,02	0,18	0,00	100,52	1,96	0,01	0,03	0,00	0,78	0,02	0,02	1,19	0,02	39,15	59,70
	Mesaba	B1-384-39	BPU xenolith	50,77	0,02	0,56	0,06	13,86	0,52	0,57	34,68	0,01	0,50	0,01	101,55	1,94	0,00	0,03	0,00	0,83	0,02	0,02	1,18	0,04	40,86	58,01
	Mesaba	B1-384-39	Mixing zone	49,15	0,18	0,47	0,00	12,61	0,58	0,57	35,59	0,00	0,00	0,00	99,15	1,94	0,01	0,02	0,00	0,78	0,03	0,02	1,25	0,00	37,96	60,78
	Mesaba	B1-384-39	Mixing zone	50,95	0,07	0,53	0,00	12,09	0,68	0,63	35,23	0,04	0,03	0,00	100,25	1,98	0,00	0,03	0,00	0,74	0,03	0,02	1,22	0,00	37,13	61,35
	Mesaba	B1-384-13	Norite	51,63	0,21	0,40	0,05	16,15	1,22	0,63	29,14	0,02	0,02	0,01	99,46	2,00	0,01	0,02	0,00	0,93	0,05	0,02	0,95	0,00	48,39	48,96
	Mesaba	B1-384-13	Norite	50,78	0,16	0,40	0,02	15,62	1,08	0,67	30,29	0,00	0,02	0,00	99,03	1,99	0,01	0,02	0,00	0,91	0,05	0,02	0,99	0,00	46,78	50,87
	Mesaba	B1-384-13	Norite	51,54	0,16	0,37	0,00	15,96	1,34	0,69	30,16	0,01	0,03	0,00	100,26	2,00	0,01	0,02	0,00	0,92	0,06	0,02	0,98	0,00	47,16	49,97
	Mesaba	B1-384-13	Norite	51,12	0,20	0,39	0,06	15,01	2,15	0,59	30,19	0,02	0,03	0,00	99,77	1,99	0,01	0,02	0,00	0,87	0,09	0,02	0,99	0,00	44,82	50,56
	Mesaba	B1-384-13	Norite	51,14	0,13	0,45	0,09	16,53	0,98	0,64	29,91	0,04	0,00	0,00	99,91	1,98	0,00	0,02	0,00	0,96	0,04	0,02	0,97	0,00	48,58	49,34
	NorthMet	DC-71	BPU xenolith	54,06	0,18	1,94	0,17	24,36	0,15	0,45	18,71	0,00	0,03	0,00	100,06	1,93	0,01	0,09	0,01	1,37	0,01	0,01	0,60	0,00	69,45	30,25
	NorthMet	DC-71	BPU xenolith	54,64	0,15	1,80	0,13	25,15	0,19	0,44	19,17	0,00	0,01	0,01	101,68	1,93	0,00	0,08	0,00	1,39	0,01	0,01	0,60	0,00	69,58	30,07
	NorthMet	DC-71	BPU xenolith	55,55	0,14	1,55	0,19	25,09	0,19	0,42	18,91	0,04	0,04	0,00	102,10	1,95	0,00	0,07	0,01	1,38	0,01	0,01	0,59	0,00	69,81	29,84
	NorthMet	DC-71	BPU xenolith	53,60	0,18	1,73	0,10	26,22	0,19	0,39	17,42	0,03	0,03	0,00	99,88	1,91	0,01	0,08	0,00	1,47	0,01	0,01	0,55	0,00	72,35	27,25
	NorthMet	DC-71	BPU xenolith	55,01	0,13	0,79	0,06	24,72	0,35	0,40	20,31	0,00	0,01	0,00	101,78	1,95	0,00	0,04	0,00	1,37	0,01	0,01	0,64	0,00	67,74	31,57
	NorthMet	DC-71	BPU xenolith	53,64	0,20	0,78	0,06	24,77	0,35	0,39	19,56	0,05	0,02	0,01	99,82	1,94	0,01	0,04	0,00	1,40	0,02	0,01	0,63	0,00	68,56	30,71
	NorthMet	DC-30	Gabbronorite	54,37	0,20	1,06	0,10	25,61	0,81	0,37	17,89	0,05	0,00	0,00	100,44	1,97	0,01	0,05	0,00	1,39	0,03	0,01	0,54	0,00	70,70	27,72
	NorthMet	DC-30	Gabbronorite	54,14	0,19	1,09	0,11	25,64	0,99	0,34	17,83	0,01	0,02	0,00	100,37	1,97	0,01	0,05	0,00	1,39	0,04	0,01	0,54	0,00	70,54	27,53
	NorthMet	DC-30	Gabbronorite	53,17	0,27	1,17	0,11	25,59	1,21	0,40	17,78	0,02	0,02	0,00	99,73	1,95	0,01	0,05	0,00	1,40	0,05	0,01	0,55	0,00	70,23	27,36
	NorthMet	DC-30	Gabbronorite	54,63	0,26	1,06	0,09	25,30	0,82	0,35	17,88	0,04	0,01	0,00	100,44	1,98	0,01	0,05	0,00	1,37	0,03	0,01	0,54	0,00	70,43	27,92

Table 3.5: Microprobe analyses of pyroxenes. Abbreviations: BPU=Bedded Pyrrhotite Unit; c.a.=contact aureole. Formulas: XEn(Pyroxene) = Mg/(Ca+Mg+Fe), XFs(Pyroxene) = Fe/(Ca+Mg+Fe).

3.8.1 PEAK TEMPERATURE IN THE BEDDED PYRRHOTITE UNIT FROM THE CONTACT AUREOLE

Bedded Pyrrhotite Unit sample A4-18-09 is from the contact aureole ~20 m from the contact with the Duluth Complex. This sample contains ~65 wt % SiO_2 and ~2 wt % ($FeO+MgO+TiO_2$) and contains the assemblage cordierite (~15 modal %) + plagioclase (~10 modal %) + K-feldspar (~15 modal %) + quartz (~10 modal %) + melt (quartz + plagioclase + K-feldspar + biotite) + sillimanite relics (<10 modal %) + graphite + sulfides +/- phlogopite and rutile. Assuming a pressure of 2.5 kbars (Labotka et al., 1981; Andrews and Ripley, 1989), the temperature at which this assemblage was produced is ~800°C, i.e. close to the beginning of the sillimanite-out field (Fig. 3.10). Modes calculated for this temperature are 45 wt % melt, 20 wt % K-feldspar, 12 wt % cordierite, 12 wt % quartz, 10 wt % plagioclase, and 1 wt % rutile. These proportions are similar to those observed in the sample.

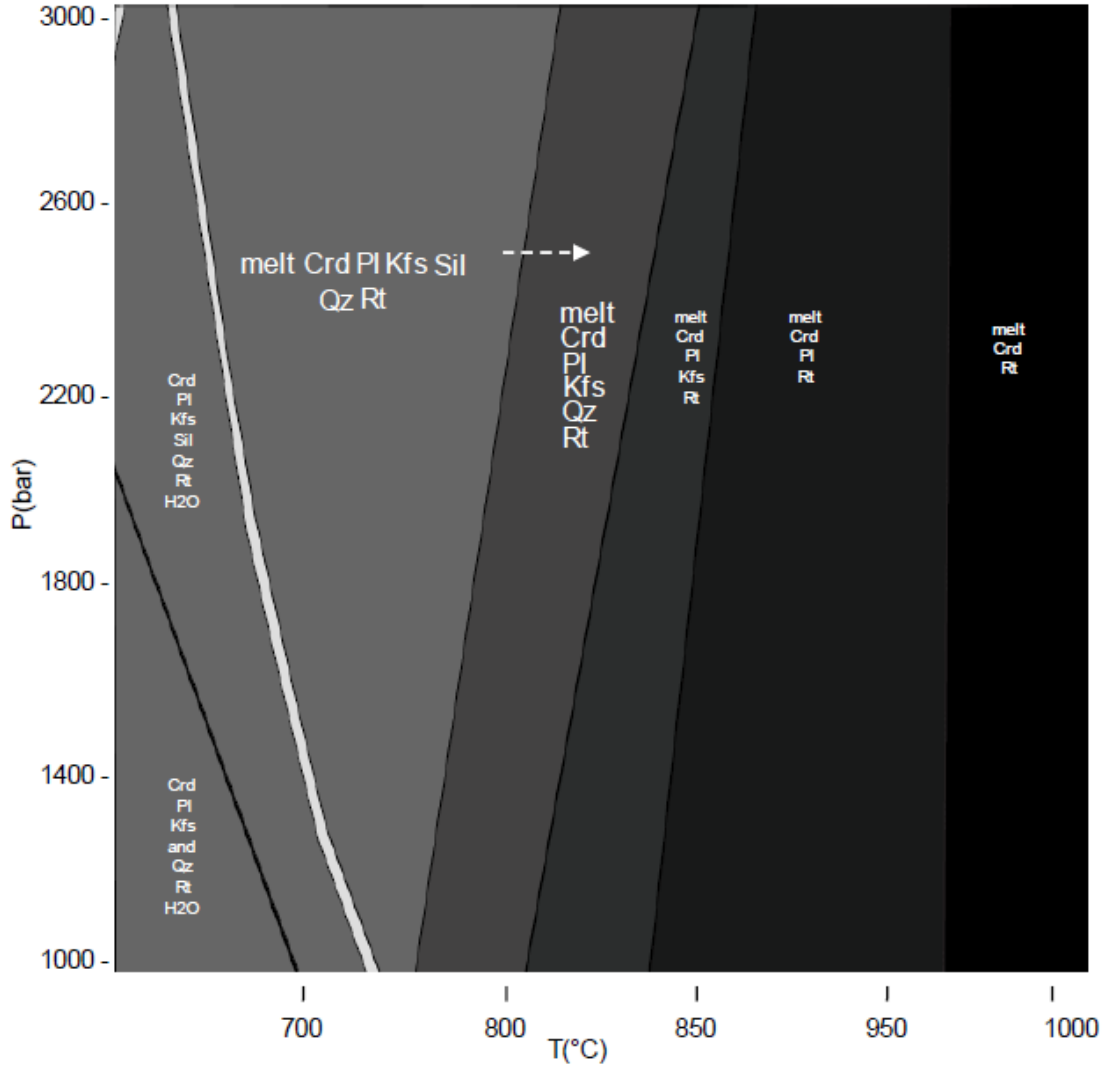

Figure 3.10: NCKFMASHMT P-T pseudosection for Bedded Pyrrhotite Unit (BPU) sample A4-18-09 from the contact aureole (Virginia Formation). Field of melt-Crd-Pl-Kfs-Qz-Rt at ~800°C and 2.5 kbars is the most consistent with the mineral assemblage in the sample A4-18-09 (white arrow). Abbreviations used for pseudosections (Whitney and Evans, 2010): Bt = Biotite; Crd = Cordierite; Hc = Hercynite; Ilm = Ilmenite; Kfs = K-feldspar; Pl = Plagioclase; Qz = Quartz; Rt = Rutile; Sil = Sillimanite.

3.8.2 TEMPERATURE IN BEDDED PYRRHOTITE UNIT XENOLITHS FROM THE MESABA DEPOSIT

Sample B1-384-34 from the Mesaba deposit contains ~5 wt % ($FeO+MgO+TiO_2$) and more than 60 wt % SiO_2 and is part of a meter-sized xenolith. The typical mineral assemblage is cordierite (~20 modal %) + plagioclase (~20 modal %) + K-feldspar (<20 modal %) + biotite (<10 modal %) + melt (quartz + plagioclase + K-feldspar + biotite) + sillimanite relics + graphite + opaques (sulfides + oxides) +/- rutile. At 2.5 kbars, orthopyroxene would be stable at a temperature higher than 850°C, and because the rock does not contain orthopyroxene, 850°C is considered to be the maximum temperature for this particular sample (Fig. 3.11a). Furthermore, Figure 3.11a shows that quartz-out occurs just above 825°C and K-feldspar-out about 25°C higher, thus a reasonable temperature "window" for this sample is ~825 to 850°C. Modes calculated at 830°C are; 50 wt % melt, 20 wt % cordierite, 15 wt % plagioclase, 10 wt % K-feldspar and 5 wt % biotite; which are close to the observed modal proportions of these minerals.

The sample B1-384-14 (also from Mesaba) is more residual than previous one (sample B1-384-34) and contains ~10 wt % ($FeO+MgO+TiO_2$) and ~ 55 wt % SiO_2. The mineral assemblage in this sample is orthopyroxene (~10 modal %) + cordierite (~10 modal %) + plagioclase (~20 modal %) + biotite (~10 modal %) + melt (quartz + K-feldspar + plagioclase + biotite) + opaques (sulfides and oxides). At 2.5 kbars, the formation of this assemblage requires wider temperature range. Figure 3.11b indicates the minimum is about 850°C. The isopleths for plagioclase, biotite and pyroxene compositions better constrain the temperature to a narrow range between 950 and 980°C. The modes in this temperature range indicate 45 wt % melt, 25 wt % plagioclase, 10 wt % biotite, 10 wt % cordierite and 10 wt % orthopyroxene; close to the observed proportions of these minerals.

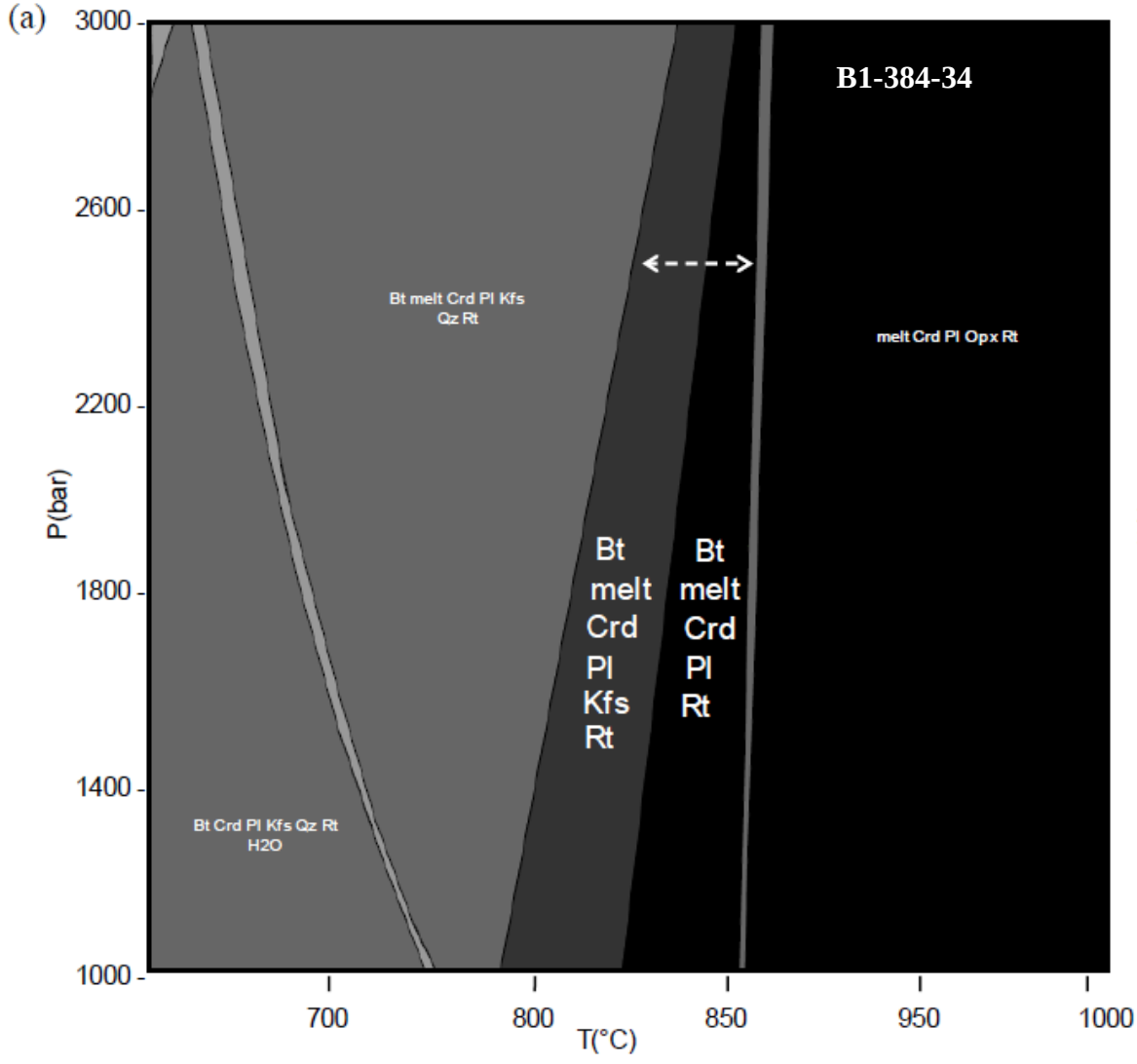
(a)
B1-384-34
3000
2600
2200
1800
1400
1000
P(bar)
Bt melt Crd Pl Kfs Qz Rt
melt Crd Pl Opx Rt
Bt melt Crd Pl Kfs Rt
Bt melt Crd Pl Rt
Bt Crd Pl Kfs Qz Rt H2O
700
800
850
950
1000
T(°C)

B1-384-14

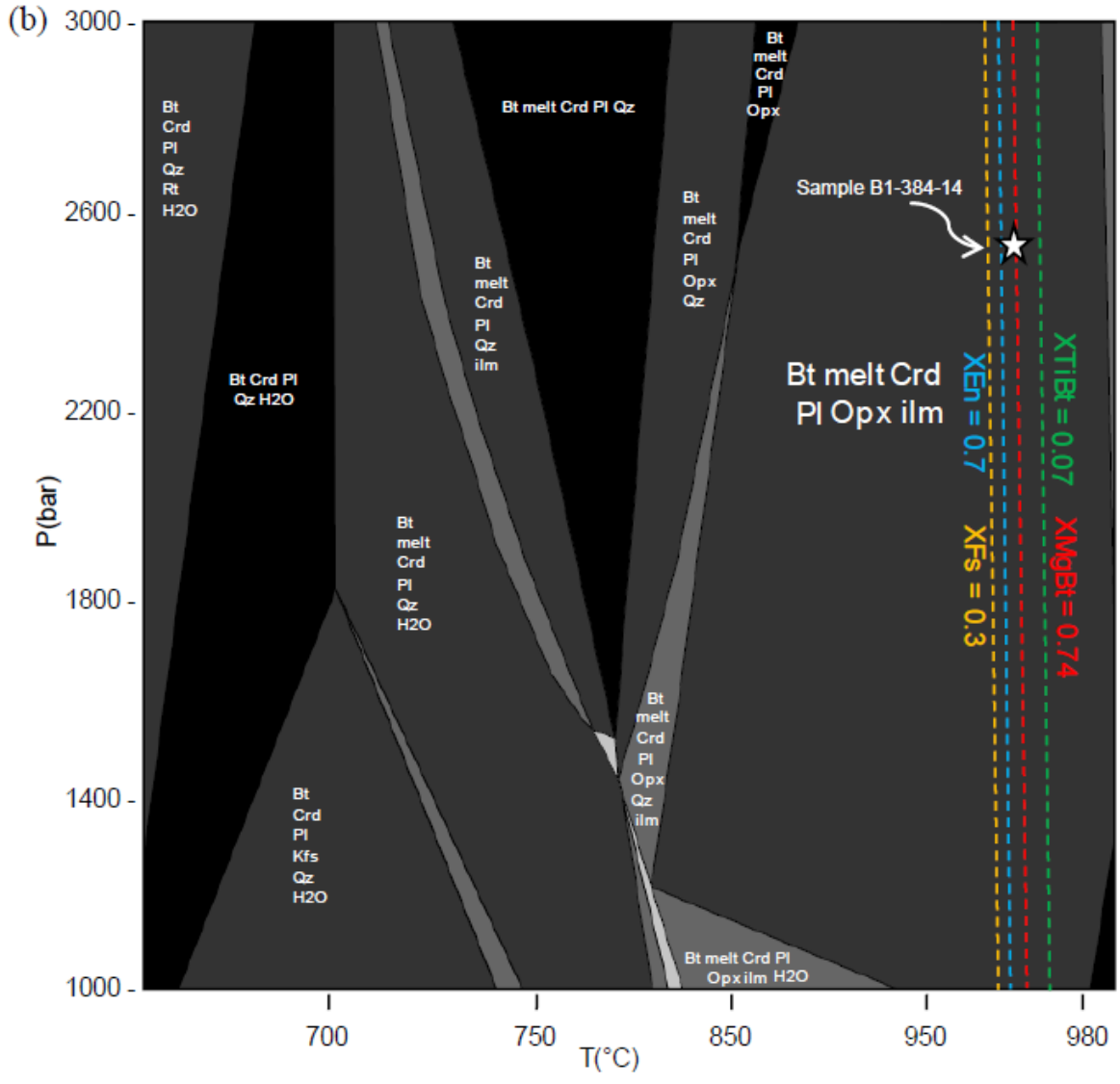
(b)
3000
2600
2200
1800
1400
1000
P(bar)
700
750
850
950
980
T(°C)
Bt Crd Pl Qz Rt H2O
Bt melt Crd Pl Qz
Bt melt Crd Pl Opx
Bt melt Crd Pl Opx Qz
Bt melt Crd Pl Qz ilm
Bt Crd Pl Qz H2O
Bt melt Crd Pl Qz H2O
Bt melt Crd Pl Opx Qz ilm
Bt Crd Pl Kfs Qz H2O
Bt melt Crd Pl Opx ilm H2O
Sample B1-384-14
Bt melt Crd Pl Opx ilm
XTiBt = 0.07
XMgBt = 0.74
XEn = 0.7
XFs = 0.3

Figure 3.11: NCKFMASHMT P-T pseudosections based on Bedded Pyrrhotite Unit (BPU) xenolith samples B1-384-34 (a) and B1-384-14 (b) from the Mesaba deposit. Arrows indicate the position at 2.5 kbars of the calculated assemblage which is the most consistent with the mineral assemblage in each sample. Calculated isopleths (dotted lines) which are added to the diagrams are consistent with values obtained from microprobe analyses. Abbreviations used for pseudosections (Whitney and Evans, 2010): Bt = Biotite; Crd = Cordierite; Hc = Hercynite; Ilm = Ilmenite; Kfs = K-feldspar; Pl = Plagioclase; Qz = Quartz; Rt = Rutile; Sil = Sillimanite.

3.8.3 TEMPERATURE IN BEDDED PYRRHOTITE UNIT XENOLITHS FROM THE NORTHMET DEPOSIT

At the NorthMet deposit xenoliths are more residual with lower SiO_2 and higher ($FeO+MgO+TiO_2$) contents than those in the Mesaba deposit. The least residual samples from NorthMet contain ~50 wt % SiO_2 and 15 wt % ($FeO+MgO+TiO_2$) and sample DC-71 is a typical example. The mineral assemblage in DC-71 is orthopyroxene (~10 modal %) + cordierite (~20 modal %) + plagioclase (~ 10 modal %) + biotite (~5 modal %) + melt (quartz + K-feldspar + plagioclase + biotite + orthopyroxene) + opaques (sulfides + oxides); the sample has no prograde quartz or K-feldspar remaining. The rock contains a small amount of prograde biotite (~5 modal %); most of the biotite crystallized from the melt but some is thought to replace orthopyroxene (Fig. 3.13a). The pseudosection for this sample (Fig. 3.12a) shows the assemblage to be stable at temperatures from ~ 800 to 950°C for the assumed pressure of 2.5 kbars. The isopleths for plagioclase, biotite and pyroxene compositions better constrain the temperature to ~ 950°C. The mineral modes calculated at this temperature indicate that 50 wt % melt is produced together with 20 wt % cordierite, 15 wt % biotite, 10 wt % plagioclase and 5 wt % orthopyroxene. These proportions match with those observed in the sample considering the observation of biotite replacing orthopyroxene.

The most residual composition for a xenolith at NorthMet deposit is that of sample DC-69 which has ~25 wt % ($FeO+MgO+TiO_2$), ~30 wt % Al_2O_3 and ~44 wt % SiO_2 and the mineral assemblage is cordierite (~50 modal %) + orthopyroxene (~20 modal %) + plagioclase (~10 modal %) + melt (quartz + K-feldspar + plagioclase + biotite + orthopyroxene) + spinel (<5 modal %) + oxides (<5 modal %) + sulfides. The prograde assemblage is quartz-, biotite- and K-feldspar-free. Biotite crystallized from the melt and

form large porphyroblasts (up to 1 mm) and some of them may be interpreted as a product of breakdown of orthopyroxene and cordierite (Fig. 3.13b). The pseudosection (Fig. 3.12b) indicates that at the assumed pressure of 2.5 kbar the assemblage is stable above a temperature of 920°C. Furthermore, Figure 3.12b shows that plagioclase-out occurs just above 1050^{o}C and because the rock contain small amount of prograde plagioclase (~10 modal %) a reasonable temperature "window" for this sample is ~900 to 1000°C. At 950°C the calculated modes predict 50 wt % cordierite, 15 wt % orthopyroxene, 10 wt % melt, 10 wt % plagioclase, 5 wt % biotite, 5 wt% ilmenite and 5 wt % hercynite. These proportions are close to those observed in the sample considering the observation of biotite replacing orthopyroxene and cordierite. The low fraction of melt for this bulk composition is significant, as will be discussed below.

DC-71

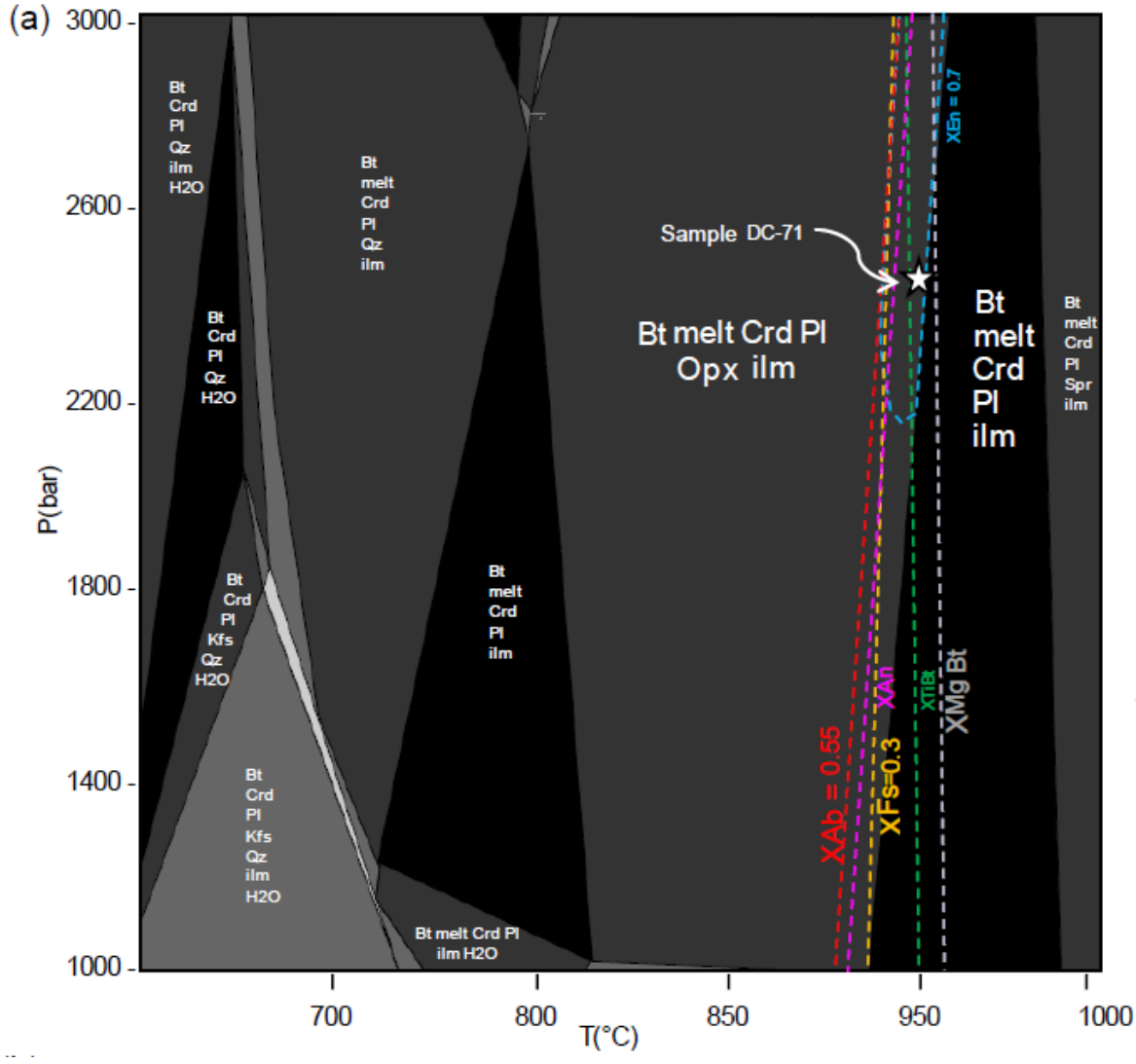
(a)
3000
2600
2200
1800
1400
1000
P(bar)
700
800
850
950
1000
T(°C)
Bt Crd Pl Qz ilm H2O
Bt melt Crd Pl Qz ilm
Bt Crd Pl Qz H2O
Bt Crd Pl Kfs Qz H2O
Bt melt Crd Pl ilm
Bt Crd Pl Kfs Qz ilm H2O
Bt melt Crd Pl ilm H2O
Sample DC-71
Bt melt Crd Pl Opx ilm
Bt melt Crd Pl ilm
Bt melt Crd Pl Spr ilm
XEn = 0.7
XAb = 0.55
XAn
XFs=0.3
XTiBt
XMg Bt

DC-69

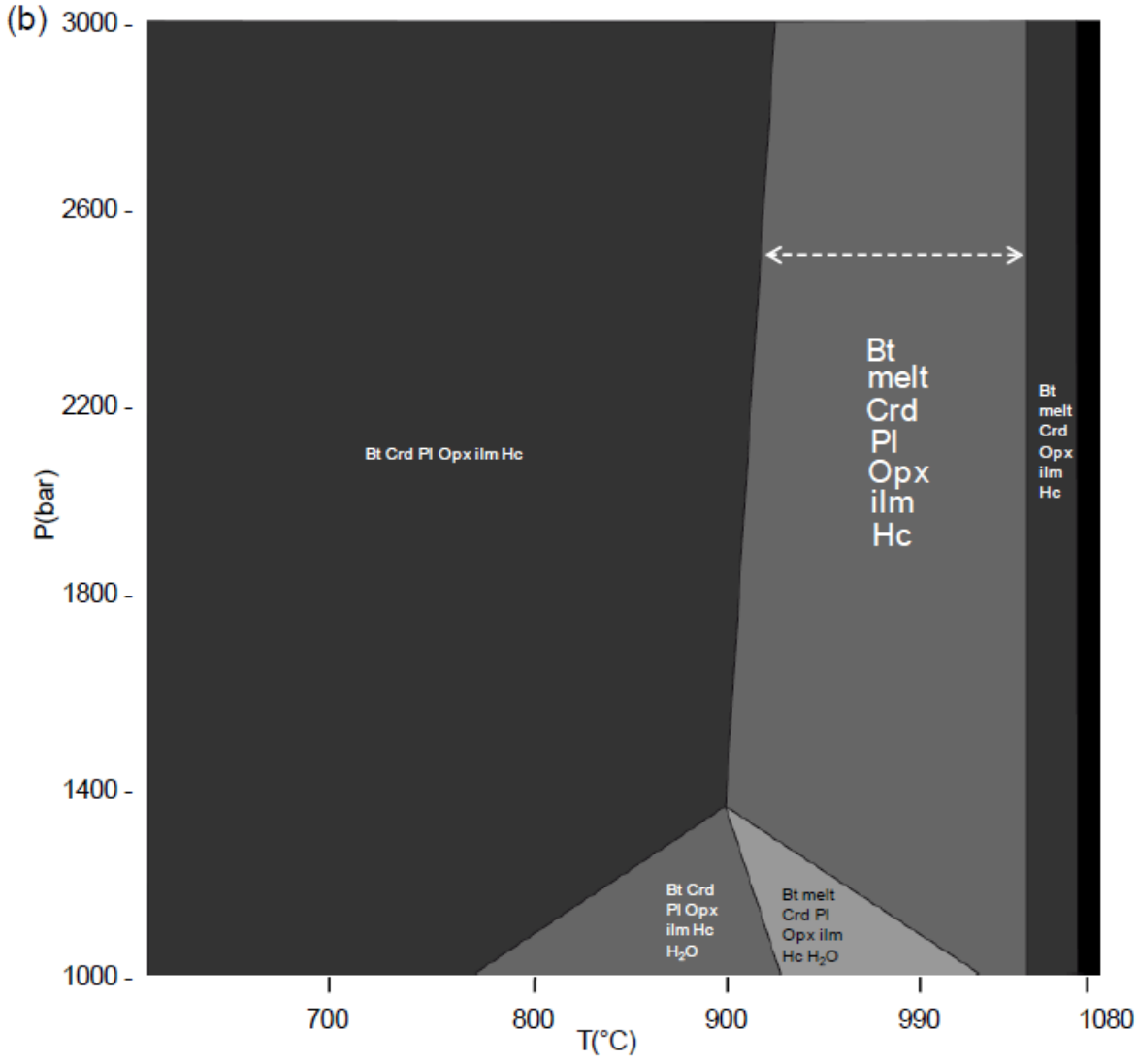
(b)
3000 -
2600 -
2200 -
1800 -
1400 -
1000 -
P(bar)
Bt Crd Pl Opx ilm Hc
Bt melt Crd Pl Opx ilm Hc
Bt melt Crd Opx ilm Hc
Bt Crd Pl Opx ilm Hc H2O
Bt melt Crd Pl Opx ilm Hc H2O
700
800
900
990
1080
T(°C)

Figure 3.12: NCKFMASHMT P-T pseudosections based on Bedded Pyrrhotite Unit (BPU) xenolith samples DC-71 (a) and DC-69 (b) from the NorthMet deposit. Arrows indicate the position of the calculated assemblage at 2.5 kbars which is the most consistent with the mineral assemblage present in each sample. Calculated isopleths (dotted lines) added to the diagrams are consistent with values obtained from microprobe analyses. Abbreviations used for pseudosections (Whitney and Evans, 2010): Bt = Biotite; Crd = Cordierite; Hc = Hercynite; Ilm = Ilmenite; Kfs = K-feldspar; Pl = Plagioclase; Qz = Quartz; Rt = Rutile; Sil = Sillimanite; Spr = Sapphirine.

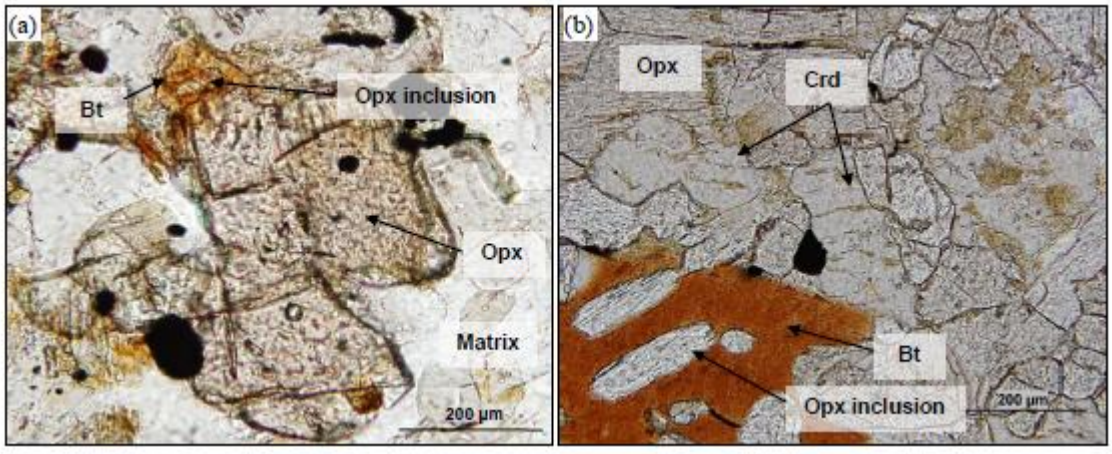

Figure 3.13: Photomicrographs of microstructure of orthopyroxene and cordierite grains replacing biotite in xenoliths DC-71 (a) and DC-69 (b) of the Bedded Pyrrhotite Unit from the NorthMet deposit. (a) Microstructure showing reaction of biotite replacing orthopyroxene. Matrix is composed of Crd+Pl+Qz. (b) Microstructure illustrating the reaction of biotite replacing orthopyroxene and cordierite. Abbreviations (Whitney and Evans, 2010): Bt = Biotite; Crd = Cordierite; Opx = Orthopyroxene; Pl = Plagioclase; Qz = Quartz.

3.9 DISCUSSION

3.9.1 PARTIAL MELTING OF THE PROTOLITH OF THE BEDDED PYRRHOTITE UNIT ROCKS AND MELT EXTRACTION HISTORY

Identifying the protolith of the xenoliths of the Bedded Pyrrhotite Unit and whether the xenoliths lost melt (components) to the mafic magma are important parameters needed to improve models of formation of Ni-Cu-PGE deposits at the Duluth Complex and elsewhere. In the Duluth Complex, the compositions of the protolith of the xenoliths in the mafic magma have not previously been well established. However, Ripley and Alawi (1988) proposed that unmetamorphosed argillites of the Virginia Formation outside the contact aureole have suitable compositions to be considered the protolith for pelitic xenoliths in the intrusion.

We have modeled the partial melting of a potential protolith of the Bedded Pyrrhotite Unit from ~700 to 1000°C using Perple_X. The starting composition we used are the bulk compositions of S-rich black shales, i.e. S>1 wt %, in the Virginia Formation from outside the contact aureole (Table 3.4). This bulk composition is similar to the average composition of black argillites in the Virginia Formation from outside the contact aureole (Rao and Ripley, 1983). Partial melting of this potential protolith begins at ~650°C and from the model calculations the fraction of melt progressively increases from ~30 wt % at 750°C, ~50 wt % at 800°C to >70 wt % at temperatures higher that 900°C (Table 3.6).

3.9.1.1 MELT COMPOSITIONS

The compositions of melt, considered to be extracted in full, was calculated at several temperature steps between 700 and 1000°C; specifically at 660, 693, 727, 760, 793, 827, 860, 893, 927, 977 and 1027°C. Batch equilibrium melting was assumed for the modeling.

The anatectic melts calculated at each of the temperature intervals in the model have monzogranitic compositions (Fig. 3.14 and Table 3.6). However, as temperatures increases the melt composition changes and describes an anticlockwise trend on the QAP plot from slightly quartz-rich through slightly K-feldspar-rich to plagioclase-rich. This sequence corresponds to the order in which phases disappear from the residuum during prograde melting (i.e. quartz-absent before K-feldspar absent). These model melt compositions are in broad agreement with those determined by experimental partial melting of pelite bulk compositions (e.g. White et al., 2011).

Leucosomes are the crystallization products derived from anatectic melt, but not necessarily the melt composition itself as mentioned earlier. In contrast to the model melts and melt compositions from partial melting experiments in the literature (e.g., Cesare et al., 2003; Bartoli et al., 2015), the leucosomes from the Bedded Pyrrhotite Unit have a much wider range of compositions from monzogranite, syenogranite, monzodiorite, granodiorite and quartz-rich granitoid (Fig. 3.14). The composition of the leucosomes associated with xenoliths of the Bedded Pyrrhotite Unit at the Mesaba and the NorthMet deposits were determined, but unfortunately the compositions of the small pockets of former melt in the xenoliths are too small to be analysed at present. At NorthMet the REE-bearing accessory phases dissolved into the melt, and were subsequently lost when that melt was extracted. The major elements indicate that the leucosomes at NorthMet are felspathic, but they are depleted in Eu, Pb, Ba, Rb, Cs (i.e. LILE) and most of the trace elements, except for U, Ta, K, Zr, Yb and Lu (Fig. 3.9d), which suggest the presence of accessory phases. In general the leucosomes do not have a trace element composition that reflects a melt composition (Fig. 3.9d).

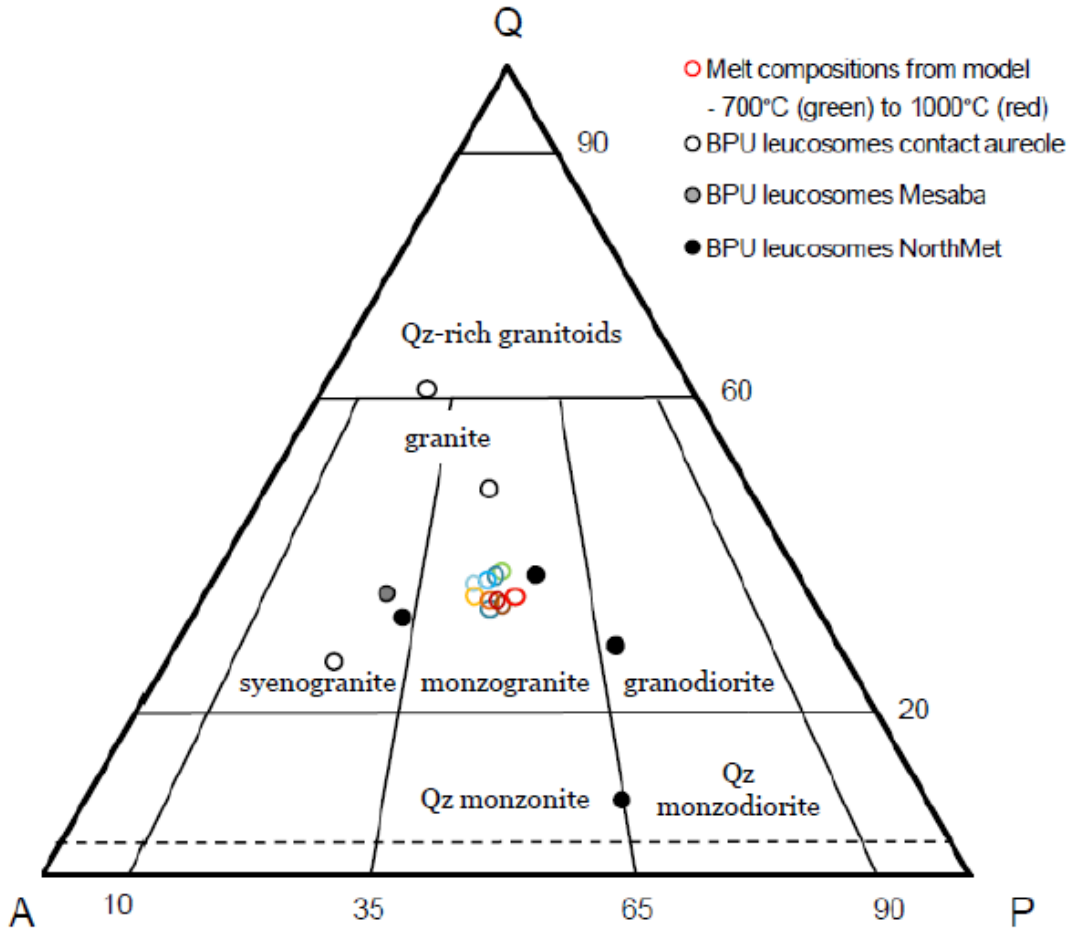

Figure 3.14: QAP (Quartz– K-feldspar –Plagioclase) ternary diagram of melt compositions calculated by the model at temperature range between 700 to 1000°C, Bedded Pyrrhotite Unit (BPU) leucosomes from the contact aureole and BPU xenoliths from Mesaba and NorthMet deposits. This diagram is generated after calculation of the norm for the melt. Melt compositions from the model which are obtained by modeling the partial melting of the potential protolith of the Bedded Pyrrhotite Unit, define a restricted field in the diagram and have monzogranitic compositions. In contrast leucosomes associated with the BPU plot over a much larger range of compositions; i.e. monzogranite, syenogranite, monzodiorite, granodiorite and quartz-rich granitoid.

			wt(%)									
	T (°C)	Melt fraction (φ)	SiO_2	TiO_2	Al_2O_3	FeO	MnO	MgO	CaO	Na_2O	K_2O	H_2O
Melt	660	15	72,68	0,00	11,94	0,00	0,00	0,00	0,09	3,20	4,87	7,22
	693	19	73,14	0,00	12,20	0,10	0,00	0,03	0,12	3,25	4,94	6,23
	727	24	73,56	0,00	12,36	0,33	0,00	0,05	0,15	3,21	5,12	5,22
	760	31	73,67	0,00	12,42	0,87	0,00	0,12	0,20	3,12	5,31	4,29
	793	43	72,50	0,00	12,07	1,46	0,00	0,22	3,20	2,85	5,37	3,41
	827	52	73,61	0,00	12,43	1,50	0,00	0,23	0,25	2,94	5,53	3,52
	860	65	73,18	0,00	12,93	1,63	0,00	0,45	0,47	2,90	5,65	2,80
	893	69	71,90	0,00	13,45	2,53	0,00	0,58	0,61	2,95	5,31	2,67
	927	73	70,66	0,00	13,96	3,25	0,00	0,80	0,83	2,93	5,03	2,54
	977	81	68,68	0,00	14,72	4,49	0,00	1,44	1,03	2,77	4,53	2,34
	1027	83	68,24	0,00	15,00	4,65	0,00	1,63	1,02	2,69	4,46	2,30
Residuum	660	15	62,12	0,00	18,61	6,58	0,00	4,11	1,16	2,08	3,61	1,04
	693	19	61,51	0,00	18,87	6,88	0,00	4,31	1,20	2,02	3,54	0,97
	727	24	60,60	0,00	19,26	7,26	0,00	4,59	1,27	1,95	3,38	0,93
	760	31	59,17	0,00	19,97	7,75	0,00	5,04	1,36	1,86	3,11	0,90
	793	43	56,97	0,00	21,85	8,77	0,00	6,01	1,42	1,79	2,60	0,85
	827	52	53,79	0,00	22,79	9,70	0,00	6,77	1,75	1,56	2,07	0,40
	860	65	45,95	0,00	26,37	13,04	0,00	9,22	1,99	1,03	0,34	0,39
	893	69	45,49	0,00	26,84	12,42	0,00	9,98	1,87	0,70	0,44	0,39
	927	73	44,73	0,00	27,57	12,00	0,00	10,86	1,47	0,39	0,44	0,38
	977	81	42,70	0,00	29,80	10,28	0,00	12,19	0,88	0,07	0,71	0,35
	1027	83	42,18	0,00	29,98	10,12	0,00	12,35	0,89	0,16	0,66	0,33

Table 3.6: Calculated melt and residuum compositions after partial melting of black shale from outside the contact aureole. See text for calculation details.

3.9.1.2 RESIDUUM COMPOSITIONS AND MELT EXTRACTION HISTORY

We approximate the residuum composition based on a batch equilibrium melting model of Protolith = Residuum + Melt. The formula from Shaw (1970) $Crt=\varphi Cm+(1-\varphi)Cr$ was used to approximate residuum compositions in which; *Crt*= whole rock composition, φ= fraction of melt, *Cm*= melt composition calculated by the model; *Cr*= residuum composition. The calculated residuum compositions are shown on Figure 3.15 and Table 3.6. The calculated residua are enriched in FeO and MgO, which are elements incompatible with the melt, and impoverished in SiO_2 and K_2O, i.e. elements compatible with the melt (Shaw, 1970). These features were previously shown by Ripley and Alawi (1988) for the pelitic xenoliths of the Duluth Complex.

Most of the Bedded Pyrrhotite Unit from the contact aureole do not show the same large compositional range as the residuum calculated from the model; their bulk compositions are partially controlled by the melt that they retained (Fig. 3.15) in pores, as the larger pockets and as microleucosomes. The retention of a significant and large melt fraction (~ 50 modal %) in the xenoliths at the Mesaba deposit is, therefore, very similar to the migmatites in general from the contact aureole at the Duluth Complex as outlined by Duchesne (2004) and Sawyer (2014). In contrast, the xenoliths of Bedded Pyrrhotite Unit at the NorthMet deposit show a much larger range in composition and many are essentially residuum (Fig. 3.15). The compositions of the most residual xenolith samples from the NorthMet deposit show that these rocks have undergone a significant loss of melt with approximately ~10 wt % melt remaining, in other words up to 80% of the melt produced was extracted (Fig. 3.15). Since the xenoliths at both locations reached similarly high temperatures, we interpret the mineral assemblage and compositional differences as

indicating that the processes of melt extraction were less effective in the xenoliths from the Mesaba deposit than in xenoliths from NorthMet deposit.

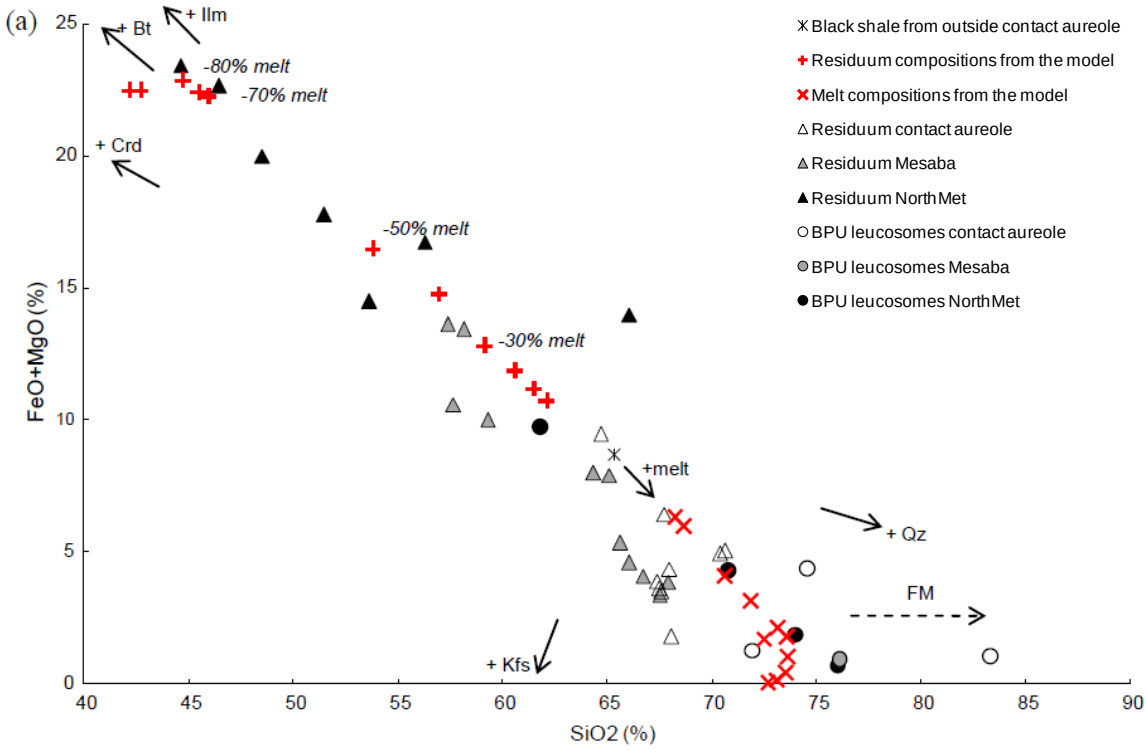
(a)
+ Bt
+ Ilm
-80% melt
-70% melt
+ Crd
-50% melt
-30% melt
+melt
+ Qz
FM
+ Kfs
FeO+MgO (%)
SiO2 (%)
Black shale from outside contact aureole
Residuum compositions from the model
Melt compositions from the model
Residuum contact aureole
Residuum Mesaba
Residuum NorthMet
BPU leucosomes contact aureole
BPU leucosomes Mesaba
BPU leucosomes NorthMet

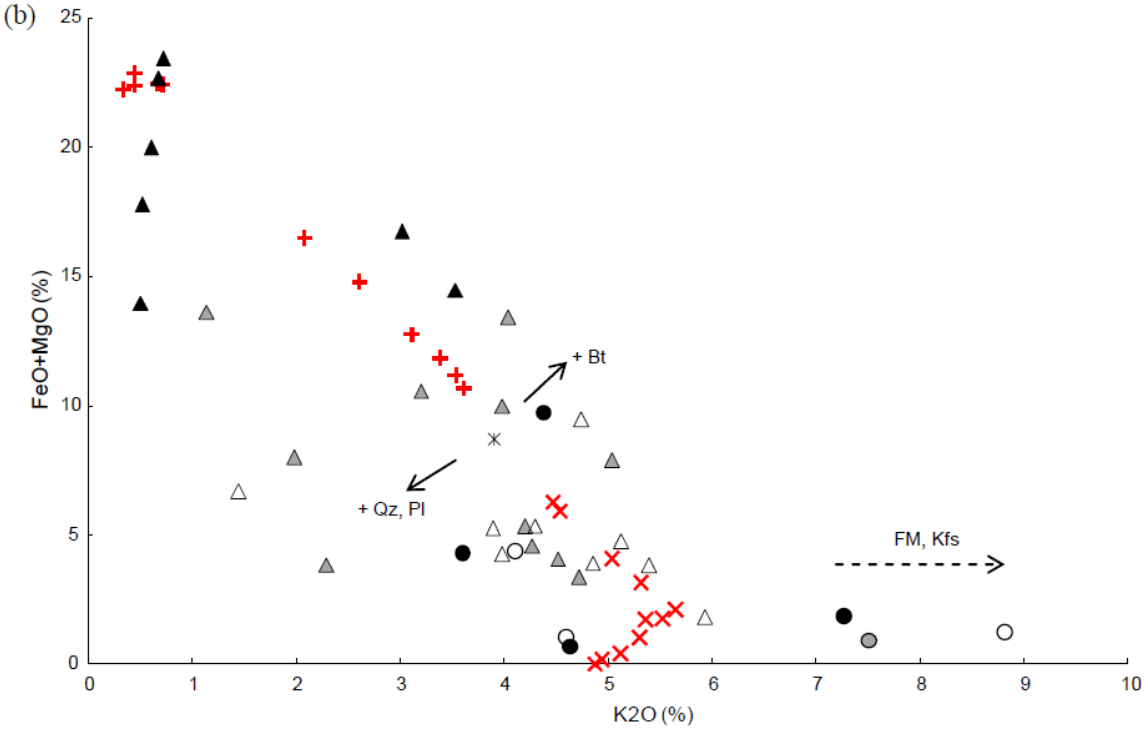
(b)
+ Bt
+ Qz, Pl
FM, Kfs
FeO+MgO (%)
K2O (%)

Figure 3.15: Plots of (a) SiO_2 and (b) K_2O vs. FeO+MgO for Bedded Pyrrhotite Unit (BPU) rocks and leucosomes from the contact aureole, BPU xenoliths and leucosomes from Mesaba and NorthMet deposits together with residuum and leucosome compositions calculated by modeling the partial melting of the potential protolith of the Bedded Pyrrhotite Unit at temperature steps from 700 to 1000°C. Abbreviations: FM = Fractionated melt.

The reasons for the difference in the extent of melt extraction from xenoliths in the Mesaba and NorthMet deposits are not well understood. In the general context of contact metamorphism, buoyancy resulting from the difference in density between melt and the solid residua and local differences in chemical potential act as driving forces for the movement and extraction of melt, whereas deviatoric and differential stresses are comparatively low, and less important driving forces. In the case of xenoliths surrounded by magma stresses are likely to be close to hydrostatic (lithostatic) and insufficient to contribute to melt segregation. Furthermore, the thermal and compositional differences between the host magma and the xenolith, and any felsic anatectic melt produced in it, are expected to be greater than in the cooler contact aureole (Turner, 1979; Robertson et al., 2015).

Our modeling shows that xenoliths in the Mesaba and NorthMet deposits formed at similar temperature ranges, and so might be expected to have experienced similar driving forces for melt extraction, but they underwent quite different degrees of extraction. Two factors which may have contributed to the different extents to which anatectic melt was extracted are the microstructure, or texture, of the rocks and the time available for the segregation process to operate.

The inner contact aureole along the contact with Paleoproterozoic pelitic and semi-pelitic rocks is characterised by the presence of diatexite migmatites and the composition of these indicates that they lost very little, or no, melt at the hand sample scale. However, some thin sections reveal that melt segregation had indeed begun in some rocks and formed pockets and microleucosomes, but it achieved only millimetre-scale separation, far too small to be evident in the sample size necessary for whole rock geochemistry

(Duchesne, 2004; Sawyer, 2014). This implies that the time interval over which temperatures were above the solidus was too short to produce macroscopically evident segregation of melt. The xenoliths at Mesaba show similar features to the contact aureole rocks and solidified before segregation had advanced far. In this scenario NorthMet, which has the smallest xenoliths, the period suprasolidus temperatures was sufficient that the length-scale for melt segregation exceeded the size of xenoliths and so they became melt depleted. However, texturally observation of different sizes of the xenoliths at NorthMet and Mesaba may also imply longer residence time for NorthMet xenoliths than those from Mesaba in the magma.

In addition, microstructure may play a role in the ability of melt to segregate (Sawyer 2014), particularly for the Bedded Pyrrhotite Unit which was derived from black shales. The Bedded Pyrrhotite Unit in the contact aureole and in the xenoliths at Mesaba both contain significant amounts (>10 modal %) of graphite which occurs as relatively large, randomly oriented tabular grains (flakes) (Fig. 3.16). This interlocking fabric of graphite may have provided sufficient resistance to the movement of melt and greatly inhibited, or prevented, the segregation of melt from the solid matrix in this case of very small deviatoric, or differential, stresses. Some of the xenoliths of Bedded Pyrrhotite Unit at NorthMet are different and contain very little graphite thus they have no interlocking microstructure of graphite flakes which might have impeded the movement of melt and so these became melt depleted. In addition, note that the amounts of graphite in xenoliths may also affect the density of these rocks, i.e. the graphite-rich xenoliths may have been more buoyant. As consequence, the more buoyant xenoliths, i.e. graphite-rich xenoliths at

Mesaba, may have undergone less “exposure” to the magma and therefore record lower temperatures than graphite-poor xenoliths at NorthMet.

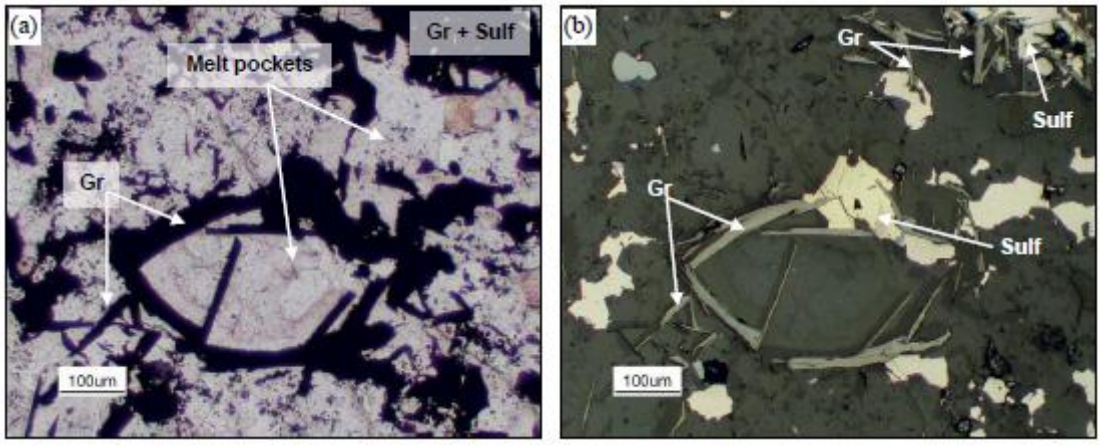

Figure 3.16: Photomicrographs of graphite grains in a xenolith of the Bedded Pyrrhotite Unit from the Mesaba deposit. (a) Graphite grains enclosing an anatectic melt pocket (Crd+Pl+Kfs+Qz). (b) Details of graphite and sulfide grains in same area of the photomicrograph (a). Abbreviations (Whitney and Evans, 2010): Crd = Cordierite; Pl = Plagioclase; Kfs = K-feldspar; Qz = Quartz; Gr = Graphite; Sulf = Sulfide.

3.9.2 WHERE DID THE EXTRACTED MELT GO?

Several lines of evidence suggest that the anatectic melt extracted from the xenoliths was mixed/mingled with the adjacent mafic magma and then formed a major component of the norites and gabbronorites in the basal Unit I. These include; 1) the presence of K-feldspar-bearing leucosomes within the host mafic rocks; 2) centimeter thick zones of mixed (hybrid) composition between the xenoliths and the mafic rocks.

We interpret the zones surrounding the xenoliths of Bedded Pyrrhotite Unit, i.e. few first centimeters of rock adjacent to the xenolith, as zone of chemical interaction between material emanating from the xenolith and the hosting mafic magma. The composition of plagioclase in these mixed zones is intermediate between An-poor plagioclase in the xenoliths and An-rich plagioclase in the mafic magma. A particular case is the plagioclase-rich leucocratic layer between the xenoliths at the NorthMet deposit and the host norite which contains felsic patches interpreted to have been large pockets of melt, or leucosomes. We suggest that these plagioclase-rich layers may represent the components left over from the reaction between felsic anatectic melt and the mafic magma. The faster diffusing components, such as H_2O, K_2O and Na_2O moved farther into the mafic magma. Complete mixing of material from the xenoliths into the mafic magma was curtailed by rapid cooling.

In summary, norites and gabbronorites from the basal Unit I, contain patches and films indicating the former presence of anatectic melt. Microstructural evidence of the intermingling of anatectic melt in the norites and gabbronorites from the basal Unit I is shown by the petrographic observation of small interspersed felsic and siliceous patches and films of anatectic melt that crystallized between the magmatic grains. In addition,

rounded grains of orthopyroxene are commonly included in the patches of former anatectic melt. We suggest that some of the orthopyroxene grains in the norites and gabbronorites of basal Unit I were derived from the partially melted xenoliths as they were consumed.

3.9.3 TEMPERATURES OF THE XENOLITHS AND IMPLICATIONS FOR NI-CU-PGE DEPOSIT FORMATION

The modeled temperatures for the Bedded Pyrrhotite Unit in the contact aureole and from the xenoliths range from 800° to ~1000°C. The lowest temperature revealed by the pseudosection modeling is based on a sample from the interior of a meter-sized xenolith. Simplified heat-transfer calculations based on heat-transfer model of Turcotte and Schubert (1982; equation 4.67) show that the heat transfer time is ~30 hours for a meter-size xenolith. These calculations are done with the following parameters: size of xenolith = 1 m; density = 2750 kg. m^{-3}; thermal capacity = 1000 $J \cdot kg^{-1} \cdot K^{-1}$ and thermal conductivity = 2.5 $W \cdot m^{-1} \cdot K^{-1}$. Xenoliths undergo rapid heat transfer suggesting that only the largest xenoliths in the Duluth Complex would resist complete heating, as suggested by Ripley and Alawi (1988) and Robertson et al. (2015). Furthermore, the rapid heating and cooling cycle in the xenoliths and slow reaction kinetics may have played a role in the preservation of low-grade assemblage in the interior of meter-size xenoliths.

The modeled temperatures for the Bedded Pyrrhotite Unit xenoliths are consistent with previous estimates that metamorphic temperatures were around 870°C (Sawyer, 2014; Benkó et al., 2015) near to the contact between the intrusion and the country rocks at Duluth. Ripley and Alawi (1988) have shown, using two-feldspar thermometry and heat transfer computations, that xenoliths at the Duluth Complex may have reached temperatures from 500 to ~1000°C. Our modeling confirms that this is a realistic

temperature range for the xenoliths there. Similar temperature ranges for xenoliths trapped in mafic magma are found in the marginal border group from the Skaergard intrusion (Markl, 2005), the Platreef in the Bushveld Complex (Johnson et al., 2010) and the Cortlandt Complex (Dorfler et al., 2015).

The maximum temperature attained by the xenoliths is a significant parameter in constraining the processes by which the enclosing magma becomes contaminated with material from the xenoliths, and which ultimately lead to the formation of Ni-Cu-PGE sulfide deposit in mafic rocks. For the Duluth Complex, Severson (1994) proposed that the Bedded Pyrrhotite Unit was the source of the S that "contaminated" the mafic magma. Queffurus and Barnes (2014) and Samalens et al. (2017) proposed a mechanism by which *in-situ* contamination of the magma by S and semimetals occurred as a consequence of the transfer of droplets of sulfide melt from the partially melted xenoliths to the host mafic magma in the extracted silicate anatectic melt. A key requirement of this proposed model is that metamorphic temperatures were high enough that the sulfide minerals melted to form droplets in the silicate anatectic melt. The temperatures of 800^{o}C to >950^{o}C calculated for the xenoliths of the Bedded Pyrrhotite Unit are, therefore, significant in this context as they support the model because at the high end they are sufficient for partial melting of the sulfide minerals (pyrrhotite and chalcopyrite) in the xenoliths to have occurred, i.e. at 800°C (Tsujimura and Kitakase, 2004).

3.10 CONCLUSIONS

The Bedded Pyrrhotite Unit from the contact aureole at the Duluth Complex also occurs as xenoliths in the basal Unit I of the Complex, both have undergone extensive

partial melting. Combining the bulk rock compositions and equilibrium thermodynamic modeling of the rocks we found that the Bedded Pyrrhotite Unit from the contact aureole and the least residual xenoliths of the Bedded Pyrrhotite Unit (mostly from the Mesaba deposit) contain similar, large fractions (~50 wt %) of silicate anatectic melt, however, the most residual of the xenoliths of the Bedded Pyrrhotite Unit, mostly at the NorthMet deposit, have lost a very large proportion of the anatectic melt that was formed in them.

The temperatures estimated to have been reached in the xenoliths are >800°C and as high as 1000°C and are sufficient that the main sulfide minerals, pyrrhotite and chalcopyrite, in them will have partially melted, and if then transported with the anatectic melt lost from the xenoliths contributed to S contamination of the host mafic magma. Thus, high temperature (T>800°C) partial melting of sulphidic pelitic country rocks in and around intrusions of mafic magmas is likely an important factor in the contamination processes which lead to the formation of Ni-Cu-PGE deposits in general.

3.11 ACKNOWLEDGMENTS

This research was funded by a Natural Science and Engineering Research Council of Canada Discovery Grant to SJB (17313) and a Canada Research Chair program grant to SJB (215503). We thank Mark Severson for providing some samples of the Bedded Pyrrhotite Unit from the contact aureole. Sadia Medhi and Dany Savard from LabMaTer are thanked for help in carrying out analyses. Editor and reviewers are thanked for helping us improve the clarity of our arguments.

3.12 REFERENCES

Acosta-Vigil, A., Buick, I., Hermann, J., Cesare, B., Rubatto, D., London, D. and Morgan, G.B., (2010) Mechanisms of crustal anatexis: A geochemical study of partially melted metapelitic enclaves and host dacite, SE Spain. Journal of Petrology, 51, 785-821.

Álvarez-Valero, A.M. and Kriegsman, L.M., (2010) Chemical, petrological and mass balance constraints on the textural evolution of pelitic enclaves. Lithos, 116, 300-309.

Álvarez-Valero, A.M. and Waters, D.J., (2010) Partially melted crustal xenoliths as a window into sub-volcanic processes: Evidence from the Neogene Magmatic Province of the Betic Cordillera, SE Spain. Journal of Petrology, 51, 973-991.

Amelin, Y., Li, C., Valeyev, O. and Naldrett, A., (2000) Nd-Pb-Sr isotope systematics of crustal assimilation in the Voisey's Bay and Mushuau intrusions, Labrador, Canada. Economic Geology, 95, 815-830.

Andrews, D. and Ripley, E., (1989) Mass transfer and sulfur fixation in the contact aureole of the Duluth Complex, Dunka road Cu-Ni deposit, Minnesota. The Canadian Mineralogist, 27, 293-310.

Arcuri, T., Ripley, E.M.and Hauck, S.A., (1998) Sulfur and oxygen isotope studies of the interaction between pelitic xenoliths and basaltic magma at the Babbitt and Serpentine Cu-Ni deposits, Duluth Complex, Minnesota. Economic Geology, 93, 1063-1075.

Bartoli, O., Acosta-Vigil, A. and Cesare, B., (2015) High-temperature metamorphism and crustal melting: working with melt inclusions. Periodico di Mineralogia 84, 3 (Special issue), 1-24.

Beard, J.S., Ragland, P.C.and Crawford, M.L., (2005) Reactive bulk assimilation: A model for crust-mantle mixing in silicic magmas. Geology 33, 681-684.

Benkó, Z., Mogessie, A., Molnár, F., Severson, M.J., Hauck, S.A. and Raič, S., (2015) Partial Melting Processes and Cu-Ni-PGE Mineralization in the Footwall of the South Kawishiwi Intrusion at the Spruce Road Deposit, Duluth Complex, Minnesota. Economic Geology, 110, 1269-1293.

Berman, G.R. and Aranovich, Y.L., (1996) Optimized standard state and solution properties of minerals. Contributions to Mineralogy and Petrology, 126, 1-24.

Bonnichsen, W., (1972) Sulfide minerals in the Duluth Complex. In; Sims, P. K., and Morey, G. W., (eds.), Geology of Minnesota, A Centennial Volume. Minnesota Geological Survey, pp. 388-393.

Bowen, N.L., (1922) The Behavior of Inclusions in Igneous Magmas. The Journal of Geology, 30, 513-570.

Cesare, B., Marchesi, C., Hermann, J. and Gómez-Pugnaire, M.T., (2003) Primary melt inclusions in andalusite from anatectic graphitic metapelites: Implications for the position of the Al2SiO5 triple point. Geology, 31, 573-576.

Chesley, J., Ruiz, J., Righter, K., Ferrari, L. and Gomez-Tuena, A., (2002) Source contamination versus assimilation: an example from the Trans-Mexican Volcanic Arc. Earth and Planetary Science Letters, 195, 211-221.

Clarke, D.B., (2007) Assimilation of xenocrysts in granitic magmas: principles, processes, proxies and problems. The Canadian Mineralogist, 45, 5-30.

Clarke, D.B., Erdmann, S., Samson, H. and Jamieson, R.A., (2009) Contamination of the South Mountain batholiths by sulfides from the country rocks. The Canadian Mineralogist, 47, 1159-1176.

Coggan. R. and Holland, T., (2002) Mixing properties of phengitic micas and revised garnet–phengite thermometers. Journal of Metamorphic Geology, 20, 683-696.

Connolly, J., (2009) The geodynamic equation of state: what and how. Geochemistry, Geophysics, Geosystems. 10, Q10014.

Connolly, J.A.D., (2005) Computation of phase equilibria by linear programming: A tool for geodynamic modeling and its application to subduction zone decarbonation. Earth and Planetary Science Letters, 236, 524-541.

Díaz-Alvarado, J., Castro, A., Fernández, C. and Moreno-Ventas, I., (2011) Assessing Bulk Assimilation in Cordierite-bearing Granitoids from the Central System Batholith, Spain; Experimental, Geochemical and Geochronological Constraints. Journal of Petrology, 52, 223-256.

Dorfler, K.M., Caddick, M.J. and Tracy, R.J., (2015) Thermodynamic Modeling of Crustal Melting Using Xenolith Analogs from the Cortlandt Complex, New York, USA. Journal of Petrology, 56, 389-408.

Duchesne, L., (2004) Fusion partielle et microstructures associées dans l'auréole de contact du complexe igné de Duluth, Minnesota: Unpublished. M.Sc. thesis, Université du Québec à Chicoutimi, 217 p.

Erdmann, S., London, D., Morgan, G.B. and Clarke, D.B., (2007) The contamination of granitic magma by metasedimentary country-rock material: an experimental study. The Canadian Mineralogist, 45, 43-61.

French, B.M., (1968) Progressive Contact Metamorphism of the Biwabik Iron-Formation, Mesabi Range, Minnesota Geological Survey, Bulletin, 45, 103p.

Gribble, C.D. and O'Hara, M.J., (1967) Interaction of basic magma with pelitic materials. Nature, 214, 1198-1201.

Harte, B., Pattison, D. R. M. and Linklater, C. M., (1991) Field relations and petrography of partially melted pelite and semipelitic rocks. In: Equilibrium and Kinetics in Contact Metamorphism: the Ballachulish Igneous Complex and its Aureole (eds. Voll, G., Topel, J., Pattison, D. R. M. and Seifert, F.), pp. 181–209. Springer-Verlag, Heidelberg.

Hauck, S.A., Severson, M.J., Zanko, L., Barnes, S.-J., Morton, P., Alminas, H., Foord, E.E. and Dahlberg, E.H., (1997) An overview of the geology and oxide, sulfide, and platinum-group element mineralization along the western and northern contacts of the Duluth Complex. Geological Society of America, Special paper, 312, 137–185.

Hiebert, R.S., Bekker, A., Wing, B.A. and Rouxel, O.J., (2013) The role of paragneiss assimilation in the origin of the Voisey's Bay Ni-Cu sulfide deposit, Labrador: Multiple S and Fe isotope evidence. Economic Geology, 108, 1459-1469.

Holland, T. and Powell, R., (1996) Thermodynamics of order-disorder in minerals: II. Symmetric formalism applied to solid solutions. American Mineralogist, 81, 1425-1437.

Holland, T. and Powell, R., (2001) Calculation of phase relations involving haplogranitic melts using an internally consistent thermodynamic dataset. Journal of Petrology, 42, 673-683.

Holland, T.J.B. and Powell, R., (1998) An internally consistent thermodynamic data set for phases of petrological interest. Journal of Metamorphic Geology, 16, 309-343.

Huppert, H.E., Sparks, R.S.J., Turner, J.S., Arndt, N.T., (1984) Emplacement and cooling of komatiite lavas. Nature, 309, 19-22.

Johnson, T.E., Brown, M. and White, R.W., (2010) Petrogenetic modeling of strongly residual metapelitic xenoliths within the southern Platreef, Bushveld Complex, South Africa. Journal of Metamorphic Geology, 28, 269-291.

Ketris, M.P. and Yudovich, Y.E., (2009) Estimations of Clarkes for Carbonaceous biolithes: World averages for trace element contents in black shales and coals. International Journal of Coal Geology, 78, 135-148.

Labotka, T.C., Papike, J.J. and Vaniman, D.T., (1981) Petrology of contact metamorphosed argillite from the Rove Formation, Gunflint Trail, Minnesota. American Mineralogist 66, 70-86.

Lesher, C.M., Arndt, N.T., and Groves, D.I., (1984) Genesis of komatiite-associated nickel sulfide deposits at Kambalda, Western Australia: A distal volcanic model. Sulfide deposits in mafic and ultramafic rocks. Institute of Mining and Metallurgy, London, 10 p.

Lesher, C.M. and Burnham, O.M., (2001) Multicomponent elemental and isotopic mixing in Ni–Cu–(PGE) ores at Kambalda, Western Australia. The Canadian Mineralogist, 39, 421-446.

Li, C. and Naldrett, A.J., (2000) Melting reactions of gneissic inclusions with enclosing magma at Voisey's Bay, Labrador, Canada: implications with respect to ore genesis. Economic Geology, 95, 801-814.

Lucente, M.E. and Morey, G.B., (1983) Stratigraphy and sedimentology of the Lower Proterozoic Virginia Formation, northern Minnesota. Minnesota Geological Survey, Report of Investigations, RI-28, 28 p.

Lyubetskaya, T. and Korenaga, J., (2007) Chemical composition of Earth's primitive mantle and its variance: 1. Method and results. Journal of Geophysical Research: Solid Earth, B03211, 112, 1-21.

Mainwaring, P.R. and Naldrett, A., (1977) Country-rock assimilation and the genesis of Cu-Ni sulfides in the Water Hen Intrusion, Duluth Complex, Minnesota. Economic Geology, 72, 1269-1284.

Naldrett, A., (1966) Role of sulphurization in genesis of iron-nickel sulphide deposits of porcupine district Ontario. Canadian Mining and Metallurgical Bulletin, 59, 489.

Markl, G., (2005) Mullite-corundum-spinel-cordierite-plagioclase xenoliths in the Skaergaard Marginal Border Group: multi-stage interaction between metasediments and basaltic magma. Contributions to Mineralogy and Petrology, 149, 196-215.

McLeod, P., Sparks, R.S.J., (1998) The dynamics of xenolith assimilation. Contributions to Mineralogy and Petrology, 132, 21-33.

Miller, J.D., Jr., and Severson, M.J., (2002) Geology of the Duluth Complex, in Miller, J.D., Jr., Green, J.C., Severson, M.J., Chandler, V.W., Hauck, S.A., Peterson, D.M., and Wahl, T.E., eds., Geology and mineral potential of the Duluth Complex and

related rocks of northeastern Minnesota. Minnesota Geological Survey, Report of Investigations, RI-58, 106-143.

Morey, G., Papike, J., Smith, R. and Weiblen, P., (1972) Observations on the contact metamorphism of the Biwabik iron-formation, east Mesabi district, Minnesota. Geological Society of America, Memoirs, 135, 225-264.

Newton, R.C., Charlu, T.V. and Kleppa, O.J., (1980) Thermochemistry of the high structural state plagioclases. Geochimica et Cosmochimica Acta, 44, 933-941.

Ojakangas, R.W., Morey, G.B. and Green, J.C., (2001) The Mesoproterozoic midcontinent rift system, Lake Superior Region, USA. Sedimentary Geology, 141–142, 421-442.

Preston, R.J., Dempster, T.J., Bell, B.R. and Rogers, G., (1999) The Petrology of Mullite-bearing Peraluminous Xenoliths: Implications for Contamination Processes in Basaltic Magmas. Journal of Petrology, 40, 549-573.

Queffurus, M. and Barnes, S.-J., (2014) Selenium and sulfur concentrations in country rocks from the Duluth Complex, Minnesota, USA: Implications for formation of the Cu-Ni-PGE sulfides. Economic Geology, 109, 785-794.

Rao, B.V. and Ripley, E.M., (1983) Petrochemical studies of the Dunka Road Cu-Ni deposit, Duluth Complex, Minnesota. Economic Geology, 78, 1222–1238.

Ripley, E.M., (1981) Sulfur isotopic studies of the Dunka road Cu-Ni deposit, Duluth Complex, Minnesota. Economic Geology, 76, 610-620.

Ripley, E.M. and Alawi, J.A., (1988) Petrogenesis of pelitic xenoliths at the Babbitt Cu-Ni deposit, Duluth Complex, Minnesota, U.S.A. Lithos, 21, 143-159.

Ripley, E.M., Park, Y-R., Li, C. and Naldrett, A., (2000) Oxygen Isotope Studies of the Voisey's Bay Ni-Cu-Co Deposit, Labrador, Canada. Economic Geology, 95, 831-844.

Ripley, E.M., Taib, N.I., Chusi, L. and Moore, C.H., (2007) Chemical and mineralogical heterogeneity in the basal zone of the Partridge River Intrusion: implications for the origin of Cu–Ni sulfide mineralization in the Duluth Complex, Midcontinent Rift System. Contributions to Mineralogy and Petrology, 154, 35-54.

Ripley, E.M. and Li, C., (2013) Sulfide saturation in mafic magmas: Is external sulfur required for magmatic Ni-Cu-(PGE) ore genesis? Economic Geology, 108, 45-58.

Ripley, E.M., (2014) Ni-Cu-PGE Mineralization in the Partridge River, South Kawishiwi, and Eagle Intrusions: A review of contrasting styles of sulfide-rich occurrences in the Midcontinent Rift System. Economic Geology, 109, 309-324.

Robertson, J., Ripley, E.M., Barnes, S.J. and Li, C., (2015) Sulfur liberation from country rocks and incorporation in mafic magmas. Economic Geology, 110, 1111-1123.

Samalens, N., Barnes, S.-J. and Sawyer, E.W., (2017) The role of black shales as a source of sulfur and semimetals in magmatic nickel-copper deposits: Example from the Partridge River Intrusion, Duluth Complex, Minnesota, USA. Ore Geology Reviews, 81, 173-187.

Sawyer, E.W., (2001) Melt segregation in the continental crust: distribution and movement of melt in anatectic rocks. Journal of Metamorphic Geology, 19, 291-309.

Sawyer, E.W., (2014) The inception and growth of leucosomes: microstructure at the start of melt segregation in migmatites. Journal of Metamorphic Geology, 32, 695-712.

Severson, M.J., (1994) Igneous stratigraphy of the South Kawishiwi intrusion, Duluth Complex, northeastern Minnesota. Natural Resources Research Institute, University of Minnesota, Technical Report, NRRI/TR-93/34, 210 p.

Severson, M.J., Patelke, R.L., Hauck, S.A. and Zanko, L.M., (1996) The Babbitt copper-nickel deposit. Part C: Igneous geology, footwall lithologies, and cross-sections Natural Resources Research Institute, University of Minnesota, Technical Report, NRRI/TR-94/21b, 48p.

Severson, M.J. and Hauck, S.A., (2008) Finish Logging of Duluth Complex Drill Core (And a Reinterpretation of the Geology at the Mesaba (Babbitt) deposit). Natural Resources Research Institute, University of Minnesota, Technical Report, NRRI/TR-2008/17, 68 p.

Shaw, D.M., (1970) Trace element fractionation during anatexis. Geochimica et Cosmochimica Acta, 34, 237-243.

Shaw, C.S.J., (2009) Caught in the act - The first few hours of xenolith assimilation preserved in lavas of the Rockeskyllerkopf volcano, West Eifel, Germany. Lithos, 112, 511-523.

Spear, F.S., Kohn, M.J. and Cheney, J.T., (1999) P-T paths from anatectic pelites. Contributions to Mineralogy and Petrology, 134, 17-32.

Tajčmanová, L., Connolly, J.A.D. and Cesare, B., (2009) A thermodynamic model for titanium and ferric iron solution in biotite. Journal of Metamorphic Geology, 27, 153-165.

Thériault, R.D., Barnes, S.-J. and Severson, M.J., (1997) The influence of country-rock assimilation and silicate to sulfide ratios (R factor) on the genesis of the Dunka

Road Cu – Ni – platinum-group element deposit, Duluth Complex, Minnesota. Canadian Journal of Earth Sciences, 34, 375-389.

Thériault, R.D. and Barnes, S.-J., (1998) Compositional variations in Cu-Ni-PGE sulfides of the Dunka road deposit, Duluth Complex, Minnesota: The importance of combined assimilation and magmatic processes. The Canadian Mineralogist, 36, 869-886.

Thériault, R.D., Barnes, S.-J. and Severson, M.J., (2000) Origin of Cu-Ni-PGE Sulfide Mineralization in the Partridge River Intrusion, Duluth Complex, Minnesota. Economic Geology, 95, 929-943.

Tracy, R.J. and Frost, B.R., (1991) Phase equilibria and thermobarometry of calcareous, ultramafic and mafic rocks, and iron formations. Reviews in Mineral. Geochem. 26, 207-289.

Tsujimura, T. and Kitakaze, A., (2004) New phase relations in the Cu–Fe–S system at 800°C; constraint of fractional crystallization of a sulfide liquid. Neues Jahrbuch für Mineralogie Monatshefte. 10, 433-444.

Turcotte, D. L. and Schubert, G., (1982) Geodynamics: Applications of continuum physics to geological problems. J. Wiley, New York. 450 pp.

Turner, J.S., (1979) Buoyancy effects in fluids: Cambridge, Cambridge University Press, 367 p.

Waldbaum, D. and Thompson, J., (1968) Mixing properties of sanidine crystalline solutions. 2. Calculations based on volume data. American Mineralogist, 53, 1-11.

Webb, P.C., Thompson, M., Potts, P.J. and Bédard, L.P., (2006) GeoPT18 - An international proficiency test for analytical geochemistry laboratories - Report on

round 18/Jan 2006 (Quartz diorite, KPT-1). International Association of Geoanalysts, Report, 32p.

White, R.W., Powell, R., Holland, T.J.B. and Worley, B., (2000) The effect of TiO2 and Fe2O3 on metapelitic assemblages at greenschist and amphibolite facies conditions: mineral equilibria calculations in the system K2O–FeO–MgO–Al2O3–SiO2–H2O–TiO2–Fe2O3. Journal of Metamorphic Geology, 18, 497-511.

White, R.W., Powell, R. and Holland, T.J.B., (2001) Calculation of partial melting equilibria in the system Na2O–CaO–K2O–FeO–MgO–Al2O3–SiO2–H2O (NCKFMASH). Journal of Metamorphic Geology, 19, 139-153.

White, R.W., Powell, R. and Holland, T.J.B., (2007) Progress relating to calculation of partial melting equilibria for metapelites. Journal of Metamorphic Geology 25, 511-527.

White, R.W., Stevens, G. and Johnson, T.E., (2011) Is the Crucible Reproducible? Reconciling Melting Experiments with Thermodynamic Calculations. Elements, 7, 241-246.

Whitney, D.L. and Evans, B.W., (2010) Abbreviations for names of rock-forming minerals. American Mineralogist, 95, 185-187.

CHAPITRE 4

A LASER ABLATION INDUCTIVELY COUPLED PLASMA MASS SPECTROMETRY STUDY OF THE DISTRIBUTION OF CHALCOPHILE ELEMENTS IN SEDIMENTARY AND MAGMATIC SULFIDES OF THE DULUTH COMPLEX, MINNESOTA, USA

SAMALENS N. [1], BARNES S.-J. [1], SAWYER E.W.[1]

[1] Université du Québec à Chicoutimi, 555 boulevard de l'Université, Saguenay, QC, G7H 2B1, Canada

ORE GEOLOGY REVIEWS, SPECIAL ISSUE, SUBMITTED DECEMBER 05, 2016

4.1 RÉSUMÉ

Des gisements de sulfures de Ni-Cu se trouvent dans la partie basale de l'Intrusion de Partridge River dans le Complexe de Duluth (Minnesota, États-Unis). Les sulfures de ces gisements se sont formés suite à l'assimilation de shales noirs protérozoïques riches en S de l'unité nommée la *Bedded Pyrrhotite Unit* sous forme de xénolithes dans le magma. De petites gouttelettes de sulfure ont été observées dans le produit de fusion partielle des xénolithes de la *Bedded Pyrrhotite Unit*. Le S a été transféré au magma lors de la libération des gouttelettes de sulfure depuis les xénolithes de la *Bedded Pyrrhotite Unit* vers le magma via le produit de fusion partielle des xénolithes. Les shales noirs sont également enrichis en Te, As, Bi, Sb et Sn (TABS). Ces éléments importants pour la formation de minéraux du groupe du platine (MGP). Ces éléments de part leur caractère chalcophile sont ajouté au magma en même temps que le S. Cependant, les concentrations et les phases hôtes des TABS sont très peu documentées dans les gisements magmatiques de Ni-Cu-Éléments du groupe du platine. Une étude pétrographique et des analyses au LA-ICP-MS (*Laser Ablation Inductively Coupled Plasma Mass Spectrometry*) des minéraux sulfurés des roches de la *Bedded Pyrrhotite Unit* et de l'unité basale contaminée de l'Intrusion de Partridge River ont été réalisées afin d'investiguer le comportement des TABS lors de la contamination du magma mafique par les shales noirs.

La proportion en sulfure de métaux communs sont varie en fonction du type de roche. L'assemblage de sulfures des roches de la *Bedded Pyrrhotite Unit* hors de l'auréole de métamorphisme de contact est constitué principalement de pyrite avec moins de 5% de pyrrhotite + chalcopyrite alors que celui des roches de la *Bedded Pyrrhotite Unit* à l'intérieur de l'auréole de contact est constitué majoritairement de pyrrhotite (>95%) avec

de faibles quantités de chalcopyrite (<2%). L'assemblage de sulfures des xénolithes de la *Bedded Pyrrhotite Unit* et des roches mafiques de l'unité basale contient deux sulfures additionnels; la pentlandite et la cubanite.

Notre étude au LA-ICP-MS a montré que les sulfures des roches de la *Bedded Pyrrhotite Unit* sont enrichis en TABS. Ces résultats confirment l'hypothèse stipulant que les shales noirs de la *Bedded Pyrrhotite Unit* sont la source des semi-métaux et que ces éléments ont été transférés au magma mafique, en même temps que le S, lors de l'assimilation des xénolithes de la *Bedded Pyrrhotite Unit*. De plus, des cartes chimiques réalisées au LA-ICP-MS de gouttelettes de sulfure piégées dans le produit de fusion partielle des xénolithes montrent que ces gouttelettes contiennent des TABS et du Pb. Ces observations supportent le modèle proposé de contamination en semi-métaux du magma mafique.

D'autre part, notre étude montre que les minéraux sulfurés ne contrôlent pas entièrement le budget en éléments chalcophiles dans les roches de la *Bedded Pyrrhotite Unit* et les roches mafiques de l'unité basale du Complexe de Duluth. Pour expliquer le budget en éléments chalcophiles, des phases autres que les sulfures concentrent ces éléments. En effet, des phases riches en matière organique pourraient jouer un rôle dans la concentration de ces éléments dans les roches de la *Bedded Pyrrhotite Unit* hors de l'auréole de contact. Dans les xénolithes et les roches mafiques entourant les xénolithes le budget en éléments chalcophiles s'explique par la contribution combinée des sulfures de métaux communs et de MGP. Les plagioclases contribuent au budget en Pb alors que les orthopyroxènes contribuent au budget en Sn.

4.2 ABSTRACT

Nickel-copper sulfide deposits occur in the basal unit of the Partridge River Intrusion, Duluth Complex (Minnesota, USA). Many evidences suggest that these sulfides are formed after assimilation of proterozoic S-rich black shales, known as the Bedded Pyrrhotite Unit, as xenoliths in the magma. The anatectic partial melt derived from xenoliths of the Bedded Pyrrhotite Unit contained small sulfide droplets. Sulfur is transferred physically to the mafic magma via these droplets. In addition to S, black shales are enriched in elements important in the formation of platinum-group minerals notably Te, As, Bi, Sb and Sn (TABS). All of these elements are chalcophile and have been added to the mafic magma along with the S. However, the concentrations and distribution of TABS in magmatic Ni-Cu-platinum-group element (PGE) deposits, are poorly documented despite their important role in formation of platinum-group minerals (PGM). In order to investigate the behavior of TABS during assimilation of black shales in mafic magma a petrographic and Laser Ablation Inductively Coupled Plasma Mass Spectrometry (LA-ICP-MS) study has been carried out on sulfide from the Bedded Pyrrhotite Unit and from the contaminated basal unit of the Partridge River Intrusion.

Petrography showed that the proportions of the base metal sulfide minerals vary with rock type. The sulfide assemblage of the Bedded Pyrrhotite Unit outside the contact metamorphism aureole consists of pyrite with a little pyrrhotite plus chalcopyrite (<5%), whereas within the contact aureole the sulfide assemblage of the Bedded Pyrrhotite Unit rocks consists dominantly of pyrrhotite (>95%) with small amount of chalcopyrite (<2%). The sulfide mineral assemblage in the xenoliths of the Bedded Pyrrhotite Unit and in the mafic rocks of the basal unit contains two additional sulfides, pentlandite and cubanite.

Our LA-ICP-MS study shows that sulfides of the Bedded Pyrrhotite Unit are rich in TABS; consistent with these S-rich black shales being the source of semimetals that contaminated the mafic magma. Furthermore, LA-ICP-MS chemical maps of sulfide droplets observed inside the anatectic melt of the Bedded Pyrrhotite Unit xenoliths show that these sulfide droplets host TABS and Pb. These observations support the proposed model for contamination of the mafic magma with the semimetals by assimilation of Bedded Pyrrhotite Unit xenoliths in the mafic magma.

On the other hand, our study shows that the entire chalcophile elements budget is not hosted by base metal sulfides and then other phases are requiered. Mass balance calculations show that chalcophile elements must be present in some other phase(s) rather than sulfides. Organic compounds may have concentrated chalcophile elements in the Bedded Pyrrhotite Unit from outside the contact aureole. In addition, platinum-group minerals and silicate phases (i.e. Pb in plagioclase and Sn in orthopyroxene) contribute to the chalcophile elements budget.

Keywords. LA-ICP-MS, black shales, TABS, Ni-Cu sulfide deposit, Duluth Complex

4.3 INTRODUCTION

Most of world's Ni-Cu-Platinum-group element (PGE) deposits are thought to have formed after contamination of a mafic magma with S-bearing sedimentary rocks (e.g., Lesher and Burnham, 2001; Ripley and Li, 2013). In particular, black shales are an ideal potential source of S. A number of mechanisms for the transfer of S from the black shales to the magma have been proposed: bulk melting of the country rock (Lesher et al., 1984), transfer by gas or hydrothermal fluids (Naldrett, 1966; Prider, 1970; Mainwaring and Naldrett, 1977; Baker et al., 2001; Ripley et al., 2007; Molnár et al., 2009; Benkó et al., 2015a, b) and transfer of sulfide droplets during partial melting (anatexis) of xenoliths (Lesher and Campbell, 1999; Lesher and Burnham, 2001; Queffurus and Barnes, 2014; Samalens et al., 2017).

In addition to S, black shales are enriched in a group of elements Te, As, Bi, Sb and Sn important in the formation of platinum-group minerals (hereafter these elements will be referred to as TABS, see also Barnes and Ripley, 2016). However, in contrast to PGE, the concentration of TABS and their host minerals are poorly documented in source rocks and in Ni-Cu-PGE sulfide deposits (Barnes and Ripley, 2016).

The Duluth Complex is an ideal place to study the distribution of TABS during the formation of a Ni-Cu-PGE sulfide deposit. At the Duluth Complex S-rich black shales of the Bedded Pyrrhotite Unit in the Virginia Formation occur both at the contact with the intrusion and as xenoliths in the basal unit of the Partridge River Intrusion (Mainwaring and Naldrett, 1977; Ripley, 1981; Andrews and Ripley, 1989; Thériault et al., 1997; Thériault and Barnes, 1998; Ripley et al., 2007; Severson and Hauck, 2008; Queffurus and Barnes, 2014). This basal unit also contains Ni-Cu-PGE deposits in the form of

disseminated and less commonly massive sulfides. Numerous drill holes across the basal unit and into the country rock allow detailed sampling. The Bedded Pyrrhotite Unit contains similar concentrations of TABS to black shales from the literature, and is enriched in these elements when compared to basaltic magmas and the average continental upper crust (Fig. 4.1). The Bedded Pyrrhotite Unit has been identified as the source of the sulfur (Zanko et al., 1994; Queffurus and Barnes, 2014) and TABS (Samalens et al., 2017) that were incorporated into the mafic magma at the Duluth Complex.

To investigate the distribution of TABS and the minerals that host them during contamination of a mafic magma by black shales we have carried out a study of the petrography and composition of the sulfide minerals. In addition we have made LA-ICP-MS chemical maps of sedimentary and magmatic sulfides and the surrounding silicates to document the distribution of TABS in the rocks.

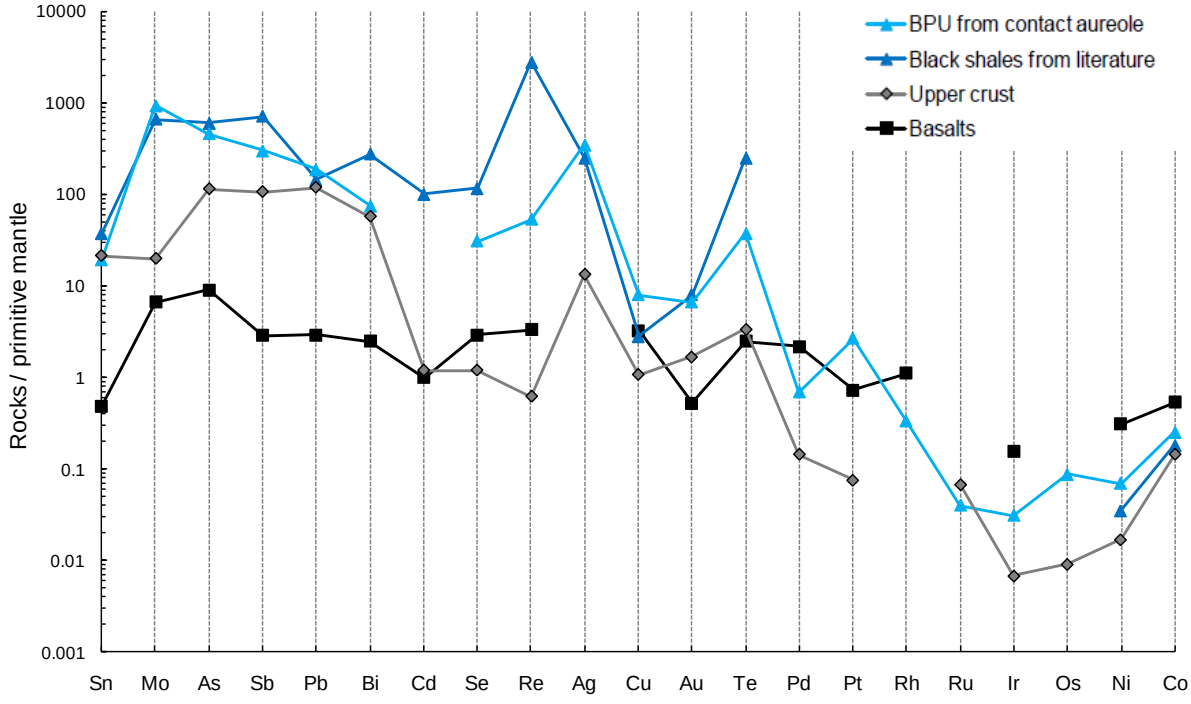

Figure 4.1: Primitive mantle-normalized plot of averages of TABS and trace metals content of the Bedded Pyrrhotite Unit, black shales, upper crust and basalts from literature (Ketris and Yudovich, 2009; Hu and Gao, 2008; Dionne-Foster, 2007; Lyubetskaya and Korenaga, 2007). Abbreviation: BPU = Bedded Pyrrhotite Unit.

4.4 GEOLOGICAL CONTEXT

The mid-Proterozoic (1100 Ma) Duluth Complex is a mafic complex located in Minnesota, USA. It consists of mainly two mafic intrusions (Fig. 4.2) that were emplaced into the Midcontinent Rift System and related to the overlying Keweenawan flood basalt (Severson and Hauck, 1997; Ojakangas et al., 2001; Miller and Severson, 2002). Magmatic Ni-Cu-PGE deposits occur at the base of two of the intrusions, the Partridge River Intrusion and the South Kawishiwi Intrusion (Fig. 4.2). The Partridge River Intrusion (see description below) and the South Kawishiwi Intrusion are well-documented (Gál et al., 2013; Benkó et al., 2015a, b; Raic et al., 2015).

Our study focused on the Mesaba, NorthMet and Wetlegs deposits of the Partridge River Intrusion (Appendix 1). The basal unit of the Partridge River Intrusion is composed of the following lithologies from the contact to the interior of the intrusion: norite, gabbronorite, troctolite and ultramafic rocks (Hauck et al., 1997; Thériault et al., 1997; Miller and Severson, 2002; Severson and Hauck, 2008). Thériault et al. (1997) and Queffurus and Barnes (2014) interpreted the norites as corresponding to the contaminated part of the magma as they are located in the vicinity of xenoliths in the basal part of the intrusion. The Ni-Cu-PGE deposits consist of disseminated to massive sulfides. The main minerals present in massive and disseminated sulfides are pyrrhotite, cubanite, chalcopyrite and pentlandite (Thériault and Barnes, 1998; Ripley, 2014). Disseminated sulfides are found throughout the basal unit of the Partridge River Intrusion, whereas massive sulfides are mainly found surrounding xenoliths of the country rocks.

The country rocks range from lower Proterozoic sediments of the Animikie Group in the south to the Archean granite-greenstone in the north (Fig. 4.2). The country rocks to the

Partridge River Intrusion are the Virginia Formation sedimentary rocks of the Animikie Group. The Virginia Formation is composed of carbonates, greywackes, pelites, black shales and siltstones (Lucente and Morey, 1983). Away from the intrusion the sedimentary rocks are essentially unmetamorphosed and the sulfide mineral present in these is pyrite (Bonnichsen, 1972; Lucente and Morey, 1983, Fig. 2A; Queffurus and Barnes, 2014). Whereas close to the intrusion, the sedimentary rocks of the Virginia Formation in the contact aureole have undergone contact metamorphism at temperatures greater than 800°C and diatexite migmatites formed close to the contact with the mafic magma, and the sulfide present in these is pyrrhotite (Labotka et al., 1981; Tracy and Frost, 1991; Sawyer, 2014).

One unit of particular interest is the Bedded Pyrrhotite Unit consisting of sulfide-rich black shales in the Virginia Formation and believed to have been deposited in restricted anoxic basins (Hauck et al., 1997). The Bedded Pyrrhotite Unit is mostly present close to the contact with the Duluth Complex (Severson and Hauck, 2008). This unit is approximately 200 m thick, but has a sporadic distribution. The basal unit of the Partridge River Intrusion (Unit I) contains numerous xenoliths of the Bedded Pyrrhotite Unit and of other facies from the Virginia Formation (Ripley and Alawi, 1988; Thériault et al., 2000; Severson and Hauck, 2008; Queffurus and Barnes, 2014).

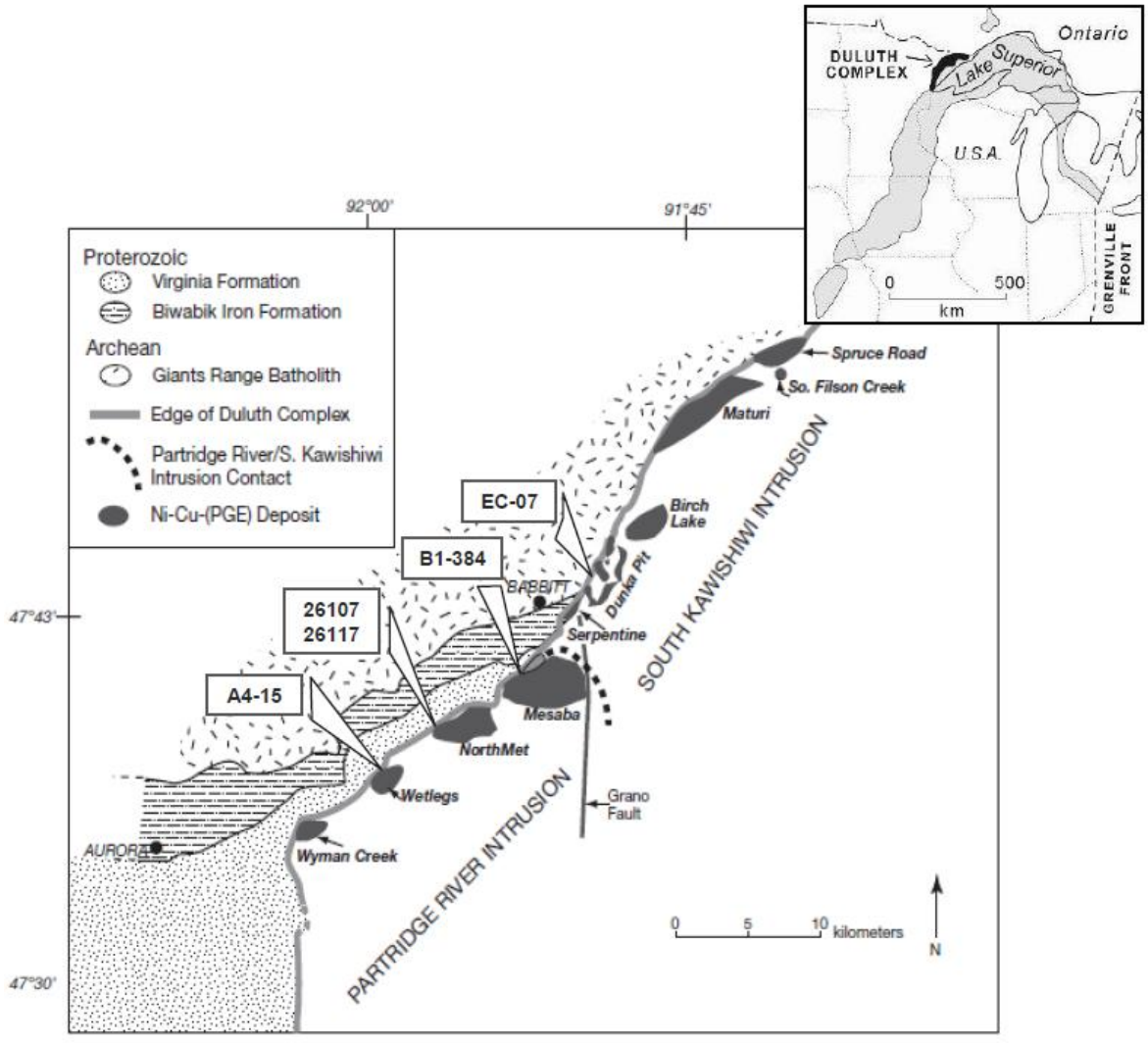

Figure 4.2: Geological and location map of the Duluth Complex (modified from Ojakangas et al., 2001; Queffurus and Barnes, 2014; Ripley, 2014). The right inset shows the position of the Duluth Complex in the Midcontinent Rift System.

4.5 METHODOLOGY

Samples of xenoliths of the Bedded Pyrrhotite Unit as well as norites and gabbronorites were collected from boreholes that crossed the basal Unit I of the Partridge River Intrusion at the Dunka Pit, NorthMet, Mesaba and Wetlegs deposits (Fig. 4.2 and Appendix 1). Thirty-five polished thin sections were examined and whole rock analyses were carried out. The results of this study are reported in Samalens et al. (2017). After a petrographic study of the textural varieties of the sulfide assemblages seventeen representative samples were selected for a more detailed investigation (this study) of the trace element contents in the sulfide minerals using LA-ICP-MS analyzes and chemical mapping.

To quantify the proportions of sulfide minerals in xenoliths of the Bedded Pyrrhotite Unit image analysis using the Image-Pro software (version 6.2) was carried out on eight thin sections. The results of the image analyses are presented in Table 4.2.

Sulfur, Se, PGE and TABS were determined on whole rock samples at LabMaTer, UQAC. Sulfur concentrations were determined by a HORIBA EMIA-220V induction furnace using the method of Bédard et al. (2008). Platinum-group elements were determined by Ni-sulfide fire assay Te-co-precipitations and ICP-MS analysis, in addition sample A4-15-01 was analysed by isotope dilution ICP-MS (Savard et al., 2010). Selenium was determined by Thiol Cotton Fiber - Instrumental Neutron Activation Analysis (TCF-INAA) at LabMaTer, UQAC (Savard et al., 2006). The TABS were determined in the black shales by solution ICP-MS using a new analytical protocol specifically designed for black shales (Henrique-Pinto et al., 2015) at LabMaTer. In the gabbronorites TABS were determined by Fusion ICP-MS (Method: WRA42B) at Activation Laboratories Ltd (Actlabs), Ontario, Canada. Data and results for the certified reference materials are given

in Appendix 5 (Samalens et al., 2017). In-situ analyses of sulfide minerals were carried out by laser ablation induced coupled plasma mass spectroscopy (LA-ICP-MS) using a 7700x Agilent ICP-MS coupled with Resolution M-50 Excimer (193nm) ArF laser. The isotopes that were monitored are ^{34}S; ^{57}Fe; ^{59}Co; ^{61}Ni; ^{65}Cu; ^{66}Zn; ^{75}As; ^{82}Se; ^{95}Mo; ^{101}Ru; ^{103}Rh; ^{105}Pd; ^{107}Ag; ^{108}Pd; ^{111}Cd; ^{118}Sn; ^{121}Sb; ^{125}Te; ^{189}Os; ^{193}Ir; ^{195}Pt; ^{197}Au; ^{208}Pb; ^{209}Bi. LA-ICP-MS operating parameters were; frequency = 15Hz; RF power = 1350W; voltage = 1,3V; beam power = 5 mJ/pulse; dwell time = 7,5 ms; speed = 5-10 µm/s; fluence = 2-5 J/cm^2. Lines scans across the surface of sulfides grains were made with beam sizes of 44 µm, 33 µm, 19 µm and 15 µm. The internal standard used was Fe. The machine was calibrated using the international reference materials po-727 (FeS doped with ~40 ppm PGE and Au, provided by Memorial University) and MASS-1 (a ZnFeCuS doped with ~50 ppm trace elements, provided by the USGS). The calibration was monitored using JBMSS-5 a FeS doped with 50-100 ppm trace elements, provided by Prof. Brenan (then at University of Toronto) and GSE-1g-A a synthetic basalt glass. Nickel and Cu argide interferences were corrected of on ^{101}Ru and ^{103}Rh using NiS and FeCuS blanks. Cadmium (^{108}Cd) interference on ^{108}Pd was corrected for using ^{111}Cd. Concentrations used for the calibration and results for the monitors are listed in Table 4.1. The LA-ICP-MS data is reported in Appendix 6. LA-ICP-MS maps were produced for small (<50µm) and large (>500µm) sulfide grains with beam sizes of 5 and 44 µm respectively, frequency of 20 and 15Hz respectively and fluence of 10 and 3 J/cm^2 respectively. In addition, 3 line scans across the entire thin section of a Bedded Pyrrhotite Unit sample were made using the following parameters: frequency = 25Hz; beam size = 75µm and fluence = 10 J/cm^2.

	^{34}S	^{57}Fe	^{59}Co	^{61}Ni	^{65}Cu	^{66}Zn	^{75}As	^{82}Se	^{95}Mo	^{101}Ru	^{103}Rh	$^{105/108}Pd$	^{107}Ag	^{111}Cd	^{118}Sn	^{121}Sb	^{125}Te	^{189}Os	^{193}Ir	^{195}Pt	^{197}Au	^{208}Pb	^{209}Bi
	%	%	ppm	%	%	ppm	ppm	ppm	ppm	ppm	ppm	ppm	ppm	ppm	ppm	ppm	ppm	ppm	ppm	ppm	ppm	ppm	ppm
Ref mat used for calibration	po-727	po-727	MASS-1	JB-MSS-5	MASS-1	MASS1	MASS-1	MASS-1	MASS-1	po-727	po-727	po-727	MASS-1	MASS-1	MASS-1	MASS-1	MASS-1	po-727	po-727	po-727	po-727	MASS-1	MASS-1
Working value	39	61	60	1,05	13,40	210000	65	51	59	36,3	41,4	43,1	50	60	59	60	15	46,9	47,8	35,4	45,8	68	60
Std dev	0	0	10	0,01	0,05	5000	3	4	9	0,3	0,3	0,4	5	7	6	9	inf val	2,5	1,2	0,8	2,3	7	inf val
source	Certif.	Certif.	Certif.	Working	Certif.	Certif.	Certif.	Certif	Certif	Certif	Certif	Certif	Certif	Certif	Certif	Certif	Certif.	Certif.	Certif.	Certif	Certif	Certif	Certif
Values obtained for in-house material																							
JB-MSS-5																							
Working values	40,57	57	n.a.	used	0,021	13	63	48,35	n.a.	21,72	61,40	64,10	53,00	0,13	0,34	61,30	36	42,50	43,98	39,9	35,9	71,5	76,1
Std dev	0,60	0,90		to	0,001	10	10	14,0	-	0,42	7,20	1,28	4,90	0,04	0,03	7,30	6	0,28	1,32	1	4,8	4,5	2,9
This study average	40,53	IS	0,90	calibrate	0,022	10,18	54,75	50,35	0,80	19,99	57,28	54,04	45,19	0,20	2,07	49,59	27,89	51,18	37,38	37,16	33,44	59,37	61,38
Std dev (n=12)	0,39	-	0,55	-	0,010	4,05	13,92	9,65	0,33	1,82	3,43	3,65	7,39	0,52	4,49	5,09	11,00	6,57	4,10	2,29	3,11	6,99	10,17
GSE-1g-A																							
Working values	n.a.	9,87	380	0,04	0,035	460	260	n.a.	390	n.a.	n.a.	n.a.	200	160	280	450	n.a.	n.a.	120	30	7	378	320
Std dev	-	0,23	20	0,003	0,002	10	90	-	30	-	-	-	20	50	50	110	-	-	-	-	-	12	30
This study average	0,11	IS	263,4	0,04	0,035	318,30	291,50	80,81	347,93	0,07	32,88	108,08	144,59	185,23	282,50	317,33	177,33	0,07	13,40	12,09	7,81	313,88	254,14
Std dev (n=8)	0,03	-	6,1	0,002	0,001	8,40	43,59	25,76	18,20	0,02	5,57	19,25	2,41	55,30	13,55	19,16	31,29	0,08	4,19	7,26	0,54	9,11	22,48

Table 4.1: Reference materials used to calibrate the LA-ICP-MS. Certif. = Value on the certificate; std dev = standard deviation; IS = internal standard; n.a. = not available.

Platinum-group minerals were identified at the CURAL laboratory, Université du Québec a Chicoutimi (UQAC), using a scanning electron microprobe (JSM-6480LV) system equipped with an energy dispersive X-ray spectrometer. Back scattered electron imaging and semi-quantitative analysis were carried out and data were treated with INCA software. Voltage was fixed at 20keV, current from ~1pA to 1µA and beam size less than 0.2 µm. Sulfides and metal standards (ASTIMEX) were used for scanning electron microprobe calibration (nickel silicide, antimony telluride, gallium arsenide, bismuth selenide, sphalerite, pentlandite, marcasite, galena and cuprite). Scanning electron microprobe results are reported in Table 4.3.

4.6 RESULTS

4.6.1 PETROGRAPHY

The modal percent of sulfide minerals present, their proportions and their morphology varies with their location and the type of host rock. The Bedded Pyrrhotite Unit samples from outside the contact aureole, ~ 3 km far from the contact with the Duluth Complex, are the least metamorphosed black shales. These samples contain 2-3 modal % sulfides consisting of very fine grained (<0.02 mm) pyrite that forms thin (<0.5 mm) sulfide beds and a small amount (<5 modal %) of pyrrhotite and chalcopyrite that are also found as sulfide beds (~100 µm) (Fig. 4.3a). The more metamorphosed samples of Bedded Pyrrhotite Unit in the contact aureole contain ~15 % sulfides in thin (3 to 10 mm) beds within a fine grained matrix of argillite. The sulfides consist of fine grained (0.1 to 0.5 mm) pyrrhotite (98 modal %) and chalcopyrite (<2 modal %) (Fig. 4.3b, Table 4.2).

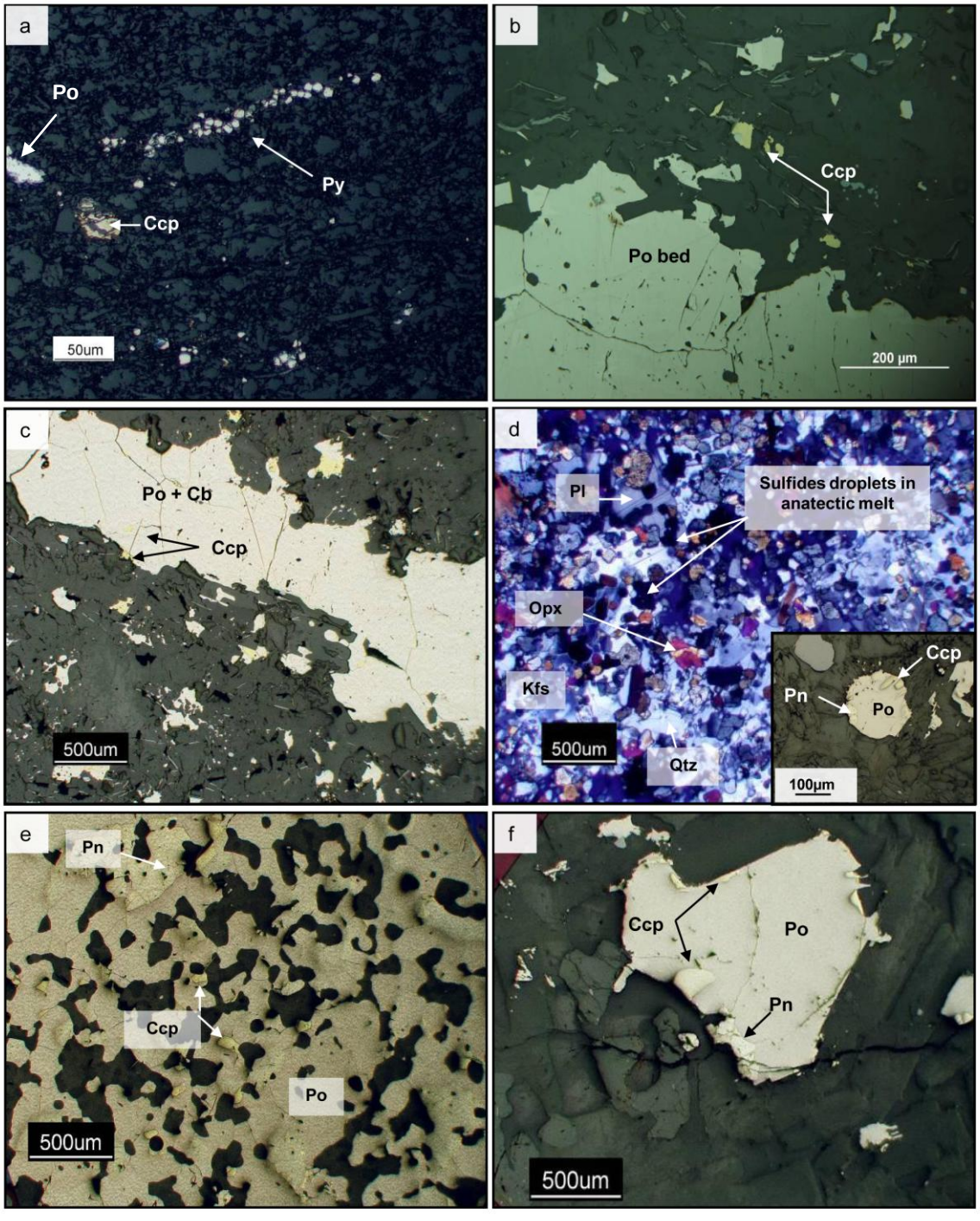
a
Po
Py
Ccp
50um
b
Ccp
Po bed
200 µm
c
Po + Cb
Ccp
500um
d
Pl
Sulfides droplets in anatectic melt
Opx
Kfs
500um
Qtz
Ccp
Pn
Po
100µm
e
Pn
Ccp
Po
500um
f
Ccp
Po
Pn
500um

Figure 4.3: Photomicrographs of sulfide textures of the Bedded Pyrrhotite Unit (BPU) from (a) outside and (b) inside the contact metamorphism aureole, from BPU xenoliths, massive sulfides and mafic magma surrounding the BPU xenoliths. a) Pyrite bed in the BPU from outside the contact aureole. b) Sulfide bed in the BPU from the contact aureole. c) Sulfide bed within a BPU xenolith. d) Partial melting texture of BPU xenolith. e) Massive sulfide surrounding BPU xenolith within the intrusion. f) Sulfide droplet within mafic magma (norite). Abbreviations: Silicates: Opx = Orthopyroxene; Pl = Plagioclase; Kfs = K-Feldspar; Qtz = Quartz. Sulfides: Ccp = Chalcopyrite; Cb = Cubanite; Po = Pyrrhotite; Pn = Pentlandite.

Sample	Rock type	Area tot sulf	Area tot	FCcp%	FPn%	FCbn%	FPo%	%Sulfide by area
DC-70	BPU contact aureole	1.6 mm^2	8,6 mm^2	2,50%	0,00%	0,00%	97,50%	18,0%
A4-15-01	BPU contact aureole	1.13 mm^2	8,6 mm^2	1,50%	0,00%	0,00%	98,50%	13,2%
Average	*BPU contact aureole*			*1,9%*	*0,0%*	*0,0%*	*98,0%*	*15,6%*
B1-384-35	BPU xenolith	2.6 mm^2	8,6 mm^2	3,1%	1,0%	8,0%	88,0%	30,1%
B1-384-19	BPU xenolith	1.35 mm^2	8,6 mm^2	6,6%	0,0%	6,5%	86,8%	15,7%
B1-384-26	BPU xenolith	3.7 mm^2	8,6 mm^2	10,3%	4,8%	13,0%	72,0%	42,8%
B1-384-34	BPU xenolith	1.6 mm^2	8,6 mm^2	14,9%	0,6%	11,0%	73,0%	18,0%
B1-384-14	BPU xenolith	2.5 mm^2	8,6 mm^2	7,3%	14,2%	10,0%	68,0%	28,7%
B1-384-33	BPU xenolith	2.9 mm^2	8,6 mm^2	5,8%	2,1%	11,0%	81,0%	33,0%
B1-384-26	BPU xenolith	0.9 mm^2	8,6 mm^2	6,7%	6,8%	16,3%	70,2%	10,6%
Average	*BPU xenoliths*			*8,0%*	*4,0%*	*11,0%*	*77,0%*	*26,0%*

Table 4.2: Summary of results of image analysis of base metal sulfides Bedded Pyrrhotite Unit xenoliths from the Mesaba deposit. Abbreviations: Ccp=chalcopyrite; Pn= pentlandite; Cbn=cubanite; Po=pyrrhotite; BPU=Bedded Pyrrhotite Unit. F(x)%=proportion of the phase x in sulfides or silicates phases; Area tot = Total area of the image; Area tot sulf = Total area of sulfides.

The petrographic evidence that the xenoliths have experienced partial melting are: quartz and feldspar patches, or minerals films filling space between the matrix grains that are interpreted as pseudomorphing former pockets of anatectic melt (Fig. 4.3d). Sulfides minerals occur in two forms. There are sulfide beds similar in width to the beds in the Bedded Pyrrhotite Unit of the contact aureole (Fig. 4.3c), and there are rounded sulfides droplets (~0.1 mm diameter) within pockets of former anatectic melt (Fig. 4.3d). In addition to pyrrhotite (~77%) and chalcopyrite (~8%) the minerals cubanite (~11%) and pentlandite (~4%) are also present. There is a greater proportion of Cu-rich sulfides (~25 % chalcopyrite and cubanite) and pentlandite (2-15 %) than observed in the contact aureole (Table 4.2). The samples contain 10 to 30 modal % sulfides.

The proportions of sulfide minerals and the assemblage in the massive sulfide close to the xenoliths of Bedded Pyrrhotite Unit are similar to sulfide assemblage in the xenoliths (Fig. 4.3e). Pyrrhotite, cubanite, chalcopyrite and pentlandite make up respectively ~60 modal %, ~30 modal %, <5 modal % and <10 modal % of the sulfide assemblage.

The groundmass in the norites and gabbronorites contains disseminated droplets of sulfide (~100µm to 1mm) (Fig. 4.3f). Norites have the same sulfide assemblage as the Bedded Pyrrhotite Unit xenoliths, but with a slightly lower percentage of pentlandite (<5% modal) and cubanite (~5-10%), whereas the sulfide mineral assemblages in the gabbronorites contain more chalcopyrite, cubanite and pentlandite but less pyrrhotite (<20 %modal).

In our samples, platinum-group minerals were only found in gabbronorites from the basal magmatic units of the Duluth Complex. The platinum-group minerals were found; within base metal sulfide grains, at the rim of sulfide grains and filling fractures within the

sulfide minerals (Fig. 4.4a to f). A total of ten platinum-group mineral grains (<5µm) were identified in the disseminated sulfides (Table 4.3). The platinum-group minerals present are possibly solid solution of polarite (PdBi), paolivite (Pd_2Sn), zvyageintsevite (Pd_3Pb), and atokite (Pd_3Sn, Pt).

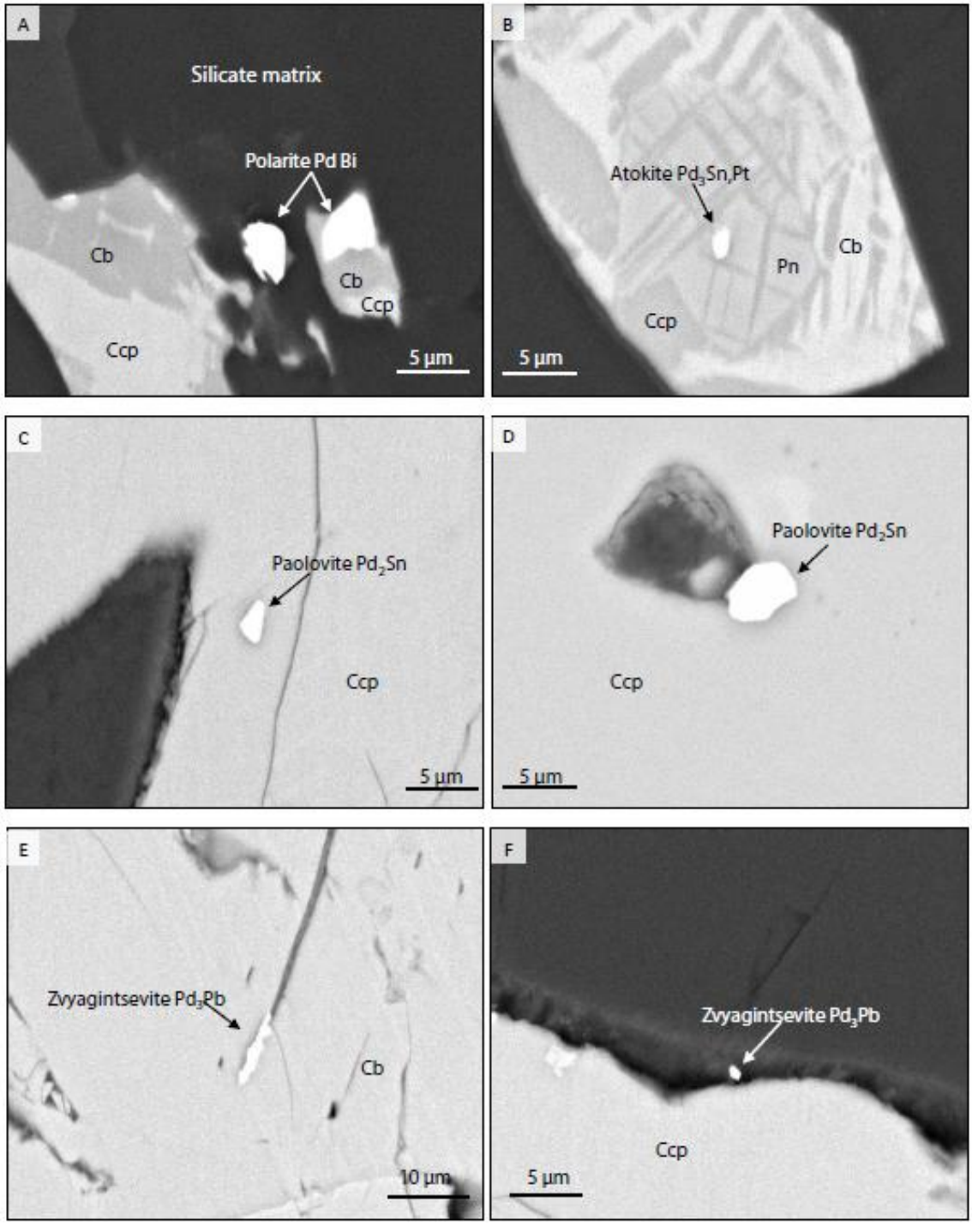
A
Silicate matrix
Polarite Pd Bi
Cb
Cb
Ccp
Ccp
5 µm
B
Atokite Pd3Sn,Pt
Pn
Cb
Ccp
5 µm
C
Paolovite Pd2Sn
Ccp
5 µm
D
Paolovite Pd2Sn
Ccp
5 µm
E
Zvyagintsevite Pd3Pb
Cb
10 µm
F
Zvyagintsevite Pd3Pb
Ccp
5 µm

Figure 4.4: Backscattered electron images of Platinum Group Minerals (PGM) hosted by chalcopyrite and cubanite sulfides from gabbronorites of the basal Unit I and II. a) Polarite (PdBi) grain in cubanite. b) Atokite (Pd_3Sn+Pt) grain in pentlandite and Cu-rich sulifdes. c) and d) Paolovite (Pd_2Sn) grains hosted by chalcopyrite. e) Zvyagintsevite (Pd_3Pb) filling a fracture in chalcopyrite. Zvyagintsevite grains fill fractures in chalcopyrite. f) Zvyagintsevite (Pd_3Pb) grain at the rim of a chalcopyrite grain. Abbreviations: Cb = Cubanite; Ccp = Chalcopyrite.

PGM	Host	Sample	Rock type	Magmatic Unit	Shape	Pd (wt%)	Pt (wt%)	Sn (wt%)	Pb (wt%)	As (wt%)	Bi (wt%)	Total (wt%)
Atokite	Ccp/Pn	DC-64	Gabbronorite	I/II	Eu	57	21	21	-	-	-	99
Paolivite	Ccp	B1-384-08	Gabbronorite	mid I	Eu	65	-	35	-	-	-	100
Paolivite	Ccp	B1-384-08	Gabbronorite	mid I	Eu	66	-	33	-	-	-	99
Paolivite	Ccp	B1-384-08	Gabbronorite	mid I	Sub	65	-	34	-	-	-	99
Paolivite	Ccp	DC-64	Gabbronorite	I/II	Eu	63	-	37	-	-	-	100
Polarite	Cb	DC-64	Gabbronorite	I/II	Sub	34	-	-	-	-	66	100
Polarite	Silicate	DC-64	Gabbronorite	I/II	Sub	37	-	-	8	-	55	100
Zyageintsevite	Silicate	DC-64	Gabbronorite	I/II	Eu	65	-	-	36	-	-	101
Zyageintsevite	Cb	DC-64	Gabbronorite	I/II	An	63	-	-	37	0,1	-	100
Zyageintsevite	Ccp	DC-64	Gabbronorite	I/II	Sub	65	-	-	35	0,1	-	100

Table 4.3: Platinum-group mineral compositions determined by energy dispersive X-ray spectroscopy. Abbreviations: Eu=Euhedral; Sub=Subeuhedral; An=Anhedral; PGE=Platinum-group elements; PGM=Platinum-group minerals; Ccp=Chalcopyrite; Cb=Cubanite; Pn=Pentlandite; mid=middle.

4.6.2 GEOCHEMISTRY

4.6.2.1 ELEMENTS CONCENTRATED IN PYRRHOTITE AND PENTLANDITE

Cobalt content provides a convenient way of separating the base metal sulfide minerals on bivariate plots such as Co versus Ni (Fig. 4.5a) because Co is present in all the minerals and has a low detection limit (Table 4.4 and Appendix 6). Cobalt concentrations are the highest in pentlandite ranging from 0.3 to 3 wt%. Cobalt concentrations in pentlandite from the xenoliths plot at the high end of this range. Pyrrhotite contains from 10 to 200 ppm Co, with the pyrrhotite from the Bedded Pyrrhotite Unit in the contact aureole having the highest contents. Pyrite from the Bedded Pyrrhotite Unit outside the contact aureole contains similar Co contents to pyrrhotite from the contact aureole. Chalcopyrite and cubanite from the mafic rocks generally contain the lowest concentration of Co ranging from 0.01 to 20 ppm, whereas chalcopyrites from xenoliths of the Bedded Pyrrhotite Unit and the Bedded Pyrrhotite Unit from outside the intrusion contain slightly more Co, from 1 to 100 ppm.

Nickel concentrations are lowest in chalcopyrite and cubanite from the mafic rocks and from the xenoliths of the Bedded Pyrrhotite Unit and range from ~10 to 150 ppm, (Fig. 4.5a, Table 4.4), whereas chalcopyrite from the Bedded Pyrrhotite Unit from outside the intrusion has higher Ni contents of ~ 1000 ppm. Pyrrhotite and pyrite are richer in Ni (~900 to 9000 ppm) and the Ni content in these minerals is similar for all the rock types. The tendency for the chalcopyrite from the sediments to be richer in Co and Ni could be the result of the absence or very low abundance of pentlandite in these rocks.

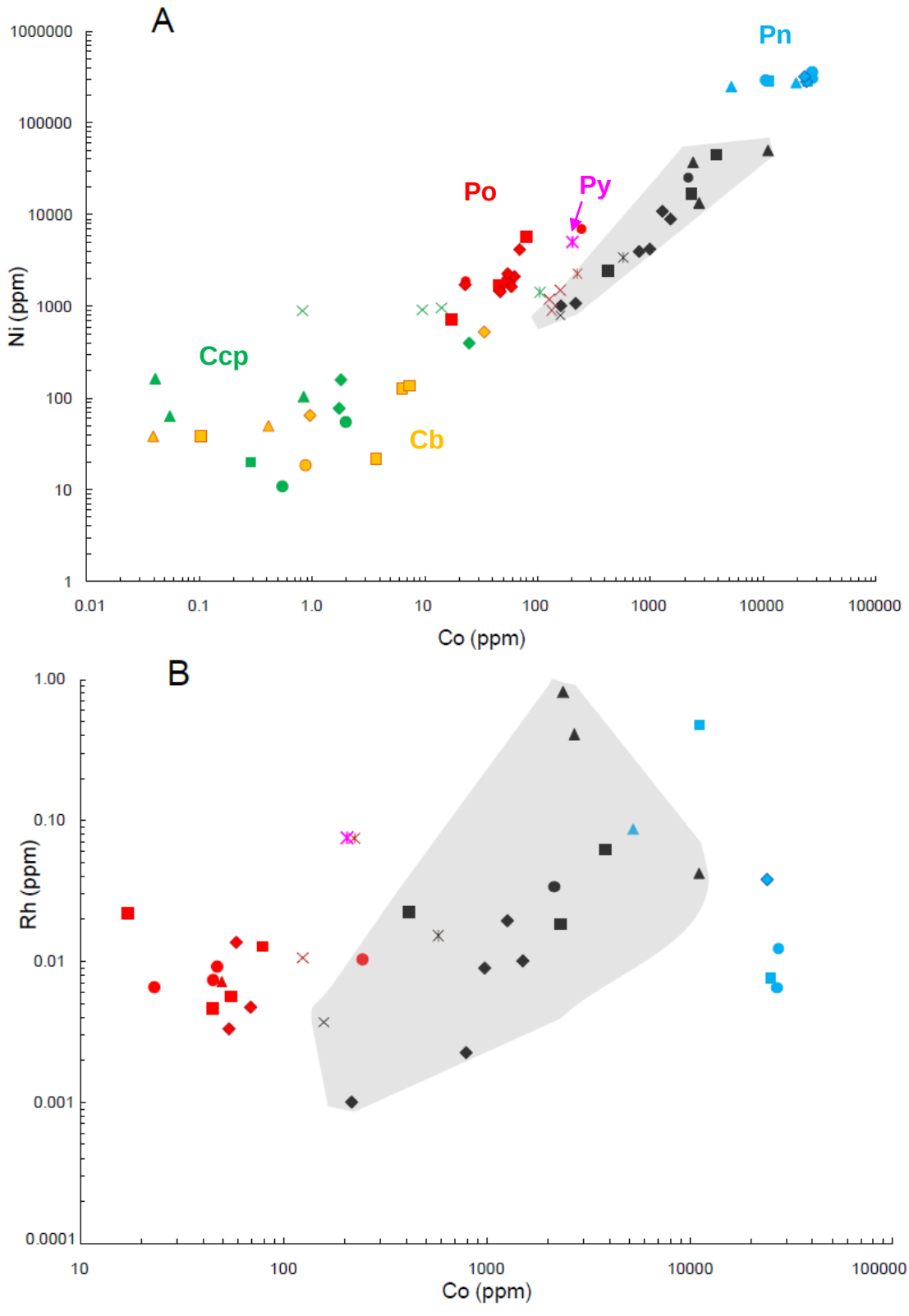
A
Pn
Po
Py
Ccp
Cb
Ni (ppm)
Co (ppm)
1000000
100000
10000
1000
100
10
1
0.01
0.1
1.0
10
100
1000
10000
100000
B
Rh (ppm)
Co (ppm)
1.00
0.10
0.01
0.001
0.0001
10
100
1000
10000
100000

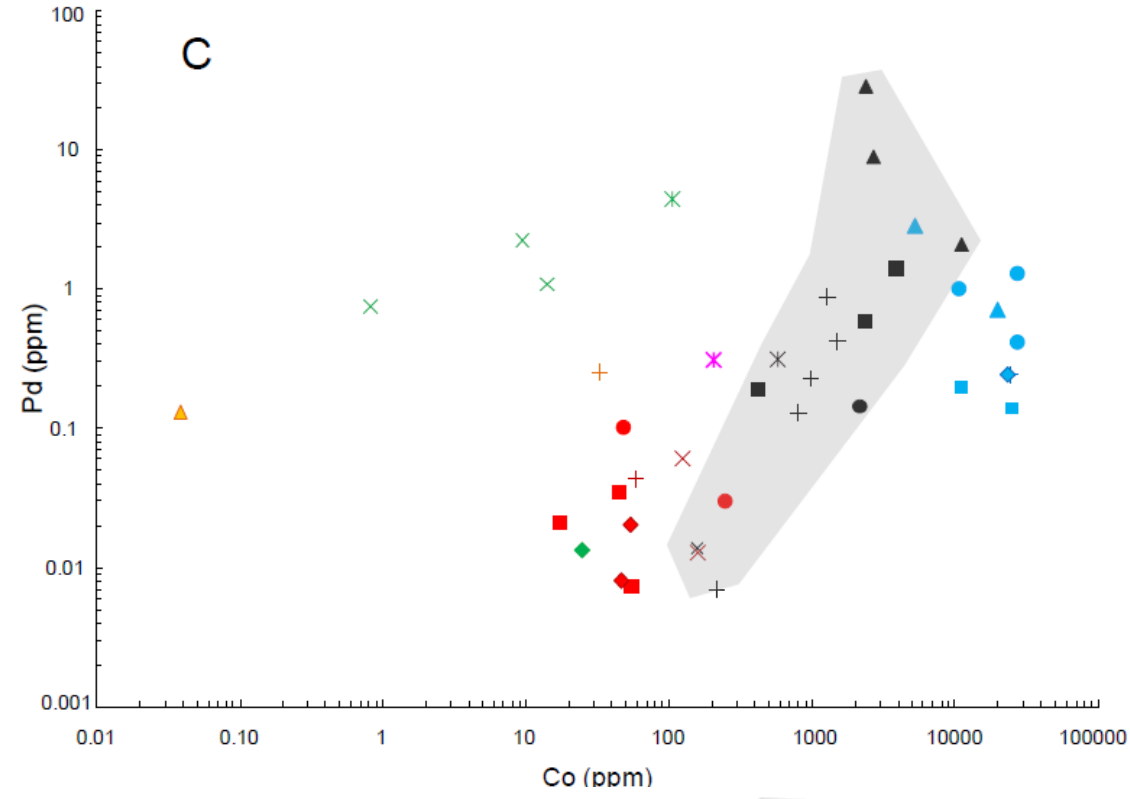
C
Pd (ppm)
100
10
1
0.1
0.01
0.001
0.01
0.10
1
10
100
1000
10000
100000
Co (ppm)

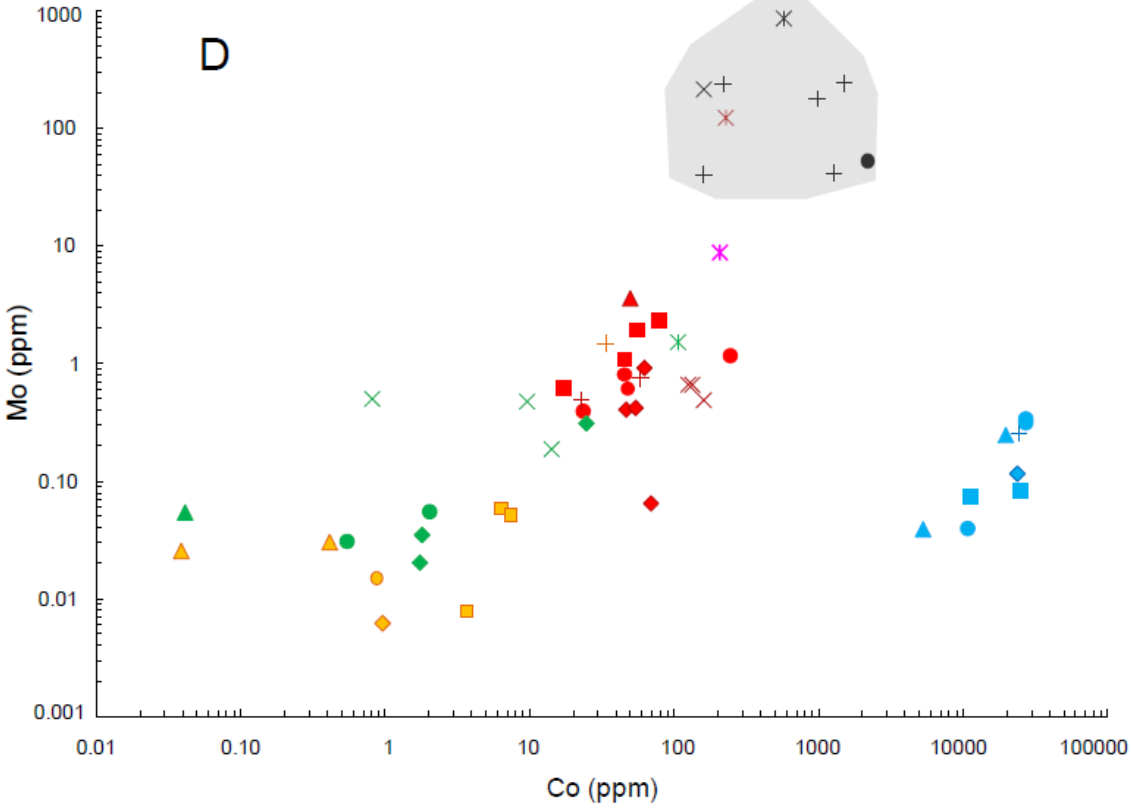
D
Mo (ppm)
1000
100
10
1
0.10
0.01
0.001
0.01
0.10
1
10
100
1000
10000
100000
Co (ppm)

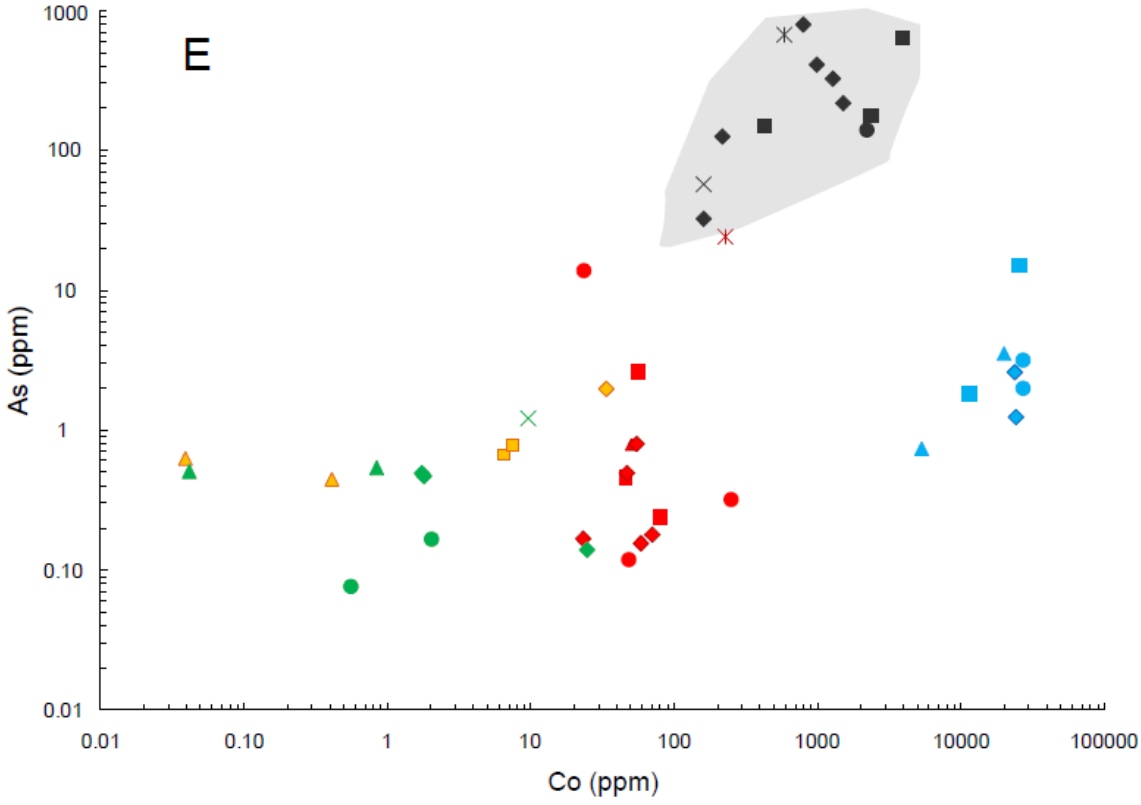

▲ Gabbronorites

■ Norites

● Massive sulfides

◆ BPU xenoliths

× BPU contact aureole

× BPU outside contact aureole

Figure 4.5: Plots of (a) Ni, (b) Rh, (c) Pd, (d) Mo and (e) As vs. Co in the Bedded Pyrrhotite Unit (BPU) rocks and the mafic rocks. Average Ni, Rh, Pd, Mo and As contents of sulfide minerals are compared to the sulfide component in the whole rock recalculated to 100 % sulfides. Field of the whole rock concentrations is shaded in grey. Abbreviations: BPU = Bedded Pyrrhotite Unit; Ccp = Chalcopyrite; Cb = Cubanite; Po = Pyrrhotite; Pn = Pentlandite.

n	Sulfide	Sample n°	Rock type	Sulfide texture	Co (ppm)	Ni (ppm)	Cu (ppm)	Zn (ppm)	As (ppm)	Se (ppm)	Mo (ppm)	Ru (ppm)	Rh (ppm)	Pd (ppm)	Ag (ppm)	Cd (ppm)	Sn (ppm)	Sb (ppm)	Te (ppm)	Os (ppm)	Ir (ppm)	Pt (ppm)	Au (ppm)	Pb (ppm)	Bi (ppm)
2	Ccp	LTV-7555	BPU outside c.a.	Sulfide bed	105	1421	299495	200	-	77,96	1,50	0,41	n.d.	4,45	282,78	1,32	0,04	6,71	-	0,004	0,019	-	-	40,29	-
2	Po	LTV-7555	BPU outside c.a.	Sulfide bed	226	2278	742	1097	24,31	141,49	122,79	n.d.	0,075	-	26,61	22,59	1,18	140,55	-	-	0,034	-	-	646,99	-
3	Py	LTV-7555	BPU outside c.a.	Sulfide bed	205	5024	673	317	-	129,88	8,69	n.d.	0,075	0,31	17,67	14,70	3,83	13,09	-	-	0,019	-	-	80,35	-
2	Ccp	A4-15-01	BPU c.a	Sulfide bed	0,8	899	380984	316	-	11,65	0,50	0,39	-	0,74	45,25	2,10	183,49	15,17	0,09	-	-	-	-	10,25	0,92
4	Ccp	A4-15-01	BPU c.a	Sulfide droplet IM	14	961	379544	304	-	17,28	0,18	0,38	-	1,08	62,44	1,53	224,17	4,01	-	-	0,021	-	-	16,13	-
1	Ccp	DC-70	BPU c.a	Sulfide bed	10	919	351162	350	1,22	13,21	0,48	0,20	-	2,22	129,63	1,95	74,86	6,33	0,40	-	-	-	-	31,65	1,70
2	Po	A4-15-01	BPU c.a	Sulfide droplet IM	126	1183	2,0	0,7	-	14,27	0,65	-	0,011	0,06	1,08	0,08	24,93	0,75	-	-	-	-	-	8,87	1,00
4	Po	A4-15-01	BPU c.a	Sulfide bed	133	900	4,0	1,0	-	14,71	0,65	0,06	-	-	0,86	-	0,11	1,68	-	-	-	-	-	4,22	0,33
3	Po	DC-70	BPU c.a	Sulfide bed	159	1490	6,0	0,8	-	14,54	0,49	-	-	0,01	0,17	0,03	0,18	-	-	-	-	-	-	3,32	1,52
1	Ccp	DC-69	BPU xenoliths	Sulfide droplet	25	396	292432	190	0,14	27,87	0,31	0,06	-	0,01	0,83	4,56	0,45	0,15	0,32	0,028	0,027	-	-	9,07	1,10
1	Ccp	DC-80	BPU xenoliths	Sulfide droplet	1,8	158	309777	593	0,47	54,10	0,03	0,08	-	-	2,08	16,13	22,97	0,07	12,20	-	-	-	-	5,72	0,47
3	Ccp	EC-07	BPU xenoliths	Sulfide droplet	1,7	78	306430	1238	0,49	38,74	0,02	0,08	-	-	3,38	38,91	8,93	0,46	4,06	-	0,003	-	0,049	15,64	1,01
8	Cb	B1-384-26	BPU xenoliths	Sulfide bed	33	527	217061	1163	1,97	30	1,5	0,15	-	0,25	10,0	8,39	4,33	0,02	7,0	-	-	-	0,02	14,09	1,59
1	Cb	B1-384-39	BPU xenoliths	Sulfide droplet	1,0	65	213157	32	-	32,22	0,01	0,20	-	-	5,19	4,28	0,32	-	1,56	-	-	-	-	5,14	-
5	Pn	B1-384-26	BPU xenoliths	Sulfide bed	24199	285486	84,9	12	1,23	23	0,3	-	0,04	0,24	1,0	0,05	0,42	0,39	1,8	0,02	-	-	0,01	4,35	1,74
2	Pn	DC-80	BPU xenoliths	Sulfide droplet	23541	319739	2,8	108	2,58	44,85	0,12	-	-	0,24	2,55	2,21	1,61	0,42	7,59		-	-	0,029	5,29	3,01
13	Po	B1-384-26	BPU xenoliths	Sulfide bed	58	1657	252,5	7	0,15	34	0,7	0,03	0,01	0,04	0,2	0,06	0,23	-	0,6	-	0,00	0,02	0,00	0,57	0,82
4	Po	B1-384-26	BPU xenoliths	Sulfide bed	46	1426	3,8	92	0,50	56	0,4	0,05	-	0,01	0,3	0,07	0,78	-	-	0,03	-	-	-	0,49	1,71
3	Po	DC-71	BPU xenoliths	Sulfide bed	23	1742	8,4	0	0,17	30	0,5	0,02	-	-	0,2	0,04	0,14	0,03	-	-	-	-	-	0,83	0,14
1	Po	B1-384-39	BPU xenoliths	Sulfide droplet	62	2092	1,2	0,1	-	26,24	0,92	0,13	-	-	0,30	-	-	-	-	0,037	-	-	-	0,17	-
1	Po	DC-69	BPU xenoliths	Sulfide droplet	69	4132	0,7	0,2	0,18	29,11	0,06	0,10	0,005	-	0,04	0,08	0,04	0,02	-	-	-	-	-	0,36	0,11
4	Po	DC-80	BPU xenoliths	Sulfide droplet	54	2252	0,6	0,7	0,81	38,97	0,42	0,03	0,003	0,02	0,09	0,01	0,10	0,03	-	-	-	-	-	0,58	0,24
1	Ccp	B1-384-39	Massive sulfides	Massive sulfides	0,5	11	307343	697	0,08	35,60	0,03	0,10	-	-	1,68	13,82	0,27	-	2,44	-	-	-	-	0,99	0,11
5	Ccp	DC-69	Massive sulfides	Massive sulfides	2,0	55	311135	275	0,17	32,80	0,06	0,08	-	-	0,49	11,37	3,83	0,03	3,72	-	-	-	0,006	6,03	0,30
2	Cb	B1-384-39	Massive sulfides	Massive sulfides	0,9	19	210688	3086	-	24,83	0,01	0,13	-	-	5,52	71,60	0,10	-	0,99	-	-	-	-	0,88	0,08
1	Pn	B1-384-26	Massive sulfides	Massive sulfides	26992	307041	2,2	0,29	1,99	38,10	0,31	-	0,007	0,41	1,10	0,01	0,40	-	0,33	-	-	-	-	1,42	1,37
1	Pn	B1-384-39	Massive sulfides	Massive sulfides	10618	294668	1,3	0,32	-	18,79	0,04	-	-	1,00	1,76	0,01	0,01	-	-	-	-	-	-	0,07	-
3	Pn	DC-69	Massive sulfides	Massive sulfides	27209	363153	10,7	0,71	3,20	25,42	0,34	-	0,012	1,30	0,39	0,03	0,04	0,13	-	-	-	-	0,007	1,79	0,32
3	Po	B1-384-26	Massive sulfides	Massive sulfides	45	1587	18,8	0,97	-	51,42	0,81	0,06	0,007	-	0,50	0,05	0,21	-	0,62	0,030	-	-	-	0,67	1,76
6	Po	B1-384-39	Massive sulfides	Massive sulfides	48	1640	4,5	0,33	0,12	25,46	0,61	0,12	0,009	0,10	0,23	0,04	0,05	-	-	0,036	-	-	0,014	0,26	0,06
2	Po	DC-69	Massive sulfides	Massive sulfides	247	6878	9,6	0,21	0,32	27,74	1,17	0,23	0,010	0,03	0,11	0,02	0,04	0,03	-	-	-	-	-	0,39	0,09
1	Po	DC-71	Massive sulfides	Massive sulfides	23	1852	223	3,68	13,96	29,23	0,39	0,01	0,006	-	0,24	0,05	0,13	-	-	-	-	-	-	1,40	0,13
3	Ccp	B1-384-12	Norite	Sulfide droplet	0,3	20	316269	270	-	66,41	-	0,29	-	-	5,88	18,39	8,35	-	4,17	-	-	-	-	2,45	1,52
5	Cb	B1-384-12	Norite	Sulfide droplet	3,7	21	219988	1878	-	72,05	0,01	0,22	-	-	44,28	104,85	5,01	-	6,39	-	-	-	-	9,93	1,06
2	Cb	B1-384-13	Norite	Sulfide droplet	6,3	126	222128	-	0,67	81,11	0,06	0,26	-	-	7,44	9,53	4,22	-	14,01	-	-	-	-	17,74	0,11
3	Cb	B1-384-16	Norite	Sulfide droplet	7,4	137	222622	-	0,79	60,44	0,05	0,23	-	-	11,74	27,98	2,48	-	14,64	-	-	-	-	11,84	0,43
3	Cb	B1-384-21	Norite	Sulfide droplet	0,1	39	221291	-	-	55,53	-	0,26	-	-	6,53	6,99	1,86	-	1,82	-	-	-	-	26,34	0,26
1	Pn	B1-384-13	Norite	Sulfide droplet	25136	281318	27	-	14,98	65,45	0,08	-	0,007	0,14	11,23	63,49	0,32	0,45	18,69	0,026	-	-	-	10,32	1,79
3	Pn	B1-384-21	Norite	Sulfide droplet	11233	290652	4906	-	1,83	40,09	0,07	-	0,475	0,20	6,63	0,09	1,75	-	1,56	0,031	-	-	-	19,46	0,13
5	Po	B1-384-13	Norite	Sulfide droplet	55	1992	8	-	2,66	64,45	1,89	0,05	0,006	0,01	0,24	0,33	0,06	-	-	0,038	-	-	-	0,31	0,32
5	Po	B1-384-16	Norite	Sulfide droplet	45	1708	14	-	0,46	46,64	1,07	0,05	0,005	0,03	0,33	0,05	0,07	-	-	-	-	-	-	0,46	0,63
4	Po	B1-384-21	Norite	Sulfide droplet	17	726	94	-	-	45,22	0,61	0,09	0,022	0,02	0,59	0,08	0,32	-	-	0,065	-	-	-	0,40	0,38
1	Po	EC-07	Norite	Sulfide droplet	79	5778	11	1,0	0,24	38,27	2,31	0,03	0,013	-	0,17	0,07	0,22	-	-	0,005	0,005	-	-	1,48	0,13
2	Ccp	B1-384-04B	Gabbronorite	Sulfide droplet	0,8	105	324992	-	0,54	38,22	-	0,35	-	-	2,39	20,53	13,83	-	3,99	-	-	-	-	3,01	-
2	Ccp	B1-384-05	Gabbronorite	Sulfide droplet	0,04	165	333361	-	0,51	106,35	0,05	0,38	-	-	5,40	3,57	19,92	-	1,58	-	-	-	-	4,46	-
2	Ccp	B1-384-08	Gabbronorite	Sulfide droplet	0,06	64	331231	-	-	92,84	-	0,33	-	-	8,44	5,86	4,12	-	1,63	-	-	-	-	3,31	-
3	Cb	B1-384-04B	Gabbronorite	Sulfide droplet	0,41	50	223321	-	0,44	36,97	0,03	0,24	-	-	9,72	10,00	1,55	-	4,81	-	-	-	-	8,85	0,06
3	Cb	B1-384-08	Gabbronorite	Sulfide droplet	0,04	38	232991	-	0,62	96,54	0,03	0,22	-	0,13	20,90	22,59	0,21	-	1,77	-	-	-	-	22,44	-
1	Pn	B1-384-04B	Gabbronorite	Sulfide droplet	19796	274481	1,1	-	3,55	28,49	0,25	-	-	0,71	1,68	0,07	1,69	0,21	0,68	-	-	-	-	2,31	0,04
2	Pn	B1-384-08	Gabbronorite	Sulfide droplet	5245	248921	674	-	0,74	84,82	0,04	-	0,087	2,85	128,94	0,35	0,76	-	1,47	0,035	-	-	-	8,58	0,10
5	Po	B1-384-04B	Gabbronorite	Sulfide droplet	50	1898	8	-	0,79	32,59	3,58	0,07	0,007	-	0,29	0,05	0,08	0,02	0,20	-	-	-	-	0,41	0,43

Table 4.4: Averages of concentrations of chalcophile elements in base metal sulfide minerals from the Partridge River Intrusion determined by LA-ICP-MS. Abbreviations: n = number of analysis; Py = Pyrite; Po = Pyrrhotite; Pn = Pentlandite; Ccp = Chalcopyrite; Cb = Cubanite; BPU = Bedded Pyrrhotite Unit; c.a. = contact aureole; IM = Sulfides inside the anatectic melt.

Rhodium concentrations are the highest in pentlandite from the mafic rocks and range from 0.005 to 0.5 ppm (Fig. 4.5b). The pentlandites from the xenoliths are typically slightly poorer in Rh (~0.03 ppm). Pyrite from the sediments outside of the aureole contains some Rh (0.08 ppm). Pyrrhotites from all rock types contain a little Rh, between 0.003 and 0.02 ppm. Concentrations of Rh in chalcopyrite and cubanite could not be determined because of the Cu interference on Rh.

Pentlandite is the base metal sulfide which has the highest Pd concentrations; ranging from 0.1 to 3 ppm (Fig. 4.5c). Pyrite in the Bedded Pyrrhotite Unit from outside the contact aureole contains ~ 0.3 ppm Pd, values similar to those measured in pentlandite of other rock types. Pyrrhotite from all rock types contains a little Pd, from ~0.01 to 0.1 ppm. For most chalcopyrites and cubanites Pd concentrations are less than detection limit. However, the chalcopyrite from the contact aureole contains significant amounts of Pd (~0.8 to 2 ppm). The isotope ^{108}Pd was used to calculate the amount of Pd present, thus this value is not a influence by Cu interference. Furthermore, cadmium levels are low (<2 ppm) in these chalcopyrites, thus the ^{108}Cd interference is insignificant. Therefore, the high Pd content in these chalcopyrites is not thought to be an artefact.

Molybdenum concentrations are the highest in the pyrrhotite from the Bedded Pyrrhotite Unit from the contact aureole and in pyrite from the Bedded Pyrrhotite Unit outside the contact aureole, and lie between ~ 0.5 and 100 ppm (Fig. 4.5d). Pyrrhotite from the other rock types contains intermediate concentrations of Mo (~0.1 to 4 ppm). Pentlandite is generally poor in Mo with values from 0.02 to 0.3 ppm. Most of the cubanite and chalcopyrite are very poor in Mo (~0.01 to 0.1 ppm). However, an exception to this is the chalcopyrite from the contact aureole which is slightly richer at ~0.1 to 1 ppm.

Arsenic concentrations are generally highest in pentlandite and values are ~ 1 to 10 ppm, and the lowest in cubanite and chalcopyrite which have concentrations of only 0.08 to 2 ppm (Fig. 4.5e). Pyrrhotite generally contains intermediate values ranging from ~ 0.1 to 10 ppm. An exception to this is pyrrhotite from outside the contact aureole which have the highest As contents of ~ 20 ppm.

4.6.2.2 ELEMENTS CONCENTRATED IN CHALCOPYRITE AND CUBANITE

Some elements, Cu, Zn, Ag, Sn, Cd and to a lesser extent Pb and Sb are concentrated in chalcopyrite and cubanite. Copper concentrations are high in some igneous pentlandites at ~0.1 to 1 wt%, however, most pentlandites and pyrrhotites contain little Cu (0.3 to 200 ppm) (Fig. 4.6a, Table 4.4 and Appendix 6). Pyrite is relatively rich in Cu with values from 200 to 1500 ppm. The tendency for the pyrite and pyrrhotite from outside the contact aureole to be richer in trace elements than the other pyrrhotites is evident for most of the trace elements.

Zinc contents in the chalcopyrite and cubanite are between 30 and 3000 ppm (Fig 4.6b). For most of the igneous pentlandites, Zn is present at concentrations less than the detection limits, whereas the pentlandites in xenoliths do contain some Zn (~100 ppm). Zinc concentrations in pyrrhotite from all rock types are low; from 0.1 to 10 ppm. An exception to this is the pyrrhotite and pyrite from the Bedded Pyrrhotite Unit from outside the contact aureole, these have Zn levels similar to those in the chalcopyrite.

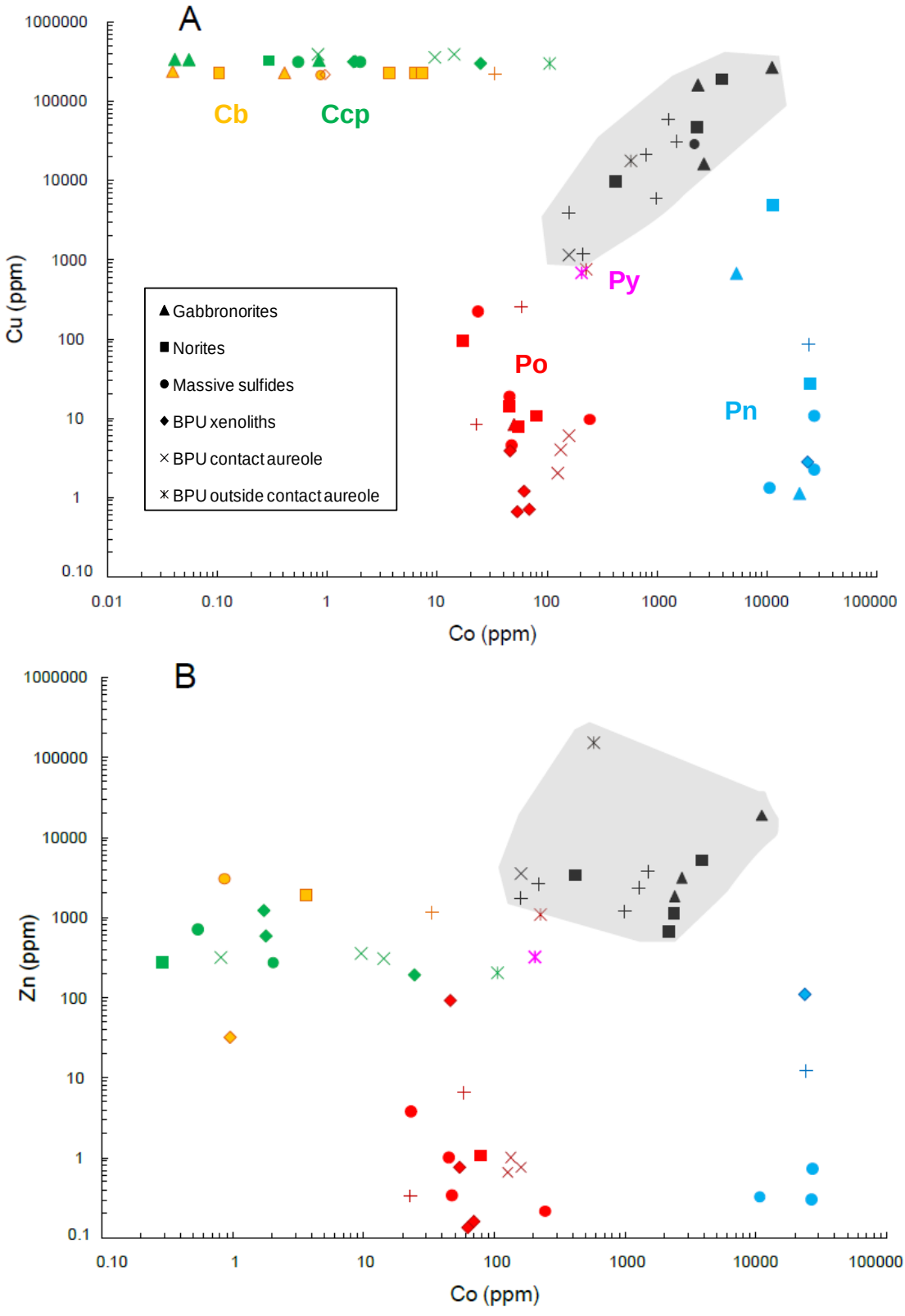
A
Cb
Ccp
Py
Po
Pn
Gabbronorites
Norites
Massive sulfides
BPU xenoliths
BPU contact aureole
BPU outside contact aureole
Cu (ppm)
Co (ppm)
1000000
100000
10000
1000
100
10
1
0.10
0.01
0.10
1
10
100
1000
10000
100000
B
Zn (ppm)
Co (ppm)
1000000
100000
10000
1000
100
10
1
0.1
0.10
1
10
100
1000
10000
100000

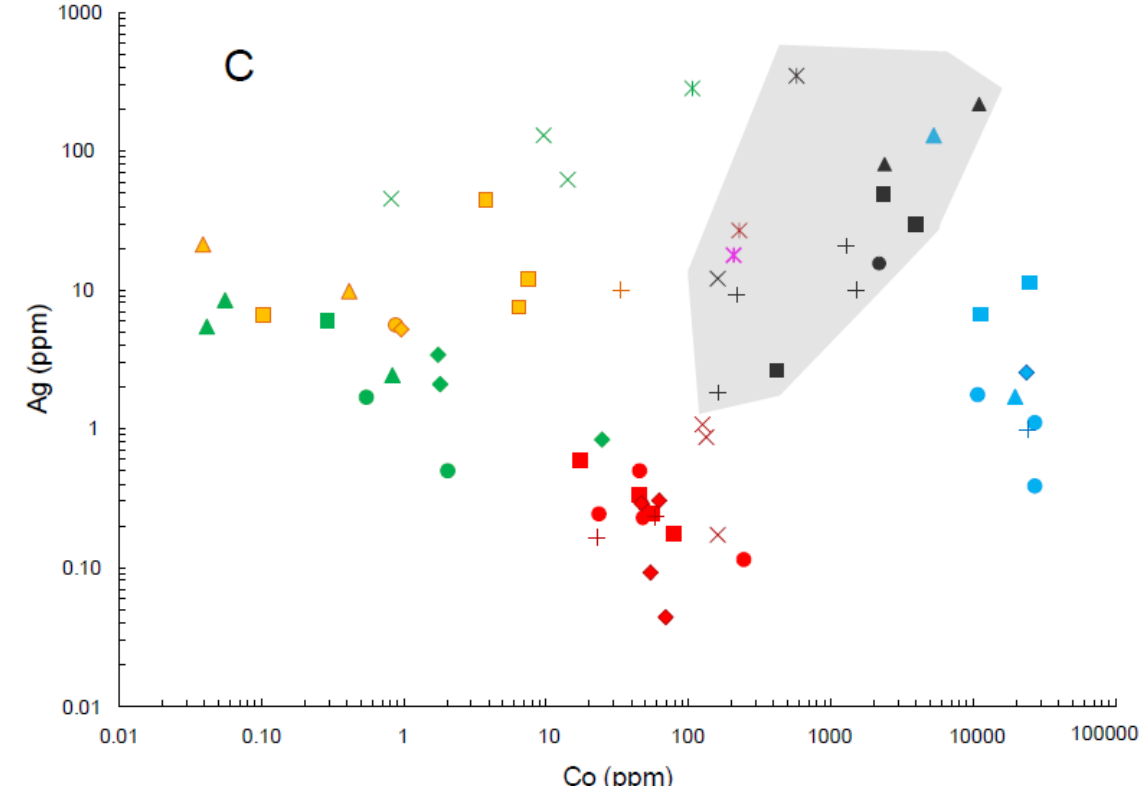
C
Ag (ppm)
Co (ppm)
1000
100
10
1
0.10
0.01
0.01
0.10
1
10
100
1000
10000
100000

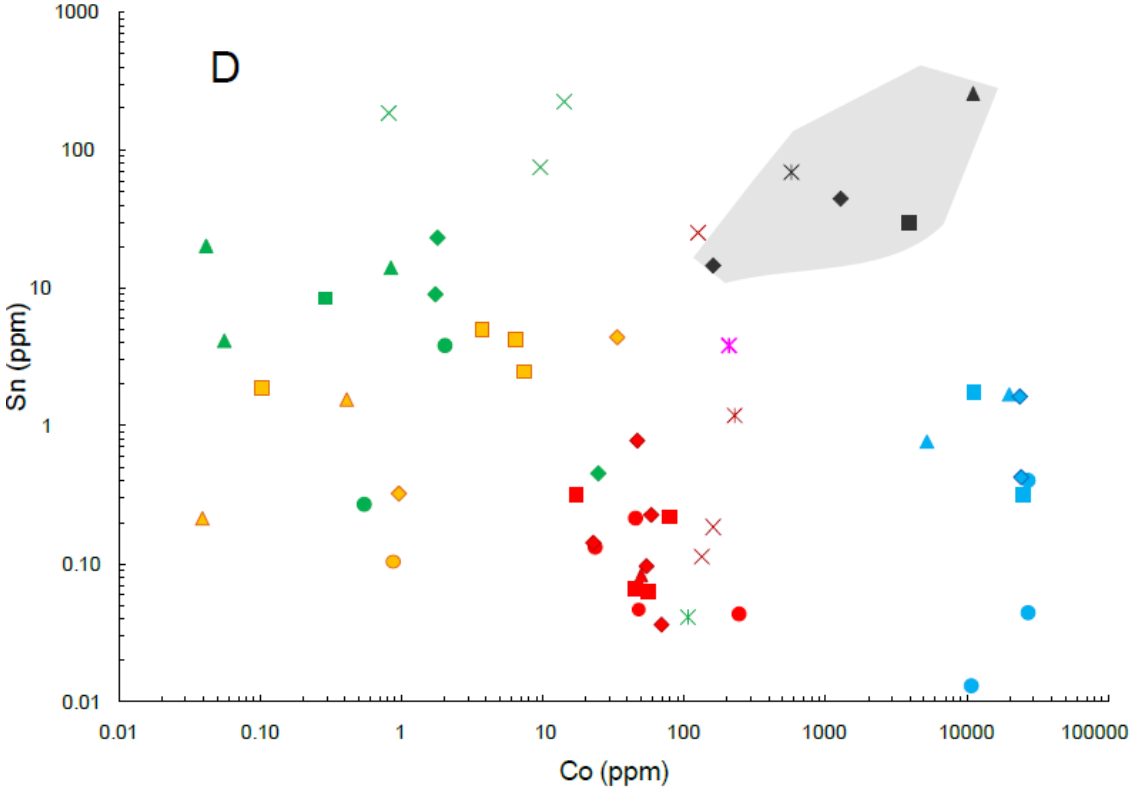
D
Sn (ppm)
Co (ppm)
1000
100
10
1
0.10
0.01
0.01
0.10
1
10
100
1000
10000
100000

Figure 4.6: Plots of (a) Cu, (b) Zn, (c) Ag and (d) Sn vs. Co in the Bedded Pyrrhotite Unit (BPU) rocks and the mafic rocks. Averages Cu, Zn, Ag and Sn content of sulfide minerals are compared to the sulfide component in the whole rock recalculated to 100 % sulfides. Field of the whole rock concentrations is shaded in grey. Abbreviations: BPU = Bedded Pyrrhotite Unit; Ccp = Chalcopyrite; Cb = Cubanite; Po = Pyrrhotite; Pn = Pentlandite.

The concentrations of Ag and Sn are the highest in chalcopyrite from the rocks inside and outside the intrusion, respectively 40 to 300 ppm and 80 to 200 ppm (Fig. 4.6c and d). Silver and Sn concentrations in chalcopyrite and cubanite from the mafic rocks are at intermediate levels; respectively in the 1 to 30 ppm and 0.1 to 20 ppm range. The chalcopyrite from the Bedded Pyrrhotite Unit xenoliths contains low levels of Ag (0.8 to 2 ppm), whereas the cubanite is notably richer (~5 ppm Ag). Pentlandite contains slightly lower Ag and Sn contents than chalcopyrite, or cubanite, generally ~0.3 to 10 ppm and ~0.02 to 2 ppm respectively. The pentlandite in the xenoliths contains less Ag and Sn than the pentlandite from the mafic rocks. Most of the pyrrhotites contain less Ag or Sn (0.03 to 2 ppm) than the other minerals. However, pyrrhotite and pyrite from outside the contact aureole are an exception to this, and contain high Ag and Sn levels (respectively ~ 10 to 30 ppm and ~ 5 to 20 ppm).

Lead concentrations are generally higher in the chalcopyrite and cubanite (~1 to 40 ppm) from the mafic rocks and xenoliths than in the pyrrhotite (~ 0.1 to 2 ppm) and the pentlandite (~ 1 to 10 ppm) regardless of the rock type. Pyrrhotite and pyrite from the contact aureole and from outside the contact aureole have the highest Pb contents at ~100 to 1000 ppm (Fig. 4.7a). Pentlandite contains intermediate levels of Pb with values between ~1 and 10 ppm.

In contrast to Ag, Sn and Pb, the Cd concentrations are lower in the chalcopyrite from the contact aureole (~ 1 to 2 ppm) than in the mafic rocks (~10 to100 ppm) (Fig. 4.7b). Both pyrrhotite and pentlandite generally have similar Cd contents ranging from 0.01 to 0.3 ppm. Pyrite and pyrrhotite of the Bedded Pyrrhotite Unit from outside the contact

aureole are generally richer in Cd than pyrrhotite and pentlandite in the other rock types, and have similar Cd contents to those in the chalcopyrite (~ 10 to 30 ppm).

Antinomy concentrations are the highest in the chalcopyrite from the Bedded Pyrrhotite Unit of the contact aureole and in the pyrite and pyrrhotite from outside the contact aureole (~10-100 ppm) (Fig. 4.7c). All the base metal sulfides from the xenoliths have very low Sb concentrations generally around 0.03 to 1 ppm. The concentrations of Sb in base metal sulfides from the mafic rocks are less than detection levels (0.02 ppm).

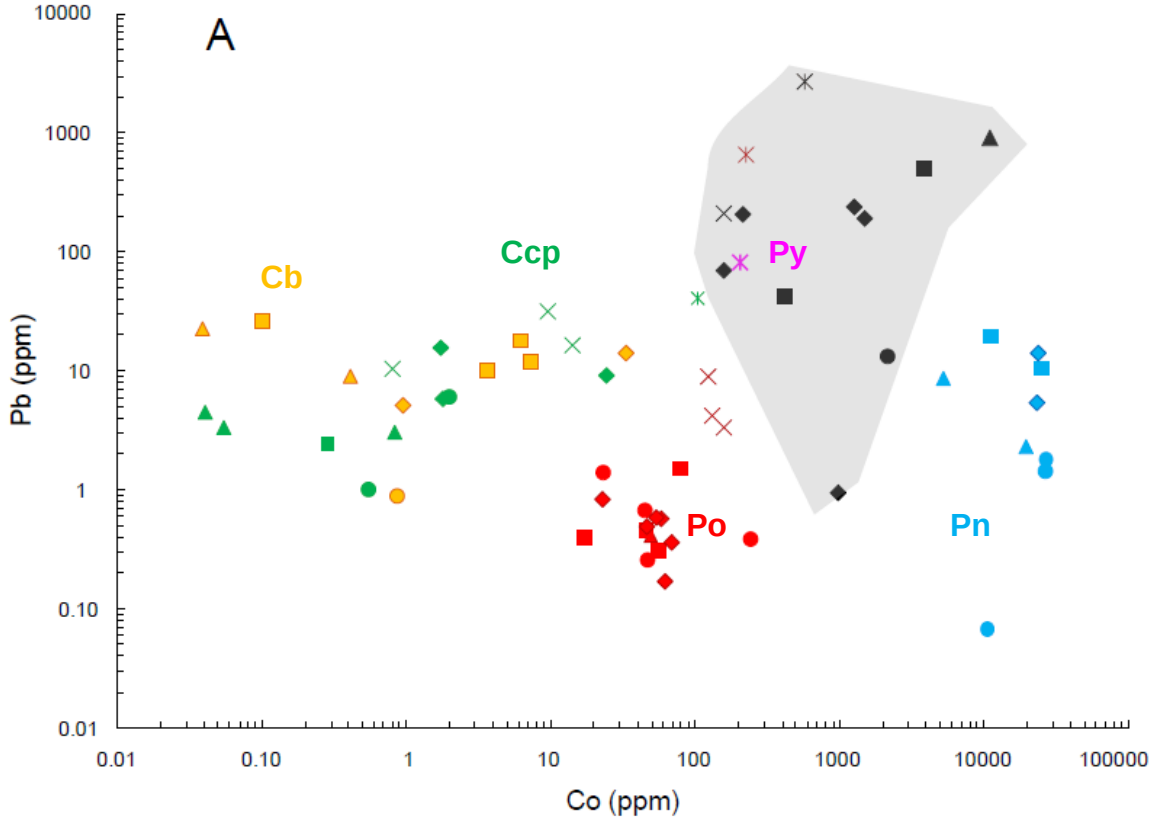
A
Cb
Ccp
Py
Po
Pn
Pb (ppm)
Co (ppm)
10000
1000
100
10
1
0.10
0.01
0.01
0.10
1
10
100
1000
10000
100000

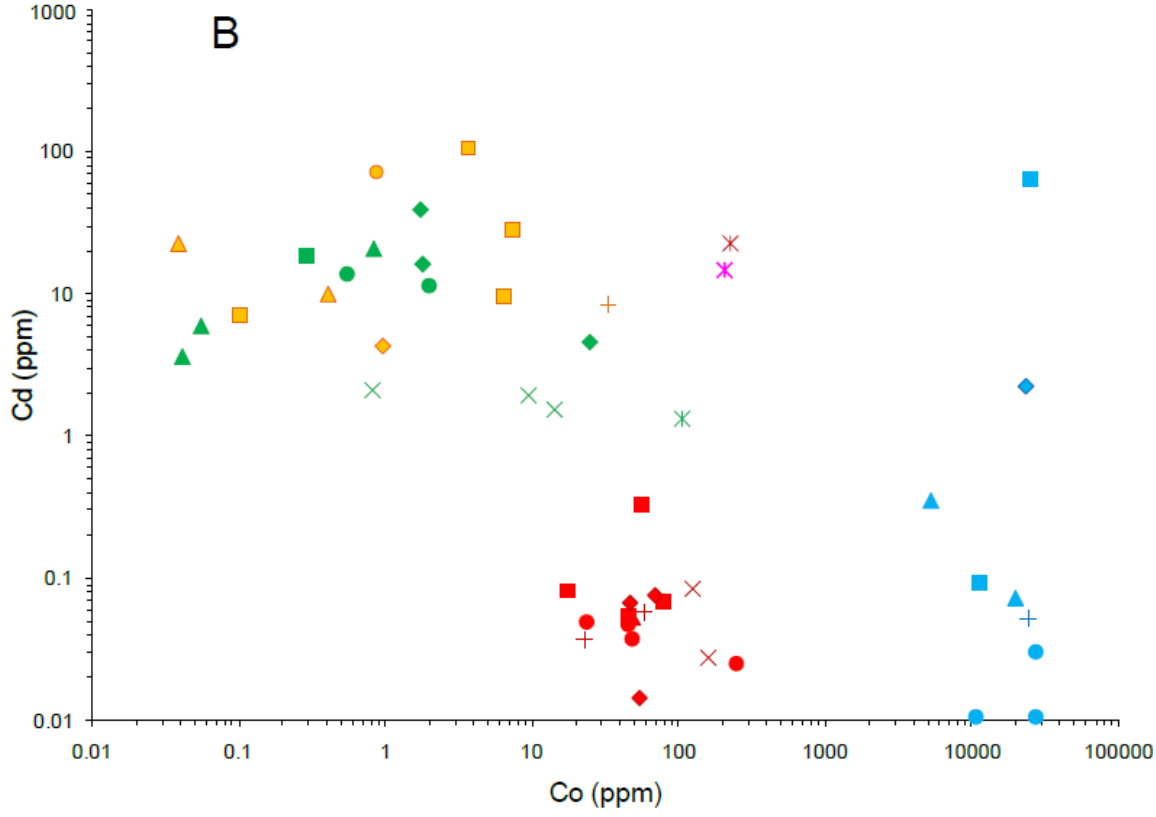
B
Cd (ppm)
Co (ppm)
1000
100
10
1
0.1
0.01
0.01
0.1
1
10
100
1000
10000
100000

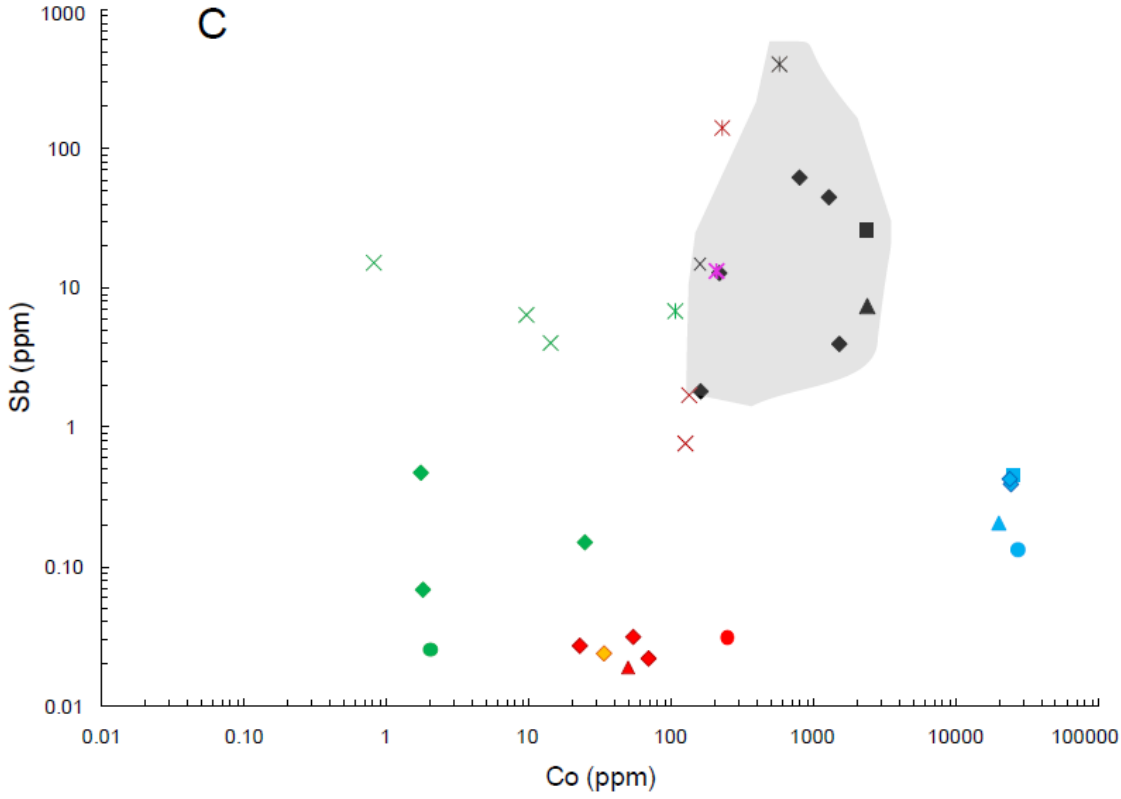

▲ Gabbronorites

■ Norites

● Massive sulfides

♦ BPU xenoliths

× BPU contact aureole

⁎ BPU outside contact aureole

Figure 4.7: Plots of (a) Pb, (b) Cd and (c) Sb vs. Co in the Bedded Pyrrhotite Unit (BPU) rocks and the mafic rocks. Average Pb, Cd and Sb contents of sulfide minerals are compared to the sulfide component in the whole rock recalculated to 100 % sulfides. Field of the whole rock concentrations is shaded in grey. Abbreviations: BPU = Bedded Pyrrhotite Unit; Ccp = Chalcopyrite; Cb = Cubanite; Po = Pyrrhotite; Pn = Pentlandite.

4.6.2.3 ELEMENTS PRESENT IN ALL BASE METAL SULFIDES

Selenium, Te and Bi are present in approximately equal amounts in all the sulfide minerals (Fig. 4.8 a, b and c). The sulfides in the mafic rocks tend to be the richest in Se and Te (respectively 40 to 100 ppm and 1 to 20 ppm). The chalcopyrite and pyrrhotite in the contact aureole are the poorest in Se and Te (respectively, 10 to 20 ppm and below the detection limit). Exception is for pyrite and pyrrhotite in outside the contact aureole that have the highest Se contents (~ 100 to 200 ppm). Bismuth occurs in approximately equal amounts in all the sulfide minerals and concentrations are in the range of 0.1 to 5 ppm.

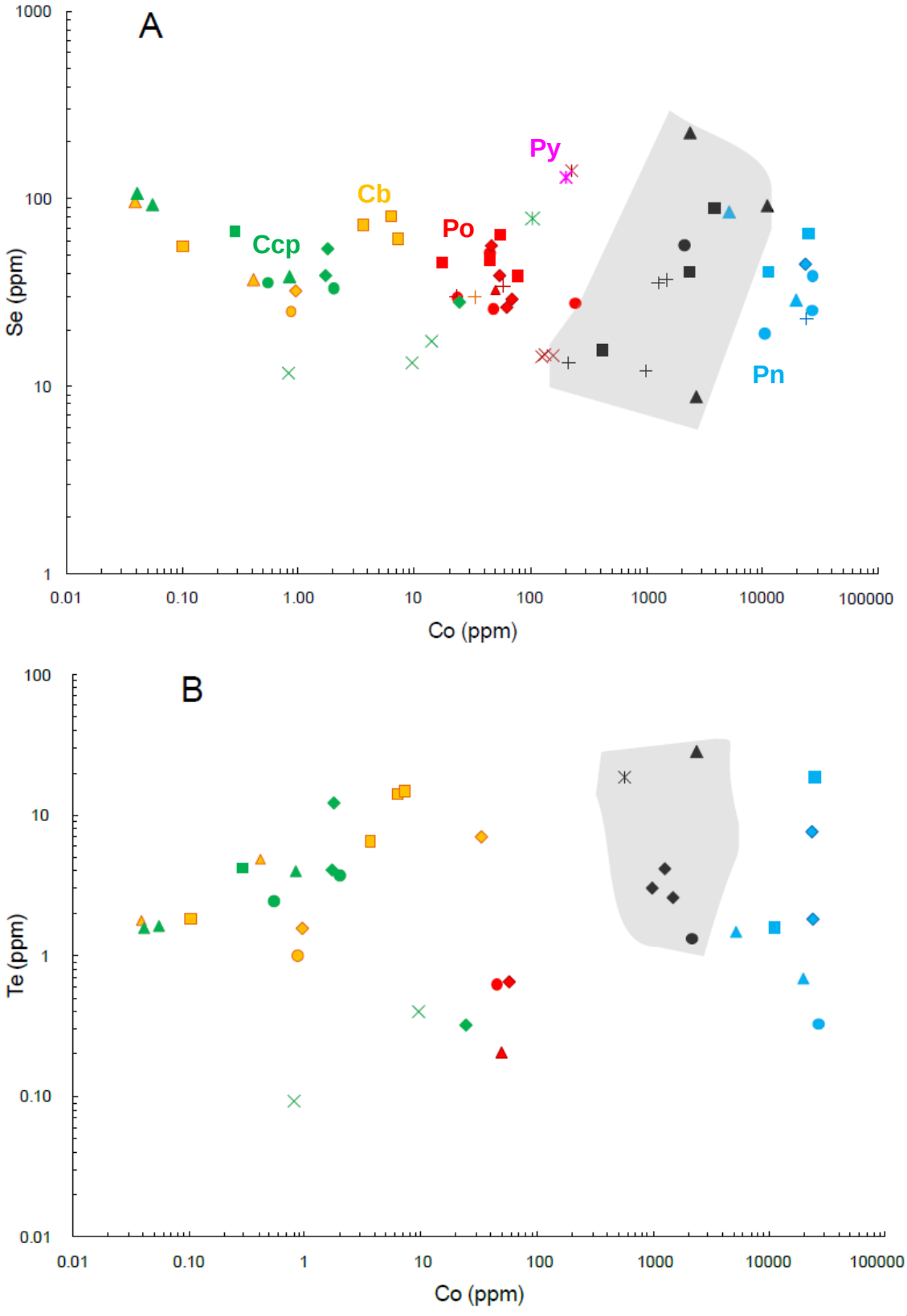
A
Se (ppm)
Co (ppm)
1000
100
10
1
0.01
0.10
1.00
10
100
1000
10000
100000
Py
Cb
Po
Ccp
Pn
B
Te (ppm)
Co (ppm)
100
10
1
0.10
0.01
0.01
0.10
1
10
100
1000
10000
100000

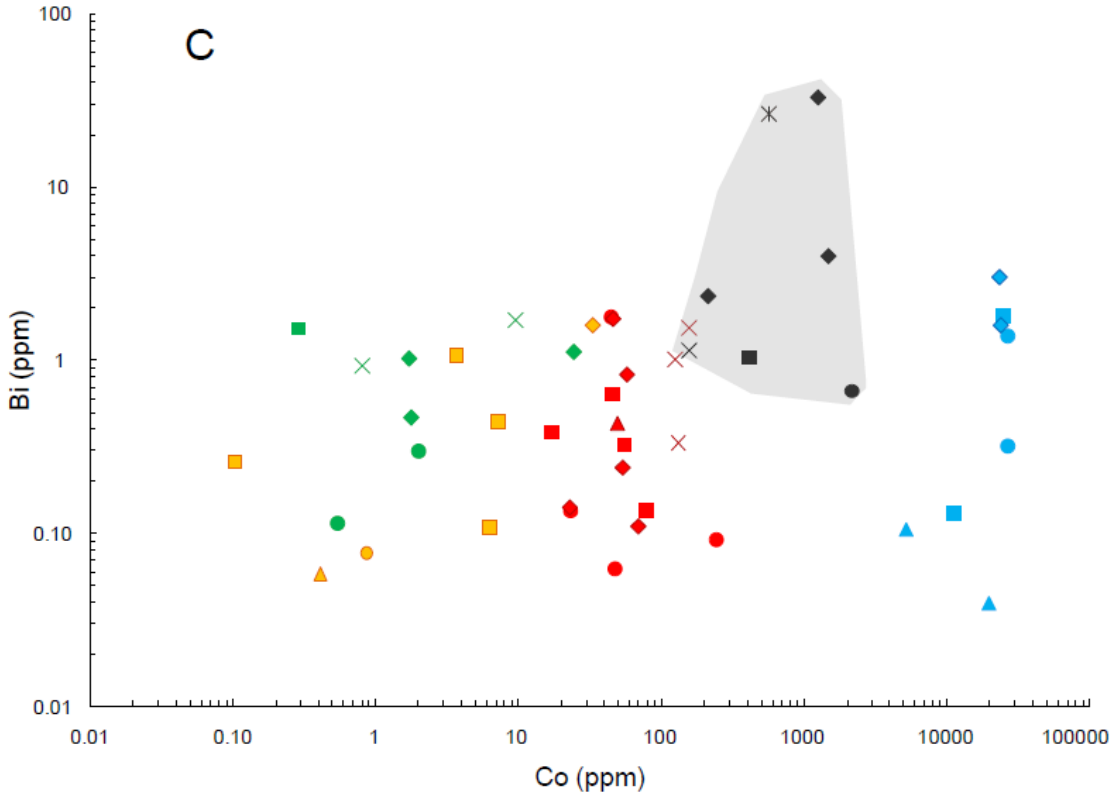

▲ Gabbronorites
■ Norites
● Massive sulfides
♦ BPU xenoliths
× BPU contact aureole
⚹ BPU outside contact aureole

Figure 4.8: Plots of (a) Se, (b) Te and (c) Bi vs. Co in the Bedded Pyrrhotite Unit (BPU) rocks and the mafic rocks. Average Se, Te and Bi contents of sulfide minerals are compared to the sulfide component in the whole rock recalculated to 100 % sulfides. Field of the whole rock concentrations is shaded in grey. Abbreviations: BPU = Bedded Pyrrhotite Unit; Ccp = Chalcopyrite; Cb = Cubanite; Po = Pyrrhotite; Pn = Pentlandite.

4.6.2.4 RECALCULATION TO 100 % SULFIDES

The concentrations of the elements in the whole rocks recalculated to 100 % sulfides (based on equation 1 in Barnes and Lightfoot, 2005) are shown on Figs. 4.5 to 4.8 and Tables 4.4 and 4.5. These concentrations are similar to the concentrations found in the base metal sulfide minerals obtained by LA-ICP-MS analysis for Ni, Cu, Co, Rh, Pd, Se and Te indicating that these elements are present mainly in the sulfides in these rocks. In contrast, Mo, As, Zn, Ag, Sn, Pb, Sb and Bi concentrations in the base metal sulfides are lower than in the whole rock recalculated to 100 % sulfides, which indicates that these elements must also be present in some other phases in the rocks. This interpretation is also support by whole rock analyses of metals and S in a previous study (Metal vs. S diagrams in Samalens et al., 2017). Note that whole rock data for Cd are not available.

Sample	Rock type	S (%)	Co (ppm)	Ni (ppm)	Cu (ppm)	Zn (ppm)	As (ppm)	Se (ppm)	Mo (ppm)	Ru (ppm)	Rh (ppm)	Pd (ppm)	Ag (ppm)	Sn (ppm)	Sb (ppm)	Te (ppm)	Os (ppm)	Ir (ppm)	Pt (ppm)	Au (ppm)	Pb (ppm)	Bi (ppm)
LTV-7555	BPU outside c.a.	1,09	17	100	510	4570	19,6	-	25,1	0,0002	0,0004	0,009	10,3	2,0	11,9	0,5	<0,159	0,0001	0,008	0,012	78,8	0,8
			577	3394	17312	155128	666,0	-	853,4	0,005	0,015	0,314	349,6	67,9	403,9	18,3	-	0,0020	0,273	0,414	2673,5	26,5
A4-15-01	BPU c.a.	6,53	28	140	200	620	10,0	-	37,0	0,0002	0,001	0,002	2,1	<1	2,6	-	0,00018	0,0001	0,009	0,016	37,0	0,2
			159	793	1133	3513	56,7	-	209,6	0,001	0,004	0,014	11,9	-	14,7	-	0,00102	0,0003	0,053	0,089	209,6	1,1
DC-69	BPU xenolith	5,90	157	670	930	190	65,2	1,9	28,4	0,008	0,001	0,036	< 0.5	< 1	< 0.2	0,5	0,00116	0,0008	0,013	0,282	0,2	<0,1
			985	4202	5832	1192	408,9	12,0	178,3	0,047	0,009	0,226	-	-	-	3,0	0,00727	0,0051	0,082	1,768	0,9	-
DC-70	BPU xenolith	4,45	26	130	140	320	15,2	1,6	28,0	<5.0	0,0001	0,001	1,1	< 1	1,5	<0,06	<1.5	0,0001	0,010	0,003	24,5	0,3
			216	1081	1164	2661	126,0	13,3	232,8	-	0,001	0,007	9,1	-	12,7	-	-	0,0005	0,081	0,023	203,9	2,3
DC-71	BPU xenolith	10,20	44	280	1060	480	9,0	0,1	11,0	-	-	-	0,5	4,0	0,5	-	-	-	-	0,228	19,0	<0,1
			160	1016	3845	1741	32,6	0,5	39,9	-	-	-	1,8	14,5	1,8	-	-	-	-	0,827	68,9	-
DC-80	BPU xenolith	1,15	25	123	646	-	24,6	-	-	<2.5	0,000	0,004	-	-	1,9	-	<0.6	0,0001	0,003	0,650	-	-
			791	3957	20784	-	791,5	-	-	-	0,002	0,129	-	-	61,5	-	-	0,0026	0,084	20,913	-	-
B1-384-26	BPU xenolith	3,74	152	900	3100	380	22,0	3,7	24,3	0,003	0,001	0,042	1,0	<1	0,4	0,3	<0.58	0,0002	0,009	0,016	19,0	0,4
			1504	8904	30668	3759	217,6	36,7	240,2	0,026	0,010	0,412	9,9	-	4,0	2,6	-	0,0023	0,092	0,160	188,1	4,0
EC-07-A	BPU xenolith	2,50	86	730	3965	160	22,0	2,4	2,8	0,001	0,001	0,058	1,4	3,0	3,0	0,3	0,00000	0,0003	0,023	0,027	15,9	2,2
			1273	10804	58683	2368	325,6	35,5	40,7	0,016	0,019	0,864	20,7	44,4	44,4	4,1	0,00000	0,0037	0,336	0,393	235,0	32,6
B1-384-39	Massive sulfide	16,30	960	12500	11200	290	61,6	24,5	23,0	0,039	0,015	0,063	6,8	<1	< 0.2	0,6	0,00852	0,0080	0,005	0,022	5,8	0,3
			2179	25423	28374	658	139,9	55,6	52,2	0,090	0,034	0,143	15,4	-	-	1,3	0,01934	0,0183	0,012	0,050	13,1	0,7
B1-384-12	Norite	1,27	134	1570	6500	180	22,0	3,1	<2	0,005	0,002	0,048	1,0	1,0	0,5	-	0,00062	0,0009	0,023	0,016	17,0	<0,1
			3904	45740	189370	5244	640,9	89,7	-	0,136	0,062	1,395	29,1	29,1	-	-	0,01806	0,0274	0,660	0,452	495,3	-
B1-384-13	Norite	1,72	108	786	2164	51	8,2	1,9	-	0,004	0,001	0,027	2,3	-	1,2	-	<0.42	0,0003	0,010	0,013	-	-
			2329	16908	46551	1104	176,4	40,2	-	0,095	0,019	0,583	48,8	-	25,8	-	-	0,0069	0,221	0,275	-	-
B1-384-16	Norite	7,17	81	470	1830	670	29,0	3,0	<2	0,005	0,004	0,037	0,5	< 1	< 0.2	-	0,00069	0,0021	0,009	0,033	8,0	0,2
			418	2425	9444	3457	149,7	15,4	-	0,026	0,022	0,190	2,6	-	-	-	0,00356	0,0108	0,048	0,172	41,3	1,0
EC-07-B	Norite	0,05	26	60	300	60	-	0,2	<2	-	-	0,001	0,6	< 1	0,4	-	-	-	0,001	-	-	0,2
			n.d.	n.d.	n.d.	n.d.	n.d.	n.d.	n.d.	n.d.	n.d.	n.d.	n.d.	n.d.	n.d.	n.d.	n.d.	n.d.	n.d.	n.d.	n.d.	n.d.
B1-384-04b	Gabbronorite	0,03	79	410	920	200	11,0	0,0	3,0	0,003	0,002	0,071	0,6	2,0	< 0.2	-	0,00027	0,0009	0,027	0,006	14,0	<0,1
			n.d.	n.d.	n.d.	n.d.	n.d.	n.d.	n.d.	n.d.	n.d.	n.d.	n.d.	n.d.	n.d.	n.d.	n.d.	n.d.	n.d.	n.d.	n.d.	n.d.	n.d.
B1-384-05	Gabbronorite	1,77	129	650	760	150	< 5	0,4	<2	0,018	0,019	0,427	< 0.5	< 1	< 0.2	<0.06	0,00267	0,0041	0,109	0,192	< 5	<0,1
			2697	13588	15887	3136	-	8,8	-	0,375	0,404	8,924	-	-	-	-	0,05581	0,0851	2,286	4,016	-	-
B1-384-08	Gabbronorite	1,80	116	1804	7718	89	<0.73	10,9	-	0,023	0,039	1,393	3,9	-	0,4	1,4	0,002	0,0102	0,422	0,170	-	-
			2383	37082	158648	1819	-	224,3	-	0,463	0,807	28,643	79,3	-	7,4	27,9	0,04111	0,2105	8,684	3,492	-	-
B1-384-21	Gabbronorite	0,29	87	390	2070	150	< 5	0,7	<2	<2.1	0,000	0,016	1,7	2,0	< 0.2	-	<.46	0,0002	0,005	0,008	7,0	<0,1
			11100	49759	264103	19138	-	91,9	-	-	0,042	2,100	216,9	255,2	-	-	-	0,0217	0,646	0,957	893,1	-

Table 4.5: Whole rock compositions of the Bedded Pyrrhotite Unit from the contact aureole, the Bedded Pyrrhotite Unit xenoliths, the norites and the gabbronorites of the Partridge River Intrusion. Abbreviations: BPU = Bedded Pyrrhotite Unit; c.a.= contact aureole; n.d.= not determined; - = not available.

4.6.2.5 LINE SCANS AND CHEMICAL MAPS

The very small size of pyrite grains (<15 µm) in Bedded Pyrrhotite Unit from outside the contact aureole made it difficult to obtain quantitative estimates of the trace element contents in the pyrite. However, line scans across the sulfide beds using a 75 micron beam, showed that most chalcophile elements are concentrated in the pyrite-rich beds by one to three orders of magnitude comparated to the matrix (Fig. 4.9). In particular, the TABS are concentrated in the pyrite-rich beds. Note that a 75 micron beam size was chosen in order to better reduce the detection limits for these elements.

In addition, chemical maps of the trace element in pyrrhotite-rich sulfide beds of the Bedded Pyrrhotite Unit from outside the contact aureole using a smaller beam size (5 microns) showed that Sb and Bi are concentrated in the chalcopyrite relative to pyrrhotite and the silicate matrix, and that Pb is present both in the sulfides and the silicate matrix (Fig. 4.10). No enrichments in Te and As were observed in, possibly this is because the concentrations are too low to be observed with a 5 micron beam, and possibly because there was no pyrite present in the mapped area.

The sulfide beds and sulfide droplets observed in the anatectic melt within xenoliths of the Bedded Pyrrhotite Unit are enriched in TABS and these are concentrated in the same area where grains of pentlandite and chalcopyrite occur (Figs. 4.11 and 4.12). Lead is found mainly in plagioclase, although there is some Pb associated with the Cu-rich sulfides.

In the sulfide droplets from the gabbronorites and norites, most of the TABS are associated with pentlandite and Cu-rich sulfides but are absent from silicates (Figs. 4.13 and 4.14). In contrast, Pb is present both in the silicate matrix plagioclases surrounding the

sulfides and in the sulfides (Fig. 4.13). Tin is partitioned between Cu-rich sulfides and orthopyroxenes. Sulfide droplets in the norite and gabbronorites have TABS-rich clusters that also contain PGE, as shown for Pd in Figures 4.13 and 4.14.

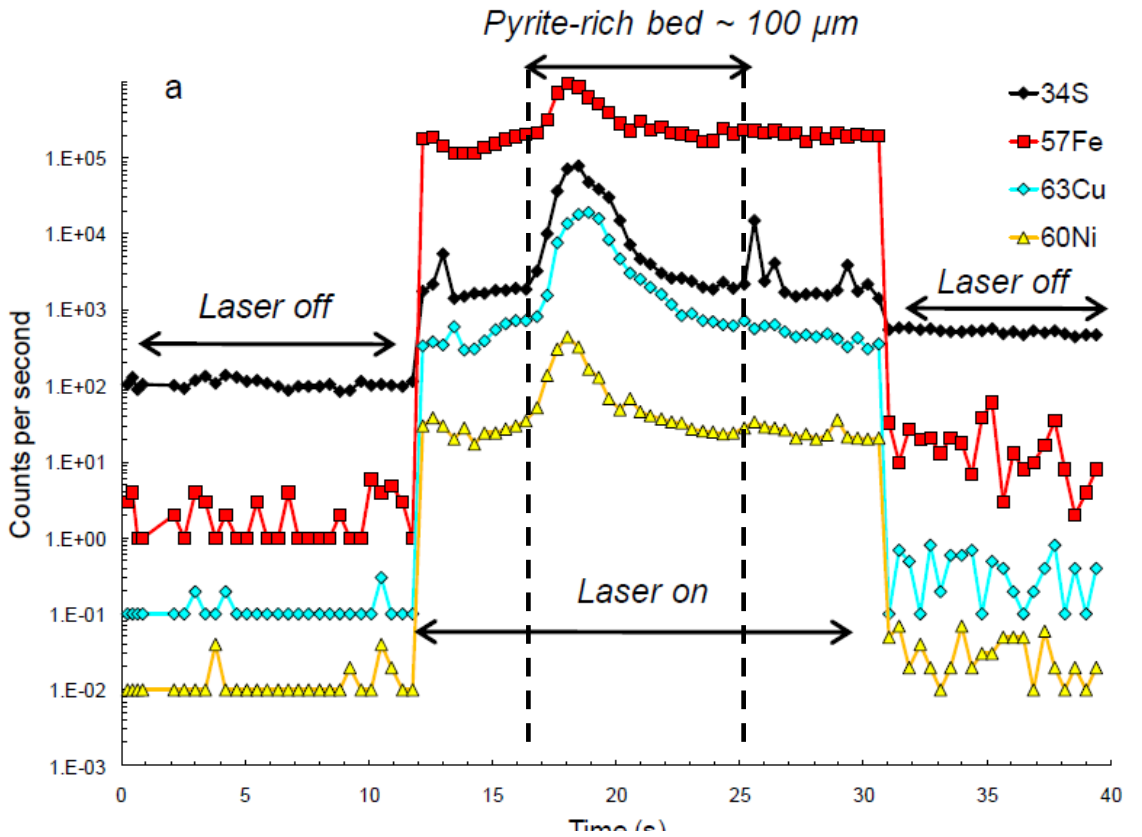
Pyrite-rich bed ~ 100 µm
a
34S
57Fe
63Cu
60Ni
Laser off
Laser off
Laser on
Counts per second
1.E+05
1.E+04
1.E+03
1.E+02
1.E+01
1.E+00
1.E-01
1.E-02
1.E-03
0
5
10
15
20
25
30
35
40

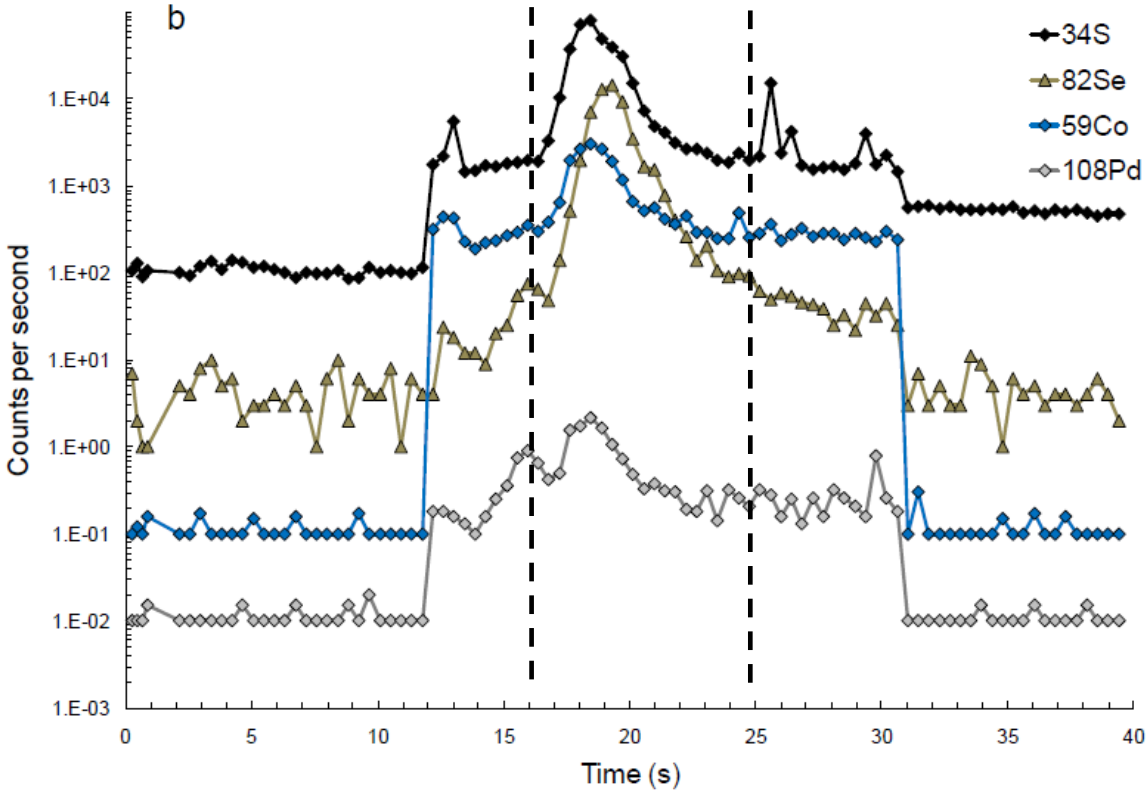
b
34S
82Se
59Co
108Pd
Counts per second
1.E+04
1.E+03
1.E+02
1.E+01
1.E+00
1.E-01
1.E-02
1.E-03
0
5
10
15
20
25
30
35
40
Time (s)

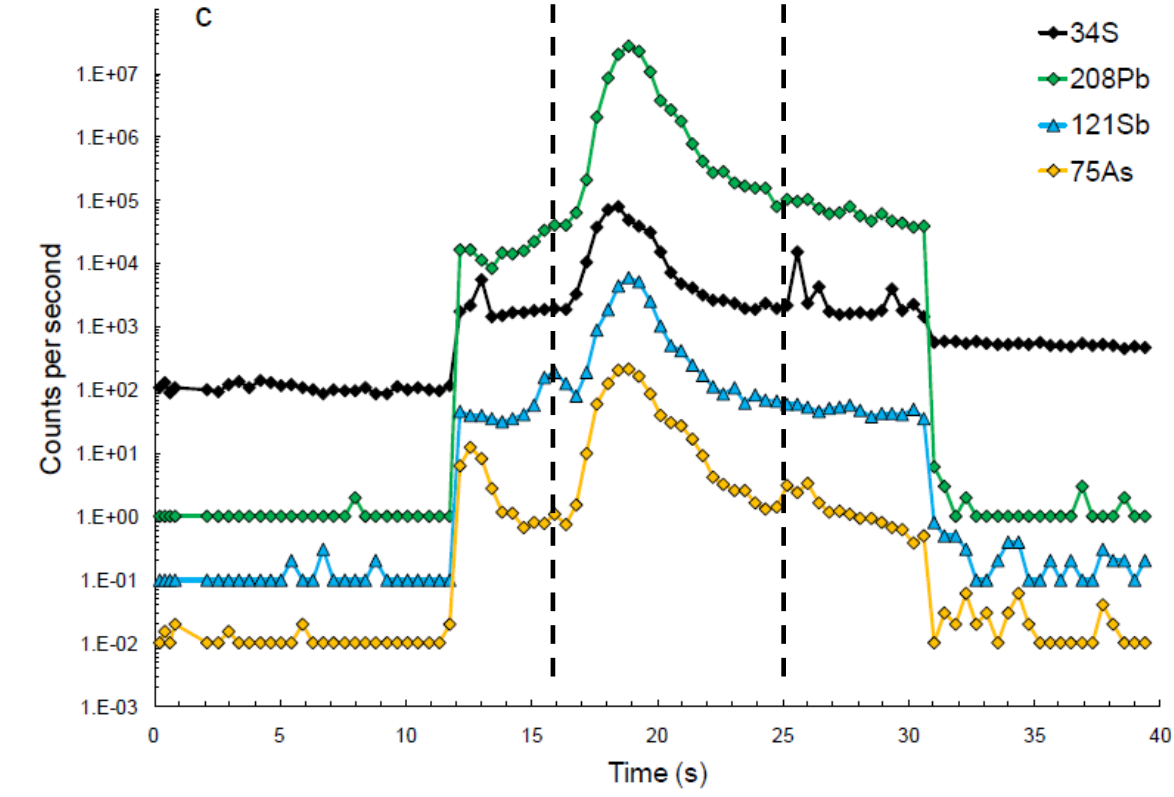
c
34S
208Pb
121Sb
75As
Counts per second
1.E+07
1.E+06
1.E+05
1.E+04
1.E+03
1.E+02
1.E+01
1.E+00
1.E-01
1.E-02
1.E-03
0
5
10
15
20
25
30
35
40
Time (s)

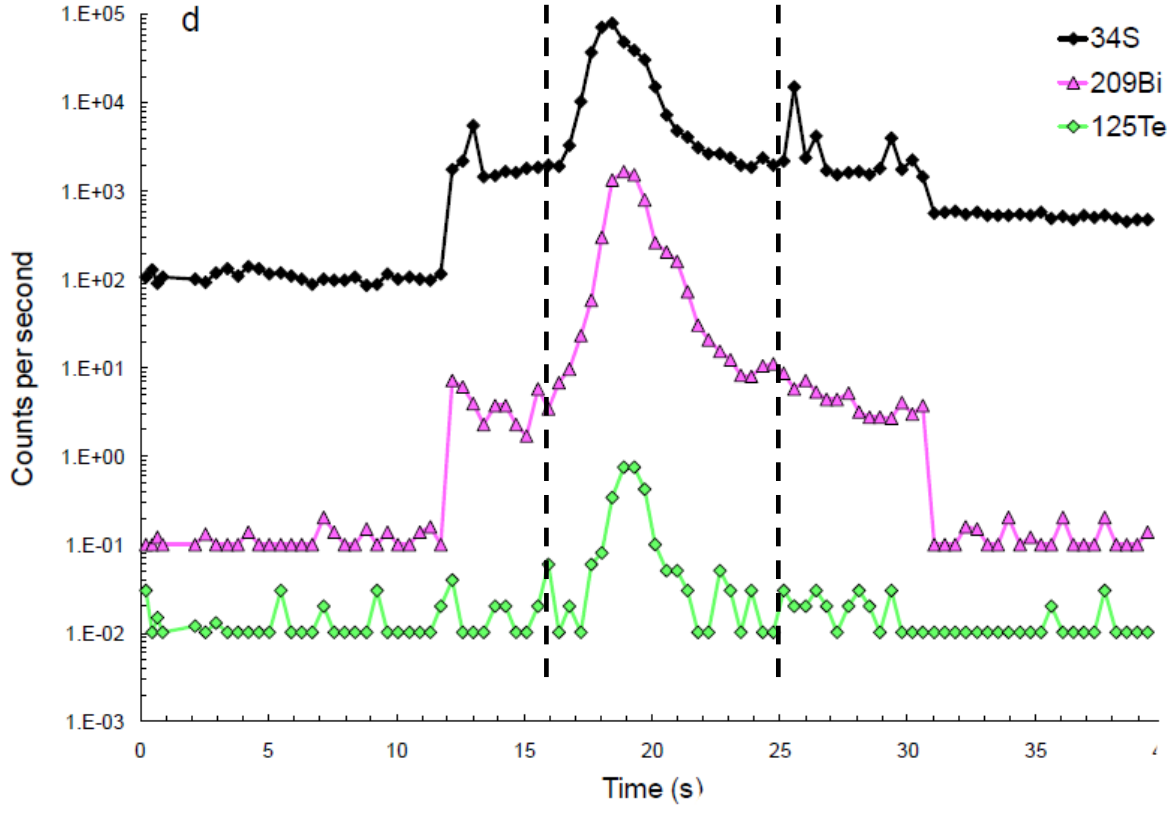
d
34S
209Bi
125Te
Counts per second
1.E+05
1.E+04
1.E+03
1.E+02
1.E+01
1.E+00
1.E-01
1.E-02
1.E-03
0
5
10
15
20
25
30
35
Time (s)

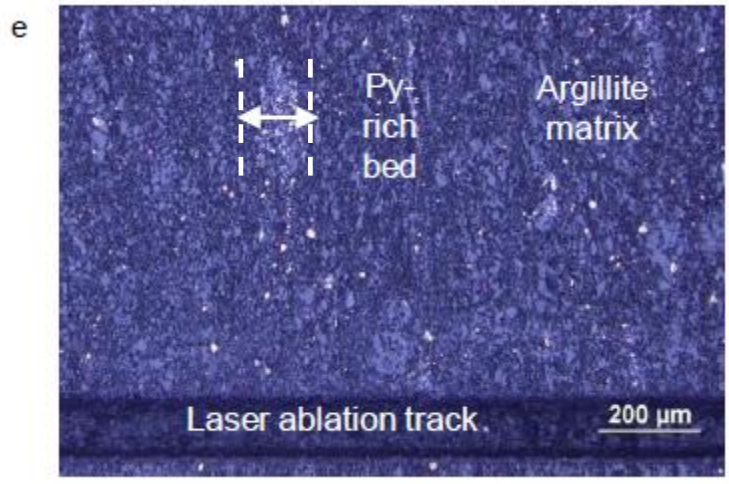

Figure 4.9: Counts per second vs. time LA-ICP-MS diagrams for a pyrite-rich bed in Bedded Pyrrhotite Unit (BPU) from outside the contact aureole (see photomicrograph e). Signals of TABS and trace metals are obtained after laser ablation (line scans) with beam size of 75µm, pulsing of 25Hz and speed of 10µm/s. The counts per second for some elements are multiplied, or divided, by 10 to 100 to improve the clarity.

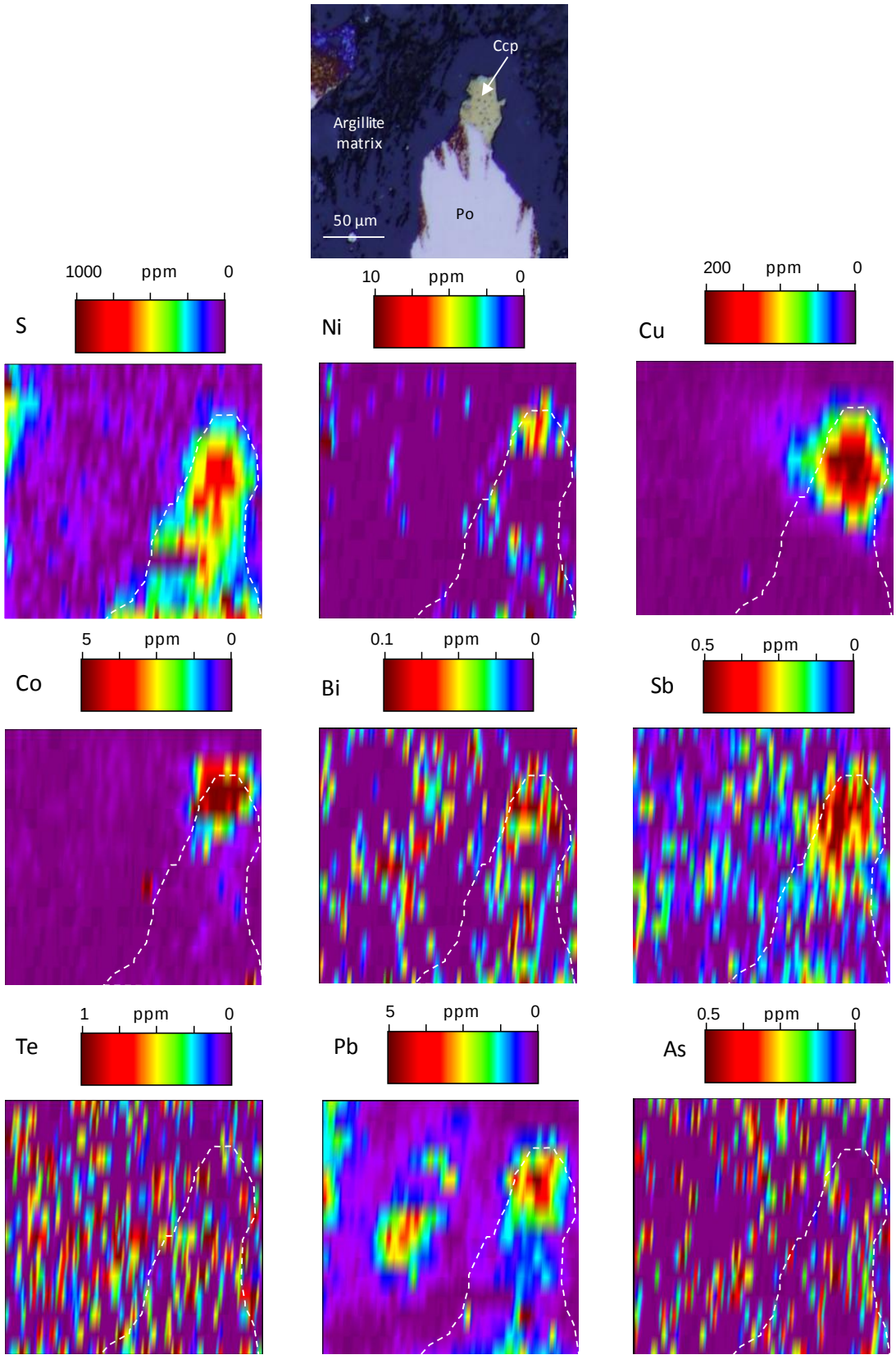
Ccp
Argillite matrix
50 µm
Po
S
1000 ppm 0
Ni
10 ppm 0
Cu
200 ppm 0
Co
5 ppm 0
Bi
0.1 ppm 0
Sb
0.5 ppm 0
Te
1 ppm 0
Pb
5 ppm 0
As
0.5 ppm 0

Figure 4.10: LA-ICP-MS maps of pyrrhotite-rich sulfide bed in Bedded Pyrrhotite Unit (BPU) from outside the contact aureole. Maps are obtained after ablation of with beam size of 5µm, frequency of 20Hz and fluence of 10J/cm^2.

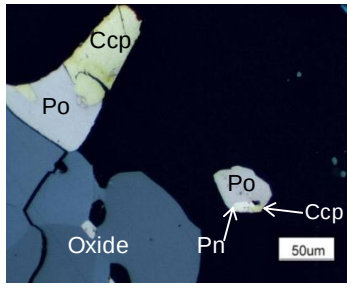
Ccp
Po
Po
Ccp
Oxide
Pn
50um

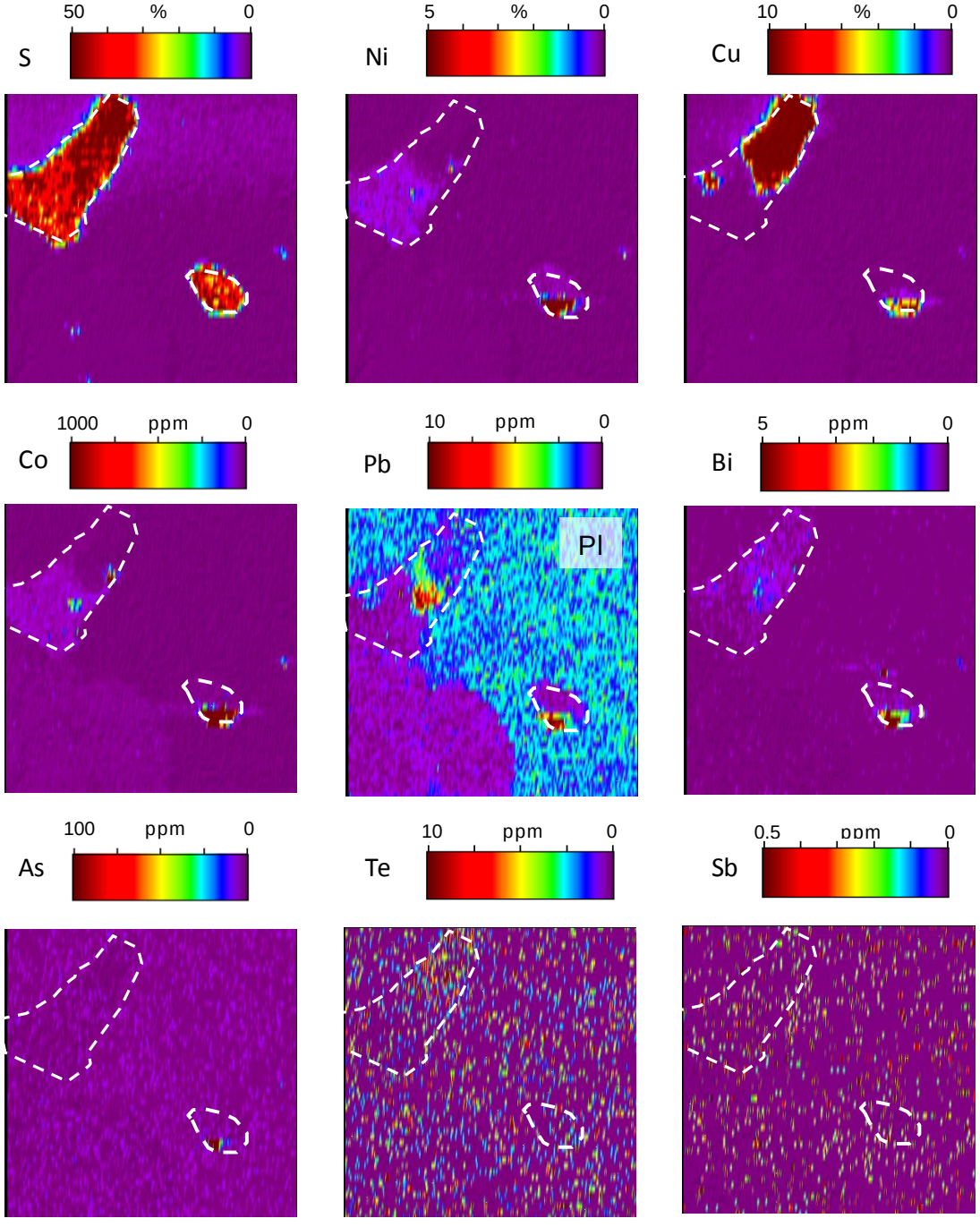
50
%
0
S
5
%
0
Ni
10
%
0
Cu
1000
ppm
0
Co
10
ppm
0
Pb
Pl
5
ppm
0
Bi
100
ppm
0
As
10
ppm
0
Te
0.5
ppm
0
Sb

Figure 4.11: LA-ICP-MS maps of sulfides in Bedded Pyrrhotite Unit (BPU) xenolith. Maps are obtained after ablation of BPU xenolith with beam size of 5µm, frequency of 20Hz and fluence of 10J/cm^2. Oxide = Ilmenite. Abbreviation: Pl = plagioclase, Ccp = Chalcopyrite; Po = Pyrrhotite; Pn = Pentlandite.

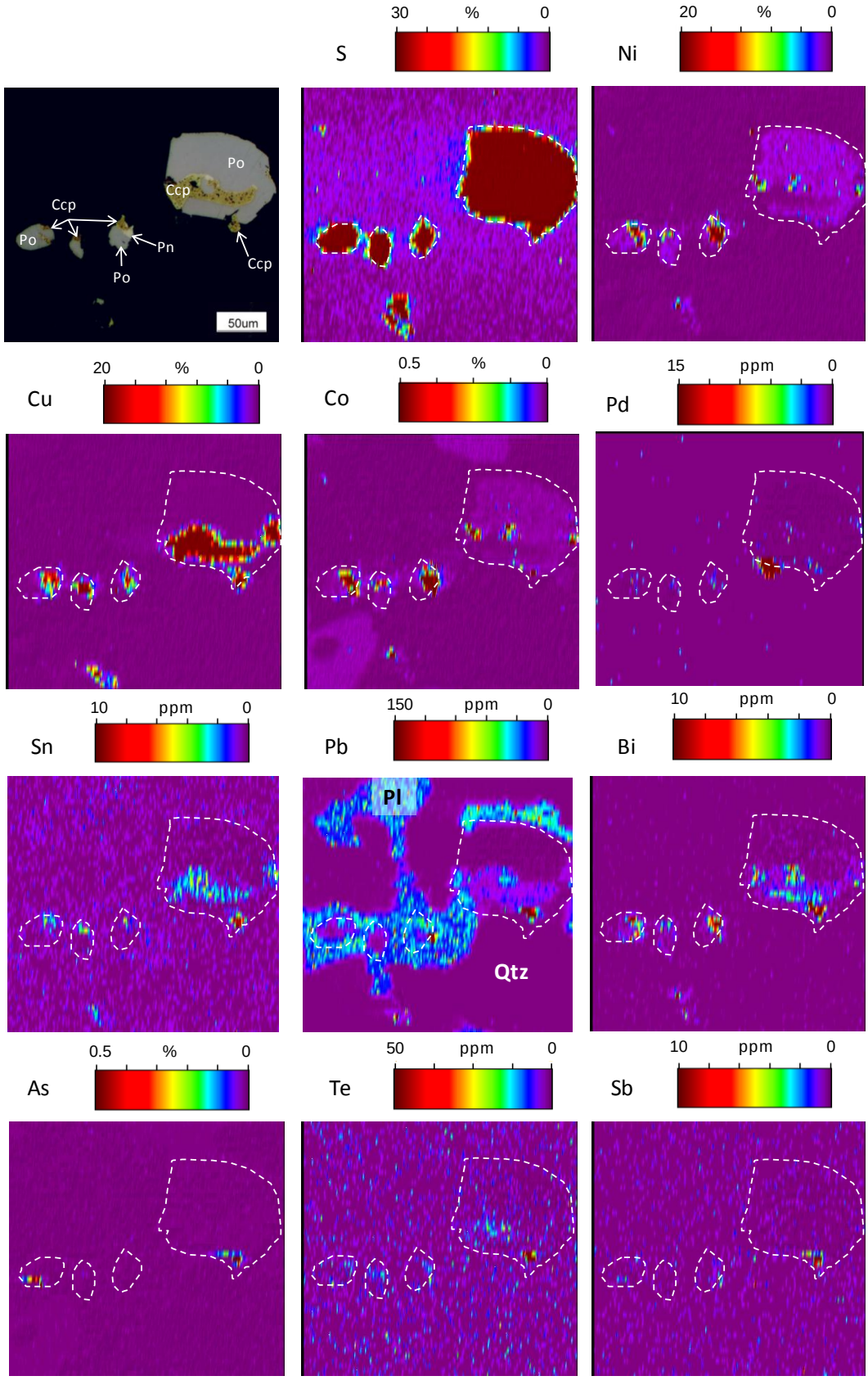
S
30 % 0
Ni
20 % 0
Po
Ccp
Ccp
Po
Pn
Po
Ccp
50um
Cu
20 % 0
Co
0.5 % 0
Pd
15 ppm 0
Sn
10 ppm 0
Pb
150 ppm 0
Bi
10 ppm 0
Pl
Qtz
As
0.5 % 0
Te
50 ppm 0
Sb
10 ppm 0

Figure 4.12: LA-ICP-MS maps of droplets of sulfide in the anatectic melt in a xenolith of Bedded Pyrrhotite Unit (BPU). Maps are obtained after ablation of BPU xenolith with beam size of 5µm, frequency of 20Hz and fluence of 10J/cm^2. Abbreviation: Pl = plagioclase, Qtz = quartz, Ccp = Chalcopyrite; Po = Pyrrhotite; Pn = Pentlandite.

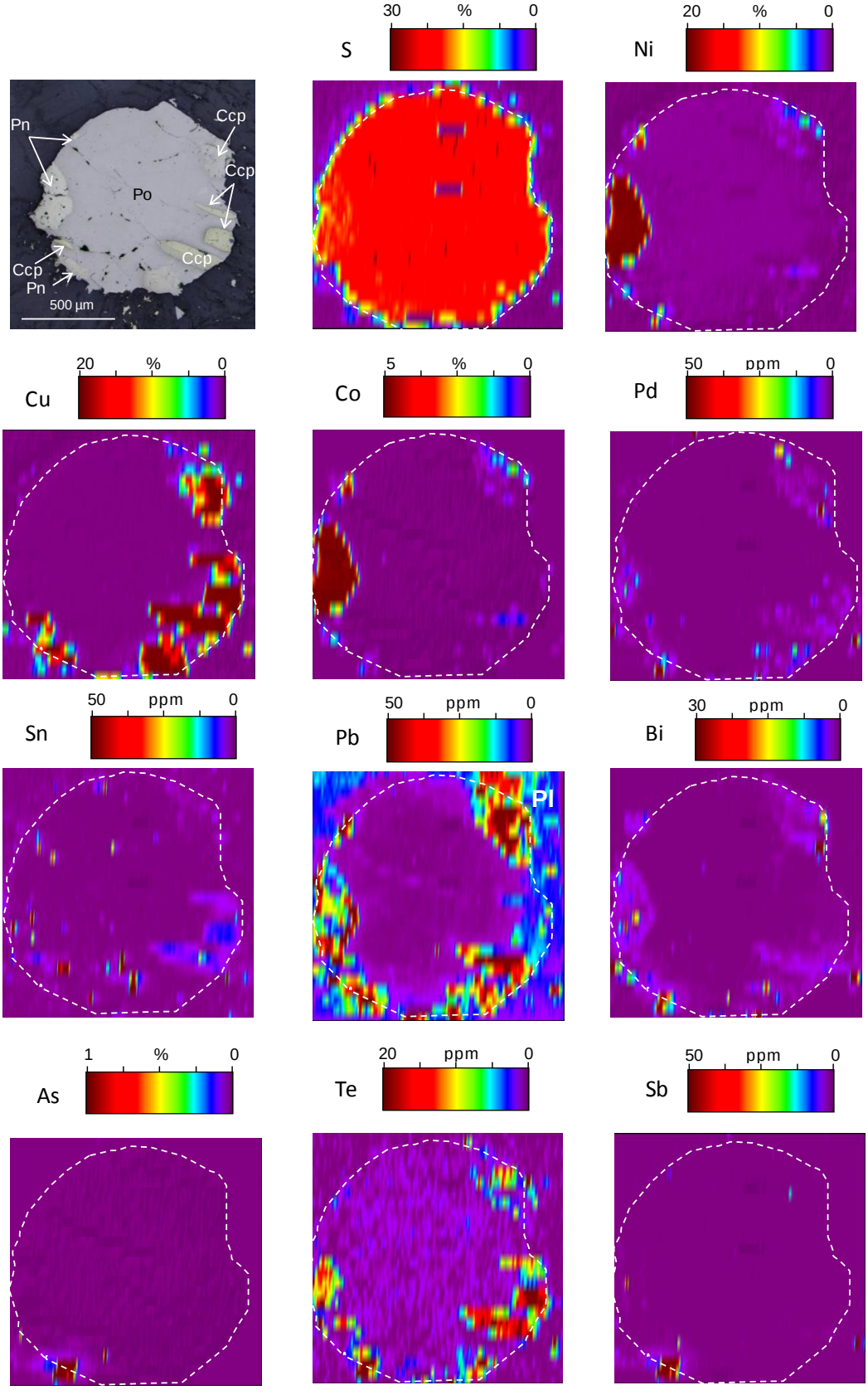
Pn
Ccp
Ccp
Po
Ccp
Ccp
Pn
500 µm
S
30 % 0
Ni
20 % 0
Cu
20 % 0
Co
5 % 0
Pd
50 ppm 0
Sn
50 ppm 0
Pb
50 ppm 0
Pl
Bi
30 ppm 0
As
1 % 0
Te
20 ppm 0
Sb
50 ppm 0

Figure 4.13: LA-ICP-MS maps of droplets of sulfide in the mafic rocks surrounding xenoliths of Bedded Pyrrhotite Unit (BPU), i.e. norite. Maps are obtained after ablation of sulfides from norite with beam size of 44µm, frequency of 15Hz and fluence of 3J/cm^2. Abbreviations: Ccp = Chalcopyrite; Po = Pyrrhotite; Pn = Pentlandite.

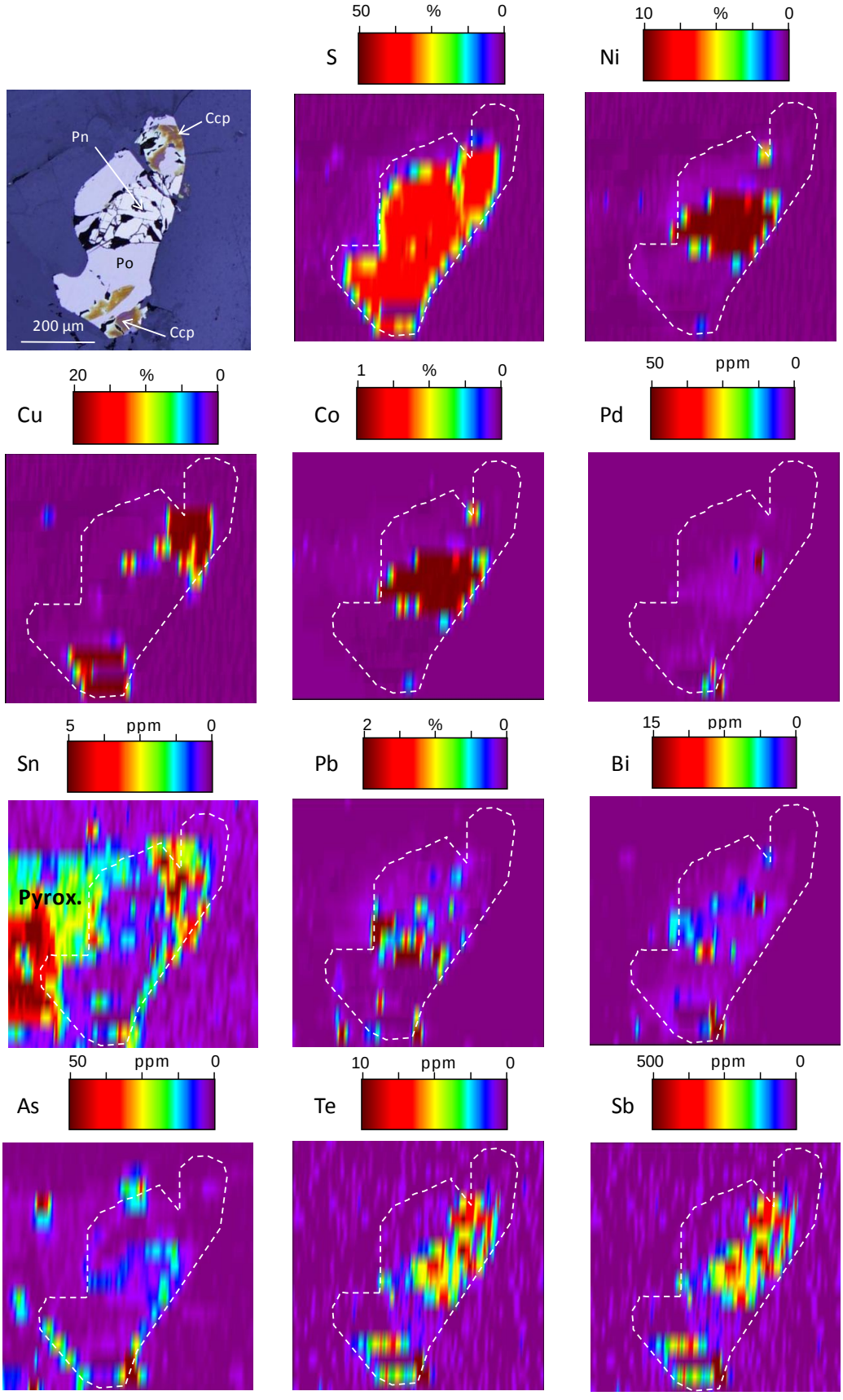
Pn
Ccp
Po
Ccp
200 µm
S
50 % 0
Ni
10 % 0
Cu
20 % 0
Co
1 % 0
Pd
50 ppm 0
Sn
5 ppm 0
Pb
2 % 0
Bi
15 ppm 0
Pyrox.
As
50 ppm 0
Te
10 ppm 0
Sb
500 ppm 0

Figure 4.14: LA-ICP-MS maps of sulfide droplets in gabbronorite. Maps are obtained after ablation of sulfides from gabbronorite with beam size of 44µm, frequency of 15Hz and fluence of 3J/cm^2. Abbreviations: Ccp = Chalcopyrite; Po = Pyrrhotite; Pn = Pentlandite.

4.7 DISCUSSION

4.7.1 TABS-HOSTED MINERALS

Most of the TABS are associated with Cu-rich sulfides and pentlandite in the Duluth Complex regardless of the rock type. Numerous authors have shown that the base metal sulfide minerals and the associated accessory PGM host much of the platinum-group element and chalcophile element budgets in magmatic Ni-Cu-PGE deposits (e.g., Barnes et al., 1997; Huminicki et al., 2005; Mungall et al., 2005; Barnes et al., 2006; Godel et al., 2007; Holwell and McDonald, 2007; Barnes et al., 2008; Godel and Barnes, 2008; Hutchinson and McDonald, 2008; Dare et al., 2010; Dare et al., 2011; Godel et al., 2012; Piña et al., 2012; Osbahr et al., 2013; Piña et al., 2013; Dare et al., 2014; Osbahr et al., 2014; Piña et al., 2014; Smith et al., 2014; Chen et al., 2015; Piña et al., 2016; Duran et al., 2016). Chalcophile elements partition into the sulfide liquid during the sulfide segregation process from a mafic magma, but the TABS do not partition into the *mss* (monosulfide solid solution) or *iss* (intermediate solid solution) that crystallize from the sulfide liquid (Table 2, Barnes and Ripley, 2016 and references therein) and hence they concentrate into the fractionated sulfide liquid along with Pt and Pd. Some PGM and other TABS minerals can crystallize from this fractionated liquid and consequently, are commonly found in association with chalcopyrite and cubanite. Platinum-group minerals and TABS minerals can also form subsolidus phases during exsolution of *mss* and *iss* to form pyrrhotite, pentlandite, chalcopyrite and cubanite. At this stage TABS and PGE maybe pushed to the grain boundaries, or into lattice defects such as dislocations, and there form PGM and TABS minerals.

The laser maps of As, Sb, Sn, Pb and Bi distributions show that these elements are concentrated within the area outlined by clusters of base metal sulfide minerals and close to Cu-rich minerals, but their distribution is irregular suggesting that they are present as inclusions within the sulfides. This interpretation is supported by the observation of Sn, Pb and Bi platinum group minerals associated with chalcopyrite (Table 4.3). In our study we did not observe Sb and As minerals, but more detailed studies report the presence of As and Sb bearing minerals maucherite; niccolite and gersdorffite with Cu-rich sulfides in the mafic rocks of the basal magmatic units (McSwiggen, 1999, Thériault et al., 1997, Severson and Hauck, 2003; Table 6a; Cervin, 2011). In addition to sulfides and platinum-group minerals the laser maps indicate that silicate phases also contain Sn and Pb in the Duluth Complex. Plagioclase and orthopyroxene host respectively Pb and Sn (Figs 4.10 to 4.14; Johnson et al., 2013).

4.7.2 TRACE ELEMENTS IN PYRITE

Pyrites of the Bedded Pyrrhotite Unit from outside the contact aureole of the Duluth Complex have similar TABS contents to the sedimentary pyrites from the literature (Gregory et al., 2015) and are enriched in TABS in comparison with magmatic pyrite from the literature (Dare et al., 2011; Piña et al., 2013; Duran et al., 2015) (Fig. 4.15). Syngenetic and diagenetic sedimentary pyrites may have been enriched in TABS during their formation in sedimentary basins (Morse, 1999; Morse and Luther, 1999; Chappaz et al., 2014).

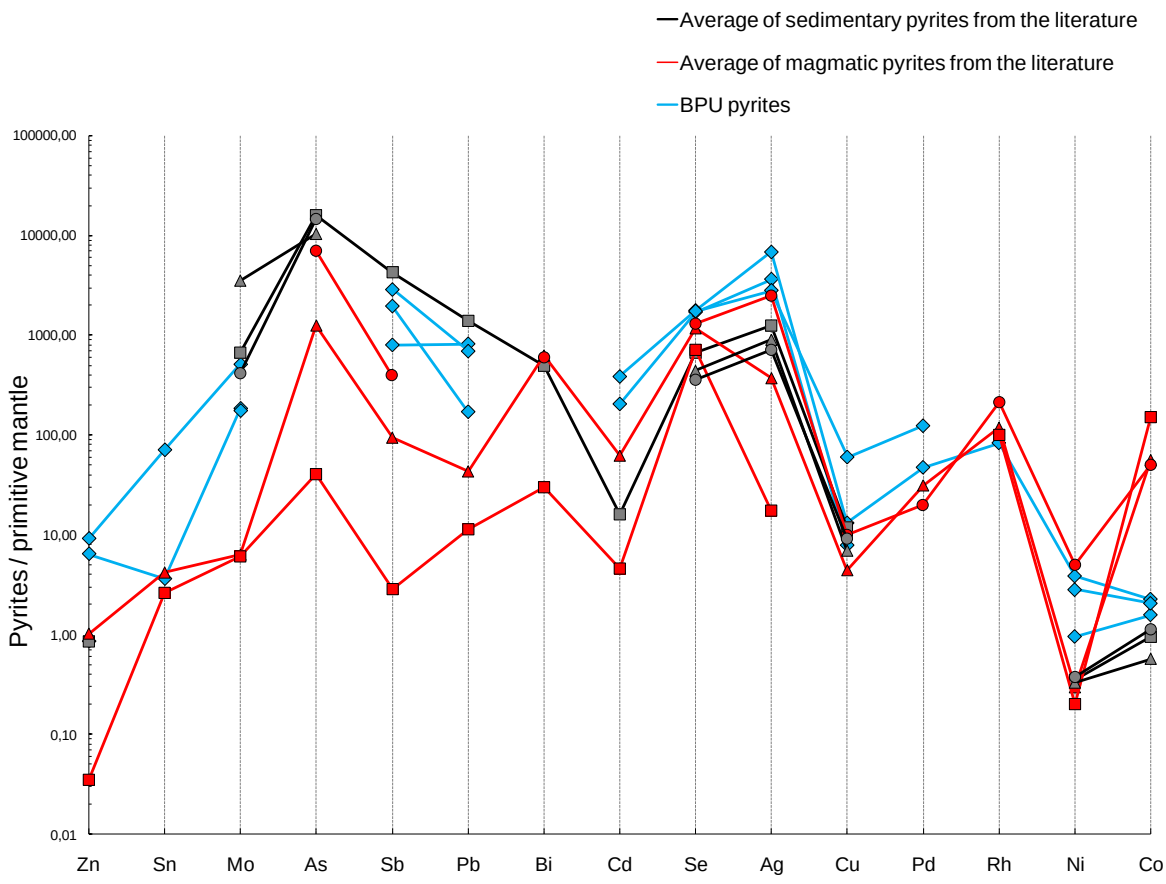

Figure 4.15: Primitive mantle-normalized plot of averages of TABS and trace metals content of the pyrites in the Bedded Pyrrhotite Unit (BPU) and from the literature. Averages of magmatic and sedimentary pyrites are shown for reference (Dare et al., 2011; Piňa et al., 2013; Duran et al., 2015; Gregory et al., 2015). Symbols: Grey triangle = Average of Paleoproterozoic pyrites in black shales (n=105); Grey circle = Average of small euhedral pyrites in black shales (n=92); Grey square = Compilation of pyrites in black shales; Red triangle = Average of pyrites in Lac des Iles deposit (n=57); Red circle = Average of pyrites in Aguablanca deposit (n=32); Red square = Average of pyrites in Mc Creedy deposit (n=23). Abbreviation: BPU = Bedded Pyrrhotite Unit.

In addition, pyrites of the Bedded Pyrrhotite Unit outside the contact aureole have lower contents of Co and platinum-group elements than magmatic pyrites from the literature (Fig. 4.15); the level of most of the platinum-group elements from the Bedded Pyrrhotite Unit pyrites are below the detection limits. Magmatic pyrites are thought to be formed either by exsolution from the *mss* (monosulfide solid solution) (Naldrett et al., 1967; Dare et al., 2011) or by the alteration of them by late magmatic hydrothermal fluids (Naldrett et al., 1999; Dare et al., 2011; Djon and Barnes, 2012; Su and Lesher, 2012). By these mechanisms magmatic pyrites are enriched in platinum-group elements (Dare et al., 2011; Lorand and Alard, 2011; Djon and Barnes, 2012; Knight et al., 2012; Piña et al., 2013; Duran et al., 2015) in comparison with sedimentary pyrite that are formed in sedimentary basins; such those from the Duluth Complex.

Metal contents of pyrites from the contact aureole normalized to less metamorphosed Bedded Pyrrhotite Unit sample from outside the contact aureole are shown in the Figure 4.16. Nickel, Co, Rh and Pd are strongly enriched in the pyrites relative to the whole rock, and they could be the main host of these elements in the black shale. Most of the other chalcophile elements are present in the pyrite at approximately the same levels as the whole rock. Pyrite makes up <3 % of the rock, thus the pyrites are not the principal host for most of the chalcophile elements and these elements are likely controlled by other phases rather than pyrite.

In contrast, line scans across the sulfide beds (using a 75 micron beam) show that Sn, Sb, Pb, Bi, Ag, Cu and Te contents are higher in the sulfide beds than in the matrix (Cu, Bi, Pb, Sb and Te are shown in the Fig. 4.9). The calculated contents of Sn, Sb, Pb, Bi, Ag, Cu and Te of the sulfide beds are 3 to 4 times higher than the whole rock (Fig. 4.16;

averages are 1 ppm, 1500 ppm, 50 ppm, 4 ppm, 350 ppm, 30 ppm and 10 ppm respectively). However, the calculated contents of As, Mo and Zn are similar to the whole rock (Fig. 4.16; averages of respectively 15 ppm, 20 ppm and 1500 ppm). The rock contains <3% sulfides, thus, even through the sulfide bed is enriched in some chalcophile elements most of the As, Mo and Zn and some of the Te, Cu, Ag, Bi Pb, Sb and Sn must be present in some other phase(s). Colloidal phases (consisting of organic compounds) absorb semimetals during sedimentary basin formation (Buffle and Leppard, 1995; Gustafsson and Gschwend, 1997; Gustafsson et al., 2000) and possibly the missing chalcophile elements are present in this form in the samples outside the contact aureole at the Duluth Complex.

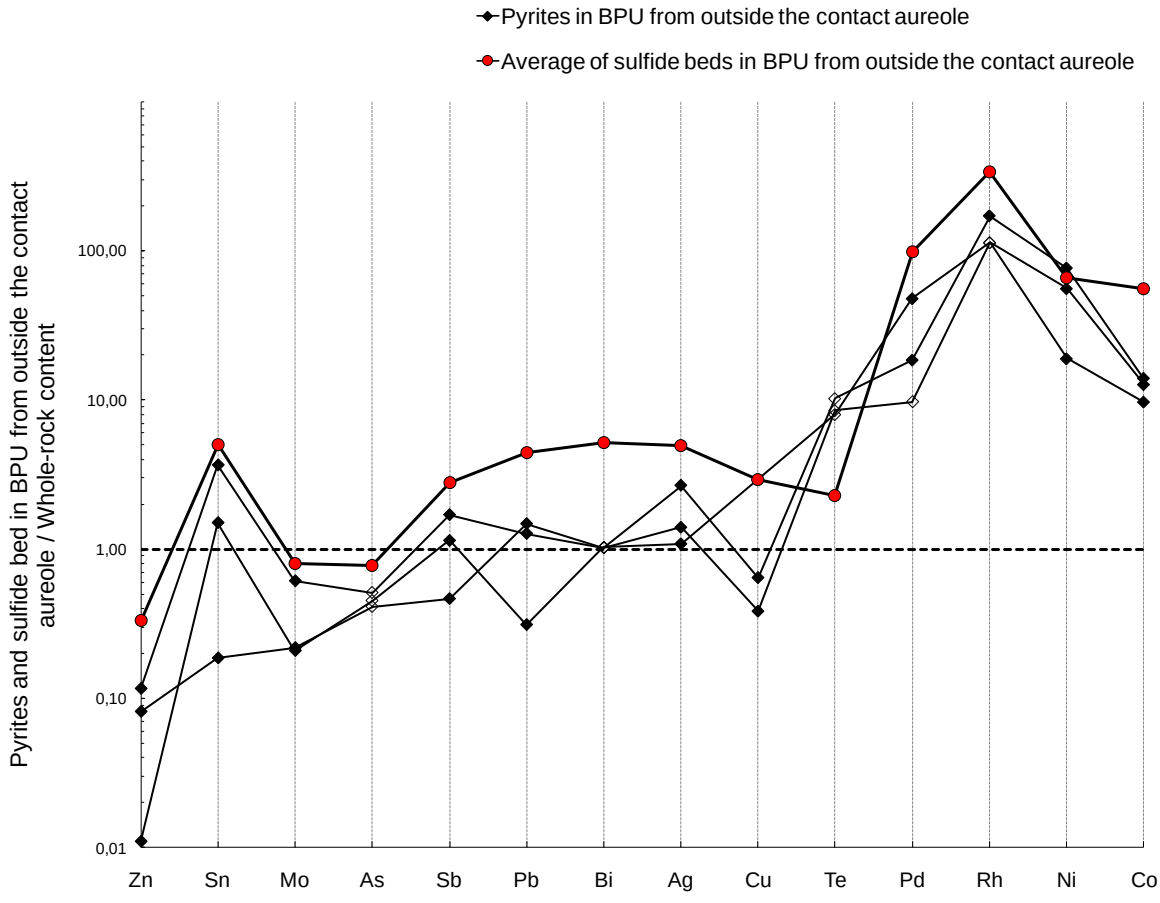

Figure 4.16: Diagram of trace metal and TABS contents of sedimentary pyrites from the Bedded Pyrrhotite Unit (BPU) outside the contact aureole normalized to whole rock concentrations. Dotted lines correspond to 1:1 ratio. Blank symbols are employed for values which are below the detection limits. Abbreviation: BPU = Bedded Pyrrhotite Unit.

4.7.3 IMPLICATIONS IN CONTAMINATION PROCESSES

The proportions of sulfide minerals in the Bedded Pyrrhotite Unit vary with location. The xenoliths of Bedded Pyrrhotite Unit contain pentlandite and have higher proportions of Cu-rich sulfides than the Bedded Pyrrhotite Unit from the contact aureole, which does not contain pentlandite. Field observations suggest that the xenoliths and contact aureole samples are from the same unit and we suggest that chemical-potential driven diffusion of Ni and Cu may occur from the magma to the xenolith as proposed by Samalens et al. (2017).

Xenoliths of the Bedded Pyrrhotite Unit have undergone partial melting in the mafic magma and then by this mechanism provide the S, TABS and Pb contamination of the mafic magma (Queffurus and Barnes, 2014; Samalens et al., 2017). Samalens et al. (2017) suggest based on a petrographic study and whole rock data that contamination of the mafic magma by S and semimetals occurs by transfer of sulfide droplets from xenoliths of the Bedded Pyrrhotite Unit to the magma via the anatectic melt produced in, and removed from, the xenolith. Our LA-ICP-MS study shows that the sulfides of the Bedded Pyrrhotite Unit are rich in TABS; consistent with these S-rich black shales being the source of semimetals that contaminated the mafic magma. In addition, LA-ICP-MS maps of sulfide droplets inside the anatectic melt in the xenoliths of Bedded Pyrrhotite Unit show that these sulfide droplets carry TABS and Pb. These observations support the proposed model for semimetals contamination of the mafic magma.

4.8 CONCLUSIONS

Petrographic study of sulfide phases show in the Duluth Complex variation in the sulfide mineralogy and mineral proportions between the Bedded Pyrrhotite Unit and the magmatic rocks. The Bedded Pyrrhotite Unit from outside the contact aureole contains mainly pyrite and a little pyrrhotite (<2%), whereas the Bedded Pyrrhotite Unit within the contact aureole contains pyrrhotite (>95%) and chalcopyrite (<2%); pyrite is absent. In addition to pyrrhotite and chalcopyrite, cubanite and pentlandite are present in the xenoliths of Bedded Pyrrhotite Unit and in the mafic rocks. Xenoliths of the Bedded Pyrrhotite Unit contain pentlandite and have higher proportions of Cu-rich sulfides than the Bedded Pyrrhotite Unit from the contact aureole, which does not contain pentlandite. These variations may be explained by Ni and Cu diffusion from the mafic magma to the xenoliths of the Bedded Pyrrhotite Unit.

Our LA-ICP-MS study shows that sulfides are enriched in TABS relative to other phases in the Duluth Complex. However, these elements are also partitioned into platinum-group minerals and silicate phases (i.e. Pb in plagioclase and Sn in orthopyroxene) in the xenoliths and the mafic rocks. Organic compounds may have concentrated chalcophile elements in the Bedded Pyrrhotite Unit from outside the contact aureole.

LA-ICP-MS maps of sulfide droplets within the anatectic melt contained in xenoliths of the Bedded Pyrrhotite Unit, and in the surrounding mafic rocks show that sulfide droplets carry TABS, PGE and Pb. These observations support previous models of semimetals contamination of mafic magma at the Duluth Complex by assimilation of Bedded Pyrrhotite Unit xenoliths; i.e. sulfide droplets are transferred from xenoliths of the

Bedded Pyrrhotite Unit to the mafic magma by the anatectic melt produced in, and then expelled from, the xenoliths.

4.9 ACKNOWLEDGMENTS

This work was funded by a Natural Science and Engineering Research Council of Canada Discovery Grant to SJB (17313) and a Canada Research Chair program grant to SJB (215503). We thank Mark Severson for providing some samples of the Bedded Pyrrhotite Unit from the contact aureole. Sadia Medhi, Dany Savard and Marko Kudrna Prašek from LabMaTer are thanked to help in carrying out analyses. Editors and reviewers are thanked for helping us improve the clarity of our manuscript.

4.10 REFERENCES

Andrews, D., Ripley, E.M., (1989) Mass transfer and sulfur fixation in the contact aureole of the Duluth Complex, Dunka Road Cu-Ni deposit, Minnesota. Can. Mineral. 27, 293-310.

Baker, D.R., Barnes, S.-J., Simon, G., Bernier, F., (2001) Fluid transport of sulfur and metals between sulfide melt and basaltic melt. Can. Mineral. 39, 537-546.

Barnes, S.-J., Makovicky, E., Makovicky, M., Rose-Hansen, J., Karup-Moller, S., (1997) Partition coefficients for Ni, Cu, Pd, Pt, Rh, and Ir between monosulfide solid solution and sulfide liquid and the formation of compositionally zoned Ni – Cu sulfide bodies by fractional crystallization of sulfide liquid. Can. J. Earth Sci. 34, 366-374.

Barnes, S.-J., Lightfoot, P.C., (2005) Formation of magmatic nickel-sulfide ore deposits and processes affecting their copper and platinum-group elements contents. Economic Geology, 100th Anniversary Volume, 179-213.

Barnes, S.-J., Cox, R., Zientek, M., (2006) Platinum-group element, gold, silver and base metal distribution in compositionally zoned sulfide droplets from the Medvezky Creek Mine, Noril'sk, Russia. Contrib. Mineral. Petrol. 152, 187-200.

Barnes, S.-J., Prichard, H.M., Cox, R.A., Fisher, P.C., Godel, B., (2008) The location of the chalcophile and siderophile elements in platinum-group element ore deposits (a textural, microbeam and whole rock geochemical study): Implications for the formation of the deposits. Chem. Geol. 248, 295-317.

Barnes, S.-J., Ripley, E.M., (2016) Highly siderophile and strongly chalcophile elements in magmatic ore deposits. Rev. Mineral. Geochem. 81, 725-774.

Bédard, L.P., Savard, D., Barnes, S.-J., (2008) Total sulfur concentration in geological reference materials by elemental infrared analyser. Geostand. Geoanal. Res. 32, 203-208.

Benkó, Z., Mogessie, A., Molnár, F., Krenn, K., Poulson, S.R., Hauck, S.A., Severson, M.J., Arehart, G.B., (2015a) Hydrothermal alteration and Cu–Ni–PGE mobilization in the charnockitic rocks of the footwall of the South Kawishiwi intrusion, Duluth Complex, USA. Ore Geol. Rev. 67, 170-188.

Benkó, Z., Mogessie, A., Molnár, F., Severson, M.J., Hauck, S.A., Raič, S., (2015b) Partial Melting Processes and Cu-Ni-PGE Mineralization in the Footwall of the South Kawishiwi Intrusion at the Spruce Road Deposit, Duluth Complex, Minnesota. Econ. Geol. 110, 1269-1293.

Bonnichsen, W., (1972) Sulfide minerals in the Duluth Complex. In Sims, P. K., and Morey, G. W., eds., Geology of Minnesota: A centennial volume: Minn. Geol. Survey. pp. 388-393.

Buffle, J., Leppard, G.G., (1995) Characterization of aquatic colloids and macromolecules. 1. Structure and behavior of colloidal material. Environ. Sci. Technol. 29, 2169–2175.

Cervin, D.O., (2011) Characterization of precious metal mineral occurrences in the NorthMet deposit of the Partridge River Intrusion, Duluth complex, Minnesota, USA: Unpublished. M.Sc. thesis, University of Minnesota, 155 p.

Chappaz, A., Lyons, T. W., Gregory, D. D., Reinhard, C. T., Gill, B. C., Li, C., Large, R. R., (2014) Does pyrite act as an important host for molybdenum in modern and ancient euxinic sediments? Geochim. Cosmochim. Acta. 126, 112-122.

Chen, L-M., Song, X-Y., Danyushevsky, L.V., Wang, Y-S., Tian, Y-L., Xiao, J-F., (2015) A laser ablation ICP-MS study of platinum-group and chalcophile elements in base metal sulfide minerals of the Jinchuan Ni–Cu sulfide deposit, NW China. Ore Geol. Rev. 65, 955-967.

Dare, S., Barnes, S.-J., Prichard, H., (2010) The distribution of platinum group elements (PGE) and other chalcophile elements among sulfides from the Creighton Ni–Cu–PGE sulfide deposit, Sudbury, Canada, and the origin of palladium in pentlandite. Miner. Deposita.45, 765-793.

Dare, S., Barnes, S.-J., Prichard, H., Fisher, P., (2011) Chalcophile and platinum-group element (PGE) concentrations in the sulfide minerals from the McCreedy East

deposit, Sudbury, Canada, and the origin of PGE in pyrite. Miner. Deposita. 46, 381-407.

Dare, S., Barnes, S.-J., Prichard, H.M., Fisher, P.C., (2014) Mineralogy and geochemistry of Cu-rich ores from the McCreedy East Ni-Cu-PGE Deposit (Sudbury, Canada): Implications for the behavior of platinum group and chalcophile elements at the end of crystallization of a sulfide liquid. Econ. Geol. 109, 343-366.

Dionne-Foster, C., (2007) Géologie et indices de Ni-Cu-EGP de la zone Frontier dans la ceinture de Cape Smith, Nouveau Québec: Unpublished. M.Sc. thesis, Université du Québec à Chicoutimi, 320 p.

Djon., M.L.N., Barnes, S.-J., (2012) Changes in sulfides and platinum-group minerals with the degree of alteration in the Roby, Twilight, and High Grade Zones of the Lac des Iles Complex, Ontario, Canada. Mineral. Deposita, 47, 875–896.

Duran, C.J., Barnes, S.-J., Corkery, J.T., (2015) Chalcophile and platinum-group element distribution in pyrites from the sulfide-rich pods of the Lac des Iles Pd deposits, Western Ontario, Canada: Implications for post-cumulus re-equilibration of the ore and the use of pyrite compositions in exploration. J. Geochem. Explor. 158, 223-242.

Duran, C.J., Barnes, S.-J., Corkery, J.T., (2016) Trace element distribution in primary sulfides and Fe–Ti oxides from the sulfide-rich pods of the Lac des Iles Pd deposits, Western Ontario, Canada: Constraints on processes controlling the composition of the ore and the use of pentlandite compositions in exploration. J. Geochem. Explor. 166, 45-63.

Gál, B., Molnár, F., Guzmics, T., Mogessie, A., Szabó, C., Peterson, D.M., (2013) Segregation of magmatic fluids and their potential in the mobilization of platinum-group elements in the South Kawishiwi Intrusion, Duluth Complex, Minnesota — Evidence from petrography, apatite geochemistry and coexisting fluid and melt inclusions. Ore Geol. Rev. 54, 59-80.

Godel, B., Barnes, S.-J., Maier, W.D., (2007) Platinum-group elements in sulphide minerals, platinum-group minerals, and whole-rocks of the Merensky Reef (Bushveld Complex, South Africa): Implications for the formation of the reef. J. Petrol. 48, 1569-1604.

Godel, B., Barnes, S.-J., (2008) Platinum-group elements in sulfide minerals and the whole rocks of the J-M Reef (Stillwater Complex): Implication for the formation of the reef. Chem. Geol. 248, 272-294.

Godel, B., González-Álvarez, I., Barnes, S.J., Barnes, S.-J., Parker, P., Day, J., (2012) Sulfides and Sulfarsenides from the Rosie Nickel Prospect, Duketon Greenstone Belt, Western Australia. Econ. Geol. 107, 275-294.

Gregory, D.D., Large, R.R., Halpin, J.A., Baturina, E.L., Lyons, T.W., Wu, S., Danyushevsky, L., Sack, P.J., Chappaz, A., Maslennikov, V.V., Bull, S.W., (2015) Trace element content of sedimentary pyrite in black shales. Econ. Geol. 110, 1389-1410.

Gustafsson, Ö., Gschwend, P.M., (1997) Aquatic colloids: Concepts, definitions, and current challenges. Limnol. Oceanogr. 42, 519–528.

Gustafsson, Ö., Widerlund, A., Andersson, P.S., Ingri, J., Roos, P., Ledin, A., (2000) Colloid dynamics and transport of major elements through a boreal river-brackish bay mixing zone. Mar. Chem. 71, 1–21.

Hauck, S.A., Severson, M.J., Zanko, L., Barnes, S.-J., Morton, P., Alminas,H., Foord, E.E., and Dahlberg, E.H., (1997) An overview of the geology and oxide, sulfide, and platinum-group element mineralization along the western and northern contacts of the Duluth Complex. Geol. Soc. Am. Special paper. 312, 137–185.

Henrique-Pinto, R., Barnes, S.-J., Savard, D., Mehdi, S., (2016) Quantification of metals and semimetals in carbon-rich rocks: a new sequential protocol including extraction from humic substances. Geostand. Geoanal. Res. http://dx.doi.org/10.1111/j.1751-908X.2015.00340.x (in press).

Holwell, D.A., McDonald, I., (2007) Distribution of platinum-group elements in the Platreef at Overysel, northern Bushveld Complex: a combined PGM and LA-ICP-MS study. Contrib. Mineral. Petrol. 154, 171-190.

Hu, Z., Gao, S., (2008) Upper crustal abundances of trace elements: A revision and update. Chem. Geol. 253, 205-221.

Huminicki, M.A.E., Sylvester, P.J., Cabri, L.J., Lesher, C.M., Tubrett, M., (2005) Quantitative mass balance of platinum-group elements in the Kelly Lake Ni-Cu-PGE deposit, Copper Cliff offset, Sudbury. Econ. Geol. 100, 1631-1646.

Hutchinson, D., McDonald, I., (2008) Laser ablation ICP-MS study of platinum-group elements in sulphides from the Platreef at Turfspruit, northern limb of the Bushveld Complex, South Africa. Miner. Deposita. 43, 695-711.

Johnson, E.R., Kamenetsky, V.S., McPhie, J., (2013) The Behavior of Metals (Pb, Zn, As, Mo, Cu) during crystallization and degassing of rhyolites from the Okataina Volcanic Center, Taupo Volcanic Zone, New Zealand. J. Petrol. 54, 1641-1659.

Ketris, M.P., Yudovich, Y.E., (2009) Estimations of Clarkes for carbonaceous biolithes: World averages for trace element contents in black shales and coals. International Journal of Coal Geology. 78, 135-148.

Knight, R.D., Prichard, H.M., McDonald, I., Ferreira Filho, C.F., (2012) PGE mineralization in the Fazenda Mirabela intrusion, Bahia State, Brazil: distribution of PGE in base metal sulphides and PGM. In ‘‘12th International Ni-Cu-PGE Symposium’’, 12–21 June 2012 Abstract Book, Guiyang, China, 118–121.

Labotka, T.C., Papike, J.J., Vaniman, D.T., (1981) Petrology of contact metamorphosed argillite from the Rove Formation, Gunflint Trail, Minnesota. Am. Mineral. 66, 70-86.

Lesher, C.M., Arndt, N.T., and Groves, D.I., (1984) Genesis of komatiite-associated nickel sulfide deposits at Kambalda, Western Australia: A distal volcanic model. Sulfide deposits in mafic and ultramafic rocks. Institute of Mining and Metallurgy, London, 10 p.

Lesher C.M., Campbell, I.H., (1993) Geochemica and Fluid Dynamic Modeling of Compositional Variations in Archean Komatiite-Hosted Nickel Sulfide Ores in Western Australia. Economic Geology, 88, 804-816.

Lesher, C.M., Burnham, O.M., (2001) Multicomponent elemental and isotopic mixing in Ni–Cu–(PGE) ores at Kambalda, Western Australia. Can. Mineral. 39, 421-446.

Lorand, J.-P., Alard, O., (2011) Pyrite tracks assimilation of crustal sulfur in Pyrenean peridotites. Miner. Petrol. 101, 115–128.

Lucente, M.E., Morey, G.B., (1983) Stratigraphy and sedimentology of the Lower Proterozoic Virginia Formation, northern Minnesota. Minnesota Geological Survey, Report of Investigations RI-28, 28 p.

Lyubetskaya, T., Korenaga, J., (2007) Chemical composition of Earth's primitive mantle and its variance: 1. Method and results. J. Geophys. Res.: Solid Earth. B03211, 112, 1-21.

Mainwaring, P.R., Naldrett, A., (1977) Country-rock assimilation and the genesis of Cu-Ni sulfides in the Water Hen Intrusion, Duluth Complex, Minnesota. Econ. Geol. 72, 1269-1284.

McSwiggen, P.L., (1999) Platinum-palladium group minerals, gold, silver, and cobalt in the Minnamax copper-nickel sulfide deposit, Duluth Complex, northeastern Minnesota. Minnesota Geological Survey, Report of Investigations RI-54, 29p.

Miller, J.D., Jr., and Severson, M.J., (2002) Geology of the Duluth Complex, in Miller, J.D., Jr., Green, J.C., Severson, M.J., Chandler, V.W., Hauck, S.A., Peterson, D.M., and Wahl, T.E., eds., Geology and mineral potential of the Duluth Complex and related rocks of northeastern Minnesota: Minnesota Geological Survey, Report of Investigations RI-58, 106-143.

Molnár, F., Arehart, G.B., Poulson, S., Hauck, S., (2009) Sulfur isotope constraints for a dynamic magmatic sulfide ore deposition model in the sill-like South Kawishiwi Intrusion of the Duluth Complex, Minnesota. Geol. Soc. America. Annual Meeting, Portland, OR. Abstr. vol. 41 (25 pp)

Morse, J. W., (1999) Sulfides in sandy sediments: new insights on the reactions responsible for sedimentary pyrite formation. Aquat. Geochem. 5, 75-85.

Morse, J. W., Luther, G. W., (1999) Chemical influences on trace metal-sulfide interactions in anoxic sediments. Geochim. Cosmochim. Acta. 63, 3373-3378.

Mungall, J.E., Andrews, D.R.A., Cabri, L.J., Sylvester, P.J., Tubrett, M., (2005) Partitioning of Cu, Ni, Au, and platinum-group elements between monosulfide solid solution and sulfide melt under controlled oxygen and sulfur fugacities. Geochim. Cosmochim. Acta. 69, 4349-4360.

Naldrett, A., (1966) Role of sulphurization in genesis of iron-nickel sulphide deposits of porcupine district Ontario. Canadian Mining and Metallurgical Bulletin, 59, 489.

Naldrett, A. J., Kullerud, G., (1967) A study of the Strathcona mine and its bearing on the origin of the nickel-copper ores of the Sudbury district, Ontario. J. Petrol. 8, 453-531.

Naldrett, A.J., Asif, M., Schandl, E., Searcy, T., Morrison, G.G., Binney, W.P., Moore, C., (1999) Platinum-group elements in the Sudbury ores: significance with respect to the origin of different ore zones and to the exploration for footwall orebodies. Econ. Geol. 94, 185–210.

Ojakangas, R.W., Morey, G.B., Green, J.C., (2001)The Mesoproterozoic midcontinent rift system, Lake Superior Region, USA. Sediment. Geol. 141–142, 421-442.

Osbahr, I., Klemd, R., Oberthür, T., Brätz, H., Schouwstra, R., (2013) Platinum-group element distribution in base-metal sulfides of the Merensky Reef from the eastern and western Bushveld Complex, South Africa. Miner. Deposita. 48, 211-232.

Osbahr, I., Oberthür, T., Klemd, R., Josties, A., (2014) Platinum-group element distribution in base-metal sulfides of the UG2 chromitite, Bushveld Complex, South Africa - a reconnaissance study. Miner. Deposita. 49, 655-665.

Piña, R., Gervilla, F., Barnes, S.-J., Ortega, L., Lunar, R., (2012) Distribution of platinum-group and chalcophile elements in the Aguablanca Ni–Cu sulfide deposit (SW Spain): Evidence from a LA-ICP-MS study. Chem. Geol. 302, 61-75.

Piña, R., Gervilla, F., Barnes, S.-J., Ortega, L., Lunar, R., (2013) Platinum-group elements-bearing pyrite from the Aguablanca Ni-Cu sulphide deposit (SW Spain): a LA-ICP-MS study. Eur. J. Mineral. 25, 241-252.

Piña, R., Gervilla, F., Barnes, S.-J., Ortega, L., Lunar, R., (2014) Liquid immiscibility between arsenide and sulfide melts: evidence from a LA-ICP-MS study in magmatic deposits at Serranía de Ronda (Spain). Miner. Deposita. 50, 265-279.

Piña, R., Gervilla, F., Barnes, S.-J., Oberthür, T., Lunar, R., (2016) Platinum-group element concentrations in pyrite from the Main Sulfide Zone of the Great Dyke of Zimbabwe. Miner. Deposita. 51, 853-872.

Prider, R.T., (1970) Nickel in Western australia. Nature, 226, 691-693.

Queffurus, M., Barnes, S.-J., (2014) Selenium and sulfur concentrations in country rocks from the Duluth Complex, Minnesota, USA: Implications for formation of the Cu-Ni-PGE sulfides. Econ. Geol. 109, 785-794.

Raič, S., Mogessie, A., Benkó, Z., Molnár, F., Hauck, S., Severson, M., (2015) Arsenic-rich Cu-Ni-PGE mineralization in Wetlegs, Duluth Complex, St. Louis County, Minnesota, USA. Can. Mineral. 53, 1-28.

Ripley, E.M., (1981) Sulfur isotopic studies of the Dunka road Cu-Ni deposit, Duluth Complex, Minnesota. Econ. Geol. 76, 610-620.

Ripley, E.M., Alawi, J.A., (1988) Petrogenesis of pelitic xenoliths at the Babbitt Cu-Ni deposit, Duluth Complex, Minnesota, U.S.A. Lithos. 21, 143-159.

Ripley, E.M., Taib, N.I., Chusi, L., Moore, C.H., (2007) Chemical and mineralogical heterogeneity in the basal zone of the Partridge River Intrusion: implications for the origin of Cu–Ni sulfide mineralization in the Duluth Complex, Midcontinent Rift System. Contrib. Mineral. Petrol. 154, 35-54.

Ripley, E.M., Li, C., (2013) Sulfide saturation in mafic magmas: Is external sulfur required for magmatic Ni-Cu-(PGE) ore genesis? Econ. Geol. 108, 45-58.

Ripley, E.M., (2014) Ni-Cu-PGE Mineralization in the Partridge River, South Kawishiwi, and Eagle Intrusions: A review of contrasting styles of sulfide-rich occurrences in the Midcontinent Rift System. Econ. Geol. 109, 309-324.

Samalens, N., Barnes, S.-J., and Sawyer, E. W., (2017) The role of black shales as a source of sulfur and semimetals in magmatic nickel-copper deposits: Example from the Partridge River Intrusion, Duluth Complex, Minnesota, USA. Ore Geol Rev. 81, 173-187.

Savard, D., Bédard, L. P., & Barnes, S. J., (2006) TCF selenium preconcentration in geological materials for determination at sub-μgg− 1 with INAA (Se/TCF-INAA). Talanta. 70, 566-571.

Savard, D., Barnes, S.-J., Meisel, T., (2010) Comparison between nickel-sulfur fire assay Te Co-precipitation and isotope dilution with high-pressure Asher acid digestion for

the determination of platinum-group elements, rhenium and gold. Geostand. Geoanal. Res. 34, 281-291.

Sawyer, E.W., (2014) The inception and growth of leucosomes: microstructure at the start of melt segregation in migmatites. J. Metamorph. Geol. 7, 695-712.

Smith, J.W., Holwell, D.A., McDonald, I., (2014) Precious and base metal geochemistry and mineralogy of the Grasvally Norite–Pyroxenite–Anorthosite (GNPA) member, northern Bushveld Complex, South Africa: implications for a multistage emplacement. Miner. Deposita. 49, 667-692.

Severson, M.J., Hauck, S.A., (1997) Igneous stratigraphy and mineralization in the basal portion of the Partridge River Intrusion, Duluth Complex, Allen Quadrangle, Minnesota: Duluth, Minnesota. University of Minnesota, Natural Resources Research Institute, Technical Report, NRRI/TR-97/19, 102 p.

Severson, M.J., Hauck, S.A., (2003) Platinum group elements (PGEs) and platinum group minerals (PGMs) in the Duluth Complex: Duluth, Minnesota. University of Minnesota, Natural Resources Research Institute, Technical Report, NRRI/TR-2003/37, 312 p.

Severson, M.J., Hauck, S.A., (2008) Finish logging of Duluth Complex Drill Core (and a reinterpretation of the geology at the Mesaba (Babbitt) deposit): Duluth. University of Minnesota, Natural Resources Research Institute, Technical Report, NRRI/TR-2008/17, 68 p.

Su, S., Lesher, C.M., (2012) Genesis of PGE mineralization in the Wengeqi mafic-ultramafic complex, Guyang County, Inner Mongolia, China. Mineral. Deposita, 47, 197–207.

Thériault, R.D., Barnes, S.-J., Severson, M.J., (1997) The influence of country-rock assimilation and silicate to sulfide ratios (R factor) on the genesis of the Dunka Road Cu – Ni – platinum-group element deposit, Duluth Complex, Minnesota. Can. J. Earth Sci. 34, 375-389.

Thériault, R.D., Barnes, S.-J., (1998) Compositional variations in Cu-Ni-PGE sulfides of the Dunka road deposit, Duluth Complex, Minnesota: The importance of combined assimilation and magmatic processes. Can. Mineral. 36, 869-886.

Thériault, R.D., Barnes, S.-J., Severson, M.J., (2000) Origin of Cu-Ni-PGE sulfide mineralization in the Partridge River Intrusion, Duluth Complex, Minnesota. Econ. Geol.

Tracy, R.J., Frost, B.R., (1991) Phase equilibria and thermobarometry of calcareous, ultramafic and mafic rocks, and iron formations. Rev. Mineral. Geochem. 26, 207-289.

Zanko, L.M., Severson, M.J., Ripley, E.M., (1994) Geology and mineralization of the Serpentine copper-nickel deposit, Duluth Complex, Minnesota. Duluth. University of Minnesota, Natural Resources Research Institute, Technical Report, NRRI/TR-93/52 (90 pp.).

CHAPITRE 5

CONCLUSION

5.1 INTRODUCTION

Les principales conclusions de ce projet de doctorat seront présentées dans ce chapitre. Les études pétrographique, texturale et géochimique ont permis de mettre en évidence un processus de contamination en S et en semi-métaux du magma et ainsi de répondre à la problématique principale de ce projet de doctorat. La contamination en S et en semi-métaux du magma se produirait lors du transfert de gouttelettes de sulfures depuis les xénolithes de la *Bedded Pyrrhotite Unit* vers le magma mafique via le produit de fusion partielle des xénolithes. De plus, une étude détaillée des conditions de fusion partielle des xénolithes et le calcul de modèles d'assemblages de minéraux à l'équilibre ont permis de mettre en évidence les conditions thermiques nécessaires à la réalisation de ce processus. Enfin, une étude détaillée de la distribution des éléments chalcophiles entre les différents minéraux a permis de mettre en évidence les phases hôtes des semi-métaux dans le Complexe de Duluth. Les réponses aux problématiques initiales seront ici abordées et discutées suivant l'ordre des trois chapitres centraux présentés dans cette thèse.

5.2 SYNTHÈSE DES RÉSULTATS

5.2.1 MÉCANISME DE CONTAMINATION EN S ET SEMI-MÉTAUX DU MAGMA

Dans ce projet de doctorat nous avons mis en évidence et décris que la contamination en S et en semi-métaux du magma se produit par le transfert de gouttelettes de sulfures des xénolithes de la *Bedded Pyrrhotite Unit* dans le magma via le produit de fusion partielle des xénolithes. Ces gouttelettes de liquide sulfurées sont transférées au magma lors de la

migration du produit de fusion partielle des xénolithes de la *Bedded Pyrrhotite Unit* vers le magma mafique. Des évidences pétrographiques et géochimiques supportent ce modèle. En effet, une décroissance progressive des rapports isotopiques du S ($\delta^{34}S$) et des rapports S/Se est observée depuis les xénolithes de la *Bedded Pyrrhotite Unit* vers les roches mafiques. Cette décroissance s'accompagne également d'une diminution du contenu en semi-métaux (c.à-.d., Te, As, Bi, Sb et Sn) des roches mafiques avec la distance depuis les xénolithes de la *Bedded Pyrrhotite Unit*. Ces variations sont observées dans les roches magmatiques de l'unité basale I, c.à-.d., à une distance d'environ 200 m depuis le contact avec les roches encaissantes.

De plus, suite à la libération de produit de fusion partielle des xénolithes de la *Bedded Pyrrhotite Unit* dans le magma mafique, la composition des roches mafiques entourant les xénolithes de la *Bedded Pyrrhotite Unit* est modifiée. En effet, les norites entourant les xénolithes de la *Bedded Pyrrhotite Unit* sont composées d'un mélange de produit de fusion partielle dérivée des xénolithes de la *Bedded Pyrrhotite Unit* et de composants d'origine magmatique.

Ce modèle explique également la présence de sulfures massifs autour des xénolithes de la *Bedded Pyrrhotite Unit*; ces sulfures étant accumulés autour des xénolithes de la *Bedded Pyrrhotite Unit* suite à la libération de gouttelettes de sulfures depuis les xénolithes.

Enfin, la diffusion de Ni, Cu et éléments du groupe du platine (EGP) depuis le magma mafique vers les xénolithes de la *Bedded Pyrrhotite Unit* a été mise en évidence. Les phases sulfurées de la *Bedded Pyrrhotite Unit* dans la Formation de Virginia sont composées majoritairement de pyrite et pyrrhotite. À l'inverse, les gouttelettes de sulfures dans le produit de fusion partielle des xénolithes de la *Bedded Pyrrhotite Unit* sont

composées de pyrrhotite, chalcopyrite, cubanite et pentlandite. De plus, des évidences géochimiques démontrent que les sulfures dans les xénolithes de la *Bedded Pyrrhotite Unit* sont plus riches en Ni, Cu et EGP que ceux des roches de la *Bedded Pyrrhotite Unit* de l'auréole de métamophisme de contact. Nous suggérons que la richesse en Ni, Cu et EGP des sulfures des xénolithes de la *Bedded Pyrrhotite Unit* résulte de la diffusion de ces éléments depuis le magma mafique vers les xénolithes. Cette diffusion est facilitée par la présence du produit de fusion partielle dérivé des xénolithes.

5.2.2 FUSION PARTIELLE DES XÉNOLITHES

Cette deuxième partie répond à la problématique initiale sur l'évaluation des conditions thermiques nécessaires pour que le processus de contamination en S et en semi-métaux du magma se produise. Les températures des xénolithes de la *Bedded Pyrrhotite Unit* sont comprises entre 800 et ~1000°C; températures obtenues suite à la réalisation de modèles thermodynamiques de fusion partielle des xénolithes résiduels de la *Bedded Pyrrhotite Unit* à l'aide du logiciel Perple_X. Ces températures supportent les températures empiriques calculées pour la fusion partielle de roches pélitiques et semi-pélitiques dans le faciès des granulites (White et al., 2003; Grant, 2009; Johnson et al., 2010; Chu and Ague, 2013).

Cette étude a montré que la majeure partie du produit de fusion partielle des xénolithes les plus résiduels de la *Bedded Pyrrhotite Unit* provenant du gisement de NorthMet a été extrait, il demeure ~10% de produit de fusion partielle dans ces xénolithes. Au contraire, les roches de la *Bedded Pyrrhotite Unit* dans l'auréole de contact ainsi que les xénolithes les moins résiduels de la *Bedded Pyrrhotite Unit* provenant du gisement de Mesaba

contiennent ~50 % de produit de fusion partielle. La libération de produit de fusion partielle dans le magma depuis les xénolithes constitue un paramètre important car suite à la libération du produit de fusion partielle des xénolithes de la *Bedded Pyrrhotite Unit* dans le magma mafique, la composition des roches mafiques entourant les xénolithes de la *Bedded Pyrrhotite Unit* sera modifiée.

5.2.3 PHASES HÔTES DES SEMI-MÉTAUX

Basé sur une étude au LA-ICP-MS du contenu en semi-métaux (Te, As, Bi, Sb et Sn) des minéraux de la *Bedded Pyrrhotite Unit* nous avons mis en évidence que les phases sulfurées des roches de la *Bedded Pyrrhotite Unit* sont enrichies en semi-métaux en comparaison avec les autres phases présentes dans la roche. Cependant, les semi-métaux ne sont pas exclusivement contenus dans les phases sulfurées. Ces éléments sont également contenus d'une part, dans les minéraux du groupe du platine (MGP) et certaines phases silicatées; c.-à-d., Pb dans les plagioclases et Sn dans les orthopyroxènes. D'autre part, dans les shales noirs à l'extérieur de l'auréole de contact ces éléments pourraient être distribués dans des phases matricielles telles que des phases riches en matière organique.

5.3 IMPLICATIONS

5.3.1 CONTAMINATION *IN-SITU* DU MAGMA

Notre étude démontre l'assimilation partielle de xénolithes de la *Bedded Pyrrhotite Unit* entraînant la contamination *in-situ* en S et en semi-métaux du magma de l'unité basale I de l'Intrusion de Partridge River du Complexe de Duluth. L'assimilation dans le magma des roches encaissantes sous forme de xénolithes riches en S se produit localement à la base de

l'Intrusion de Partridge River suite à la mise en place de l'intrusion (Ripley et Al-Jassar, 1987; Ripley et Alawi, 1988; Andrews et Ripley, 1989; Ripley et al., 1999; Thériault et al., 2000; Queffurus et Barnes, 2014; Williams et al., 2010; Robertson et al., 2015). En effet, la mise en place de l'intrusion dans la croûte entraîne une érosion thermomécanique des roches encaissantes et l'inclusion de xénolithes de roches encaissantes dans le magma. Ces xénolithes vont subir un épisode de fusion partielle dans le magma et libérer localement, c.-à-d., *in-situ*, une partie de leur produit de fusion partielle dans le magma. Lors de la libération de ce produit de fusion partielle dans le magma des gouttelettes de sulfures pourront être transférées selon le modèle proposé dans cette thèse de doctorat.

Ce mécanisme s'oppose à celui par lequel le magma serait contaminé à par une phase fluide riche en S dérivée des roches encaissantes (Ripley and Alawi, 1986; Ripley and Al-Jassar, 1987; Andrews and Ripley, 1989).

5.3.2 CONTAMINATION EN SEMI-MÉTAUX DU MAGMA

La richesse en semi-métaux des shales noirs est un facteur essentiel pour la formation des gisements de Ni-Cu-EGP. En effet, les semi-métaux sont des éléments importants pour la concentration des EGP dans les gisements de Ni-Cu-EGP car ils constituent les anions nécessaires pour la formation des minéraux du groupe du platine (Godel and Barnes, 2008; Dare et al., 2010; Chen et al., 2014). La contamination en semi-métaux du magma pour le Complexe de Duluth est donc une étape majeure pour la formation des gisements.

Notre étude montre que les shales noirs de la *Bedded Pyrrhotite Unit*, de part leur richesse en semi-métaux, constituent une source intéressante pour la contamination en semi-métaux du magma. De plus, des minéraux du groupe du platine ont été mis en

évidence dans cette étude, en complément de travaux antérieurs, et peuvent être formés suite à la contamination en semi-métaux du magma.

5.3.3 COMPOSITION DES SULFURES DANS LES ROCHES MAFIQUES

Dans le Complexe de Duluth, la composition des sulfures dans les roches mafiques est typiquement magmatique, les sulfures n'ayant pas subi de remobilisation hydrothermale (Thériault et al., 1997). La composition relativement homogène des sulfures dans les roches mafiques du Complexe de Duluth, leurs textures et l'absence d'évidences d'altération supporte cet argument.

La composition des sulfures dans les roches mafiques à proximité des xénolithes de roche encaissante admet une composante sédimentaire suite à l'assimilation des xénolithes dans le magma mafique (Thériault et al., 1997; Queffurus et Barnes, 2014). Thériault et al. (1997) proposent que le contenu en métaux des sulfures contenus dans les norites et les gabbronorites résulte de différents degrés de contamination du magma mafique et dépend du facteur R (rapport liquide silicaté / liquide sulfuré).

Notre étude montre que le contenu en métaux des sulfures dans les roches mafiques est dépendant du degré de contamination du magma et du facteur R tel que proposé par Thériault et al. (1997) et Queffurus et Barnes (2014). De plus, les analyses géochimiques roche totale montrent que le contenu en semi-métaux des sulfures dans le magma dépend de ces deux paramètres mais est également fortement dépendant du coefficient de partage pour les semi-métaux dans le liquide sulfuré (Li et Audétat, 2015; Brenan, 2015).

5.3.4 CONDITIONS THERMIQUES POUR LA CONTAMINATION DU MAGMA

L'assimilation de roches encaissantes par leur fusion partielle dans le magma est un mécanisme décrit par de nombreux auteurs (Gribble and O'Hara, 1967; Ripley and Alawi, 1988; Preston et al., 1999; Chesley et al., 2002; Beard et al., 2005; Markl, 2005; Clarke, 2007; Erdmann et al., 2007; Clarke et al., 2009; Shaw, 2009; Díaz-Alvarado et al., 2011; Hiebert et al., 2013; Dorfler et al., 2015; Robertson et al., 2015). De nombreux auteurs ont démontré l'importance de la fusion partielle des roches encaissantes pour la formation de gisements de Ni-Cu-EGP (Ripley et Alawi, 1988; Thériault et al., 1997; Thériault and Barnes, 1998; Amelin et al., 2000; Li and Naldrett, 2000; Ripley et al., 2000; Johnson et al., 2010; Queffurus and Barnes, 2014; Robertson et al., 2015).

Notre étude démontre une importante contribution de la fusion partielle des xénolithes de la *Bedded Pyrrhotite Unit* pour la formation des gisements de Ni-Cu-EGP dans le Complexe de Duluth. Les xénolithes subissent une fusion partielle dans le magma et leur température a atteint entre 800 et ~1000°C. Ces températures constituent un facteur critique dans la formation des gisements de l'Intrusion de Partridge River par le modèle de contamination en S et en semi-métaux du magma proposé dans cette étude. En effet, les températures sont suffisamment hautes pour permettre la fusion des sulfures dans les xénolithes (pyrrhotite et chalcopyrite) de la *Bedded Pyrrhotite Unit* et ainsi permettre leur transfert au magma sous forme de gouttelettes de sulfure lors de la libération de produit de fusion partielle des xénolithes dans le magma mafique.

5.3.5 EXPLORATION

Dans le cas du Complexe de Duluth les shales noirs riches en S de la *Bedded Pyrrhotite Unit* sont à l'origine de la contamination en S et en semi-métaux du magma mafique. La présence de shales noirs à proximité d'intrusions mafiques peut constituer une cible d'exploration pour identifier d'éventuels gisements de sulfures de Ni-Cu-EGP.

La présence de sulfures massifs autour des xénolithes de roches encaissantes est également un paramètre important pour l'exploration. En effet, les sulfures massifs se trouvent dans les zones basales de l'intrusion, à proximité des xénolithes de roches encaissantes.

Enfin, cette étude a montré que la présence de sulfures massifs pauvres en EGP, c.à-.d., formés avec un faible facteur R, dans la partie basale de l'intrusion n'exclue pas la présence de sulfures disséminés riches en EGP dans les unités magmatiques sus-jacentes.

5.4 APPORTS AUX DÉBATS ACTUELS

Notre étude s'inscrit dans la problématique actuelle d'améliorer notre compréhension des mécanismes de formation des gisements de Ni-Cu-EGP. De nombreux auteurs ont mis en évidence la connexion entre la fusion partielle des roches encaissantes riches en S et la formation de gisements mondiaux de Ni-Cu-EGP (Ripley and Alawi, 1988; Thériault et al., 1997; Thériault and Barnes, 1998; Amelin et al., 2000; Li and Naldrett, 2000; Ripley et al., 2000; Johnson et al., 2010; Queffurus and Barnes, 2014; Robertson et al., 2015). Le modèle de contamination *in-situ* en S et en semi-métaux du magma pour le Complexe de Duluth proposé dans ce projet de doctorat apporte ainsi des évidences supplémentaires pour ces mécanismes de formation. Nos travaux renforcent et supportent le modèle de contamination *in-situ* en S du magma proposé par Queffurus et Barnes (2014) et Thériault

et Barnes (1998) pour le Complexe de Duluth. Le modèle de contamination en S et en semi-métaux du magma proposé pour le Complexe de Duluth pourrait être applicable à la formation d'autres gisements sulfurés de Ni-Cu-EGP.

Enfin, les semi-métaux sont des éléments importants fréquemment mentionnées lors des débats actuels sur les énergies renouvelables; ce sont des éléments essentiels notamment pour la production de panneaux solaires photovoltaïques. Les shales noirs et les sulfures de métaux communs en tant que produit secondaire dans les gisements de Cu sont des sources potentielles de semi-métaux. Cependant, peu de données sur le contenu en semi-métaux des shales noirs et sur le contenu en semi-métaux des sulfures magmatiques sont présentées dans la littérature. Cela s'explique notamment par la difficulté de mesurer leurs concentrations dans les matériaux géologiques. En effet, ces éléments peuvent être retenus dans la matière organique ou encore se comporter comme des éléments volatiles lors des analyses et le contenu en semi-métaux des shales noirs sera alors sous estimé. Selon la méthode d'analyse choisie; c.-à-d. attaques avec acides, digestion haute température, analyses par activation neutronique (INAA), ces éléments peuvent également montrer des limites de détection trop hautes. En cela, les données obtenues sur le contenu en semi-métaux des shales noirs dans ce projet de doctorat s'ajoutent aux bases de données existantes et viennent les compléter.

5.5 INVESTIGATIONS FUTURES

Plusieurs questions peuvent être relevées suite à cette étude:

- Dans les shales noirs les moins métamorphisés à l'extérieur de l'auréole de métamorphisme de contact, quelles autres phases de la matrice contiennent les semi-métaux? Est-ce réellement des phases organiques ?

- Quelle est l'échelle de la contamination en S et en semi-métaux du magma mafique dans le Complexe de Duluth ? Cette étude répond en partie à cette question en proposant une contamination du magma en ces éléments pour une distance d'environ 200m depuis le contact avec les roches encaissantes dans les unités basales du Complexe de Duluth. Pourrait-on envisager une contamination à plus grande échelle ?

- Quelle est l'échelle des processus de diffusion de Ni, Cu et EGP ? Quels autres éléments pourraient avoir été impliqués dans ce processus de diffusion ?

- Peut-on évoquer d'autres mécanismes de ségrégation du produit de fusion partielle depuis les xénolithes vers le magma mafique ?

5.6 RÉFÉRENCES

Amelin, Y., Li, C., Valeyev, O. and Naldrett, A., (2000) Nd-Pb-Sr isotope systematics of crustal assimilation in the Voisey's Bay and Mushuau intrusions, Labrador, Canada. Economic Geology, 95, 815-830.

Andrews, D. and Ripley, E., (1989) Mass transfer and sulfur fixation in the contact aureole of the Duluth Complex, Dunka road Cu-Ni deposit, Minnesota. The Canadian Mineralogist, 27, 293-310.

Beard, J.S., Ragland, P.C. and Crawford, M.L., (2005) Reactive bulk assimilation: A model for crust-mantle mixing in silicic magmas. Geology 33, 681-684.

Brenan, J.M., Andrews, D., (2001) High-temperature stability of laurite and Ru–Os–Ir alloy and their role in PGE fractionation in mafic magmas. The Canadian Mineralogist, 39, 341-360.

Chen, L-M., Song, X-Y., Danyushevsky, L.V., Wang, Y-S., Tian, Y-L., Xiao, J-F., (2015) A laser ablation ICP-MS study of platinum-group and chalcophile elements in base metal sulfide minerals of the Jinchuan Ni–Cu sulfide deposit, NW China. Ore Geology Reviews. 65, 955-967

Chesley, J., Ruiz, J., Righter, K., Ferrari, L. and Gomez-Tuena, A., (2002) Source contamination versus assimilation: an example from the Trans-Mexican Volcanic Arc. Earth and Planetary Science Letters, 195, 211-221.

Chu, X., Ague, J.J., (2013) Phase equilibria for graphitic metapelite including solution of CO_2 in melt and cordierite: implications for dehydration, partial melting and graphite precipitation. J. Metamorph. Geol. 31, 843-862.

Clarke, D.B., (2007) Assimilation of xenocrysts in granitic magmas: principles, processes, proxies and problems. The Canadian Mineralogist, 45, 5-30.

Clarke, D.B., Erdmann, S., Samson, H. and Jamieson, R.A., (2009) Contamination of the South Mountain batholiths by sulfides from the country rocks. The Canadian Mineralogist, 47, 1159-1176.

Dare, S., Barnes, S.-J., Prichard, H., Fisher, P., (2010) The timing and formation of Platinum-Group minerals from the Creighton Ni-Cu-Platinum-Group Element Sulfide Deposit, Sudbury, Canada: Early crystallization of PGE-rich sulfarsenides. Economic Geology, 105, 1071-1096.

Díaz-Alvarado, J., Castro, A., Fernández, C. and Moreno-Ventas, I., (2011) Assessing Bulk Assimilation in Cordierite-bearing Granitoids from the Central System Batholith, Spain; Experimental, Geochemical and Geochronological Constraints. Journal of Petrology, 52, 223-256.

Dorfler, K.M., Caddick, M.J. and Tracy, R.J., (2015) Thermodynamic Modeling of Crustal Melting Using Xenolith Analogs from the Cortlandt Complex, New York, USA. Journal of Petrology, 56, 389-408.

Erdmann, S., London, D., Morgan, G.B. and Clarke, D.B., (2007) The contamination of granitic magma by metasedimentary country-rock material: an experimental study. The Canadian Mineralogist, 45, 43-61.

Godel, B., Barnes, S.-J., (2008) Platinum-group elements in sulfide minerals and the whole rocks of the J-M Reef (Stillwater Complex): Implication for the formation of the reef. Chemical Geology. 248, 272-294.

Grant, J.A., (2009) Thermocalc and experimental modeling of melting of pelite, Morton Pass, Wyoming. J. Metamorph. Geol. 27, 571-578.

Gribble, C.D. and O'Hara, M.J., (1967) Interaction of basic magma with pelitic materials. Nature, 214, 1198-1201.

Hiebert, R.S., Bekker, A., Wing, B.A. and Rouxel, O.J., (2013) The role of paragneiss assimilation in the origin of the Voisey's Bay Ni-Cu sulfide deposit, Labrador: Multiple S and Fe isotope evidence. Economic Geology, 108, 1459-1469.

Johnson, T.E., Brown, M. and White, R.W., (2010) Petrogenetic modeling of strongly residual metapelitic xenoliths within the southern Platreef, Bushveld Complex, South Africa. Journal of Metamorphic Geology, 28, 269-291.

Li, C. and Naldrett, A.J., (2000) Melting reactions of gneissic inclusions with enclosing magma at Voisey's Bay, Labrador, Canada: implications with respect to ore genesis. Economic Geology, 95, 801-814.

Li, Y., Audétat, A., (2015) Effects of temperature, silicate melt composition, and oxygen fugacity on the partitioning of V, Mn, Co, Ni, Cu, Zn, As, Mo, Ag, Sn, Sb, W, Au, Pb, and Bi between sulfide phases and silicate melt. Geochim. Cosmochim. Acta. 162, 25-45.

Markl, G., (2005) Mullite-corundum-spinel-cordierite-plagioclase xenoliths in the Skaergaard Marginal Border Group: multi-stage interaction between metasediments and basaltic magma. Contributions to Mineralogy and Petrology, 149, 196-215.

Preston, R.J., Dempster, T.J., Bell, B.R. and Rogers, G., (1999) The Petrology of Mullite-bearing Peraluminous Xenoliths: Implications for Contamination Processes in Basaltic Magmas. Journal of Petrology, 40, 549-573.

Queffurus, M. and Barnes, S.-J., (2014) Selenium and sulfur concentrations in country rocks from the Duluth Complex, Minnesota, USA: Implications for formation of the Cu-Ni-PGE sulfides. Economic Geology, 109, 785-794.

Ripley, E.M., Alawi, J.A., (1986) Sulfide mineralogy and chemical evolution of the Babbitt Cu-Ni deposit, Duluth Complex, Minnesota. The Canadian Mineralogist, 24, 347-368.

Ripley, E.M., Al-Jassar, T.J., (1987) Sulfur and oxygen isotope studies of melt-country rock interaction, Babbitt Cu-Ni deposit, Duluth Complex, Minnesota. Economic Geology, 82, 87-107.

Ripley, E.M. and Alawi, J.A., (1988) Petrogenesis of pelitic xenoliths at the Babbitt Cu-Ni deposit, Duluth Complex, Minnesota, U.S.A. Lithos, 21, 143-159.

Ripley, E.M., Lambert, D.D., Frick, L.R., (1999) Re-Os, Sm-Nd, and Pb isotopic constraints on mantle and crustal contributions to magmatic sulfide mineralization in the Duluth Complex. Geochimica et Cosmochimica Acta, 62, 3349-3365.

Ripley, E.M., Park, Y-R., Li, C. and Naldrett, A., (2000) Oxygen Isotope Studies of the Voisey's Bay Ni-Cu-Co Deposit, Labrador, Canada. Economic Geology, 95, 831-844.

Robertson, J., Ripley, E.M., Barnes, S.J., Li, C., (2015) Sulfur liberation from country rocks and incorporation in mafic magmas. Economic Geology, 110, 1111-1123.

Shaw, C.S.J., (2009) Caught in the act - The first few hours of xenolith assimilation preserved in lavas of the Rockeskyllerkopf volcano, West Eifel, Germany. Lithos, 112, 511-523.

Thériault, R.D., Barnes, S.-J. and Severson, M.J., (1997) The influence of country-rock assimilation and silicate to sulfide ratios (R factor) on the genesis of the Dunka Road Cu – Ni – platinum-group element deposit, Duluth Complex, Minnesota. Canadian Journal of Earth Sciences, 34, 375-389.

Thériault, R.D. and Barnes, S.-J., (1998) Compositional variations in Cu-Ni-PGE sulfides of the Dunka road deposit, Duluth Complex, Minnesota: The importance of combined assimilation and magmatic processes. The Canadian Mineralogist, 36, 869-886.

Thériault, R.D., Barnes, S.-J. and Severson, M.J., (2000) Origin of Cu-Ni-PGE Sulfide Mineralization in the Partridge River Intrusion, Duluth Complex, Minnesota. Economic Geology, 95, 929-943.

White, R.W., Powell, R., Clarke, G.L., (2003) Prograde metamorphic assemblage evolution during partial melting of metasedimentary rocks at low pressures: Migmatites from Mt Stafford, Central Australia. J. Petrol. 44, 1937-1960.

Williams, C.D., Ripley, E.M., Li, C., (2010) Variations in Os ratios of pyrrhotite as a result of water-rock and magma-rock interaction: Constraints from Virginia Formation-Duluth Complex contact zone. Geochimica et Cosmochimica Acta, 74, 4772-4792.

ANNEXES

ANNEXE 1: POSITION STRATIGRAPHIQUE DES ÉCHANTILLONS

Note:

La figure est renseignée en anglais dans un souci de cohérence avec les publications présentées dans ce mémoire de doctorat.

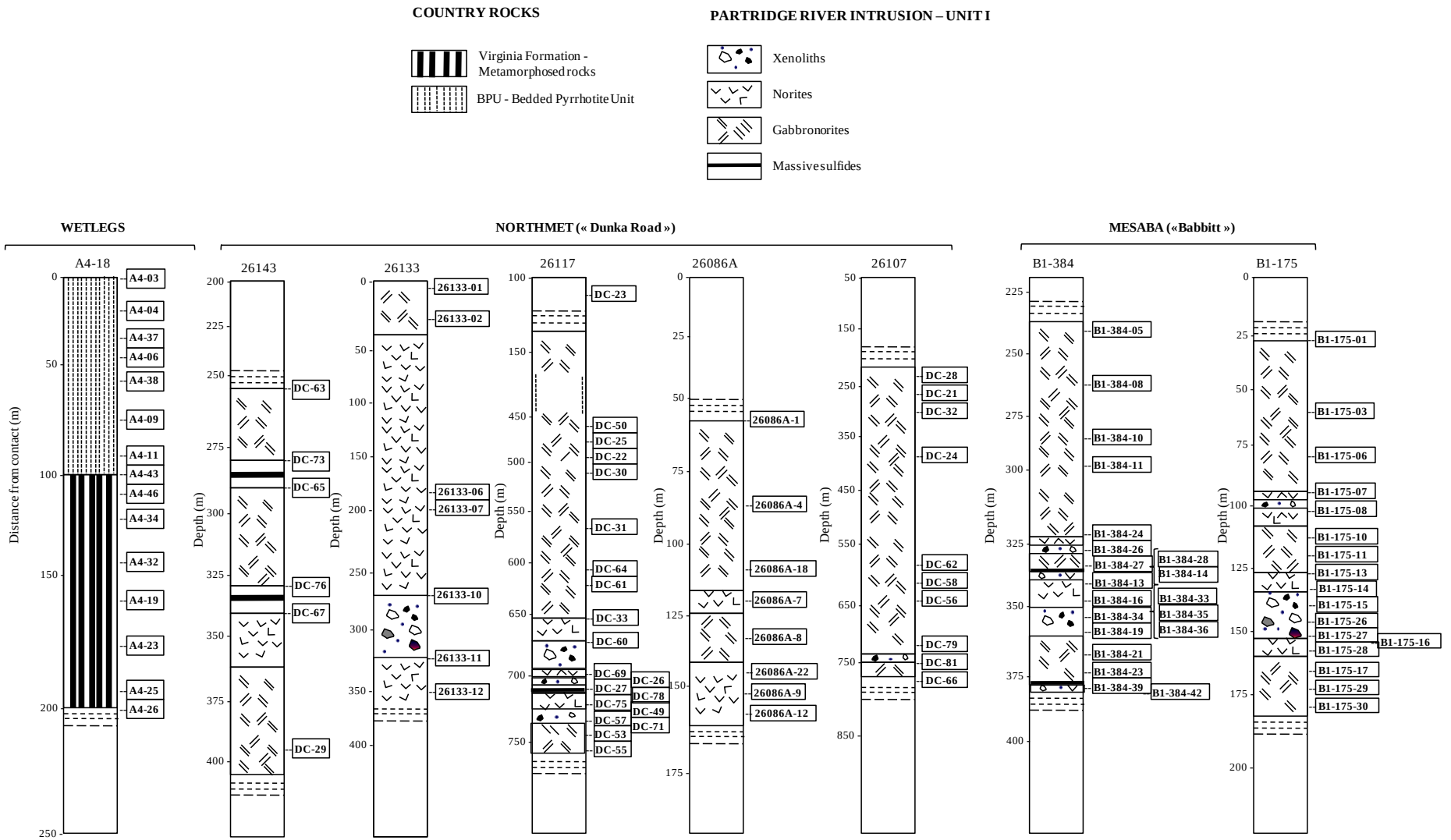
COUNTRY ROCKS
Virginia Formation - Metamorphosed rocks
BPU - Bedded Pyrrhotite Unit
PARTRIDGE RIVER INTRUSION – UNIT I
Xenoliths
Norites
Gabbronorites
Massive sulfides
WETLEGS
NORTHMET (« Dunka Road »)
MESABA («Babbitt »)
A4-18
26143
26133
26117
26086A
26107
B1-384
B1-175
Distance from contact (m)
Depth (m)
A4-03
A4-04
A4-37
A4-06
A4-38
A4-09
A4-11
A4-43
A4-46
A4-34
A4-32
A4-19
A4-23
A4-25
A4-26
DC-63
DC-73
DC-65
DC-76
DC-67
DC-29
26133-01
26133-02
26133-06
26133-07
26133-10
26133-11
26133-12
DC-23
DC-50
DC-25
DC-22
DC-30
DC-31
DC-64
DC-61
DC-33
DC-60
DC-69
DC-27
DC-75
DC-57
DC-53
DC-55
DC-26
DC-78
DC-49
DC-71
26086A-1
26086A-4
26086A-18
26086A-7
26086A-8
26086A-22
26086A-9
26086A-12
DC-28
DC-21
DC-32
DC-24
DC-62
DC-58
DC-56
DC-79
DC-81
DC-66
B1-384-05
B1-384-08
B1-384-10
B1-384-11
B1-384-24
B1-384-26
B1-384-27
B1-384-13
B1-384-16
B1-384-34
B1-384-19
B1-384-21
B1-384-23
B1-384-39
B1-384-28
B1-384-14
B1-384-33
B1-384-35
B1-384-36
B1-384-42
B1-175-01
B1-175-03
B1-175-06
B1-175-07
B1-175-08
B1-175-10
B1-175-11
B1-175-13
B1-175-14
B1-175-15
B1-175-26
B1-175-27
B1-175-28
B1-175-16
B1-175-17
B1-175-29
B1-175-30

ANNEXE 2: ANALYSES ISOTOPIQUES DU S ($\delta^{34}S$)

Abréviations:

BPU = Bedded Pyrrhotite Unit

Note:

Les tableaux sont renseignés en anglais dans un souci de cohérence avec les publications présentées dans ce mémoire de doctorat.

Samples	Rock type	Deposit	$\delta^{34}S$ (‰ VCDT)
DC-70	BPU contact aureole	Dunka Pit	16.3
A4-04	BPU contact aureole	Wetlegs	20.4
A4-09	BPU contact aureole	Wetlegs	16.7
A4-11	BPU contact aureole	Wetlegs	18.3
A4-38	BPU contact aureole	Wetlegs	19.5
B1-384-14	BPU xenolith	Mesaba	9.5
B1-384-19	BPU xenolith	Mesaba	11.5
B1-384-26	BPU xenolith	Mesaba	18.1
B1-384-33	BPU xenolith	Mesaba	10.7
B1-384-34	BPU xenolith	Mesaba	11.7
B1-384-35	BPU xenolith	Mesaba	12.2
B1-384-36	BPU xenolith	Mesaba	14.2
DC-69	BPU xenolith	NorthMet	16.9
DC-71	BPU xenolith	NorthMet	15.9
B1-384-28	Massive sulfides	Mesaba	12.0
B1-384-39	Massive sulfides	Mesaba	12.3
DC-73	Massive sulfides	NorthMet	8.4
DC-75	Massive sulfides	NorthMet	16.0
DC-76	Massive sulfides	NorthMet	12.0
B1-384-13	norite	Mesaba	13.2
B1-384-16	norite	Mesaba	12.5
B1-384-42	norite	Mesaba	12.2
DC-27	norite	NorthMet	14.5
DC-49	norite	NorthMet	8.2
DC-52	norite	NorthMet	13.7
DC-54	norite	NorthMet	12.5
DC-60	norite	NorthMet	10.4
DC-67	norite	NorthMet	5.3
B1-175-07	norite	Serpentine	10.6
B1-175-14	norite	Serpentine	15.3
B1-384-05	Gabbronorite	Mesaba	12.0
B1-384-08	Gabbronorite	Mesaba	6.1
B1-384-10	Gabbronorite	Mesaba	7.7
B1-384-21	Gabbronorite	Mesaba	12.4
26086A-18	Gabbronorite	NorthMet	10.7
26086A-21	Gabbronorite	NorthMet	12.8
DC-53	Gabbronorite	NorthMet	6.7
DC-55	Gabbronorite	NorthMet	9.0
DC-56	Gabbronorite	NorthMet	9.2
DC-58	Gabbronorite	NorthMet	6.6
DC-61	Gabbronorite	NorthMet	7.5
DC-62	Gabbronorite	NorthMet	1.6
DC-63	Gabbronorite	NorthMet	7.1
DC-64	Gabbronorite	NorthMet	2.8
DC-65	Gabbronorite	NorthMet	11.9
DC-66	Gabbronorite	NorthMet	9.8
DC-79	Gabbronorite	NorthMet	7.6
B1-175-06	Gabbronorite	Serpentine	13.7
B1-175-30	Gabbronorite	Serpentine	15.2

ANNEXE 3: MATÉRIAUX DE RÉFÉRENCE POUR LES ANALYSES ISOTOPIQUES DU S ($\delta^{34}S$)

Note:

Les tableaux sont renseignés en anglais dans un souci de cohérence avec les publications présentées dans ce mémoire de doctorat.

University of Waterloo Whole-rock $\delta^{34}S$	$\delta^{34}S$ (‰ VCDT)
DC-64 (This study)	3.0
DC-64 (Duplicate this study)	2.8
DC-64 (Thériault and Barnes, 1998)	2.5
B1-384-26 (This study)	18.4
B1-384-26 (Duplicate this study)	18.6
B1-384-26 (Queffurus and Barnes, 2014)	17.3

ANNEXE 4: GÉOCHIMIE SUR ROCHE TOTALE

Abréviations:

BS = Black shales

c.a. = Auréole de métamorphisme de contact

out. c.a.= Roches à l'extérieur de l'auréole de métamorphisme de contact

BPU = Bedded Pyrrhotite Unit

Kew. basalt = Basaltes de Keweenawan

Notes:

La composante sulfurée a été enlevée pour les éléments majeurs. Pour cela, le contenu en Fe des sulfures a été extrait du contenu de Fe total pour chaque analyse. Une normalisation à 100% des résultats a ensuite été réalisée. Ces données ont ensuite été utilisées pour les calculs des modèles présentés dans le chapitre 3.

Les tableaux sont renseignés en anglais dans un souci de cohérence avec les publications présentées dans ce mémoire de doctorat.

Les échantillons B1-384-19, B1-384-34, B1-384-35 et B1-384-36 correspondent à la partie interne (cœur) des xénolithes.

Samples	M-2-874	DC-08	M-2-1526	LTV-08	LTV-7555	DC-70	B1-331-01	B1-338-01	A4-01	A4-03	A4-04	A4-09
Rock type	BS out. c.a.	BS out. c.a.	BS out. c.a.	BS out. c.a.	BS out. c.a.	BPU c.a.	BPU c.a.	BPU c.a.	BPU c.a.	BPU c.a.	BPU c.a.	BPU c.a.
Deposit	B-2	B-2	B-2	LTV Mine	LTV Mine	Dunka Pit	Mesaba	Mesaba	Wetlegs	Wetlegs	Wetlegs	Wetlegs
S (%)	3.3	1.1	1.0	2.2	1.1	4.5	4.3	5.6	6.5	2.3	6.3	4.2
SiO_2 (wt%)	53.2	61.8	61.6	61.4	65.8	63.2	63.3	61.7	62.3	67.5	52.4	64.8
TiO_2 (wt%)	1.7	0.8	0.7	0.7	0.7	0.8	0.8	0.8	0.8	0.8	0.7	0.6
Al_2O_3 (wt%)	20.4	17.5	15.6	16.1	13.9	17.8	17.5	17.2	17.6	16.8	15.3	16.5
FeO (wt%)	7.6	5.5	4.1	4.0	4.9	2.0	1.9	1.1	1.2	3.7	0.7	0.1
MnO (wt%)	0.05	0.05	0.03	0.03	0.02	0.03	0.03	0.03	0.03	0.04	0.02	0.02
MgO (wt%)	3.0	3.3	2.7	3.4	2.1	2.9	3.2	3.2	2.3	2.7	1.6	1.7
CaO (wt%)	1.8	0.6	0.8	0.5	0.3	1.2	1.0	0.7	1.0	1.2	0.8	0.9
Na_2O (wt%)	4.0	2.1	1.9	1.1	1.4	2.0	2.0	1.5	1.6	1.7	1.6	1.6
K_2O (wt%)	2.8	3.7	3.4	3.9	3.5	3.6	4.0	4.7	4.4	1.4	4.3	5.4
P_2O_5 (wt%)	0.29	0.20	0.14	0.16	0.12	0.15	0.12	0.11	0.12	0.09	0.07	0.11
LOI	5.3	4.6	9.1	8.7	7.3	6.3	6.2	8.8	8.5	4.1	11.3	8.1
Ba (ppm)	745	583	471	531	581	469	585	488	498	309	494	558
Ce (ppm)	130.0	50.9	85.0	90.0	48.9	63.5	65.6	63.1	61.7	84.1	74.1	62.6
Cs (ppm)	5.4	9.5	10.6	8.5	8.6	7.8	8.1	12.0	7.8	4.7	8.7	11.1
Dy (ppm)	-	3.6	-	-	4.0	5.2	5.0	4.6	5.0	-	-	5.8
Eu (ppm)	2.9	1.2	1.7	2.1	0.8	1.8	1.6	1.5	1.3	1.5	2.1	1.5
Hf (ppm)	7.0	3.5	3.8	4.6	3.0	3.1	4.0	3.3	3.1	5.7	3.7	2.9
La (ppm)	64.7	26.0	41.7	38.2	25.7	33.3	34.6	33.2	32.7	38.7	34.1	32.2
Lu (ppm)	0.7	0.3	0.6	0.6	0.4	0.6	0.5	0.5	0.5	0.3	0.7	0.6
Nb (ppm)	-	10.5	-	-	9.3	10.0	11.3	10.0	9.5	-	8.0	8.8
Nd (ppm)	59.5	22.9	39.2	35.5	22.9	32.0	33.8	31.5	31.6	36.3	33.2	31.1
Pb (ppm)	-	13.0	-	-	78.8	24.5	20.0	42.7	37.0	12.6	-	35.0
Pr (ppm)	-	6.1	-	-	6.2	8.2	8.7	8.3	8.2	-	-	8.0
Rb (ppm)	102	145	140	155	154	101	142	178	159	52	172	191
Sm (ppm)	12.7	4.6	8.9	8.7	4.5	6.2	6.5	6.2	6.5	6.7	9.0	6.5
Sr (ppm)	-	72	-	-	62	237	196	132	106	-	112	138
Ta (ppm)	3.3	0.9	0.9	1.2	0.7	0.7	0.8	0.7	0.8	0.6	0.7	0.6
Tb (ppm)	1.3	0.6	0.8	0.9	0.6	0.9	0.9	0.8	0.8	0.8	1.0	0.9
Th (ppm)	13.8	10.4	10.0	10.4	9.1	8.3	8.9	8.3	8.2	10.8	9.7	8.1
U (ppm)	11.6	6.6	15.7	12.5	21.0	16.5	8.0	15.3	21.2	3.6	23.3	20.8
Y (ppm)	-	23.0	-	-	25.0	37.1	31.6	28.5	32.7	-	30.0	39.6
Yb (ppm)	4.1	2.3	3.1	3.1	2.7	3.8	3.4	3.0	3.4	1.7	3.8	4.1
Zr (ppm)	536	139	181	311	123	129	166	136	134	191	125	120
As (ppm)	6.2	14.0	20.6	2.6	19.6	15.2	29.0	13.8	10.0	31.6	22.4	13.0
Sb (ppm)	6.1	4.2	12.1	9.6	11.9	1.5	0.5	2.6	2.6	1.5	5.9	2.2
Bi (ppm)	-	<0,1	-	-	0.8	0.3	0.5	0.5	0.2	0.2	-	0.1
Te (ppm)	-	-	-	-	0.5	<0.06	0.2	0.1	-	<0.06	-	-
Ni (ppm)	95	80	137	200	100	130	120	90	187	289	140	80
Cu (ppm)	85	50	177	188	510	140	170	290	197	313	200	140
Co (ppm)	27	26	19	21	17	26	22	25	28	27	-	22
Ag (ppm)	<1.7	1.1	2.9	2.3	10.3	1.1	1.7	1.5	2.1	1.3	-	1.1
Se (ppm)	1.4	2.9	5.9	-	-	1.6	-	-	-	1.1	2.4	3.1
Pb(ppm)	-	13.0	-	-	78.8	24.5	20.0	42.7	37.0	12.6	-	35.0
Mo (ppm)	-	5.0	-	-	25.1	28.0	20.7	30.0	37.0	-	-	26.0
Os (ppb)	0.3	<0,159	<.30	0.5	<0,159	<1.5	0.3	0.3	0.2	-	-	0.4
Ir (ppb)	0.1	0.0	0.1	0.1	0.1	0.1	-	0.1	0.1	-	-	0.1
Ru (ppb)	5.0	<0,033	2.9	5.7	0.2	<5.0	0.2	0.2	0.2	-	-	0.2
Rh (ppb)	0.3	0.1	<.53	0.2	0.4	0.1	0.2	0.2	0.7	-	-	0.3
Pt (ppb)	2.4	1.7	12.5	4.1	8.0	4.9	3.1	9.7	9.3	-	-	-
Pd (ppb)	5.2	1.1	5.9	5.0	9.3	0.8	2.2	1.2	2.4	-	-	1.8
Au (ppb)	10.2	1.7	12.0	7.0	12.2	1.7	2.3	2.7	15.8	-	-	7.1

Samples	A4-11	A4-12A	A4-19	A4-38	A4-43	EC-07-A	B1-384-14	B1-384-18	B1-384-19	B1-384-207	B1-384-26	B1-384-33
Rock type	BPU c.a.	BPU c.a.	BPU c.a.	BPU c.a.	BPU c.a.	BPU xenolith	BPU xenolith	BPU xenolith	BPU xenolith	BPU xenolith	BPU xenolith	BPU xenolith
Deposit	Wetlegs	Wetlegs	Wetlegs	Wetlegs	Wetlegs	Dunka Pit	Mesaba	Mesaba	Mesaba	Mesaba	Mesaba	Mesaba
S (%)	6.7	5.9	0.3	2.2	1.5	2.5	7.1	7.7	5.5	1.2	3.7	5.3
SiO_2 (wt%)	62.0	61.9	64.7	60.7	65.4	48.7	51.8	53.7	59.7	55.5	54.2	56.4
TiO_2 (wt%)	0.8	0.9	0.9	0.8	0.8	2.1	0.7	0.7	0.8	0.7	0.5	0.7
Al_2O_3 (wt%)	17.7	18.3	17.6	16.3	16.5	18.2	18.3	19.1	18.4	19.2	18.5	16.9
FeO (wt%)	0.9	1.0	6.1	3.9	3.9	9.1	4.7	4.5	1.9	8.1	7.0	10.3
MnO (wt%)	0.03	0.05	0.07	0.05	0.04	0.17	0.11	0.04	0.03	0.06	0.15	0.04
MgO (wt%)	2.6	2.9	3.3	3.5	2.8	6.8	4.8	4.6	3.0	4.7	5.9	2.8
CaO (wt%)	0.7	1.1	0.6	1.3	1.2	10.0	3.0	1.9	1.0	1.0	4.1	0.9
Na_2O (wt%)	1.5	1.7	1.8	1.5	1.7	2.3	3.5	2.4	2.3	2.2	2.9	1.8
K_2O (wt%)	4.9	3.6	4.7	3.2	2.5	1.0	2.9	3.6	3.8	3.9	1.1	3.9
P_2O_5 (wt%)	0.08	0.14	0.13	0.16	0.13	0.27	0.08	0.10	0.14	0.12	0.09	0.11
LOI	8.8	8.4	-	3.4	1.9	1.2	10.1	9.4	9.0	4.5	5.5	6.2
Ba (ppm)	574	493	689	619	584	228	603	323	537	990	641	561
Ce (ppm)	59.9	71.5	83.4	79.9	68.6	36.0	62.7	54.5	77.7	83.2	62.6	72.5
Cs (ppm)	9.9	10.3	9.5	7.0	7.0	2.6	2.3	9.2	11.4	5.6	7.0	10.2
Dy (ppm)	4.4	5.3	-	-	-		-	-	-	-	4.2	-
Eu (ppm)	1.3	1.7	1.8	1.5	1.8	1.6	1.9	1.7	1.9	1.8	1.6	1.6
Hf (ppm)	3.0	3.3	3.9	4.4	4.6	3.4	3.0	2.4	3.6	3.7	3.2	3.2
La (ppm)	31.6	36.5	35.9	42.0	34.0	16.6	33.7	27.4	36.4	41.3	32.7	38.8
Lu (ppm)	0.5	0.5	0.4	0.4	0.4	0.3	0.5	0.6	0.8	0.4	0.4	0.7
Nb (ppm)	9.1	10.4	-	11.0	8.0		-	-	-	-	10.1	-
Nd (ppm)	30.1	36.8	28.8	39.7	31.4	20.1	26.9	26.2	36.3	37.8	30.6	35.5
Pb (ppm)	38.0	27.0	-	-	-	15.9	20.5	-	37.4	-	19.0	44.0
Pr (ppm)	7.8	9.4	-	-	-		-	-	-	-	8.1	-
Rb (ppm)	169	144	162	125	112	36	57	153	169	117	86	154
Sm (ppm)	5.9	7.4	6.3	6.8	6.0	4.8	4.9	6.4	9.8	7.7	6.0	7.4
Sr (ppm)	106	125	-	152	177	275	260	-	-	-	177	172
Ta (ppm)	0.8	0.8	0.7	0.8	0.6	1.6	1.3	0.5	0.8	0.9	0.9	1.9
Tb (ppm)	0.8	0.9	0.7	0.8	0.8	0.7	0.7	0.5	1.0	0.6	0.7	1.0
Th (ppm)	7.6	9.1	11.1	12.1	8.8	2.4	7.6	6.0	10.0	12.6	8.0	10.0
U (ppm)	20.9	18.3	7.7	5.2	4.1	0.9	3.7	10.6	21.0	4.9	13.5	20.2
Y (ppm)	29.3	34.3	-	27.0	26.0	-	-	-	-	-	26.3	-
Yb (ppm)	3.0	3.4	2.6	2.2	2.6	-	-	3.2	4.1	2.5	2.6	-
Zr (ppm)	124	134	151	162	166	139	130	<150	136	202	135	138
As (ppm)	22.9	27.0	14.1	31.4	35.0	22.0	47.0	63.2	112.4	25.0	22	36.4
Sb (ppm)	1.9	1.9	2.0	1.4	1.2	3.0	1.1	10.5	4.9	6.3	0.4	2.7
Bi (ppm)	0.5	0.1	-	-	-	2.2	1.5	-	0.5	-	0.4	0.7
Te (ppm)	0.6	-	-	-	-	0.3	0.1	-	0.6	-	0.3	0.5
Ni (ppm)	150	150	135	101	67	730	2720	2192	607	457	900	1120
Cu (ppm)	260	310	58	130	59	3965	4129	4666	1986	981	3100	3371
Co (ppm)	34	29	18	-	-	86	307	218	54	48	152	129
Ag (ppm)	0.9	1.6	1.6	-	-	1.4	1.4	4.2	7.5	-	1.0	2.4
Se (ppm)	4.4		0.5	2.2	1.4	2.4	6.2	-	2.5	-	3.7	2.3
Pb(ppm)	38.0	27.0	-	-	-	15.9	20.5	-	37.4	-	19.0	44.0
Mo (ppm)	23.9	31.0	-	-	-	2.8	25.0	-	-	-	24.3	20.4
Os (ppb)	<0.2	0.2	-	-	-	-	0.3	<1.2	0.4	0.2	<0.6	0.3
Ir (ppb)	-	0.1	-	-	-	0.3	-	0.6	0.1	-	0.2	-
Ru (ppb)	0.1	0.2	-	-	-	1.1	0.2	<7.3	3.3	2.9	2.6	0.2
Rh (ppb)	0.1	0.3	-	-	-	1.3	0.3	2.1	<0.1	<2.2	1.0	-
Pt (ppb)	6.1	6.2	-	-	-	22.7	15.3	4.0	0.9	1.4	9.3	1.4
Pd (ppb)	1.2	8.0	-	-	-	58.4	144.8	27.4	12.5	<9.1	41.7	11.5
Au (ppb)	3.5	8.5	-	-	-	26.6	6.2	14.8	11.1	24.2	16.2	4.3

Samples	B1-384-34	B1-384-35	B1-384-36	B1-46-02	B1-46-05a	26014-01a	26015-01b	26086A-11	DC-26	DC-69	DC-71	DC-78
Rock type	BPU xenolith	BPU xenolith	BPU xenolith	BPU xenolith	BPU xenolith	BPU xenolith	BPU xenolith	BPU xenolith	BPU xenolith	BPU xenolith	BPU xenolith	BPU xenolith
Deposit	Mesaba	Mesaba	Mesaba	Mesaba	Mesaba	NorthMet	NorthMet	NorthMet	NorthMet	NorthMet	NorthMet	NorthMet
S (%)	5.2	6.4	6.4	0.5	2.7	1.2	0.0	3.8	0.7	5.9	10.2	1.6
SiO_2 (wt%)	60.7	62.7	61.5	64.3	59.8	50.9	55.5	62.7	47.9	43.9	48.6	45.6
TiO_2 (wt%)	0.8	0.8	0.8	0.8	0.7	1.2	0.8	0.4	0.1	0.7	0.8	1.8
Al_2O_3 (wt%)	18.7	18.8	18.7	17.0	17.0	18.8	16.6	10.4	29.6	29.5	20.7	27.5
FeO (wt%)	1.2	0.1	0.5	4.4	4.3	10.9	11.6	8.3	8.6	12.8	7.7	12.8
MnO (wt%)	0.03	0.05	0.05	0.03	0.02	0.21	0.10	0.22	0.06	0.06	0.07	0.07
MgO (wt%)	3.0	3.4	3.2	3.6	2.9	6.7	4.9	5.0	11.2	10.3	5.5	9.4
CaO (wt%)	1.2	1.7	0.8	4.1	0.4	6.7	2.8	6.8	0.5	0.2	1.6	0.1
Na_2O (wt%)	2.1	2.4	2.2	3.6	1.9	2.9	3.2	0.5	0.2	0.2	2.6	0.2
K_2O (wt%)	3.9	2.1	4.2	2.0	4.6	0.5	3.0	0.5	0.6	0.7	3.2	0.7
P_2O_5 (wt%)	0.14	0.12	0.12	0.18	0.12	0.05	0.17	0.09	-	-	0.05	0.02
LOI	8.1	7.7	7.8	-	8.1	1.1	1.3	5.1	1.3	1.7	9.3	1.9
Ba (ppm)	545	388	580	505	489	241	197	191	24	15	339	102
Ce (ppm)	79.8	69.2	65.1	68.9	69.7	51.6	52.4	45.0	<.83	1.4	42.4	3.6
Cs (ppm)	13.1	10.4	10.4	5.5	7.8	4.3	27.1	2.1	5.6	3.2	3.3	6.2
Dy (ppm)	-	-	-	-	-	-	-	-	-	0.2	3.1	-
Eu (ppm)	1.8	1.7	1.6	1.5	1.4	3.1	1.5	1.6	<.13	0.0	2.4	0.0
Hf (ppm)	3.6	3.5	3.4	4.3	4.3	1.9	3.4	2.8	<.38	0.3	1.6	0.8
La (ppm)	36.2	36.0	34.5	36.3	33.8	30.9	25.6	18.8	0.4	0.7	22.9	1.8
Lu (ppm)	0.9	0.7	0.7	0.5	0.6	0.4	0.5	0.3	0.1	0.0	0.4	0.1
Nb (ppm)	-	33.0	-	-	-	-	-	-	-	2.3	10.4	-
Nd (ppm)	37.4	35.4	33.3	33.0	32.7	20.0	21.5	17.5	3.3	0.6	19.6	1.1
Pb (ppm)	29.7	31.0	17.9	-	-	-	-	-	-	0.2	19.0	-
Pr (ppm)	-	-	-	-	-	-	-	-	-	0.2	5.2	-
Rb (ppm)	196	86	132	93	157	25	287	15	53	37	37	40
Sm (ppm)	10.1	7.2	7.0	7.8	7.7	3.1	5.0	5.1	0.1	0.1	3.6	0.4
Sr (ppm)	-	214	150	-	-	-	-	-	-	7	271	-
Ta (ppm)	1.0	2.0	1.6	1.2	0.9	0.7	0.8	0.5	5.0	0.9	0.7	0.9
Tb (ppm)	1.0	1.1	1.0	0.7	0.9	0.3	0.6	0.7	<.13	0.0	0.5	<0,04
Th (ppm)	9.9	10.0	9.3	10.8	10.0	0.8	5.2	4.8	<.15	0.2	2.4	1.1
U (ppm)	22.3	24.8	21.5	10.3	9.2	0.3	4.7	1.7	<.19	0.1	5.4	0.3
Y (ppm)	-	-	-	-	-	-	-	-	-	1.0	20.9	-
Yb (ppm)	4.1	-	-	2.8	3.6	2.8	2.9	1.9	0.2	0.2	2.9	0.6
Zr (ppm)	<210	137	134	97	411	89	192	92	-	10	63	-
As (ppm)	48.0	40.1	23.0	35.5	34.2	18.6	22.0	36.4	14.4	65.2	9.0	6.0
Sb (ppm)	2.4	2.8	2.8	6.2	8.9	4.8	30.8	2.3	1.1	< 0.2	0.5	0.2
Bi (ppm)	0.5	1.0	0.8	-	-	-	-	-	-	<0.1	<0.1	-
Te (ppm)	0.6	0.5	0.3	-	-	-	-	-	-	0.5	-	-
Ni (ppm)	535	430	410	125	264	195	166	973	150	670	280	355
Cu (ppm)	1221	1926	2067	144	438	251	2	1123	422	930	1060	732
Co (ppm)	32	73	60	18	23	46	27	82	166	157	44	69
Ag (ppm)	5.9	1.3	1.3	1.4	1.7	-	<2.2	2.3	-	0.5	-	-
Se (ppm)	2.7	2.4	2.8	-	1.4	1.2	0.0	-	-	1.9	0.1	-
Pb(ppm)	29.7	31.0	17.9	-	-	-	-	-	-	0.2	19.0	-
Mo (ppm)		24.6	18.5	-	-	-	-	-	-	28.4	11.0	-
Os (ppb)	0.2	0.3	0.3	<0.2	0.6	<.35	<0.37	<0.2	0.7	1.2	<0.6	0.7
Ir (ppb)	-	-	-	-	-	0.1	0.1	0.6	0.3	0.8	0.3	0.2
Ru (ppb)	2.8	-	0.2	<2.7	2.5	4.0	2.3	5.3	<2.9	7.5	0.3	1.7
Rh (ppb)	0.2	-	0.1	<0.2	0.2	0.5	0.2	4.5	0.7	1.4	1.3	0.4
Pt (ppb)	51.4	0.7	1.7	2.9	1.7	2.2	<1.2	<1.6	6.0	13.1	3.6	9.0
Pd (ppb)	3.9	3.5	9.6	2.7	3.5	2.6	4.5	93.9	2.9	36.1	40.7	5.3
Au (ppb)	2.0	2.9	6.3	4.9	2.9	6.0	2.5	2.7	144.0	282.0	43.0	122.0

Samples	DC-81	B1-175-08	B1-175-15	B1-175-26	B1-175-27	26133-11	B1-384-04b	26014-01b	26015-03a	26015-1	DC-80	A4-06
Rock type	BPU xenolith	BPU xenolith	BPU xenolith	BPU xenolith	BPU xenolith	BPU xenolith	Leucosome	Leucosome	Leucosome	Leucosome	Leucosome	Leucosome c.a.
Deposit	NorthMet	Serpentine	Serpentine	Serpentine	Serpentine	Wyman creek	Mesaba	NorthMet	NorthMet	NorthMet	NorthMet	Wetlegs
S (%)	0.4	1.3	4.5	4.9	5.5	1.2	0.0	0.0	0.1	0.4	1.2	1.4
SiO_2 (wt%)	46.7	51.0	60.6	61.1	52.8		75.7	75.5	73.5	69.7	61.0	70.2
TiO_2 (wt%)	1.6	1.4	0.7	0.7	0.9	0.6	0.1	0.1	0.1	0.6	0.8	0.2
Al_2O_3 (wt%)	22.0	22.0	17.9	18.0	17.8	53.4	12.7	13.0	13.6	14.8	17.4	15.1
FeO (wt%)	14.5	12.0	1.6	1.0	4.1	21.5	0.4	0.5	1.1	2.7	6.2	0.4
MnO (wt%)	0.11	0.10	0.03	0.02	0.05	0.05	0.01	0.01	0.02	0.02	0.05	0.01
MgO (wt%)	10.1	7.5	2.9	2.5	3.9	23.4	0.5	0.2	0.7	1.5	3.4	0.8
CaO (wt%)	0.4	1.3	0.7	0.5	1.2		0.7	2.6	0.7	0.7	0.9	0.3
Na_2O (wt%)	1.0	1.9	2.3	2.3	2.1	1.2	1.8	2.8	2.2	4.6	4.8	1.9
K_2O (wt%)	0.6	1.6	5.0	5.0	8.3		7.5	4.6	7.2	3.5	4.3	8.6
P_2O_5 (wt%)	0.02	0.05	0.12	0.12	0.14		0.01	0.04	0.13	0.22	0.01	0.13
LOI	2.9	1.1	7.3	7.7	7.6	-	0.5	0.7	0.7	1.5	1.2	2.4
Ba (ppm)	18	581	562	584	623	65	140	90	129	169	539	1066
Ce (ppm)	13.0	56.1	73.7	74.0	76.5	14.2	35.0	9.7	11.6	22.7	71.8	32.3
Cs (ppm)	3.2	3.7	8.3	7.3	4.8	6.8	4.9	6.7	3.3	0.3	5.1	2.6
Dy (ppm)	-	-	-	-	-	-	3.0	-	-	-	-	-
Eu (ppm)	0.5	2.2	1.5	1.5	1.7	0.2	1.3	0.1	0.8	0.9	1.2	2.8
Hf (ppm)	1.3	2.6	4.0	4.2	3.7	1.0	2.5	2.1	3.4	3.2	3.5	1.0
La (ppm)	6.4	32.0	37.2	36.5	39.9	6.1	19.2	5.3	4.9	8.8	34.0	13.2
Lu (ppm)	0.4	0.4	0.7	0.7	0.4	0.3	0.3	0.5	0.9	1.0	0.4	0.5
Nb (ppm)	-	-	-	-	-	-	12.8	-	-	-	-	-
Nd (ppm)	3.2	23.3	34.6	33.8	36.6	4.6	16.0	5.9	8.1	15.7	32.1	9.4
Pb (ppm)	-	-	-	-	-	-	14.0	-	-	-	-	-
Pr (ppm)	-	-	-	-	-	-	4.2	-	-	-	-	-
Rb (ppm)	43	43	156	143	267	47	167	270	198	46	5	223
Sm (ppm)	1.0	3.9	8.3	8.6	7.6	1.5	3.1	3.5	4.6	6.5	6.4	5.3
Sr (ppm)	-	-	-	-	-	65	166	-	-	-	-	108
Ta (ppm)	0.6	0.9	0.8	0.9	0.6	0.1	1.1	3.5	1.1	1.6	0.6	0.2
Tb (ppm)	0.1	0.4	0.9	0.9	0.7	0.8	0.5	0.4	0.4	0.5	0.8	0.4
Th (ppm)	0.5	5.1	9.9	10.1	9.6	2.2	4.2	4.1	6.5	6.3	15.2	4.6
U (ppm)	0.1	0.9	10.9	12.3	5.7	2.2	3.1	8.4	25.6	34.2	5.3	31.2
Y (ppm)	-	-	-	-	-	-	18.8	-	-	-	-	-
Yb (ppm)	1.9	2.4	3.7	3.5	2.6	1.4	2.2	2.1	4.4	4.1	1.7	2.0
Zr (ppm)	-	99	<56	108	<80	27	101	<69	243	<200	-	43
As (ppm)	82.9	11.4	178.9	50.6	73.4	22.2	11.0	19.3	4.1	24.2	24.6	14.3
Sb (ppm)	1.1	4.2	9.5	8.3	5.5	1.3	< 0.2	7.6	3.8	0.3	1.9	2.0
Bi (ppm)	-	-	-	-	-	-	<0,1	-	-	-	-	-
Te (ppm)	-	-	-	-	-	-	-	-	-	-	-	-
Ni (ppm)	291	414	867	697	1086	366	410	0	95	41	123	154
Cu (ppm)	420	662	1928	1590	2196	202	920	2	2	86	646	51
Co (ppm)	83	67	70	55	133	66	79	2	1	9	25	3
Ag (ppm)	-	8.7	5.3	4.6	0.9	-	0.6	<0.90	<1.5	2.0	-	1.0
Se (ppm)	-	0.8	1.6	1.1	1.4	-	0.0	0.0	0.1	0.3	-	0.5
Pb(ppm)	-	-	-	-	-	-	14.0	-	-	-	-	-
Mo (ppm)	-	-	-	-	-	-	3.0	-	-	-	-	-
Os (ppb)	0.6	0.5	0.4	0.3	0.3	-	0.3	<.34	<0.5	<0.43	<0.6	-
Ir (ppb)	0.3	0.5	0.1	0.1	0.1	0.2	0.9	0.1	0.0	0.0	0.1	-
Ru (ppb)	<2.6	8.5	3.9	1.9	10.1	8.6	3.0	1.3	3.7	1.6	<2.5	-
Rh (ppb)	0.3	1.5	0.4	8.8	0.2	1.8	2.4	<0.55	<0.74	<0.31	0.1	-
Pt (ppb)	7.4	9.0	4.8	0.9	2.6	33.4	26.9	<1.4	<1.0	<0.82	2.6	-
Pd (ppb)	8.3	11.2	17.9	8.2	23.0	8.7	70.8	6.4	<2.3	2.4	4.0	-
Au (ppb)	72.0	4.8	13.6	6.9	9.4	13.4	5.9	2.6	<0.7	2.7	650.0	-

Samples Rock type Deposit	A4-34 Leucosome c.a. Wetlegs	A4-37 Leucosome c.a. Wetlegs	B1-384-39 Massive sulfides Mesaba	DC-73 Massive sulfides NorthMet	DC-74 Massive sulfides NorthMet	DC-75 Massive sulfides NorthMet	DC-76 Massive sulfides NorthMet	B1-384-04a norite Mesaba	B1-384-12 norite Mesaba	B1-384-13 norite Mesaba	B1-384-15 norite Mesaba	B1-384-16 norite Mesaba
S (%)	0.2	1.1	16.3	19.6	22.2	31.2	34.9	0.0	1.3	1.7	1.6	7.2
SiO_2 (wt%)	73.1	82.1	34.4	37.3	44.2	33.5	27.7	51.9	49.8	47.6	46.0	47.6
TiO_2 (wt%)	0.1	0.3	1.9	4.8	0.9	1.4	3.8	1.4	1.8	5.4	4.5	5.4
Al_2O_3 (wt%)	13.3	9.1	10.7	7.5	13.7	12.3	4.5	23.3	19.0	15.1	14.8	16.6
FeO (wt%)	2.7	0.4	29.7	31.4	25.6	37.6	42.5	6.3	11.3	14.1	16.1	12.2
MnO (wt%)	0.05	0.01	0.15	0.28	0.21	0.12	0.25	0.07	0.16	0.20	0.20	0.23
MgO (wt%)	1.6	0.6	2.9	9.7	4.9	6.8	5.4	2.7	6.1	6.5	5.7	5.6
CaO (wt%)	1.0	0.3	3.3	6.7	1.0	4.1	11.8	9.5	8.1	9.0	9.0	5.7
Na_2O (wt%)	2.0	1.1	2.2	1.0	1.7	1.0	1.3	3.6	2.5	1.7	2.6	3.1
K_2O (wt%)	4.0	4.5	1.4	0.3	2.7	0.4	1.2	0.8	0.5	0.3	0.9	0.7
P_2O_5 (wt%)	0.24	0.09	0.50	0.04	0.04		1.56	0.14	0.15	0.15	0.28	0.13
LOI	1.9	1.5	8.0	0.5	2.4	0.7	-	0.2	0.6	0.0	0.0	2.3
Ba (ppm)	176	442	179	56	99	<59	-	178	165	159	231	137
Ce (ppm)	8.4	18.0	29.4	3.7	10.9	<.88	-	31.2	26.5	22.6	44.8	19.6
Cs (ppm)	1.8	2.7	0.9	<.43	0.9	<.48	-	9.2	1.9	1.1	1.5	0.8
Dy (ppm)	-	-	2.2	-	-	-	-	3.2	2.3	-	-	3.5
Eu (ppm)	1.0	1.2	0.8	0.6	0.4	0.2	-	1.8	1.3	1.7	2.1	1.6
Hf (ppm)	2.7	2.2	0.8	0.9	0.6	<.19	-	1.8	1.4	2.2	4.1	1.4
La (ppm)	4.1	9.4	14.8	2.4	6.6	1.5	-	15.2	13.6	11.8	17.8	10.1
Lu (ppm)	0.4	0.3	0.2	0.1	0.1	<.02	-	0.3	0.3	0.3	0.4	0.3
Nb (ppm)	-	-	7.6	-	-	-	-	9.9	6.9	-	-	12.7
Nd (ppm)	3.0	8.4	15.4	5.0	3.7	<2.8	-	14.4	11.8	13.8	21.5	10.7
Pb (ppm)	-	-	5.8	-	-	-	-	7.0	17.0	-	-	8.0
Pr (ppm)	-	-	3.8	-	-	-	-	3.9	3.2	-	-	2.6
Rb (ppm)	64	118	32	12	28	<7.8	-	77	21	15	27	8
Sm (ppm)	6.2	4.0	3.1	1.2	1.0	0.2	-	3.2	2.4	3.6	5.7	2.6
Sr (ppm)	58	70	73	-	-	-	-	394	242	-	-	192
Ta (ppm)	1.5	0.4	8.0	0.5	0.2	-	-	1.0	0.5	1.2	1.2	0.8
Tb (ppm)	0.3	0.4	0.4	<.22	<.09	<.08	-	0.5	0.4	0.5	0.9	0.5
Th (ppm)	2.4	6.5	1.6	0.7	3.1	1.3	-	4.1	3.2	2.0	2.8	0.7
U (ppm)	48.2	19.9	0.7	<.31	0.3	1.1	-	2.9	1.7	1.3	0.9	1.3
Y (ppm)	-	-	13.2	-	-	-	-	19.3	11.9	-	-	20.5
Yb (ppm)	2.4	1.6	1.0	0.9	0.4	<.12	-	2.0	1.5	1.9	2.5	2.3
Zr (ppm)	54	70	23	-	-	-	-	67	53	97	73	55
As (ppm)	8.5	24.3	44.0	33.3	25.2	174.8	104.4	<5	22.0	8.2	8.5	29.0
Sb (ppm)	3.4	1.6	0.1	0.2	0.4	0.4	2.4	< 0.2	0.5	1.2	1.7	< 0.2
Bi (ppm)	-	-	0.2	0.6	1.8	0.6	1.4	<0.1	<0.1	-	-	0.2
Te (ppm)	-	-	2.6	0.4	0.5	1.1	0.9	<0.06	<0.06	-	-	-
Ni (ppm)	-	22	9890	10691	14518	6840	18731	260	1570	786	1100	470
Cu (ppm)	15	43	30108	12154	18206	11369	5423	950	6500	2164	4862	1830
Co (ppm)	5	7	960	1097	1586	1245	-	18	134	108	125	81
Ag (ppm)	-	-	6.8	1.1	2.0	11.5	-	-	1.0	2.3	2.3	0.5
Se (ppm)	0.2	1.0	24.5	25.0	22.0	13.0	43.0	1.5	3.1	1.9	-	3.0
Pb(ppm)	-	-	5.8	-	-	-	-	7.0	17.0	-	-	8.0
Mo (ppm)	-	-	23.0	-	-	-	-	2.0	<2	-	-	<2
Os (ppb)	-	-	8.5	1.2	3.5	3.8	4.6	0.8	0.6	<0.4	<0.4	0.7
Ir (ppb)	-	-	8.0	38.2	9.3	2.3	27.0	0.6	0.9	0.3	0.7	2.1
Ru (ppb)	-	-	39.5	26.9	18.9	<9.3	39.9	2.5	4.7	4.4	3.4	5.1
Rh (ppb)	-	-	14.9	116.4	32.0	11.8	116.9	1.2	2.1	0.9	1.8	4.3
Pt (ppb)	-	-	5.4	88.9	32.5	23.2	34.6	9.0	22.7	10.3	23.5	9.3
Pd (ppb)	-	-	63.1	469.9	626.5	876.7	1590.0	10.9	47.9	27.1	52.4	36.8
Au (ppb)	-	-	22.1	286	3471	1310	<2	1.2	15.5	12.8	27.5	33.3

Samples Rock type Deposit	B1-384-24 norite Mesaba	B1-384-27 norite Mesaba	B1-384-30 norite Mesaba	B1-384-42 norite Mesaba	26086A-05 norite NorthMet	26086A-06. norite NorthMet	26086A-07 norite NorthMet	26086A-09 norite NorthMet	26086A-10 norite NorthMet	26086A-12 norite NorthMet	26086A-22 norite NorthMet	DC-27 norite NorthMet
S (%)	3.2	2.3	2.3	6.3	2.8	3.6	1.6	1.5	5.5	0.9	3.4	0.8
SiO_2 (wt%)	49.4	47.2	46.3	50.3	45.7	50.2	45.6	50.1	47.5	48.7	48.3	43.5
TiO_2 (wt%)	2.0	3.6	4.4	3.3	7.5	2.7	5.3	2.2	3.9	2.9	2.7	6.9
Al_2O_3 (wt%)	18.0	16.9	15.5	14.1	10.7	15.1	13.9	16.6	15.2	15.5	14.1	6.6
FeO (wt%)	12.5	14.6	14.9	16.0	18.4	12.3	15.2	11.2	15.7	14.0	15.0	23.8
MnO (wt%)	0.20	0.19	0.21	0.23	0.24	0.15	0.22	0.14	0.19	0.19	0.20	0.25
MgO (wt%)	6.9	7.0	5.9	3.3	8.6	6.8	6.5	6.3	6.0	5.7	8.8	12.0
CaO (wt%)	6.9	8.0	8.8	6.7	4.3	4.5	8.7	7.7	7.3	8.3	6.9	4.2
Na_2O (wt%)	2.3	2.0	2.5	2.8	1.7	2.6	1.5	1.6	1.5	3.0	1.8	0.8
K_2O (wt%)	0.5	0.3	0.7	0.4	0.9	1.0	0.6	0.8	0.4	1.3	0.7	0.2
P_2O_5 (wt%)	0.11	0.17	0.24	1.19	0.22	0.08	0.34	0.28	0.17	0.40	0.29	0.52
LOI	1.1	0.0	0.5	1.5	1.6	4.1	2.0	2.9	1.7	0.0	1.1	1.2
Ba (ppm)	157	190	212	218	157	282	290	256	198	314	204	57
Ce (ppm)	22.4	21.5	31.6	87.9	36.6	37.3	42.1	46.0	23.8	63.0	41.1	23.0
Cs (ppm)	1.7	0.8	1.4	0.4	1.7	2.0	1.5	2.8	2.2	2.1	1.7	< 0.1
Dy (ppm)	-	-	-	-	-	-	-	-	-	-	-	3.5
Eu (ppm)	1.8	2.2	2.1	3.1	1.5	2.4	2.3	2.5	2.0	2.5	2.1	1.2
Hf (ppm)	2.0	2.4	3.9	4.9	4.5	2.5	4.5	6.1	2.0	6.8	3.7	1.7
La (ppm)	12.5	11.0	16.0	41.5	16.1	20.6	17.3	20.6	11.9	28.7	18.0	10.4
Lu (ppm)	0.2	0.3	0.3	0.7	0.4	0.4	0.5	0.4	0.3	0.6	0.4	0.3
Nb (ppm)	-	-	-	-	-	-	-	-	-	-	-	25.4
Nd (ppm)	11.7	12.7	20.2	59.1	18.3	17.0	22.4	25.9	13.2	36.4	22.5	14.8
Pb (ppm)	-	-	-	-	-	-	-	-	-	-	-	6.0
Pr (ppm)	-	-	-	-	-	-	-	-	-	-	-	3.2
Rb (ppm)	21	17	31	5	37	42	32	42	30	51	28	2
Sm (ppm)	2.7	3.2	5.1	12.9	4.2	3.7	6.2	6.4	3.3	8.7	5.6	3.4
Sr (ppm)	-	-	-	-	-	-	-	-	-	-	-	97
Ta (ppm)	0.6	1.0	1.2	2.0	1.7	1.3	1.6	1.1	0.9	1.4	1.0	2.7
Tb (ppm)	0.4	0.4	0.7	1.7	0.6	0.4	1.0	0.9	0.5	1.3	0.8	0.6
Th (ppm)	2.5	1.6	2.7	1.0	3.1	3.2	2.3	4.5	1.8	4.5	2.5	0.5
U (ppm)	1.4	0.6	0.9	1.0	1.5	2.0	1.0	1.9	1.4	1.4	1.0	0.3
Y (ppm)	-	-	-	-	-	-	-	-	-	-	-	19.7
Yb (ppm)	1.5	1.7	2.4	5.1	2.9	2.5	3.2	2.7	1.8	4.2	2.9	2.1
Zr (ppm)	120	47	187	403	119	46	102	169	<60	147	70	70
As (ppm)	9.1	21.5	9.1	6.5	28.1	51.2	14.3	21.2	33.1	3.8	41.0	10.0
Sb (ppm)	1.9	0.9	1.6	0.2	1.9	2.2	1.7	3.2	2.5	2.4	2.0	< 0.2
Bi (ppm)	-	-	-	0.1	-	-	-	-	-	-	-	0.1
Te (ppm)	-	-	-	1.1	-	-	-	-	-	-	-	-
Ni (ppm)	976	2179	1240	3513	1269	1200	1031	724	2264	560	1212	330
Cu (ppm)	2280	2974	4336	11649	4887	3131	3615	1615	6020	2499	3438	860
Co (ppm)	144	172	134	257	135	101	112	85	252	74	149	101
Ag (ppm)	0.7	3.7	2.4	3.9	7.3	2.2	4.4	1.7	2.1	2.4	2.7	0.7
Se (ppm)	4.1	-	-	-	-	-	2.0	1.3	-	1.7	2.6	0.9
Pb(ppm)	-	-	-	-	-	-	-	-	-	-	-	6.0
Mo (ppm)	-	-	-	-	-	-	-	-	-	-	-	6.0
Os (ppb)	0.8	<1.4	0.6	2.9	0.7	1.0	1.0	<0.8	2.7	<0.5	<0.5	<0.6
Ir (ppb)	1.3	2.5	0.7	2.3	1.5	0.3	1.3	0.8	9.7	0.6	1.0	0.3
Ru (ppb)	5.2	7.5	2.3	12.1	3.7	9.7	4.9	2.1	7.8	4.2	5.2	<2.6
Rh (ppb)	2.9	7.0	1.9	5.1	14.6	1.5	<0.5	3.5	16.3	3.1	4.4	0.9
Pt (ppb)	13.6	105.5	25.2	1.9	53.0	13.3	141.8	180.6	245.4	38.6	35.2	12.8
Pd (ppb)	43.1	1132.2	64.3	92.0	340.3	94.2	282.3	143.3	2126.4	151.2	171.7	22.7
Au (ppb)	18.7	480.0	23.9	22.1	76.6	48.2	48.2	17.7	31.9	30.8	29.3	-

Samples	DC-49	DC-52	DC-54	DC-57	DC-60	DC-67	DC-68	B1-175-03	B1-175-07	B1-175-09	B1-175-10	B1-175-13
Rock type	norite	norite	norite	norite	norite	norite	norite	norite	norite	norite	norite	norite
Deposit	NorthMet	NorthMet	NorthMet	NorthMet	NorthMet	NorthMet	NorthMet	Serpentine	Serpentine	Serpentine	Serpentine	Serpentine
S (%)	0.2	0.7	0.3	1.5	1.6	3.4	3.4	4.0	7.1	8.4	3.2	4.8
SiO_2 (wt%)	49.2	55.0	45.8	53.0	40.3	57.0	57.2	45.3	47.1	47.9	47.1	48.6
TiO_2 (wt%)	2.9	1.0	1.4	2.2	7.4	2.8	2.7	2.1	3.4	2.5	2.3	1.6
Al_2O_3 (wt%)	15.5	18.3	20.1	19.1	14.3	14.3	14.3	16.2	15.0	15.7	17.0	16.8
FeO (wt%)	14.9	8.8	13.8	7.5	19.8	9.5	9.6	9.3	13.7	13.7	13.2	14.6
MnO (wt%)	0.18	0.08	0.12	0.09	0.23	0.10	0.10	0.16	0.18	0.19	0.17	0.17
MgO (wt%)	5.3	5.5	8.6	2.6	7.4	3.5	3.5	7.9	7.0	7.1	6.8	6.7
CaO (wt%)	7.0	2.1	2.0	8.4	6.9	5.3	5.2	7.8	8.0	7.0	8.2	6.8
Na_2O (wt%)	2.8	2.9	1.5	3.7	2.2	3.8	3.8	2.3	1.7	2.2	2.3	2.3
K_2O (wt%)	0.5	4.0	0.7	1.3	0.5	2.4	2.4	0.6	0.4	0.3	0.7	0.9
P_2O_5 (wt%)	0.54	0.07	0.02	1.01	0.13	0.72	0.70	0.26	0.40	0.36	0.34	0.29
LOI	1.1	2.2	5.8	1.1	0.9	0.6	0.4	7.5	2.6	2.5	1.7	1.1
Ba (ppm)	199	673	198	434	164	300	258	191	177	125	226	323
Ce (ppm)	44.5	60.1	22.6	78.6	21.1	61.3	62.4	40.1	45.8	30.7	47.6	40.7
Cs (ppm)	0.6	2.6	2.8	4.2	0.5	9.2	9.2	3.1	0.7	0.4	1.3	1.4
Dy (ppm)	-	-	-	-	-	-	-	-	-	-	-	-
Eu (ppm)	2.8	2.7	2.0	3.5	1.6	1.4	1.4	1.9	1.7	1.3	2.1	1.6
Hf (ppm)	2.3	2.5	1.0	1.2	2.5	2.5	2.7	3.2	3.6	1.6	4.3	2.6
La (ppm)	19.3	31.5	14.1	31.2	8.7	27.1	27.2	16.4	18.5	12.8	21.5	18.1
Lu (ppm)	0.5	0.6	0.3	0.4	0.3	0.4	0.4	0.3	0.4	0.3	0.4	0.3
Nb (ppm)	-	-	-	-	-	-	-	-	-	-	-	-
Nd (ppm)	24.3	21.3	7.5	51.1	11.5	34.5	36.4	17.6	21.8	17.3	24.7	20.7
Pb (ppm)	-	-	-	-	-	-	-	-	-	-	-	-
Pr (ppm)	-	-	-	-	-	-	-	-	-	-	-	-
Rb (ppm)	7	86	31	39	12	124	122	23	7	7	25	45
Sm (ppm)	6.0	3.9	1.2	11.2	3.1	7.6	7.7	4.8	6.2	4.5	5.8	5.0
Sr (ppm)	-	-	-	-	-	-	-	-	-	-	-	-
Ta (ppm)	1.2	-0.3	0.7	0.6	1.3	1.0	1.1	0.7	1.0	0.6	0.9	0.7
Tb (ppm)	0.9	0.2	<.17	1.3	0.6	0.4	0.3	0.6	0.9	0.6	0.8	0.7
Th (ppm)	0.8	4.7	0.5	3.9	1.4	7.2	7.2	2.4	1.8	1.6	2.9	2.5
U (ppm)	1.3	2.1	0.3	4.6	0.4	4.6	5.0	0.7	0.8	1.3	0.8	1.2
Y (ppm)	-	-	-	-	-	-	-	-	-	-	-	-
Yb (ppm)	2.8	3.2	1.7	2.3	1.5	2.1	2.2	2.2	2.7	1.8	2.8	2.0
Zr (ppm)	-	-	-	-	-	-	-	65	124	<54	145	191
As (ppm)	2.0	6.3	2.8	29.0	3.4	6.9	2.1	17.5	13.8	26.5	15.3	14.6
Sb (ppm)	1.6	1.4	0.8	2.5	0.6	0.6	0.1	3.5	0.3	0.5	1.5	1.6
Bi (ppm)	-	-	-	-	-	5.2	0.8	-	0.5	-	-	-
Te (ppm)	-	-	-	-	-	2.1	0.4	-	2.3	-	-	-
Ni (ppm)	151	186	265	1885	1140	1570	1553	1680	3037	3768	1867	1511
Cu (ppm)	373	293	622	8140	3000	13996	14052	5424	5397	5491	5450	2471
Co (ppm)	52	40	62	96	127	138	137	179	344	404	170	233
Ag (ppm)	-	-	-	3.9	0.8	2.0	2.5	4.2	2.6	2.7	3.7	-
Se (ppm)	-	-	-	-	-	-	-	4.2	5.8	4.9	5.0	5.0
Pb(ppm)	-	-	-	-	-	-	-	-	-	-	-	-
Mo (ppm)	-	-	-	-	-	-	-	-	-	-	-	-
Os (ppb)	<0.5	<0.9	0.7	2.5	<1.3	4.1	2.9	0.5	0.8	2.5	0.7	1.8
Ir (ppb)	0.1	0.3	0.2	7.6	1.2	2.0	1.7	0.9	1.5	2.3	1.2	1.1
Ru (ppb)	<5.0	4.9	<5.0	7.7	<5.0	5.3	<5.3	6.9	3.5	4.1	3.5	5.8
Rh (ppb)	<0.2	0.7	0.6	16.9	4.8	7.1	7.2	2.0	2.0	4.7	3.5	2.3
Pt (ppb)	2.5	3.7	6.9	554.5	50.2	835.3	642.4	26.0	6.7	10.6	38.8	16.2
Pd (ppb)	5.4	11.1	8.1	423.5	104.7	974.2	932.3	100.3	84.3	59.1	88.1	49.4
Au (ppb)	<2	<2	23.0	309.0	185.0	2763.0	2133.0	47.1	23.9	45.1	90.2	19.3

Samples	B1-175-14	B1-175-28	CN-7-3	CN-7-6	26133-06	26133-07	26133-10	26133-12	LE-3-01	B1-384-05	B1-384-08	B1-384-10
Rock type	norite	norite	norite	norite	norite	norite	norite	norite	Gabbronorite	Gabbronorite	Gabbronorite	Gabbronorite
Deposit	Serpentine	Serpentine	Water-hen	Water-hen	Wyman creek	Wyman creek	Wyman creek	Wyman creek	Longear	Mesaba	Mesaba	Mesaba
S (%)	2.4	0.7	0.3	1.8	1.3	0.8	0.1	0.1	0.0	1.8	1.8	4.0
SiO_2 (wt%)	49.4	48.5	-	48.1	-	-	-	-	48.4	46.1	45.4	47.3
TiO_2 (wt%)	3.2	3.3	14.5	1.5	1.9	6.9	8.6	7.8	0.6	0.5	0.6	2.2
Al_2O_3 (wt%)	15.5	15.2	18.8	20.2	45.9	17.8	9.8	37.6	20.7	21.8	18.4	19.9
FeO (wt%)	15.7	15.3	40.1	10.0	22.1	40.5	47.3	30.2	8.2	9.4	12.3	10.5
MnO (wt%)	0.19	0.20	0.56	0.15	0.30	0.62	0.64	0.44	0.11	0.12	0.16	0.12
MgO (wt%)	5.7	5.8	23.7	7.7	24.7	32.5	32.5	17.7	9.5	7.7	11.0	4.7
CaO (wt%)	7.9	8.1	-	10.7	-	-	-	-	9.3	9.4	8.6	10.2
Na_2O (wt%)	1.4	2.2	2.3	1.5	5.2	1.6	1.2	6.3	2.8	2.5	2.2	3.0
K_2O (wt%)	0.3	0.9	-	0.1	-	-	-	-	0.4	0.3	0.3	0.6
P_2O_5 (wt%)	0.51	0.45	-	0.09	-	-	-	-	0.06	0.07	0.10	0.16
LOI	0.2	0.0	-	-	-	-	-	-	-	2.0	1.0	1.3
Ba (ppm)	322	404	49	64	136	36	65	149	111	77	82	156
Ce (ppm)	73.2	69.5	8.8	2.1	18.5	9.8	21.7	34.6	9.3	9.3	11.2	19.6
Cs (ppm)	2.3	1.4	0.5	0.2	0.2	0.4	1.4	0.4	0.3	0.3	0.3	0.8
Dy (ppm)	-	-	-	-	-	-	-	-	-	1.0	-	-
Eu (ppm)	2.6	3.1	1.4	1.0	1.2	0.9	1.1	1.9	1.0	0.7	1.0	1.5
Hf (ppm)	6.8	6.2	1.4	0.3	1.3	1.6	2.4	3.6	0.7	0.9	1.0	2.3
La (ppm)	32.1	29.5	3.7	1.7	7.9	3.6	8.8	14.5	4.6	4.4	5.7	9.7
Lu (ppm)	0.6	0.6	0.2	0.1	0.1	0.2	0.2	0.3	0.1	0.1	0.1	0.2
Nb (ppm)	-	-	-	-	-	-	-	-	-	3.3	-	-
Nd (ppm)	38.3	36.1	5.3	1.3	9.3	7.3	12.9	19.4	4.1	4.9	6.8	12.2
Pb (ppm)	-	-	-	-	-	-	-	-	-	< 5	-	-
Pr (ppm)	-	-	-	-	-	-	-	-	-	1.2	-	-
Rb (ppm)	22	34	8	7	1	0	8	3	3	5	5	22
Sm (ppm)	9.5	9.2	1.7	0.2	2.0	1.9	3.2	4.4	1.1	1.1	1.5	3.1
Sr (ppm)	-	-	108	414	332	263	71	290	263	177	-	-
Ta (ppm)	1.4	1.5	2.1	0.3	0.3	0.5	1.0	0.8	0.1	0.8	0.2	0.7
Tb (ppm)	1.4	1.3	0.8	0.1	0.4	0.4	0.7	0.8	0.2	0.2	0.2	0.5
Th (ppm)	4.6	3.5	0.2	0.1	0.8	0.2	1.1	2.0	0.5	0.7	0.6	1.8
U (ppm)	1.7	1.5	-	-	0.1	0.0	0.4	0.6	0.1	0.2	0.2	0.5
Y (ppm)	-	-	-	-	-	-	-	-	-	5.4	-	-
Yb (ppm)	4.4	4.2	0.9	0.3	0.9	1.2	1.6	2.3	0.5	0.6	0.7	1.4
Zr (ppm)	196	322	25	20	25	79	251	5	37	35	<72	84
As (ppm)	10.7	6.4	4.6	25.1	0.7	0.9	2.9	0.9	0.2	<5	1.9	0.7
Sb (ppm)	2.6	1.6	0.3	0.2	0.1	0.1	0.2	0.1	0.0	< 0.2	0.1	0.9
Bi (ppm)	-	-	-	-	-	-	-	-	-	<0.1	0.8	-
Te (ppm)	-	-	-	-	-	-	-	-	-	<0.06	1.4	-
Ni (ppm)	1114	364	497	1002	2071	1462	703	279	430	650	1804	2337
Cu (ppm)	1226	537	673	1121	6525	3828	630	309	48	760	7718	27472
Co (ppm)	177	81	115	142	112	139	144	62	61	129	116	96
Ag (ppm)	-	-	-	1.4	3.0	0.4	-	-	-	-	3.9	15.0
Se (ppm)	2.1	1.1	-	-	-	-	-	-	-	0.4	10.9	-
Pb(ppm)	-	-	-	-	-	-	-	-	-	< 5	<5	-
Mo (ppm)	-	-	-	-	-	-	-	-	-	<2	-	-
Os (ppb)	0.3	0.5	1.4	-	0.9	1.4	1.7	1.3	1.1	2.7	2.0	1.8
Ir (ppb)	0.3	0.2	0.1	-	3.4	1.3	1.0	0.8	0.1	4.1	10.0	2.4
Ru (ppb)	<3.9	2.3	9.4	-	4.3	7.8	5.4	7.1	6.7	17.9	22.5	13.8
Rh (ppb)	0.9	0.5	0.6	-	4.3	4.1	3.3	1.8	0.6	19.3	39.3	1.7
Pt (ppb)	2.6	2.3	10.5	-	43.2	56.7	378.8	18.2	7.8	109.4	422.5	58.6
Pd (ppb)	13.8	7.1	5.9	-	8.7	11.1	38.7	1.7	3.8	426.9	1393.4	296.1
Au (ppb)	7.6	<1.0	3.8	-	16.9	44.2	4.2	1.2	0.4	192.1	169.9	119.2

Samples	B1-384-11	B1-384-21	B1-384-23	26086A-01	26086A-03	26086A-04	26086A-08	26086A-18	26086A-21	DC-21	DC-22	DC-23
Rock type	Gabbronorite	Gabbronorite	Gabbronorite	Gabbronorite	Gabbronorite	Gabbronorite	Gabbronorite	Gabbronorite	Gabbronorite	Gabbronorite	Gabbronorite	Gabbronorite
Deposit	Mesaba	Mesaba	Mesaba	NorthMet	NorthMet	NorthMet	NorthMet	NorthMet	NorthMet	NorthMet	NorthMet	NorthMet
S (%)	1.9	0.3	2.8	0.1	1.3	1.3	0.8	0.5	5.0	0.3	0.0	0.0
SiO_2 (wt%)	45.2	45.8	46.1	48.0	47.9	46.4	47.4	47.9	46.7	48.7	47.1	46.8
TiO_2 (wt%)	2.7	2.0	2.5	1.4	1.2	1.0	1.1	1.2	1.1	0.5	0.4	0.6
Al_2O_3 (wt%)	16.4	15.6	16.8	19.9	21.6	19.6	19.9	21.5	20.9	17.3	21.7	20.4
FeO (wt%)	15.6	17.4	15.0	9.9	8.0	10.9	11.0	8.8	9.8	9.4	9.1	11.0
MnO (wt%)	0.19	0.20	0.19	0.13	0.10	0.13	0.13	0.11	0.12	0.14	0.11	0.13
MgO (wt%)	9.0	9.5	7.3	7.2	6.1	8.6	7.7	6.8	7.1	8.8	7.7	8.0
CaO (wt%)	7.5	7.1	8.1	9.5	10.0	9.5	9.3	10.1	9.5	11.2	9.9	9.5
Na_2O (wt%)	2.6	1.6	2.8	3.2	3.1	2.6	2.7	2.9	2.6	2.7	2.9	2.4
K_2O (wt%)	0.5	0.5	0.7	0.6	0.6	0.4	0.5	0.6	0.4	0.4	0.3	0.3
P_2O_5 (wt%)	0.18	0.21	0.31	0.23	0.18	0.11	0.13	0.14	0.12	0.02	0.06	0.04
LOI	0.0	0.0	0.0	0.0	1.1	0.7	0.0	0.0	1.4	0.8	0.7	0.9
Ba (ppm)	165	316	209	220	165	122	140	186	107	117	136	85
Ce (ppm)	24.2	49.2	34.8	36.6	32.2	18.0	21.2	22.8	17.8	4.8	8.0	5.5
Cs (ppm)	0.8	1.5	1.1	1.7	0.9	0.6	0.8	1.7	0.7	<.57	<.23	0.4
Dy (ppm)	-	5.0	-	-	-	-	-	-	-	-	-	0.4
Eu (ppm)	1.7	1.9	1.8	1.9	1.5	1.2	1.3	1.5	1.1	0.9	1.0	0.8
Hf (ppm)	3.0	3.2	3.8	2.9	2.8	1.6	1.9	2.0	2.0	0.3	0.2	0.3
La (ppm)	12.1	23.4	17.2	14.7	13.1	7.8	9.2	9.7	8.5	2.3	4.1	3.0
Lu (ppm)	0.3	0.4	0.3	0.3	0.3	0.2	0.2	0.2	0.1	0.1	0.1	0.0
Nb (ppm)	-	13.5	-	-	-	-	-	-	-	-	-	2.3
Nd (ppm)	14.9	27.0	21.2	16.5	15.2	8.6	10.8	11.1	9.0	5.1	5.9	2.6
Pb (ppm)	-	7.0	-	-	-	-	-	-	-	-	-	< 5
Pr (ppm)	-	6.4	-	-	-	-	-	-	-	-	-	0.6
Rb (ppm)	22	27	29	19	21	10	13	16	10	<5.2	10	3
Sm (ppm)	3.5	6.0	5.1	4.4	3.9	2.2	2.7	2.8	2.2	1.2	0.9	0.5
Sr (ppm)	-	241	-	-	-	-	-	-	-	-	-	301
Ta (ppm)	0.9	1.0	1.0	0.7	0.6	0.3	0.5	0.5	0.4	0.6	1.0	0.2
Tb (ppm)	0.5	0.9	0.7	0.7	0.6	0.3	0.4	0.4	0.3	0.2	0.1	0.1
Th (ppm)	1.7	2.7	2.3	1.7	2.0	0.9	1.4	1.2	1.4	<.15	0.3	0.2
U (ppm)	0.5	1.0	0.6	0.6	0.6	0.3	0.4	0.4	0.4	<.14	0.1	0.1
Y (ppm)	-	28.1	-	-	-	-	-	-	-	-	-	2.4
Yb (ppm)	1.8	2.6	2.3	2.0	1.9	1.1	1.3	1.3	1.1	0.6	0.3	0.3
Zr (ppm)	122	148	94	244	154	<87	32	48	93			13
As (ppm)	5.8	<5	4.4	1.0	1.4	1.1	1.3	3.5	21.7	<0.33	<0.33	<5
Sb (ppm)	0.9	< 0.2	1.2	1.9	1.1	0.7	0.9	2.0	0.8	0.3	0.5	< 0.2
Bi (ppm)	-	<0.1	-	-	-	-	-	-	-	-	-	<0.1
Te (ppm)	-	<0.06	-	-	-	-	-	-	-	-	-	<0.06
Ni (ppm)	4524	390	1556	312	3075	7379	1233	520	3382	228	295	310
Cu (ppm)	5767	2070	10153	512	5834	3065	4386	772	5231	112	169	270
Co (ppm)	230	87	131	53	97	188	80	58	272	76	84	66
Ag (ppm)	4.4	-	4.7	-	3.9	1.4	3.2	0.7	2.9	-	-	-
Se (ppm)	-	0.7	-	0.5	-	3.3	2.8	0.7	-	-	-	0.2
Pb(ppm)	-	7.0	-	-	-	-	-	-	-	-	-	< 5
Mo (ppm)	-	<2	-	-	-	-	-	-	-	-	-	<2
Os (ppb)	1.8	<0.5	0.6	0.3	2.0	1.8	0.9	1.1	0.2	<0.9	<0.5	<1.3
Ir (ppb)	3.1	0.2	0.8	0.6	6.4	3.3	3.3	0.4	3.3	0.2	0.0	0.3
Ru (ppb)	13.5	<2.1	5.1	2.1	8.6	15.8	9.2	10.8	<14	<8.2	<5.4	4.9
Rh (ppb)	14.2	0.3	1.7	1.9	29.8	29.5	19.2	2.2	14.7	0.2	<0.2	0.8
Pt (ppb)	59.7	5.1	168.3	24.8	443.0	71.6	176.1	9.9	54.3	4.5	<2.4	6.7
Pd (ppb)	510.6	16.5	39.0	88.5	1085.3	2083.1	961.4	42.8	315.6	4.5	<2.8	10.6
Au (ppb)	26.9	7.5	12.1	7.2	939.0	57.9	291.9	5.4	129.6	-	2.0	32.0

Samples	DC-24	DC-25	DC-28	DC-29	DC-30	DC-31	DC-32	DC-33	DC-50	DC-53	DC-55	DC-56
Rock type	Gabbronorite	Gabbronorite	Gabbronorite	Gabbronorite	Gabbronorite	Gabbronorite	Gabbronorite	Gabbronorite	Gabbronorite	Gabbronorite	Gabbronorite	Gabbronorite
Deposit	NorthMet	NorthMet	NorthMet	NorthMet	NorthMet	NorthMet	NorthMet	NorthMet	NorthMet	NorthMet	NorthMet	NorthMet
S (%)	0.1	<.01	0.0	0.0	<.01	<.01	0.0	0.1	0.1	0.2	1.1	1.4
SiO_2 (wt%)	47.0	49.5	47.1	49.3	48.4	50.6	46.9	47.4	45.3	48.2	47.5	46.3
TiO_2 (wt%)	1.4	0.8	0.3	1.0	0.4	0.8	0.3	0.6	5.0	2.3	1.8	1.3
Al_2O_3 (wt%)	19.9	21.9	21.1	24.0	23.0	16.1	21.0	19.1	13.7	16.5	16.8	17.3
FeO (wt%)	11.3	7.1	8.4	4.9	7.2	8.0	8.3	11.9	14.5	12.6	13.4	13.8
MnO (wt%)	0.15	0.09	0.11	0.05	0.09	0.14	0.11	0.14	0.20	0.18	0.18	0.15
MgO (wt%)	6.6	5.5	8.3	2.9	6.1	7.8	7.5	8.9	7.3	6.4	7.6	8.4
CaO (wt%)	9.4	11.3	9.3	10.4	10.7	12.8	10.2	8.4	10.4	8.6	8.3	8.5
Na_2O (wt%)	3.1	3.2	3.0	4.2	3.1	2.8	2.9	2.8	2.5	3.2	2.9	2.8
K_2O (wt%)	0.5	0.5	0.4	0.5	0.4	0.4	0.5	0.4	0.4	1.0	0.8	0.6
P_2O_5 (wt%)	0.16	0.07	0.02	0.04	0.05	0.02	0.03	0.04	0.05	0.31	0.24	0.12
LOI	0.6	0.0	2.1	2.6	0.5	0.7	2.2	0.3	0.5	0.8	0.4	0.8
Ba (ppm)	176	115	99	165	100	88	133	118	110	276	204	162
Ce (ppm)	21.7	13.5	3.8	10.1	8.9	7.4	5.7	9.3	14.6	48.4	35.6	21.8
Cs (ppm)	0.5	0.7	1.2	<.36	0.2	<.34	1.1	0.2	< 0.1	1.7	1.5	0.4
Dy (ppm)	-	-	-	-	0.8	-	-	-	3.3	-	-	-
Eu (ppm)	1.5	1.2	0.7	1.6	0.9	1.3	0.8	1.2	1.4	2.4	1.9	1.3
Hf (ppm)	2.2	0.4	0.3	0.6	0.6	0.4	0.2	0.3	1.9	4.3	3.3	2.2
La (ppm)	9.7	5.3	2.0	4.7	4.4	2.4	2.5	4.4	6.0	21.1	15.6	9.4
Lu (ppm)	0.2	0.1	0.0	0.1	0.1	0.2	0.1	0.1	0.3	0.5	0.4	0.3
Nb (ppm)	-	-	-	-	2.9	-	-	-	12.8	-	-	-
Nd (ppm)	10.7	6.1	4.2	4.5	4.4	4.0	2.3	2.8	10.9	25.3	19.0	8.3
Pb (ppm)	-	-	-	-	< 5	-	-	-	< 5	-	-	-
Pr (ppm)	-	-	-	-	1.1	-	-	-	2.2	-	-	-
Rb (ppm)	8	7	4	4	5	5	4	7	2	34	21	9
Sm (ppm)	2.8	1.6	0.4	0.9	0.9	1.4	0.6	0.7	3.0	5.9	4.4	2.5
Sr (ppm)	-	-	-	-	321	-	-	-	208	-	-	-
Ta (ppm)	1.0	1.3	0.5	0.6	0.1	0.9	0.6	0.5	1.0	0.9	0.7	0.3
Tb (ppm)	0.4	0.2	<.05	<.11	0.1	0.4	0.1	<.10	0.6	0.6	0.6	0.2
Th (ppm)	1.3	0.7	0.1	0.5	0.4	<.18	0.1	0.3	0.2	3.8	2.2	1.3
U (ppm)	0.3	0.2	<.16	<.11	0.2	<.13	<.08	<.22	0.1	1.0	0.6	0.3
Y (ppm)	-	-	-	-	4.6	-	-	-	18.5	-	-	-
Yb (ppm)	1.3	0.7	0.2	0.3	0.4	0.9	0.3	0.3	1.8	2.7	2.1	1.4
Zr (ppm)	-	-	-	-	25	-	-	-	76	-	-	-
As (ppm)	0.9	0.3	<0.39	0.8	<5	<0.44	<0.50	<0.43	<5	2.2	2.7	3.5
Sb (ppm)	1.6	0.3	0.5	4.4	< 0.2	0.6	1.1	0.5	< 0.2	1.0	0.1	2.9
Bi (ppm)	-	-	-	-	<0.1	-	-	-	<0.1	-	0.2	-
Te (ppm)	-	-	-	-	<0.06	-	-	-	<0.06	-	0.5	-
Ni (ppm)	189	198	266	123	150	97	244	190	180	230	1073	1909
Cu (ppm)	164	129	62	155	30	87	132	173	450	514	3652	5550
Co (ppm)	74	62	74	44	36	62	69	97	60	55	89	170
Ag (ppm)	-	-	-	-	-	-	-	-	-	-	0.3	1.4
Se (ppm)	-	-	-	-	0.0	-	-	-	0.2	-	-	-
Pb(ppm)	-	-	-	-	< 5	-	-	-	< 5	-	-	-
Mo (ppm)	-	<2	-	-	-	-	-	-	<2	-	-	-
Os (ppb)	1.1	0.4	<1.3	<0.6	<0.7	0.5	<0.9	<0.8	<1.2	<0.8	0.9	1.6
Ir (ppb)	0.1	0.3	0.4	0.4	0.3	0.1	0.1	0.1	0.3	0.6	1.0	2.8
Ru (ppb)	<2.7	<2.0	<3.1	<2.5	<3.3	<5.0	<1.7	<4.1	<2.2	<5.0	6.9	12.9
Rh (ppb)	0.2	0.5	0.1	0.4	1.5	0.9	0.4	0.3	0.5	1.5	5.1	14.4
Pt (ppb)	3.1	<5.3	<5.1	8.5	<6.0	9.6	5.5	<4.7	7.4	10.2	42.1	111.7
Pd (ppb)	3.7	6.1	<2.8	6.9	17.0	2.0	3.3	3.1	14.2	39.0	174.3	402.1
Au (ppb)	48.0	31.0	19.0	59.0	421.0	18.0	89.0	265.0	<2	-	322.0	476.0

Samples	DC-58	DC-59	DC-61	DC-62	DC-63	DC-64	DC-65	DC-66	DC-79	B1-175-01	B1-175-06	B1-175-11
Rock type	Gabbronorite	Gabbronorite	Gabbronorite	Gabbronorite	Gabbronorite	Gabbronorite	Gabbronorite	Gabbronorite	Gabbronorite	Gabbronorite	Gabbronorite	Gabbronorite
Deposit	NorthMet	NorthMet	NorthMet	NorthMet	NorthMet	NorthMet	NorthMet	NorthMet	NorthMet	Serpentine	Serpentine	Serpentine
S (%)	2.0	0.1	1.5	1.7	2.5	0.6	2.2	4.3	1.1	3.2	0.9	2.0
SiO_2 (wt%)	47.4	47.9	47.0	45.4	43.9	46.6	46.7	46.0	46.7	44.2	47.2	46.8
TiO_2 (wt%)	1.4	0.8	0.3	1.5	3.1	0.6	4.4	2.2	0.7	3.3	2.3	2.8
Al_2O_3 (wt%)	19.5	18.5	20.6	14.8	12.9	20.1	13.8	14.9	20.3	16.4	16.8	15.7
FeO (wt%)	10.8	10.7	9.8	15.1	18.9	10.3	15.3	18.6	10.4	13.7	12.9	14.4
MnO (wt%)	0.14	0.15	0.11	0.19	0.24	0.13	0.19	0.18	0.10	0.17	0.17	0.18
MgO (wt%)	7.6	9.2	9.0	11.9	9.9	8.9	5.5	6.3	9.3	7.4	7.5	7.2
CaO (wt%)	9.4	8.4	9.3	7.7	7.3	9.7	9.8	7.7	8.3	9.0	8.5	8.4
Na_2O (wt%)	3.0	3.2	2.7	2.3	2.1	2.5	2.3	2.1	2.2	2.6	2.6	2.9
K_2O (wt%)	0.6	0.7	0.4	0.6	0.6	0.4	0.6	0.7	0.5	0.6	0.8	1.0
P_2O_5 (wt%)	0.07	0.15	0.04	0.20	0.08	0.10	0.33	0.28	0.08	0.35	0.29	0.40
LOI	0.1	0.3	0.8	0.4	0.9	0.6	0.9	1.0	1.3	2.0	0.8	0.1
Ba (ppm)	143	150	81	152	146	80	116	276	19	172	245	262
Ce (ppm)	13.5	21.7	6.5	27.4	17.7	8.5	27.4	44.3	16.8	40.7	45.1	54.6
Cs (ppm)	<.33	0.6	<.27	0.7	1.2	0.2	1.1	1.5	2.1	1.4	2.2	1.8
Dy (ppm)	-	-	-	-	-	0.9	-	-	-	-	-	-
Eu (ppm)	1.4	1.6	0.9	1.4	1.5	0.7	2.0	1.8		1.9	1.9	2.4
Hf (ppm)	1.1	1.8	0.3	2.7	1.3	0.8	3.7	6.0	1.4	3.3	2.8	4.9
La (ppm)	5.6	9.6	2.9	11.5	8.5	4.1	10.7	19.4	7.4	15.3	18.1	23.5
Lu (ppm)	0.2	0.2	0.0	0.3	0.2	0.1	0.5	0.5		0.3	0.4	0.4
Nb (ppm)	-	-	-	-	-	3.0	-	-	-	-	-	-
Nd (ppm)	7.0	10.6	1.1	14.1	10.9	4.7	17.2	25.8	8.4	18.1	20.8	27.8
Pb (ppm)	-	-	-	-	-	< 5	-	-	-	-	-	-
Pr (ppm)	-	-	-	-	-	1.1	-	-	-	-	-	-
Rb (ppm)	7	11	<6.3	13	16	5	<7.9	21	19	12	25	40
Sm (ppm)	1.8	2.5	0.6	3.6	2.4	1.1	4.9	6.2	1.8	5.3	5.5	7.1
Sr (ppm)	-	-	-	-	-	250	-	-	-	-	-	-
Ta (ppm)	0.2	0.3	<.11	0.4	0.7	0.1	1.4	0.9	0.2	1.1	0.9	1.2
Tb (ppm)	0.2	0.3	<.09	0.6	0.4	0.1	0.9	1.1		0.8	0.8	1.0
Th (ppm)	0.7	1.3	0.2	1.5	0.9	0.5	1.4	2.6	1.1	1.8	2.1	3.7
U (ppm)	0.2	0.4	<.21	0.4	0.1	0.1	0.4	0.8	0.3	0.6	0.8	1.0
Y (ppm)	-	-	-	-	-	4.8	-	-	-	-	-	-
Yb (ppm)	0.8	1.0	0.2	1.7	1.3	0.5	2.6	2.8	-	2.2	2.5	3.1
Zr (ppm)	-	-	-	-	-	37	-	-	-	90	86	327
As (ppm)	0.7	0.3	<0.38	2.7	7.5	<5	14.8	22.6	4.7	12.4	20.8	17.9
Sb (ppm)	2.7	1.1	0.6	0.1	0.1	<0.2	1.4	0.4	0.6	1.6	2.4	2.0
Bi (ppm)	-	-	-	0.2	0.4	<0.1	-	0.7	-	-	-	-
Te (ppm)	-	-	-	0.3	0.4	<0.06	-	0.8	-	-	-	-
Ni (ppm)	2439	567	2051	3742	824	640	1465	2283	2246	2506	783	1017
Cu (ppm)	10228	1014	7129	12249	2210	690	15662	6395	7120	8240	2719	5362
Co (ppm)	113	68	113	150	180	75	109	310	120	198	89	127
Ag (ppm)	0.8	-	1.2	1.6	0.5	-	3.9	1.0	-	6.3	3.2	4.3
Se (ppm)	-	-	-	-	-	3.3	-	-	-	5.5	1.3	2.6
Pb(ppm)	-	-	-	-	-	< 5	-	-	-	-	-	-
Mo (ppm)	-	-	-	-	-	<2	-	-	-	-	-	-
Os (ppb)	1.9	<1.4	2.5	3.2	1.2	4.1	2.3	2.2	1.3	<0.9	<0.7	0.6
Ir (ppb)	3.0	0.1	3.8	10.5	0.9	8.6	0.4	4.3	3.0	1.5	0.4	0.8
Ru (ppb)	10.3	<3.1	16.2	34.2	<5.0	31.5	<5.0	20.3	10.1	4.6	3.1	1.9
Rh (ppb)	19.3	0.3	18.2	79.9	3.2	58.0	2.9	23.0	15.0	3.4	1.7	1.7
Pt (ppb)	160.7	<5.4	124.3	559.7	15.6	299.1	371.1	35.1	163.9	18.4	17.4	85.6
Pd (ppb)	712.2	5.1	501.3	2250.6	62.9	1630.4	600.7	463.7	583.0	133.0	60.0	65.8
Au (ppb)	1440.0	-	589.0	4214.0	184.0	887.0	2650.0	451.0	667.0	45.7	20.4	20.9

Samples Rock type Deposit	B1-175-16 Gabbronorite Serpentine	B1-175-17 Gabbronorite Serpentine	B1-175-29 Gabbronorite Serpentine	B1-175-30 Gabbronorite Serpentine	26133-01 Gabbronorite Wyman creek	26133-02 Gabbronorite Wyman creek	DC-36 Kew. basalt NorthMet	DC-37 Kew. basalt NorthMet	DC-38 Kew. basalt NorthMet
S (%)	6.5	4.6	2.3	3.0	0.0	0.0	<0.01	<0.01	<0.01
SiO_2 (wt%)	49.6	45.8	47.1	46.0	-	-	50.5	49.1	48.9
TiO_2 (wt%)	3.4	1.6	1.9	1.9	1.8	2.0	2.4	0.8	1.0
Al_2O_3 (wt%)	15.4	16.7	17.7	17.9	58.1	56.4	11.2	17.2	16.9
FeO (wt%)	9.2	13.1	12.8	12.3	17.3	19.3	13.4	8.4	9.0
MnO (wt%)	0.20	0.17	0.16	0.15	0.24	0.26	0.21	0.14	0.15
MgO (wt%)	4.9	8.5	7.0	7.7	15.8	15.0	7.1	8.3	8.6
CaO (wt%)	10.5	8.1	8.0	8.2	-	-	10.6	10.6	10.8
Na_2O (wt%)	2.6	2.4	2.7	2.6	6.7	7.1	2.5	2.4	2.5
K_2O (wt%)	0.7	0.8	1.0	0.9	-	-	0.4	0.4	0.4
P_2O_5 (wt%)	0.52	0.21	0.30	0.26	-	-	0.29	0.07	0.10
LOI	2.5	2.4	1.2	1.9	-	-	1.4	2.7	1.6
Ba (ppm)	508	177	205	234	113	151	116	79	84
Ce (ppm)	71.2	30.3	44.6	44.3	15.0	13.4	12.3	13.4	15.1
Cs (ppm)	0.5	2.0	1.8	2.3	0.4	0.7	< 0.1	<.56	0.4
Dy (ppm)	-	-	-	-	-	-	3.0	-	-
Eu (ppm)	2.9	1.5	1.9	1.8	1.1	1.5	1.4	0.6	0.9
Hf (ppm)	6.2	2.8	4.1	3.9	1.1	1.2	1.8	0.8	1.0
La (ppm)	29.8	13.2	18.2	18.4	5.9	6.1	5.1	4.6	5.4
Lu (ppm)	0.6	0.3	0.3	0.3	0.1	0.1	0.2	0.2	0.3
Nb (ppm)	-	-	-	-	-	-	12.5	-	-
Nd (ppm)	39.1	15.9	21.0	20.0	7.3	6.9	9.2	5.9	5.8
Pb (ppm)	-	-	-	-	-	-	< 5	-	-
Pr (ppm)	-	-	-	-	-	-	1.9	-	-
Rb (ppm)	12	25	30	36	5	8	2	<11	<6.2
Sm (ppm)	9.6	4.0	5.5	5.3	1.5	1.5	2.5	1.9	2.5
Sr (ppm)	-	-	-	-	337	415	217	-	-
Ta (ppm)	1.4	0.6	0.9	0.9	0.3	0.3	3.1	0.2	0.4
Tb (ppm)	1.4	0.6	0.7	0.7	0.3	0.3	0.5	0.3	0.4
Th (ppm)	1.3	2.2	2.4	3.0	0.8	0.8	0.1	0.2	0.4
U (ppm)	0.9	0.6	0.9	1.0	0.2	0.2	0.1	<.16	<.16
Y (ppm)	-	-	-	-	-	-	16.4	-	-
Yb (ppm)	4.6	1.8	2.5	2.3	0.7	0.7	1.6	1.3	1.7
Zr (ppm)	342	80	143	193	42	130	71	-	-
As (ppm)	35.1	3.7	11.7	3.3	0.3	0.4	< 5	<.20	0.2
Sb (ppm)	0.6	2.2	2.0	0.2	0.1	0.1	< 0.2	0.7	1.4
Bi (ppm)	-	-	-	0.3	-	-	<0,1	-	-
Te (ppm)	-	-	-	0.9	-	-	-	-	-
Ni (ppm)	1194	2541	1427	2257	205	236	160	221	218
Cu (ppm)	4190	9797	14283	5318	51	43	420	97	117
Co (ppm)	173	225	115	193	43	48	56	59	62
Ag (ppm)	2.0	3.3	9.2	3.2	-	-	< 0.5	<.48	<.48
Se (ppm)	2.1	5.2	3.3	3.9	-	-	0.3	0.2	0.1
Pb(ppm)	-	-	-	-	-	-	< 5	-	-
Mo (ppm)	-	-	-	-	-	-	<2	-	-
Os (ppb)	2.3	0.9	0.8	0.5	0.8	-	0.4	<.47	<1.1
Ir (ppb)	1.0	1.4	1.0	1.0	0.1	0.1	0.9	0.2	0.2
Ru (ppb)	10.0	2.8	4.0	2.5	7.1	0.5	<2.1	<1.4	<5.0
Rh (ppb)	2.5	2.4	2.5	2.4	1.4	0.8	0.8	0.4	0.4
Pt (ppb)	<1.4	21.8	70.4	25.5	7.0	4.3	21.3	10.1	7.0
Pd (ppb)	39.2	55.8	91.8	68.7	0.5	0.4	11.7	9.2	10.7
Au (ppb)	35.9	20.0	36.7	25.2	0.5	0.3	213.0	28.0	0.0

ANNEXE 5: MATÉRIAUX DE RÉFÉRENCE POUR LES ANALYSES SUR ROCHE TOTALE

Abréviations:

BS = Shales noirs

c.a. = Auréole de métamorphisme de contact

out.c.a.= Roches à l'extérieur de l'auréole de contact

BPU = Bedded Pyrrhotite Unit

Kew. basalt = Basaltes de Keweenawan

LOI = Perte au feu

Notes:

Les tableaux sont renseignés en anglais dans un souci de cohérence avec les publications présentées dans ce mémoire de doctorat.

Les valeurs des standards analysés sont présentées en italique dans les tableaux suivant.

Références:

Henrique-Pinto, R., Barnes, S.-J., Savard, D., Mehdi, S. Quantification of metals and semimetals in carbon-rich rocks: A new sequential protocol including extraction from humic substances. Geostand. Geoanal. Res. doi: 10.1111/j.1751-908X.2015.00340.x (in press).

Li, C., Chai, C., Li, X., Mao, X., 1998. Determination of Platinum-Group Elements and Gold in Two Russian Candidate Reference Materials SCHS-1 and SLg-1 by ICP-MS after Nickel Sulfide Fire Assay Preconcentration. Geostand. Newslett. 22, 195-197.

Petrov, L.L., Kornakov, Y.N., Korotaeva, Il.,Anchutina, E.A., Persikova, L.A., Susloparova, V.E., Fedorova, I.N., Shibanov, V.A., 2004. Multi-Element Reference Samples of Black Shale. Geostand. Geoanal. Res. 28, 89-102.

Savard, D., Bédard, L.P., Barnes, S.-J., 2009. Selenium Concentrations in Twenty-Six Geological Reference Materials: New Determinations and Proposed Values. Geostand. Geoanal. Res. 33, 249-259.

Savard, D., Barnes, S.-J., Meisel, T., 2010. Comparison between Nickel-Sulfur Fire Assay Te Co-precipitation and Isotope Dilution with High-Pressure Asher Acid Digestion for the Determination of Platinum-Group Elements, Rhenium and Gold. Geostand. Geoanal. Res. 34, 281-291.

Webb, P.C., Thompson, M., Potts, P.J., Bédard, L.P., 2006. GeoPT18 - An international proficiency test for analytical geochemistry laboratories - Report on round 18/Jan 2006 (Quartz diorite, KPT-1). International Association of Geoanalysts, Report, 32p.

ACTLAB Fusion followed by ICP-MS	KPT-1this study	KPT-1 (Webb et al., 2006)
SiO_2 (wt%)	55.39	54.14 +/- 1.19
TiO_2 (wt%)	0.89	0.9 +/- 0.04
Al_2O_3 (wt%)	14.33	14.41 +/- 0.39
Fe_2O_3 (wt%)	12.00	12.24 +/- 0.34
MnO (wt%)	0.15	0.143 +/- 0.01
MgO (wt%)	4.27	4.3 +/- 0.14
CaO (wt%)	6.87	6.89 +/- 0.21
Na_2O (wt%)	2.61	2.61 +/- 0.09
K_2O (wt%)	1.66	1.65 +/- 0.06
P_2O_5 (wt%)	0.16	0.17 +/- 0.01
LOI	1.47	-
Total	99.80	-
Ba (ppm)	471	465.27 +/- 29.53
Ce (ppm)	53.87	55.71 +/- 4.87
Cs (ppm)	4.40	4.42 +/- 0.57
Dy (ppm)	4.45	4.47 +/- 0.57
Eu (ppm)	1.22	1.24 +/- 0.19
Hf (ppm)	3.75	4.41 +/- 0.56
La (ppm)	26.65	26.91 +/- 2.62
Lu (ppm)	0.41	0.42 +/- 0.08
Nb (ppm)	7.90	8.48 +/- 0.98
Nd (ppm)	24.63	24.64 +/- 2.43
Pb (ppm)	67.50	81.07 +/- 6.69
Pr (ppm)	6.28	6.39 +/- 0.77
Rb (ppm)	66	61.45 +/- 5.29
Sm (ppm)	5.0	4.9 +/- 0.62
Sr (ppm)	264	261.04 +/- 18.07
Ta (ppm)	0.57	0.6 +/- 0.1
Tb (ppm)	0.74	0.74 +/- 0.12
Th (ppm)	6.99	7.27 +/- 0.86
U (ppm)	1.75	1.76 +/- 0.26
Y (ppm)	24.70	25.82 +/- 2.53
Yb (ppm)	2.67	2.69 +/- 0.37
Zr (ppm)	161	158.12 +/- 11.81

LabMaTer S determination by infrared spectrometry S-C analyser	S (%)
KPT-1 this work	1.08
KPT-1 (Webb et al. 2006)	*1.029+/-.034*

LabMaTer Semimetals determined by black shale method	As (ppm)	Sb (ppm)	Bi (ppm)	Te (ppm)
SDO-1 this study	68.41	4.69	0.37	0.29
SDO-1 (Henrique-Pinto et al., in press)	*62.6+/-1.7*	*4.11+/-0.09*	*0.27+/-0.01*	*0.131+/-0.02*
SBC-1 this study	34.19	1.19	0.77	0.28
SBC-1 (Henrique-Pinto et al., 2016)	*29.4+/-1.8*	*1.22+/-0.26*	*0.6+/-0.01*	*0.184+/-0.04*
SCHS-1 this study	56.19	0.1	0.13	0.07
SCHS-1 (Henrique-Pinto et al., 2016)	*50.1+/-0.4*	*0.072+/-0.001*	*0.102+/-0.002*	-
SH-1 this study	27.91	1.54	1.45	0.25
SH-1 (UQAC)	*22.5+/-2.2*	*1.17+/-0.03*	*1.19+/-0.03*	*0.198+/-0.014*
KPT-1	2.57	8.49	0.45	0.48
KPT-1 (Webb et al., 2006)	*2.2+/-0.53*	*10.01+/-1.13*	*0.95+/-0.153*	*0.35+/-0.090*
WMS-1a	24.39	5.31	0.73	3.28
WMS-1a (Certificate values CANMET)	*30.9+/-4.8*	*6.29+/-0.98*	*1.2*	*3.7 +/-0.64*

LabMaTer Selenium determination by TCF-INAA	Se (ppm)
MRG-1	0.24
MRG-1(Savard et al., 2009)	*0.199+/-0.008*

ACTLAB Fusion followed by ICP-MS	Ni (ppm)	Cu (ppm)	Co (ppm)	Ag (ppm)	As (ppm)	Sb (ppm)	Bi (ppm)	Pb (ppm)	Mo (ppm)
KPT-1this study	880	950	83	1.4	7	9.7	0.8	68	2
KPT-1 (Webb et al., 2006)	*1093+/-71*	*1112+/-102*	*78.92+/-5*	*0.75+/-0.15*	*2.2+/-0.53*	*10+/-1.13*	*0.95+/-0.15*	*81.07+/-0.994*	*1.72+/-0.118*

LabMaTer Ni-FA-ICP-MS	Os (ppb)	Ir (ppb)	Ru (ppb)	Rh (ppb)	Pt(ppb)	Pd (ppb)	Au (ppb)
OKUM - this study	0.7	0.9	4.5	1.4	10.4	12.0	1.0
OKUM (Savard et al., 2010)	*0.98+/-0.34*	*0.99 +/- 0.07*	*4.25+/-0.3*	*1.40 +/- 0.13*	*11+/-0.6*	*11.7+/-0.5*	*1.4*
SLg-1 black shale - this study FA	<0.16	0.05	0.38	0.52	3.85	1.37	1760
SLg-1 black shale - this study ID	<0.03	0.06	0.66	-	3.06	0.98	-
SLg-1 (Li et al., 1998)	*n.d.*	*0.02+/- 0.013*	*0.27+/-0.03*	*0.32+/-0.05*	*1.39+/-0.12*	*1.49+/-0.13*	*1690+/-900*
SLg-1 (Petrov et al., 2004)	*n.d.*	*n.d.*	*1+/-0.4*	-	*2.2+/-0.5*	*2.3+/-0.6*	*2500+/-300*

ANNEXE 6: ANALYSES DES SULFURES AU LA-ICP-MS

Abréviations:

c.a. = Auréole de contact

BPU = Bedded Pyrrhotite Unit

Py=Pyrite

Po=Pyrrhotite

Pn=Pentlandite

Ccp=Chalcopyrite

Cb=Cubanite

n.a. = Données non disponibles

Notes:

Les tableaux sont renseignés en anglais dans un souci de cohérence avec les publications présentées dans ce mémoire de doctorat.

Les valeurs sont présentées en ppm dans les tableaux de données de cette annexe.

Les valeurs obtenues pour les matériaux de référence pour les analyses de sulfures au LA-ICP-MS sont présentées dans le Chapitre 4.

Les valeurs au dessus limites de détection sont reportées dans cette annexe ainsi que les valeurs inférieures aux limites de détection, c-à.-d. <LOD.

SULFURES SHALES NOIRS BPU HORS DE L'AURÉOLE DE CONTACT :

Sulfides	**Ccp**	**Ccp**	**Po**	**Po**	**Py**	**Py**	**Py**
Samples	LTV-7555	LTV-7555	LTV-7555	LTV-7555	LTV-7555	LTV-7555	LTV-7555
Deposits	LTV Pit	LTV Pit	LTV Pit	LTV Pit	LTV Pit	LTV Pit	LTV Pit
Rock types	BPU outside c.a.	BPU outside c.a.	BPU outside c.a.	BPU outside c.a.	BPU outside c.a.	BPU outside c.a.	BPU outside c.a.
Sulfide textures	Sulfide bed	Sulfide bed	Sulfide bed	Sulfide bed	Sulfide bed	Sulfide bed	Sulfide bed
Co	115.63	95.06	208.81	243.09	164.79	235.61	215.66
Ni	1089	1753	2163	2394	1890	7598	5585
Cu	343859	255130	704.33	779.13	195.51	326.61	1495.92
Zn	235.83	164.60	1234.13	959.88	372.40	529.81	49.86
As	<7.63	<7.63	<8.35	24.31	<8.04	<10	<8.83
Se	67.86	88.06	119.05	163.93	126.62	133.39	129.65
Mo	2.68	0.32	159.56	86.02	5.49	15.33	5.24
Ru	n.a.	n.a.	<0.79	<0.06	<0.30	<0.60	<0.5
Rh	<0.03	<0.03	0.08	<0.11	<0.05	0.08	<0.05
Pd	5.93	2.97	<0.11	<0.27	<0.09	0.17	0.44
Ag	380.38	185.18	34.84	18.39	14.43	27.43	11.16
Cd	0.94	1.69	19.01	26.18	10.15	19.26	<2.43
Sn	<1.62	0.04	1.18	<4.31	0.37	7.29	<3.00
Sb	10.04	3.37	176.39	104.71	5.54	20.13	13.59
Te	<3.52	<3.52	<4.49	<7.11	<4.60	<5.54	<4.31
Os	<0.01	0.004	<1.02	<1.64	<0.33	<0.37	<0.37
Ir	0.01	0.03	0.03	<0.08	<0.12	0.01	0.02
Pt	<0.28	<0.28	<0.52	<0.57	<0.36	<0.42	<0.18
Au	<0.27	<0.3	<0.45	<0.65	<0.51	<0.31	<0.32
Pb	48.08	32.51	658.20	635.77	116.84	99.73	24.50
Bi	<0.80	<0.81	<0.80	<0.79	<0.80	<0.83	<0.80

SULFURES ROCHES BPU AURÉOLE DE CONTACT:

Sulfides	**Ccp**	**Ccp**	**Ccp**	**Ccp**	**Ccp**	**Ccp**	**Po**
Samples	A4-15-01	A4-15-01	A4-15-01	A4-15-01	A4-15-01	A4-15-01	A4-15-01
Deposits	Wetlegs	Wetlegs	Wetlegs	Wetlegs	Wetlegs	Wetlegs	Wetlegs
Rock types	BPU c.a	BPU c.a	BPU c.a	BPU c.a	BPU c.a	BPU c.a	BPU c.a
Sulfide textures	Sulfide bed	Sulfide bed	Sulfide droplet	Sulfide droplet	Sulfide droplet	Sulfide droplet	Sulfide bed
Co	0.87	0.76	0.56	19.78	0.29	36.21	131.33
Ni	900.73	897.69	1004.19	885.51	982.89	971.14	522.95
Cu	377636	384331	422368	313429	426020	356359	1.27
Zn	395.59	236.14	240.70	517.31	240.09	216.86	0.87
As	<2.22	<2.04	<4.82	<7.19	<7.3	<4.95	<3.63
Se	11.47	11.84	16.43	18.26	15.52	18.93	13.46
Mo	0.42	0.58	0.15	0.27	<0.94	0.13	0.57
Ru	0.30	0.49	0.58	0.16	0.52	0.28	0.04
Rh	<0.02	<0.03	<0.02	<0.12	<0.01	<0.01	<0.005
Pd	0.51	0.98	0.21	1.22	1.51	1.36	<0.1
Ag	39.29	51.21	15.91	80.03	78.51	75.30	1.43
Cd	3.07	1.13	<0.9	2.13	1.40	1.07	<0.65
Sn	182.88	184.10	273.87	203.88	200.84	218.10	<0.78
Sb	8.12	22.21	1.52	5.54	1.46	7.53	0.12
Te	<0.63	0.09	<1.69	<2.85	<2.58	<2.22	<1.59
Os	<0.057	<0.18	<0.14	<0.22	<0.50	<0.35	<0.2
Ir	<0.05	<0.03	0.030	0.020	<0.05	<0.11	<0.05
Pt	<0.15	<0.13	<0.24	<0.3	<0.34	<0.41	<0.14
Au	<0.08	<0.1	<0.23	<0.28	<0.24	<0.17	<0.11
Pb	8.73	11.78	9.40	20.78	9.10	25.22	4.83
Bi	0.89	0.96	<0.80	<0.84	<0.80	<0.91	0.46

SULFURES ROCHES BPU AURÉOLE DE CONTACT (Suite):

Sulfides	**Po**	**Po**	**Po**	**Po**	**Po**	**Ccp**	**Po**	**Po**	**Po**
Samples	A4-15-01	A4-15-01	A4-15-01	A4-15-01	A4-15-01	DC-70	DC-70	DC-70	DC-70
Deposits	Wetlegs	Wetlegs	Wetlegs	Wetlegs	Wetlegs	Dunka Pit	Dunka Pit	Dunka Pit	Dunka Pit
Rock types	BPU c.a	BPU c.a	BPU c.a	BPU c.a	BPU c.a	BPU c.a	BPU c.a	BPU c.a	BPU c.a
Sulfide textures	Sulfide bed	Sulfide bed	Sulfide bed	Sulfide droplet	Sulfide droplet	Sulfide bed	Sulfide bed	Sulfide bed	Sulfide bed
Co	144.73	118.55	136.50	129.96	121.23	9.52	164.55	155.83	156.57
Ni	756.06	863.27	1458.52	1157.47	1209.20	918.99	1558.25	1483.45	1427.36
Cu	1.50	12.78	0.37	0.54	3.43	351162	<32.36	6.23	5.80
Zn	1.62	0.44	1.00	0.62	0.69	349.95	0.98	0.54	<2.04
As	<0.40	<2.82	<3.69	<2.81	<4.15	1.22	<3.01	<2.21	<3.23
Se	13.46	14.83	17.08	15.27	13.28	13.21	17.20	15.33	11.09
Mo	0.70	0.84	0.48	0.65	<0.59	0.48	0.26	0.27	0.93
Ru	0.08	<0.13	<0.11	<0.08	<0.30	0.20	<0.30	<0.30	<0.30
Rh	<0.02	<0.03	<0.06	<0.03	0.010	<0.02	<0.005	<0.005	<0.014
Pd	<0.1	<0.07	<0.03	<0.16	0.06	2.22	0.00	0.01	0.02
Ag	1.07	0.07	0.87	1.62	0.53	129.63	0.20	0.15	0.17
Cd	<0.85	<0.81	<0.79	0.16	0.01	1.95	<0.09	0.03	<0.48
Sn	<0.63	<0.75	0.11	<0.74	24.93	74.86	0.11	0.26	<0.77
Sb	3.24	<0.50	<0.58	<0.50	0.75	6.33	<2.30	<2.33	<0.50
Te	<1.11	<0.94	<1.57	<0.69	<1.62	0.40	<2.69	<1.81	<0.90
Os	<0.1	<0.22	<0.18	<0.27	<0.12	<0.06	<0.2	<0.04	<0.13
Ir	<0.04	<0.05	<0.06	<0.02	<0.04	<0.03	<0.01	<0.05	<0.05
Pt	<0.16	<0.14	<0.19	<0.11	<0.20	<0.14	<0.03	<0.03	<0.17
Au	<0.10	<0.09	<0.10	<0.08	<0.10	<0.10	<0.04	<0.03	<0.17
Pb	7.23	3.30	1.50	1.98	15.77	31.65	3.55	3.43	2.99
Bi	0.44	0.15	0.28	0.73	1.27	1.70	2.06	2.41	0.09

SULFURES ROCHES XÉNOLITHES BPU:

Sulfides	**Cb**	**Cb**	**Cb**	**Cb**	**Cb**	**Pn**	**Pn**	**Pn**
Samples	B1-384-26	B1-384-26	B1-384-26	B1-384-26	B1-384-26	B1-384-26	B1-384-26	B1-384-26
Deposits	Mesaba	Mesaba	Mesaba	Mesaba	Mesaba	Mesaba	Mesaba	Mesaba
Rock types	BPU xenoliths	BPU xenoliths	BPU xenoliths	BPU xenoliths	BPU xenoliths	BPU xenoliths	BPU xenoliths	BPU xenoliths
Sulfide textures	Sulfide bed	Sulfide bed	Sulfide bed	Sulfide bed	Sulfide bed	Sulfide bed	Sulfide bed	Sulfide bed
Co	0.13	2.05	16.05	182.29	51.03	27253	24713	24583
Ni	<3.00	38.27	128.00	2839	502	301180	273504	282946
Cu	223033	227560	206079	211346	213445	20.51	6.32	68.38
Zn	119.34	190.94	1597	481.46	3992	1.76	13.51	38.10
As	<1.21	<1.60	0.12	0.11	0.09	1.29	1.19	1.10
Se	28.11	25.97	22.47	22.80	26.62	15.08	16.12	15.47
Mo	<0.03	<0.03	<0.03	<0.03	<0.03	0.17	0.75	0.22
Ru	0.22	0.25	0.06	0.06	0.07	<0.02	<0.02	<0.02
Rh	<0.01	<0.01	<0.005	<0.006	<0.004	<0.006	<0.006	<0.005
Pd	<0.01	<0.01	0.02	0.16	0.43	0.12	0.22	0.15
Ag	5.60	8.72	7.13	23.66	4.40	0.82	1.39	1.21
Cd	2.43	4.40	6.17	1.84	2.59	0.01	0.00	0.02
Sn	5.02	10.49	6.05	5.93	3.66	0.31	0.54	0.77
Sb	<1.51	<1.78	<0.02	0.03	0.02	0.06	0.16	0.17
Te	6.54	6.91	6.67	6.46	7.98	<0.20	1.26	<0.19
Os	<0.03	<0.02	<0.03	<0.01	<0.01	<0.03	<0.02	<0.02
Ir	<0.05	<0.05	<0.006	<0.004	<0.003	<0.007	<0.007	<0.004
Pt	<0.01	<0.002	<0.01	<0.008	<0.004	<0.01	<0.005	<0.005
Au	<0.01	<0.02	<0.006	0.010	<0.002	<0.008	<0.002	<0.002
Pb	6.21	16.17	8.44	11.52	7.78	3.13	9.57	5.70
Bi	2.67	1.28	0.32	0.98	1.19	0.76	3.91	1.11

SULFURES XÉNOLITHES BPU (Suite) :

Sulfides	**Po**	**Po**	**Po**	**Po**	**Po**	**Cb**	**Cb**	**Cb**
Samples	B1-384-26	B1-384-26	B1-384-26	B1-384-26	DC-71	B1-384-26	B1-384-26	B1-384-26
Deposits	Mesaba	Mesaba	Mesaba	Mesaba	NorthMet	Mesaba	Mesaba	Mesaba
Rock types	BPU xenoliths	BPU xenoliths	BPU xenoliths	BPU xenoliths	BPU xenoliths	BPU xenoliths	BPU xenoliths	BPU xenoliths
Sulfide textures	Sulfide bed	Sulfide bed	Sulfide bed	Sulfide bed	Sulfide bed	Sulfide droplet	Sulfide droplet	Sulfide droplet
Co	67.13	49.49	64.76	87.89	19.33	1.15	14.40	0.30
Ni	1783	1657	1560	1851	1669	31.27	146	4.65
Cu	9.97	<188.75	140.87	92.25	11.72	223856	220646	210523
Zn	0.19	<1.08	5.73	48.62	0.41	2140	67.90	716
As	<2.1	<1.76	0.19	<0.13	0.12	8.39	2.96	0.12
Se	26.93	17.76	17.27	20.44	28.98	32.39	23.70	55.51
Mo	1.28	0.89	1.05	0.36	0.21	0.01	4.32	0.04
Ru	0.01	<0.03	<0.04	<0.05	<0.04	0.23	0.21	0.07
Rh	<0.005	<0.04	0.01	0.01	<0.007	<0.01	<0.02	<0.001
Pd	<0.15	<0.15	0.03	<0.03	<0.01	<0.01	0.53	0.13
Ag	0.13	0.16	0.30	0.21	0.20	15.47	5.60	9.04
Cd	0.05	<0.10	0.02	0.03	0.03	37.04	1.56	11.07
Sn	0.24	0.21	1.37	0.10	0.06	0.85	2.53	0.13
Sb	<1.83	<1.92	<0.03	<0.03	<0.03	<2.07	<1.31	0.02
Te	0.31	<1.87	<0.25	<0.24	<0.26	10.00	7.04	4.26
Os	<0.03	<0.03	<0.03	<0.01	<0.04	<0.03	<0.03	<0.02
Ir	0.001	<0.01	<0.007	<0.007	<0.01	<0.05	<0.05	<0.05
Pt	<0.01	<0.03	<0.02	<0.02	<0.03	<0.004	<0.004	<0.01
Au	<0.02	0.003	<0.01	<0.009	<0.01	<0.10	0.03	<0.10
Pb	0.31	0.21	0.14	0.22	1.33	13.46	3.91	45.27
Bi	1.27	3.57	0.02	0.06	0.25	1.48	4.77	0.05

SULFURES XÉNOLITHES BPU (suite):

Sulfides	**Pn**	**Pn**	**Po**	**Po**	**Po**	**Po**	**Po**	**Po**
Samples	B1-384-26	B1-384-26	B1-384-26	B1-384-26	B1-384-26	B1-384-26	B1-384-26	B1-384-26
Deposits	Mesaba	Mesaba	Mesaba	Mesaba	Mesaba	Mesaba	Mesaba	Mesaba
Rock types	BPU xenoliths	BPU xenoliths	BPU xenoliths	BPU xenoliths	BPU xenoliths	BPU xenoliths	BPU xenoliths	BPU xenoliths
Sulfide textures	Sulfide droplet	Sulfide droplet	Sulfide droplet	Sulfide droplet	Sulfide droplet	Sulfide droplet	Sulfide droplet	Sulfide droplet
Co	23801	20643	32.35	18.82	34.41	100.16	19.95	63.76
Ni	281970	287830	1004	885	1558	2256	1004	1832
Cu	244	<38.38	2.18	8.73	2.37	2.06	<25.62	<125.59
Zn	6.84	0.46	<0.06	274	1.87	0.61	0.30	<3.00
As	0.72	1.86	<1.67	0.50	<2.13	<1.69	<1.58	<2.08
Se	48.85	18.95	60.46	52.73	57.97	53.54	27.43	36.77
Mo	0.08	0.04	0.46	0.37	0.41	0.39	1.71	1.50
Ru	<0.01	<0.01	0.08	0.05	0.03	<0.03	0.04	<0.01
Rh	0.04	<0.01	<0.02	<0.02	<0.01	<0.005	<0.01	<0.04
Pd	0.50	0.20	0.01	<0.08	<0.03	<0.05	0.019	<0.01
Ag	0.42	1.07	0.22	0.37	0.36	0.21	0.16	0.06
Cd	0.21	0.01	0.09	0.09	0.02	<0.04	0.14	<0.05
Sn	0.13	0.35	2.24	0.31	0.30	0.26	0.17	0.17
Sb	1.17	<1.85	<2.01	<2.21	<2.53	<2.01	<2.12	<2.05
Te	0.88	3.26	<1.48	<1.94	<2.49	<1.96	<1.70	1.31
Os	0.02	<0.01	<0.01	0.03	0.03	<0.01	<0.02	<0.03
Ir	<0.01	<0.007	<0.01	<0.04	<0.01	<0.01	<0.05	<0.01
Pt	<0.02	<0.019	<0.02	<0.04	<0.03	<0.02	<0.009	<0.03
Au	0.01	0.01	<0.03	<0.09	<0.04	<0.03	<0.01	<0.03
Pb	2.12	1.23	0.21	0.59	0.58	0.57	0.19	0.10
Bi	0.65	2.28	4.36	1.12	0.12	1.25	1.94	1.83

SULFURES XÉNOLITHES BPU (suite):

Sulfides	Po	Po	Po	Po	Po	Po	Po	Cb
Samples	B1-384-26	B1-384-26	B1-384-26	B1-384-26	B1-384-26	B1-384-26	B1-384-26	B1-384-39
Deposits	Mesaba	Mesaba	Mesaba	Mesaba	Mesaba	Mesaba	Mesaba	Mesaba
Rock types	BPU xenoliths	BPU xenoliths	BPU xenoliths	BPU xenoliths	BPU xenoliths	BPU xenoliths	BPU xenoliths	BPU xenoliths
Sulfide textures	Sulfide droplet	Sulfide droplet	Sulfide droplet	Sulfide droplet	Sulfide droplet	Sulfide droplet	Sulfide droplet	Sulfide droplet
Co	71.55	68.50	74.80	67.50	52.05	28.68	42.51	0.95
Ni	2063	1975	2018	1850	1576	975	1394	64.61
Cu	0.62	935	879	135	82	1.56	249	213157
Zn	<0.83	2.99	0.69	2.06	1.22	0.72	2.56	31.69
As	<2.57	0.23	0.07	0.09	0.21	0.17	0.12	<1.79
Se	21.19	49.24	48.87	40.95	61.08	39.83	38.71	32.22
Mo	1.02	0.17	0.18	0.39	0.56	0.20	0.40	0.01
Ru	<0.01	<0.08	0.03	0.01	0.05	0.02	0.05	0.20
Rh	0.00	0.03	0.02	<0.01	0.01	<0.009	0.01	<0.01
Pd	<0.01	0.09	<0.02	<0.02	0.05	0.06	0.01	<0.03
Ag	0.10	0.21	0.12	0.21	0.47	0.25	0.62	5.19
Cd	<0.05	<0.05	0.05	0.02	0.06	<0.05	0.08	4.28
Sn	0.19	0.06	0.30	0.04	0.03	0.03	0.05	0.32
Sb	<2.50	<0.03	<0.03	<0.03	<0.03	<0.03	<0.03	<1.29
Te	0.44	<0.51	<0.40	<0.44	0.52	<0.38	<0.3	1.56
Os	<0.03	<0.02	<0.03	<0.05	<0.05	<0.04	<0.02	<0.03
Ir	<0.01	<0.01	<0.009	<0.01	<0.01	<0.009	<0.007	<0.05
Pt	<0.02	<0.03	<0.03	<0.02	0.02	<0.02	<0.02	<0.009
Au	<0.03	<0.02	<0.01	<0.02	<0.02	<0.01	<0.008	<0.10
Pb	0.14	1.38	0.77	0.77	0.42	0.77	1.98	5.14
Bi	1.62	0.12	0.07	0.03	0.07	0.09	0.04	<0.90

SULFURES XÉNOLITHES BPU (suite):

Sulfides	**Po**	**Ccp**	**Po**	**Po**	**Po**	**Ccp**	**Pn**	**Pn**
Samples	B1-384-39	DC-69	DC-69	DC-71	DC-71	DC-80	DC-80	DC-80
Deposits	Mesaba	NorthMet	NorthMet	NorthMet	NorthMet	NorthMet	NorthMet	NorthMet
Rock types	BPU xenoliths	BPU xenoliths	BPU xenoliths	BPU xenoliths	BPU xenoliths	BPU xenoliths	BPU xenoliths	BPU xenoliths
Sulfide textures	Sulfide droplet	Sulfide droplet	Sulfide droplet	Sulfide droplet	Sulfide droplet	Sulfide droplet	Sulfide droplet	Sulfide droplet
Co	62.27	24.65	69.25	28.62	20.76	1.80	23639	23443
Ni	2092	396	4133	1740	1818	158.24	317460	322018
Cu	1.18	292432	0.69	1.58	11.78	309777	2.02	3.52
Zn	0.13	190	0.16	0.32	0.26	593	3.81	212
As	<1.74	0.14	0.18	0.18	0.19	0.47	3.71	1.45
Se	26.24	27.87	29.11	29.92	30.67	54.10	46.07	43.63
Mo	0.92	0.31	0.06	0.71	0.55	0.03	0.09	0.14
Ru	0.13	0.06	0.10	0.02	<0.03	0.08	<0.04	<0.03
Rh	<0.005	<0.009	0.005	<0.006	<0.006	<0.005	<0.005	<0.005
Pd	<0.02	0.01	<0.02	<0.02	<0.02	<0.01	0.20	0.28
Ag	0.30	0.83	0.04	0.16	0.13	2.08	2.03	3.06
Cd	<0.05	4.56	0.08	0.05	<0.05	16.13	0.09	4.33
Sn	<0.25	0.45	0.04	0.32	0.04	22.97	1.95	1.27
Sb	<1.56	0.15	0.02	<0.03	0.03	0.07	0.48	0.36
Te	<1.22	0.32	<0.37	<0.18	<0.31	12.20	8.47	6.71
Os	0.04	0.03	<0.01	<0.02	<0.02	<0.01	<0.02	<0.007
Ir	<0.002	0.03	<0.01	<0.01	<0.008	<4.45	<0.007	<0.007
Pt	<0.02	<0.02	<0.03	<0.02	<0.02	<0.009	<0.02	<0.024
Au	<0.04	<0.003	<0.02	<0.007	<0.008	<0.003	0.03	<0.03
Pb	0.17	9.07	0.36	0.24	0.92	5.72	4.49	6.09
Bi	<1.06	1.10	0.11	0.04	0.14	0.47	3.02	3.00

SULFURES XÉNOLITHES BPU (suite):

Sulfides	**Po**	**Po**	**Po**	**Po**	**Ccp**	**Ccp**	**Ccp**
Samples	DC-80	DC-80	DC-80	DC-80	EC-07	EC-07	EC-07
Deposits	NorthMet	NorthMet	NorthMet	NorthMet	Dunka Pit	Dunka Pit	Dunka Pit
Rock types	BPU xenoliths	BPU xenoliths	BPU xenoliths	BPU xenoliths	BPU xenoliths	BPU xenoliths	BPU xenoliths
Sulfide textures	Sulfide droplet	Sulfide droplet	Sulfide droplet	Sulfide droplet	Sulfide droplet	Sulfide droplet	Sulfide droplet
Co	29.17	75.42	54.98	56.60	3.62	0.34	1.25
Ni	1838	2238	2371	2562	173.45	26.84	33.47
Cu	0.77	0.51	0.60	0.71	306430	309169	303691
Zn	2.12	0.37	0.19	0.32	484	369	2860
As	2.28	0.19	0.32	0.43	1.37	0.09	0.01
Se	25.37	43.88	41.70	44.94	43.12	41.02	32.07
Mo	0.08	0.78	0.30	0.53	0.02	0.02	0.01
Ru	<0.03	0.03	<0.04	<0.05	0.07	0.09	0.07
Rh	<0.006	<0.009	<0.008	0.003	<0.005	<0.004	<0.006
Pd	0.02	<0.02	<0.02	<0.02	<0.006	<0.006	<0.01
Ag	0.10	0.10	0.07	0.10	1.76	0.36	8.03
Cd	<0.05	0.01	0.01	0.02	35.60	26.05	55.08
Sn	0.23	0.05	0.04	0.07	12.57	12.72	1.50
Sb	0.03	<0.03	<0.03	<0.03	0.19	0.03	1.17
Te	<0.18	<0.34	<0.32	<0.19	6.12	4.95	1.12
Os	<0.03	<0.01	<0.009	<0.02	<0.03	<0.03	<0.01
Ir	<0.004	<0.006	<0.005	<0.007	<0.002	0.003	<5.85
Pt	<0.02	<0.03	<0.03	<0.01	<0.01	<0.01	<0.02
Au	<0.008	<0.01	<0.01	<0.005	<0.10	<0.10	0.05
Pb	1.15	0.29	0.30	0.58	8.28	4.49	34.14
Bi	0.11	0.27	0.26	0.31	0.24	0.20	2.59

SULFURES MASSIFS:

Sulfides	**Pn**	**Po**	**Po**	**Po**	**Cb**	**Ccp**	**Pn**	**Po**
Samples	B1-384-26	B1-384-26	B1-384-26	B1-384-26	B1-384-39	B1-384-39	B1-384-39	B1-384-39
Deposits	Mesaba	Mesaba	Mesaba	Mesaba	Mesaba	Mesaba	Mesaba	Mesaba
Rock types	Massive sulfides	Massive sulfides	Massive sulfides	Massive sulfides	Massive sulfides	Massive sulfides	Massive sulfides	Massive sulfides
Sulfide textures	Massive sulfides	Massive sulfides	Massive sulfides	Massive sulfides	Massive sulfides	Massive sulfides	Massive sulfides	Massive sulfides
Co	26992	51.36	43.88	40.83	1.48	0.54	10618	20.69
Ni	307041	1770	1515	1477	30.86	10.86	294668	1464
Cu	2.21	3.86	50.49	1.93	210688	307343	1.30	0.64
Zn	0.29	1.87	0.87	0.17	2757	697	0.32	0.18
As	1.9900	<2.10	<1.92	<1.76	<1.28	0.0800	<1.43	<2.05
Se	38.10	53.60	54.23	46.44	22.39	35.60	18.79	25.43
Mo	0.31	1.23	0.77	0.43	0.02	0.03	0.04	0.63
Ru	<0.02	0.04	0.08	0.05	0.21	0.10	<0.02	0.18
Rh	0.01	0.01	0.01	<0.04	<0.002	<0.005	<0.005	<0.003
Pd	0.41	<0.01	<0.02	<0.01	<0.003	<0.01	1.00	<0.005
Ag	1.10	0.30	0.73	0.47	7.53	1.68	1.76	0.27
Cd	0.01	<0.03	0.05	<0.05	79.83	13.82	0.01	<0.05
Sn	0.40	0.34	0.18	0.12	0.08	0.27	0.01	0.12
Sb	<1.48	<1.83	<1.67	<1.92	<1.11	<0.02	<1.33	<1.60
Te	0.33	0.56	0.69	<1.87	0.41	2.44	<1.32	<1.38
Os	<0.03	<0.04	0.03	<0.04	<0.03	<0.03	<0.03	0.03
Ir	<0.01	<0.01	<0.01	<0.05	<0.05	<0.005	<0.007	<0.05
Pt	<0.03	<0.01	<0.01	<0.01	<0.01	<0.02	<0.006	<0.01
Au	<0.03	<0.02	<0.02	<0.03	<0.10	<0.003	<0.02	<0.02
Pb	1.42	0.63	0.79	0.59	0.89	0.99	0.07	0.30
Bi	1.37	2.99	0.56	1.73	<0.81	0.11	<1.06	<1.27

SULFURES MASSIFS (Suite):

Sulfides	**Po**	**Po**	**Po**	**Po**	**Po**	**Ccp**	**Ccp**	**Ccp**
Samples	B1-384-39	B1-384-39	B1-384-39	B1-384-39	B1-384-39	DC-69	DC-69	DC-69
Deposits	Mesaba	Mesaba	Mesaba	Mesaba	Mesaba	NorthMet	NorthMet	NorthMet
Rock types	Massive sulfides	Massive sulfides	Massive sulfides	Massive sulfides	Massive sulfides	Massive sulfides	Massive sulfides	Massive sulfides
Sulfide textures	Massive sulfides	Massive sulfides	Massive sulfides	Massive sulfides	Massive sulfides	Massive sulfides	Massive sulfides	Massive sulfides
Co	53.04	46.37	51.73	49.49	65.01	2.46	0.72	5.69
Ni	1657	1517	1664	1722	1816	42.30	48.38	121.72
Cu	0.98	1.42	1.53	8.17	14.34	312760	311482	314038
Zn	0.19	0.09	0.17	0.95	0.39	359	253	259
As	<1.77	<1.64	<1.55	0.1600	0.0800	0.0700	0.2600	0.2600
Se	25.74	25.87	27.30	23.37	25.06	33.69	33.90	32.01
Mo	0.93	0.61	0.45	0.48	0.53	<0.03	<0.03	0.06
Ru	0.13	0.13	0.12	0.08	0.11	0.08	0.08	0.07
Rh	<0.005	<0.005	<0.005	0.01	<0.007	<0.003	<0.003	<0.002
Pd	0.0020	<0.006	<0.02	0.20	<0.01	<0.01	<0.008	<0.009
Ag	0.24	0.18	0.18	0.34	0.14	0.15	1.49	0.34
Cd	0.04	<0.05	<0.05	0.04	<0.03	12.48	11.69	10.99
Sn	0.02	<0.16	0.04	0.02	0.03	3.21	3.20	4.42
Sb	<1.41	<1.16	<1.36	<0.03	<0.03	0.03	0.03	0.03
Te	<1.21	<1.07	<1.22	<0.22	<0.23	3.18	4.71	3.39
Os	0.03	0.05	<0.04	<0.04	<0.03	<0.03	<0.003	<0.009
Ir	<0.05	<0.05	<0.05	<0.05	<0.006	<0.005	<0.005	<0.005
Pt	<0.01	<0.01	<0.01	<0.01	<0.03	<0.01	<0.007	<0.01
Au	0.01	<0.04	<0.04	<0.003	<0.003	<0.10	<0.10	0.006
Pb	0.14	0.30	0.25	0.36	0.19	4.34	10.51	5.25
Bi	<1.25	<1.03	<1.11	0.05	0.07	0.28	0.43	0.27

SULFURES MASSIFS (Suite):

Sulfides	**Ccp**	**Ccp**	**Pn**	**Pn**	**Pn**	**Po**	**Po**	**Po**
Samples	DC-69	DC-69	DC-69	DC-69	DC-69	DC-69	DC-69	DC-71
Deposits	NorthMet	NorthMet	NorthMet	NorthMet	NorthMet	NorthMet	NorthMet	NorthMet
Rock types	Massive sulfides	Massive sulfides	Massive sulfides	Massive sulfides	Massive sulfides	Massive sulfides	Massive sulfides	Massive sulfides
Sulfide textures	Massive sulfides	Massive sulfides	Massive sulfides	Massive sulfides	Massive sulfides	Massive sulfides	Massive sulfides	Massive sulfides
Co	0.83	0.37	27676	28002	25950	364	129	23.35
Ni	33.81	30.98	360439	367277	361742	8140	5616	1852
Cu	311603	305791	2.08	3.97	26.05	1.81	17.45	223
Zn	226	281	1.04	0.58	0.50	0.18	0.25	3.68
As	0.1800	0.0500	6.0600	2.2700	1.2800	0.4900	0.1600	13.9600
Se	34.60	29.82	25.75	25.89	24.62	27.11	28.36	29.23
Mo	<0.03	<0.03	0.11	0.36	0.54	0.21	2.14	0.39
Ru	0.09	0.07	<0.03	<0.02	<0.03	0.24	0.22	0.01
Rh	<0.003	<0.003	<0.005	0.01	0.01	0.01	0.01	0.01
Pd	<0.01	<0.006	1.17	1.23	1.50	<0.02	0.03	<0.01
Ag	0.22	0.26	0.37	0.31	0.48	0.16	0.06	0.24
Cd	11.11	10.62	0.03	0.04	0.03	0.02	<0.03	0.05
Sn	4.70	3.64	0.05	0.05	0.03	0.05	0.03	0.13
Sb	<0.02	0.02	0.12	0.18	0.09	0.03	<0.03	<0.03
Te	4.06	3.24	<0.20	<0.20	<0.20	<0.19	<0.23	<0.15
Os	<0.03	<0.01	<0.03	<0.01	<0.03	<0.03	<0.008	<0.01
Ir	<0.005	<0.005	<0.007	<0.007	<0.01	<0.01	<0.006	<0.006
Pt	<0.008	<0.009	<0.02	<0.02	<0.01	<0.02	<0.02	<0.01
Au	<0.10	<0.02	0.007	<0.01	<0.007	<0.009	<0.02	<0.008
Pb	2.50	7.55	0.91	3.91	0.54	0.72	0.05	1.40
Bi	0.21	0.30	0.38	0.38	0.20	0.16	0.02	0.13

SULFURES DANS LES NORITES :

Sulfides	**Cb**	**Cb**	**Cb**	**Cb**	**Cb**	**Ccp**	**Ccp**	**Ccp**
Samples	B1-384-12	B1-384-12	B1-384-12	B1-384-12	B1-384-12	B1-384-12	B1-384-12	B1-384-12
Deposits	Mesaba	Mesaba	Mesaba	Mesaba	Mesaba	Mesaba	Mesaba	Mesaba
Rock types	Norite	Norite	Norite	Norite	Norite	Norite	Norite	Norite
Sulfide textures	Sulfide droplet	Sulfide droplet	Sulfide droplet	Sulfide droplet	Sulfide droplet	Sulfide droplet	Sulfide droplet	Sulfide droplet
Co	<0.79	11.93	0.69	1.52	0.63	<0.33	<0.72	0.29
Ni	7.0	81.07	4.98	7.00	7.41	14.91	34.08	10.71
Cu	216449	218918	225914	222622	216038	319515	313733	315559
Zn	370	914	2058	3045	3004	268	320	223
As	<1.30	<1.83	<1.20	<1.15	<1.35	<1.53	<1.21	<1.24
Se	47.49	72.22	85.47	85.80	69.26	52.64	60.16	86.42
Mo	0.01	0.01	0.01	0.01	0.01	<0.02	<0.02	<0.02
Ru	0.24	0.21	0.24	0.21	0.20	0.30	0.30	0.27
Rh	<0.01	<0.02	<0.03	<0.01	<0.01	<0.01	<0.01	<0.01
Pd	<0.01	<0.01	<0.03	<0.01	<0.01	<0.01	<0.01	<0.01
Ag	16.67	25.14	60.74	34.85	83.99	5.21	5.96	6.47
Cd	24.28	59.26	132.91	187.64	120.16	16.52	20.36	18.29
Sn	1.01	1.73	19.75	1.44	1.13	5.55	10.32	9.19
Sb	<1.21	<1.57	<1.57	<1.15	<1.72	<1.22	<1.12	<1.10
Te	1.19	6.25	9.51	8.27	6.75	3.13	2.71	6.66
Os	<0.04	<0.03	<0.03	<0.03	<0.03	<0.01	<0.03	<0.03
Ir	<0.01	<0.01	<0.01	<0.01	<0.01	<0.01	<0.01	<0.01
Pt	<0.008	<0.02	<0.02	<0.01	<0.01	<0.006	<0.008	<0.01
Au	<0.01	<0.02	<0.01	<0.01	<0.03	<0.02	<0.01	<0.008
Pb	6.60	9.71	8.15	10.41	14.77	1.90	3.62	1.84
Bi	<0.53	1.98	0.76	0.78	0.74	2.43	0.91	1.22

SULFURES DANS LES NORITES (Suite) :

Sulfides	**Cb**	**Cb**	**Pn**	**Po**	**Po**	**Po**	**Po**	**Po**
Samples	B1-384-13	B1-384-13	B1-384-13	B1-384-13	B1-384-13	B1-384-13	B1-384-13	B1-384-13
Deposits	Mesaba	Mesaba	Mesaba	Mesaba	Mesaba	Mesaba	Mesaba	Mesaba
Rock types	Norite	Norite	Norite	Norite	Norite	Norite	Norite	Norite
Sulfide textures	Sulfide droplet	Sulfide droplet	Sulfide droplet	Sulfide droplet	Sulfide droplet	Sulfide droplet	Sulfide droplet	Sulfide droplet
Co	7.20	5.47	25136	52.98	52.54	53.29	58.34	59.46
Ni	141	111	281318	2169	1994	1965	1931	1901
Cu	225502	218753	27.35	1.33	1.23	1.85	32.41	1.68
Zn	<0.06	<0.06	<0.06	<0.06	<0.06	<0.1	<0.1	<0.1
As	0.62	0.72	14.98	4.49	0.82	<0.97	<0.79	<0.87
Se	97.53	64.69	65.45	50.67	58.09	66.38	72.55	74.55
Mo	<0.02	0.06	0.08	2.66	1.91	1.56	1.57	1.75
Ru	0.26	0.26	<0.03	0.04	0.06	0.05	0.04	0.07
Rh	<0.002	<0.003	0.01	<0.008	<0.01	<0.01	<0.005	0.006
Pd	<0.009	<0.02	0.14	0.005	<0.03	0.01	<0.03	<0.03
Ag	9.66	5.23	11.23	0.23	0.24	0.15	0.32	0.26
Cd	9.63	9.42	63.49	0.08	<0.03	0.04	1.06	0.13
Sn	5.76	2.67	0.32	0.14	0.01	<0.12	0.06	0.04
Sb	<0.32	<0.29	0.45	<0.43	<0.46	<0.38	<0.46	<0.53
Te	20.41	7.61	18.69	<1.25	<1.72	<1.17	<1.08	<1.29
Os	<0.03	<0.03	0.03	0.04	<0.04	<0.06	<0.05	<0.06
Ir	<0.01	<0.01	<0.02	<0.02	<0.02	<0.02	<0.02	<0.02
Pt	<0.02	<0.03	<0.03	<0.05	<0.05	<0.03	<0.04	<0.06
Au	<0.03	<0.02	<0.02	<0.02	<0.05	<0.02	<0.02	<0.02
Pb	23.54	11.93	10.32	0.54	0.05	0.14	0.41	0.40
Bi	0.11	<0.30	1.79	0.31	0.65	0.22	0.10	<0.42

SULFURES DANS LES NORITES (Suite) :

Sulfides	**Cb**	**Cb**	**Cb**	**Po**	**Po**	**Po**	**Po**	**Po**
Samples	B1-384-16	B1-384-16	B1-384-16	B1-384-16	B1-384-16	B1-384-16	B1-384-16	B1-384-16
Deposits	Mesaba	Mesaba	Mesaba	Mesaba	Mesaba	Mesaba	Mesaba	Mesaba
Rock types	Norite	Norite	Norite	Norite	Norite	Norite	Norite	Norite
Sulfide textures	Sulfide droplet	Sulfide droplet	Sulfide droplet	Sulfide droplet	Sulfide droplet	Sulfide droplet	Sulfide droplet	Sulfide droplet
Co	0.19	2.96	18.93	45.50	47.12	59.77	47.18	26.80
Ni	37.65	84.36	288	1882	1814	1907	1596	1340
Cu	220564	226737	220564	0.77	1.05	56.10	10.60	0.82
Zn	<0.06	<0.06	<0.06	<0.1	<0.1	<0.1	<0.1	<0.1
As	0.82	0.77	<0.8	0.46	<0.9	<0.8	<0.9	<0.8
Se	60.49	60.66	60.16	43.76	43.38	50.74	46.69	48.62
Mo	0.04	0.07	0.04	0.94	1.44	1.50	0.61	0.87
Ru	0.22	0.23	0.25	0.04	0.05	0.08	0.04	0.05
Rh	<0.01	<0.003	<0.007	<0.006	0.004	0.005	<0.009	<0.01
Pd	<0.01	<0.01	<0.03	<0.03	<0.02	0.06	<0.02	0.01
Ag	6.11	9.63	19.46	0.32	0.28	0.37	0.22	0.46
Cd	30.86	25.10	27.98	0.09	0.04	<0.09	<0.03	0.03
Sn	2.42	4.94	0.07	0.08	0.03	0.06	0.03	0.14
Sb	<0.46	<0.42	<0.49	<0.49	<0.48	<0.54	<0.46	<0.52
Te	15.51	15.39	13.00	<1.15	<1.13	<1.58	<1.13	<1.26
Os	<0.03	<0.03	<0.05	<0.05	<0.04	<0.06	<0.07	<0.05
Ir	<0.008	<0.008	<0.01	<0.01	<0.01	<0.01	<0.02	<0.01
Pt	<0.03	<0.02	<0.03	<0.03	<0.04	<0.04	<0.03	<0.04
Au	<0.02	<0.02	<0.03	<0.02	<0.03	<0.02	<0.02	<0.03
Pb	8.11	13.74	13.66	0.17	0.37	0.16	0.63	0.95
Bi	0.19	0.67	<0.42	0.90	0.87	0.22	0.43	0.72

SULFURES DANS LES NORITES (Suite) :

Sulfides	**Cb**	**Cb**	**Cb**	**Pn**	**Pn**	**Pn**	**Po**	**Po**	**Po**	**Po**	**Po**
Samples	B1-384-21	B1-384-21	B1-384-21	B1-384-21	B1-384-21	B1-384-21	B1-384-21	B1-384-21	B1-384-21	B1-384-21	EC-07
Deposits	Mesaba	Mesaba	Mesaba	Mesaba	Mesaba	Mesaba	Mesaba	Mesaba	Mesaba	Mesaba	Dunka Pit
Rock types	Norite	Norite	Norite	Norite	Norite	Norite	Norite	Norite	Norite	Norite	Norite
Sulfide textures	Sulfide droplet	Sulfide droplet	Sulfide droplet	Sulfide droplet	Sulfide droplet	Sulfide droplet	Sulfide droplet	Sulfide droplet	Sulfide droplet	Sulfide droplet	Sulfide droplet
Co	0.18	0.03	0.10	11591	11494	10615	14.90	14.35	11.30	28.24	79.03
Ni	42.18	35.80	38.19	297598	296622	277737	636	571	582	1114	5778
Cu	219042	221387	223445	9377.00	2735.00	2605.00	1.73	0.46	374.00	1.22	10.78
Zn	<0.06	<0.06	<0.06	<0.06	<0.06	<0.06	<0.06	<0.06	<0.06	<0.06	1.03
As	<0.8	<0.8	<0.8	1.77	2.21	1.51	<0.7	<0.9	<0.9	<0.9	0.24
Se	63.95	57.73	44.89	34.84	33.99	51.44	47.87	44.19	41.82	47.00	38.27
Mo	<0.02	<0.02	<0.02	0.09	0.08	0.05	1.17	0.49	0.37	0.41	2.31
Ru	0.28	0.26	0.26	<0.04	<0.03	<0.03	0.04	0.13	0.10	0.07	0.03
Rh	<0.002	<0.006	<0.008	0.960	0.31	0.16	0.03	<0.01	0.02	<0.007	0.01
Pd	<0.02	<0.007	<0.02	0.23	0.24	0.13	0.01	<0.01	0.03	<0.02	<0.009
Ag	6.51	4.12	8.97	6.12	7.81	5.96	0.68	0.59	0.55	0.53	0.17
Cd	2.40	2.84	15.72	0.19	0.03	0.05	0.07	0.03	0.08	0.14	0.07
Sn	2.94	0.12	2.51	0.81	1.63	2.80	0.11	0.05	0.73	0.39	0.22
Sb	<0.46	<0.39	<0.20	<0.20	<0.20	<0.38	<0.43	<0.48	<0.55	<0.20	<0.20
Te	2.00	1.65	<0.97	<1.13	<0.91	1.56	<1.15	<1.35	<1.28	<1.35	<0.19
Os	<0.04	<0.03	<0.05	0.03	0.03	<0.07	<0.04	<0.03	0.07	<0.03	0.005
Ir	<0.01	<0.01	<0.006	<0.01	<0.008	<0.008	<0.01	<0.02	<0.01	<0.008	0.01
Pt	<0.03	<0.02	<0.04	<0.04	<0.03	<0.03	<0.02	<0.05	<0.03	<0.03	<0.02
Au	<0.03	<0.03	<0.02	<0.02	<0.02	<0.02	<0.05	<0.04	<0.03	<0.03	<0.008
Pb	18.85	48.15	12.02	3.45	6.09	48.84	0.15	0.19	0.94	0.30	1.48
Bi	0.15	0.30	0.32	<0.35	0.13	<0.29	0.45	0.34	0.49	0.24	0.13

SULFURES DANS LES GABBRONORITES :

Sulfides	**Cb**	**Cb**	**Cb**	**Ccp**	**Ccp**	**Pn**	**Po**	**Po**
Samples	B1-384-04B	B1-384-04B	B1-384-04B	B1-384-04B	B1-384-04B	B1-384-04B	B1-384-04B	B1-384-04B
Deposits	Mesaba	Mesaba	Mesaba	Mesaba	Mesaba	Mesaba	Mesaba	Mesaba
Rock types	Gabbronorite	Gabbronorite	Gabbronorite	Gabbronorite	Gabbronorite	Gabbronorite	Gabbronorite	Gabbronorite
Sulfide textures	Sulfide droplet	Sulfide droplet	Sulfide droplet	Sulfide droplet	Sulfide droplet	Sulfide droplet	Sulfide droplet	Sulfide droplet
Co	1.12	0.05	0.06	0.97	0.70	19797	41.57	48.18
Ni	76.95	36.34	36.75	131.00	79.12	274481	1985	1747
Cu	221922	223609	224432	324080	325905	1.11	0.92	1.25
Zn	<0.06	<0.06	<0.06	<0.06	<0.06	<0.06	<0.83	<0.83
As	<0.58	0.45	0.44	0.52	0.55	3.55	1.83	0.65
Se	38.06	35.72	37.12	34.87	41.57	28.49	33.41	31.29
Mo	0.04	0.02	0.03	<0.03	<.0.03	0.25	3.20	3.13
Ru	0.25	0.24	0.23	0.32	0.37	<0.02	0.08	0.08
Rh	<0.005	<0.006	<0.007	<0.003	<0.006	<0.004	0.01	0.01
Pd	<0.01	<0.01	<0.02	<0.02	<0.008	0.71	<0.01	<0.02
Ag	9.20	10.55	9.42	2.95	1.84	1.68	0.49	0.25
Cd	20.99	5.80	3.20	8.79	32.26	0.07	0.04	0.04
Sn	1.60	1.89	1.15	15.95	11.72	1.69	0.12	0.11
Sb	<0.27	<0.21	<0.40	<0.23	<0.24	0.21	0.02	<0.36
Te	4.92	4.40	5.10	3.16	4.81	0.68	0.40	<0.57
Os	<0.03	<0.05	<0.06	<0.04	<0.05	<0.03	<0.04	<0.05
Ir	<0.004	<0.01	<0.01	<0.01	<0.01	<0.01	<0.02	<0.009
Pt	<0.03	<0.02	<0.03	<0.02	<0.01	<0.02	<0.04	<0.01
Au	<0.02	<0.02	<0.02	<0.03	<0.03	<0.02	<0.02	<0.03
Pb	5.92	12.92	7.72	3.04	2.99	2.31	0.54	0.27
Bi	0.06	<0.28	<0.35	<0.23	<0.29	0.04	<0.34	<0.38

SULFURES DANS LES GABBRONORITES (Suite) :

Sulfides	**Po**	**Po**	**Po**	**Ccp**	**Ccp**	**Cb**	**Cb**	**Cb**	**Ccp**	**Ccp**	**Pn**	**Pn**
Samples	B1-384-04B	B1-384-04B	B1-384-04B	B1-384-05	B1-384-05	B1-384-08	B1-384-08	B1-384-08	B1-384-08	B1-384-08	B1-384-08	B1-384-08
Deposits	Mesaba	Mesaba	Mesaba	Mesaba	Mesaba	Mesaba	Mesaba	Mesaba	Mesaba	Mesaba	Mesaba	Mesaba
Rock types	Gabbronorite	Gabbronorite	Gabbronorite	Gabbronorite	Gabbronorite	Gabbronorite	Gabbronorite	Gabbronorite	Gabbronorite	Gabbronorite	Gabbronorite	Gabbronorite
Sulfide textures	Sulfide droplet	Sulfide droplet	Sulfide droplet	Sulfide droplet	Sulfide droplet	Sulfide droplet	Sulfide droplet	Sulfide droplet	Sulfide droplet	Sulfide droplet	Sulfide droplet	Sulfide droplet
Co	48.18	57.53	52.98	0.05	0.03	0.03	0.07	0.02	0.03	0.08	5451	5040
Ni	1801	1960	1995	156	174	36.42	37.24	41.40	59.95	68.16	247782	250061
Cu	0.42	0.66	38.64	334426	332296	229452	229617	239905	331991	330470	274	1075
Zn	<0.83	<0.83	<0.83	<0.06	<0.06	<0.06	<0.06	<0.06	<0.06	<0.06	<0.06	<0.06
As	0.33	0.69	0.45	0.55	0.46	0.47	0.58	0.82	<0.34	<0.44	0.79	0.69
Se	32.47	32.16	33.60	108.64	104.07	76.05	107.40	106.17	91.81	93.88	84.33	85.31
Mo	1.03	4.06	6.48	<.0.03	0.05	0.02	<0.02	0.03	<.0.03	<.0.03	0.03	0.05
Ru	0.07	0.07	0.07	0.33	0.43	0.24	0.16	0.27	0.32	0.34	<0.02	<0.02
Rh	<0.008	<0.008	<0.005	<0.004	<0.005	<0.004	<0.003	<0.006	<0.004	<0.004	0.04	0.13
Pd	<0.01	<0.03	<0.03	<0.01	<0.02	0.04	<0.02	0.22	<0.02	<0.02	5.26	0.44
Ag	0.30	0.26	0.14	6.54	4.26	32.96	16.34	13.41	11.84	5.04	132.84	125.03
Cd	0.09	0.05	0.03	5.48	1.66	0.28	67.07	0.40	6.42	5.29	0.35	<0.07
Sn	0.04	0.09	0.05	20.18	19.66	0.05	0.41	0.18	6.15	2.09	1.43	0.09
Sb	<0.40	<0.40	<0.36	<0.28	<0.24	<0.20	<0.35	<0.29	<0.30	<0.24	<0.34	<0.23
Te	0.18	0.08	0.16	1.49	1.66	1.88	1.33	2.10	0.92	2.34	1.69	1.24
Os	<0.05	<0.06	<0.02	<0.04	<0.03	<0.05	<0.03	<0.04	<0.04	<0.04	<0.06	0.04
Ir	<0.006	<0.01	<0.01	<0.007	<0.008	<0.009	<0.02	<0.005	<0.01	<0.008	<0.006	<0.008
Pt	<0.03	<0.03	<0.01	<0.03	<0.02	<0.03	<0.02	<0.03	<0.05	<0.02	<0.02	<0.02
Au	<0.03	<0.02	<0.04	<0.02	<0.02	<0.01	<0.03	<0.03	<0.02	<0.01	<0.02	<0.02
Pb	0.64	0.46	0.12	5.15	3.78	9.59	5.47	52.26	2.18	4.44	7.55	9.61
Bi	0.67	<0.36	0.19	<0.28	<0.28	<0.40	<0.27	<0.24	<0.32	<0.23	0.10	<0.25

ANNEXE 7 : T-X(H_20) PSEUDOSECTIONS DANS LE SYSTÈME NCKFMASHMT

Abréviations (Whitney et Evans, 2010):

Bt = Biotite

Crd = Cordiérite

Hc = Hercynite

Ilm = Ilménite

Kfs = Feldspath potassique

Opx = Orthopyroxène

Pl = Plagioclase

Qz = Quartz

Rt = Rutile

Sil = Sillimanite

Notes:

Les pseudosections sont renseignées en anglais dans un souci de cohérence avec les publications présentées dans ce mémoire de doctorat.

Les pseudosections ont été réalisées à partir de compositions roche totale (Chapitre 3 de ce mémoire de doctorat) de xénolithes de la Bedded Pyrrhotite Unit.

Le contenu en H_2O nécessaire à l'obtention de paragénèses sous saturées en H_2O pour les deux échantillons présentés est inférieur à 0.1 mol (~2wt%).

Bedded Pyrrhotite Unit xenolith B1-384-14; NCKFMASHMT; P = 2.5 kbars

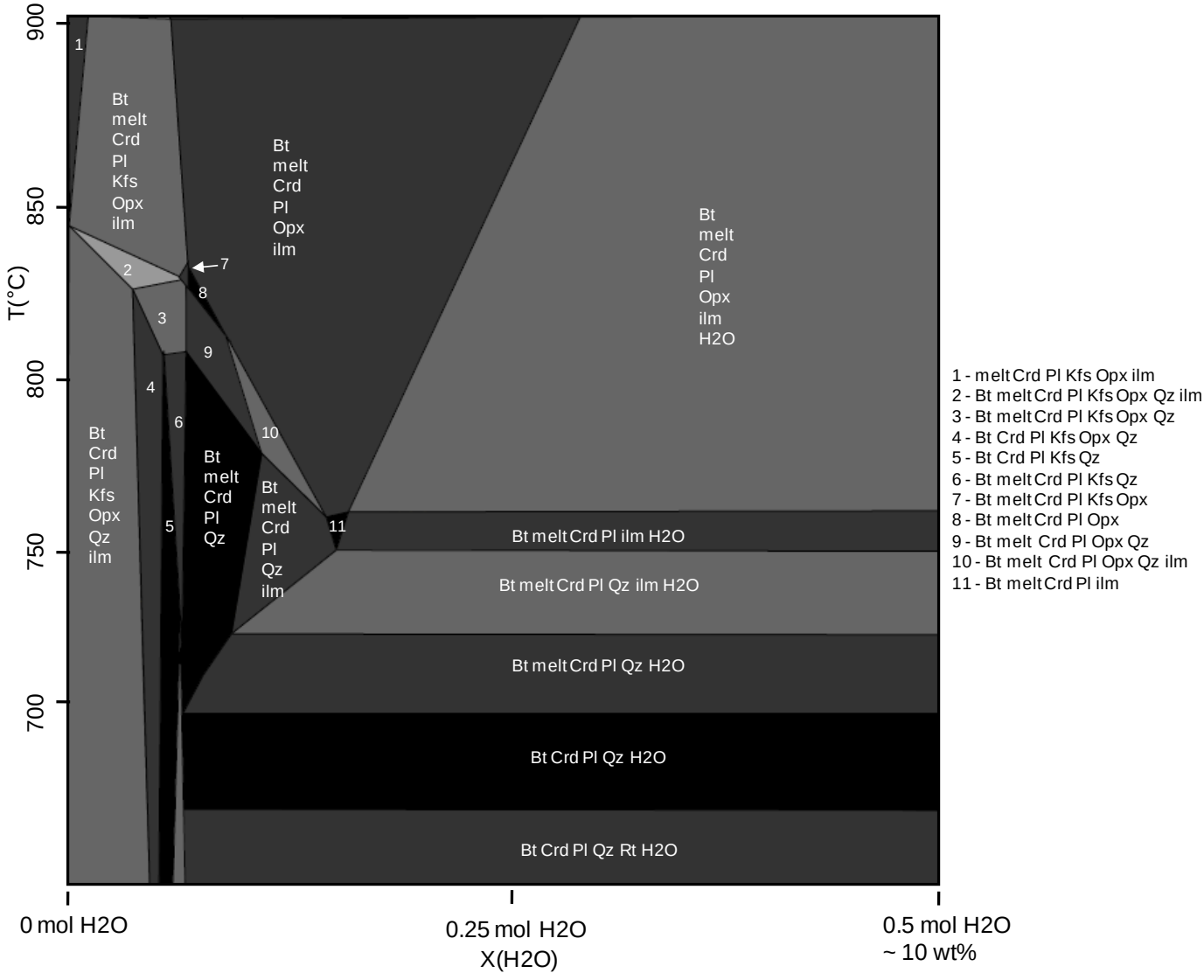

Bedded Pyrrhotite Unit xenolith DC-69; NCKFMASHMT; P = 2.5 kbars

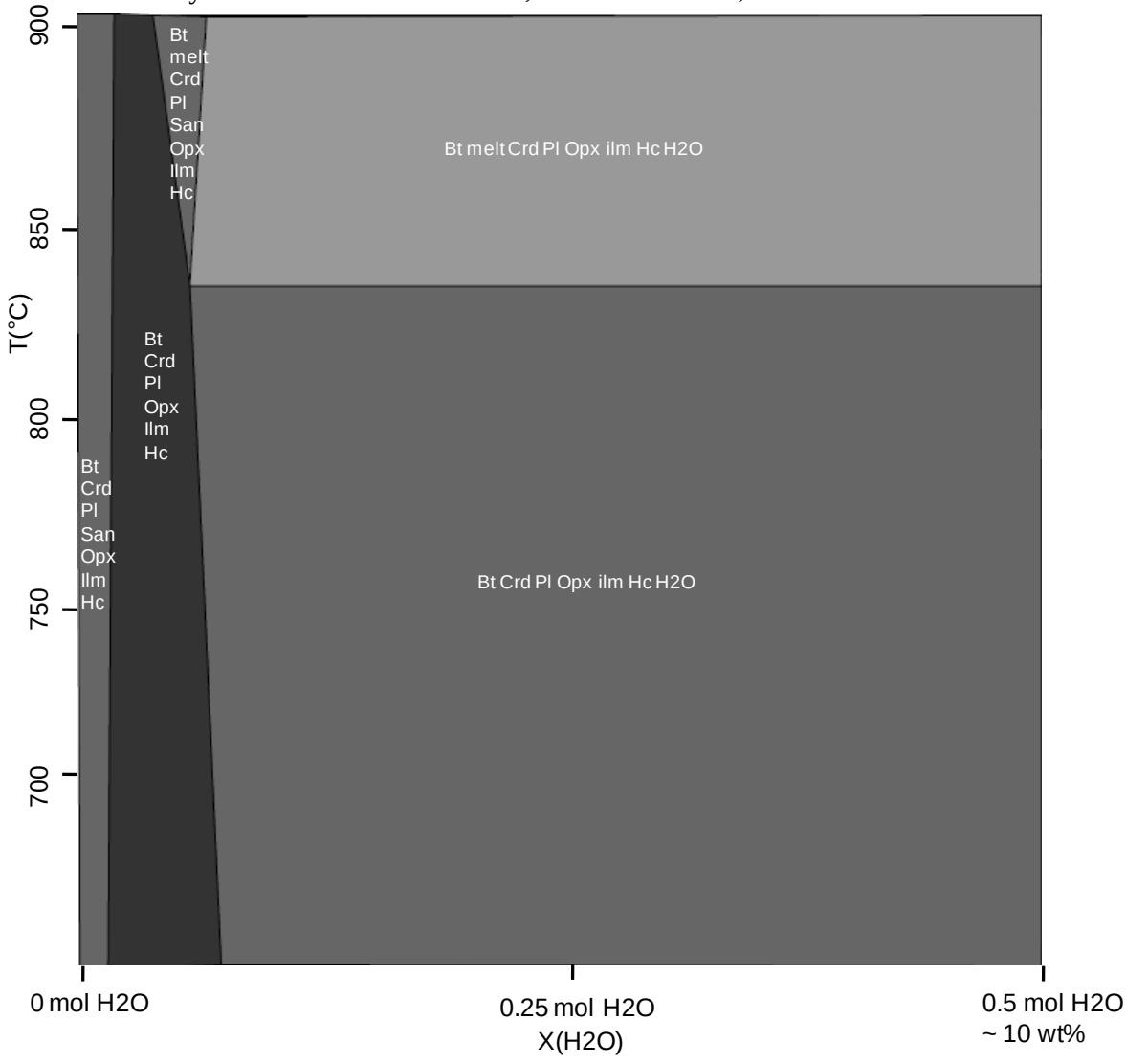

ANNEXE 8: CARTOGRAPHIE XRF – BORDURE FONDUE DE XÉNOLITHE

Abréviations:

BPU = Bedded Pyrrhotite Unit

Pl = Plagioclase

Qtz = Quartz

Kfs = Feldspath potassique

Opx = Orthopyroxène

Note:

Les figures sont renseignées en anglais dans un souci de cohérence avec les publications présentées dans ce mémoire de doctorat.

Légende:

La figure A représente une cartographie chimique obtenue par cartographie XRF d'une marge de xénolithe BPU et du magma avoisinant. La zone riche en potassium en marge du xénolithe est interprétée comme étant le produit de fusion partielle du xénolithe. Les figures B et C montrent le détail de gouttelettes de sulfure à l'extérieur (B) et piégées (C) dans le produit de fusion partielle (Plg+Kfs+Qtz+OPX) du xénolithe.

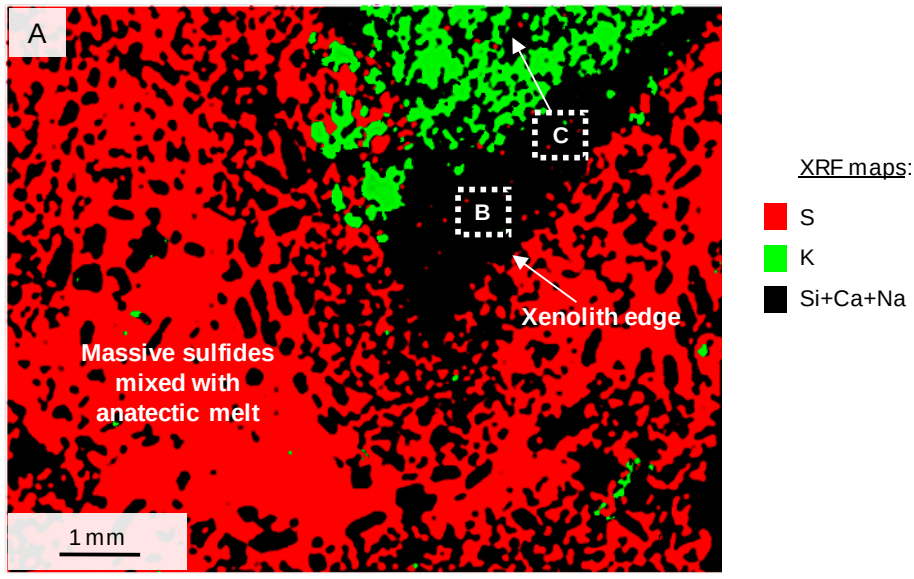
A
C
B
Xenolith edge
Massive sulfides
mixed with
anatectic melt
1 mm
XRF maps:
S
K
Si+Ca+Na

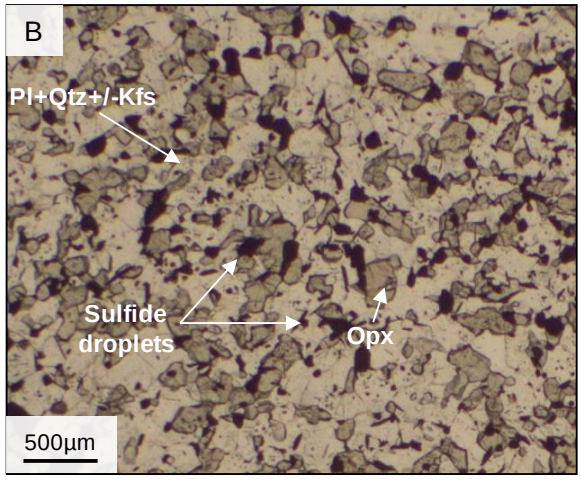
B
Pl+Qtz+/-Kfs
Sulfide
droplets
Opx
500µm

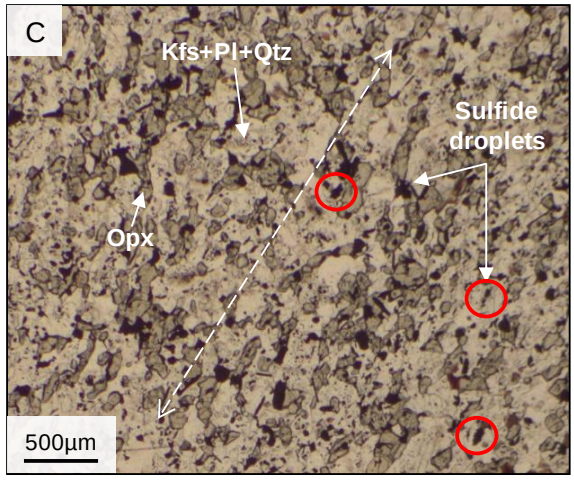
C
Kfs+Pl+Qtz
Sulfide
droplets
Opx
500µm

- **GAC-MAC Fredericton, Canada (Mai 2014)**

Proterozoic black shales: a source of S and semimetals for the formation of Cu-Ni-PGE magmatic deposits

Samalens N., Barnes S.-J., Sawyer E. W.

Département des sciences de la Terre, Université du Québec à Chicoutimi

Many black shale units close to magmatic nickel-copper-PGE (Platinum Group Elements) rich intrusions are thought to be the source of sulphur and semimetals in the ores. Contamination of a magma by country rock is thought to be essential to form magmatic Ni-Cu-PGE deposits.

The Duluth Complex (Minnesota, USA) represent an interesting example for studying the contamination processes. Many intrusions in the Duluth Complex, such as Partridge River Intrusion, are surrounded by sedimentary rocks of the Virginia Formation. Bedded Pyrrhotite Unit (BPU) in the Virginia Formation consists of black shales with sulfide-rich beds. In contrast to PGE-rich Devonian black shales the Proterozoic BPU black shales are PGE-poor. Furthermore, BPU black shales contain less Ni and Cu than average black shales.

Black shales in the BPU outside the contact aureole contain mainly pyrite whereas inside the aureole they contain various sulphur minerals, such as pyrrhotite and chalcopyrite. Presence of chalcopyrite requires Cu, and its source is currently unknown. In the less metamorphosed zones of the contact aureole framboidal pyrite is found. In the more metamorphosed parts of the contact aureole, pyrite has been transformed to pyrrhotite. BPU black shales are enriched in semimetals (As and Sb), have S/Se ratios greater than 20000 and an average $\delta^{34}S$ of 18‰.

Contamination processes occur in the basal part of the intrusion, close to the contact with BPU black shales units. Some fragments (xenoliths) of BPU are found inside the magma as a consequence of thermal erosion of the Virginia Formation during emplacement of the intrusion. BPU xenoliths in the magma are thought to be responsible for the sulphur and semimetals contamination of the magma. Progressive decrease in the S/Se ratios and $\delta^{34}S$ is recorded from the contacts to the interior of the intrusion. BPU xenoliths trapped in the magma contain mostly pyrrhotite, chalcopyrite and pentlandite sulfide assemblages. Gabbronorites close to xenoliths are enriched in semimetals and an increase in the S/Se ratios and $\delta^{34}S$ values occurs in gabbronorites surrounding fragments of BPU. Contamination of the magma in sulphur and semimetals is the result of melt transfer from xenoliths into the mafic magma as the xenoliths undergo partial melting. In

conclusion, black shales of BPU are the source of contamination of the magma in semimetals and sulphur essential for the formation of Ni-Cu-PGE deposits in the Duluth Complex.

- **SGA Nancy, France (Août 2015)**

Proterozoic black-shales: a source of sulfur and semi-metals for the formation of Ni-Cu-Platinum-group element deposits

Nadège Samalens, Sarah-Jane Barnes, Edward William Sawyer
Unité des Sciences de la Terre, Université du Québec à Chicoutimi, G7H 2B1, QC, Canada
Abstract. The basal unit of the Duluth Complex (Minnesota, USA) contains Ni-Cu sulfides. The S in these is thought to be derived from a sulfide-rich black shale unit known as the Bedded Pyrrhotite Unit (BPU) a stratigraphic unit within part of the host rocks. Numerous boreholes have been drilled through the basal unit of the Duluth Complex into the country rock and these allow investigation of the processes whereby S in the country rock was transferred to the mafic magma. The basal unit contains partially melted xenoliths of the Bedded Pyrrhotite Unit and the mafic rocks surrounding these show a progressive decreases in: S/Se, $\delta^{34}S$, and semi-metal contents away from the xenoliths. The partial melt of the xenoliths contained small sulfide droplets. We suggest that sulfur and semi-metals (Sb, Bi, As and Pb) were transferred to the mafic magma via the droplets. The sulfide droplets then equilibrated with the mafic magma and collect Ni, Cu and platinum-group elements (PGE). During the final stage of crystallization of the sulfide liquid the semi-metals combined with the PGE to form platinum-group minerals.

Keywords. Duluth Complex, Proterozoic black-shales, *in-situ* assimilation, Ni deposits, magmatic sulfides, LA-ICP-MS

1 Introduction

Most of world's Ni-Cu-PGE deposits were formed after the addition of sulfur to the magma from an external source in the country rocks (Ripley and Li 2013). It is generally thought that this S is derived from black shales. Black shales are also rich in semi-metals (As, Sb, Te and Bi). Interestingly, these elements are necessary for the formation of many of the platinum-group minerals (PGM). Thus the question arises: are these elements also derived from the black-shales?

The Partridge River Intrusion of the Duluth Complex represents an ideal and well-documented location for studying contamination processes. Mineralization is found in the basal part of the intrusion close to its contact with sedimentary country rocks of the Virginia Formation (Severson and Hauck 2008).

A particular unit in the Proterozoic Virginia Formation, called Bedded Pyrrhotite Unit, is composed of pyrrhotite-rich black-shales. Thériault and Barnes (1998) proposed that sulfur was transferred to the mafic magma after partial melting of entrained xenoliths in the magma. Subsequently, the Bedded Pyrrhotite Unit has been identified as the source of the sulfur that contaminated the mafic magma (Queffurus and Barnes 2014). However, the exact mechanism by which the S is transferred by the partial melt is poorly understood.

Therefore, we have carried a petrographic, mineralogical and geochemical study of the interactions between xenoliths of the Bedded Pyrrhotite Unit and the enclosing mafic magma in the basal part of the Partridge River Intrusion.

2 Geological setting

The Duluth Complex is a Keweenawan-age (1100 Ma) mafic complex located in Minnesota, USA. The Complex is composed of several mafic intrusions related to a mantle plume that was located beneath the mid-continental rift system (Ojakangas et al. 2001). The country rocks to the Duluth Complex consist of sediments ranging from banded iron formation through carbonates, but are predominately greywackes and pelites. Of particular interest is the Bedded Pyrrhotite Unit, a sulfide-rich black shale believed to have been deposited in restricted anoxic basins. This unit is approximately 200 m thick, but has a sporadic distribution.

The Duluth Complex can be divided into three mafic intrusions: the Partridge River Intrusion, the Bathtub Intrusion and the South Kawishiwi Intrusion. The basal unit (Unit I) of the Partridge River Intrusion contains abundant xenoliths of the host-rocks and most of the sulfide mineralization (Severson and Hauck 2008). Unit 1 is composed of the following lithologies: norite, gabbronorite and troctolite, from the base to the center of the intrusion. Norites are found near to the contact with the Virginia Formation country rocks and around xenoliths of country rock. Disseminated to massive Ni-Cu sulfides occur in Unit I. Sulfides are commonly found around the xenoliths.

Samples were chosen on from boreholes that crossed the contact between the Virginia Formation and Partridge River Intrusion at the Dunka Road, Mesaba and Wetlegs deposits.

3 Results

3.1 Petrography

Temperatures of greater than 800°C have been reported from diatexite migmatites found close to the contact with the intrusion (Sawyer 2014).

The Bedded Pyrrhotite Unit is divided into unmetamorphosed and metamorphosed depending upon whether inside or outside of the contact aureole that is developed around the intrusion. Unmetamorphosed Bedded Pyrrhotite Unit, outside the contact aureole, contains pyrite and few grains of chalcopyrite. Metamorphosed Bedded Pyrrhotite Unit in the contact aureole, is composed of pyrrhotite-rich beds with chalcopyrite. Pentlandite is absent.

Xenoliths of the Bedded Pyrrhotite Unit in the basal unit of the intrusion contain disrupted, or delaminated, pyrrhotite-rich beds that also have cubanite, chalcopyrite and pentlandite (Fig. 1a).

Former anatectic melt occurs as pockets (pores) and interconnected networks in the xenoliths of the Bedded Pyrrhotite Unit and in the Bedded Pyrrhotite Unit country rock immediately adjacent to the contact with the intrusion. Rounded grains of sulfide occur widely within in the anatectic melt, and commonly appear to be trapped in pockets (Fig. 1b). These are interpreted to be globules of a former sulfide melt carried by the silicate anatectic melt.

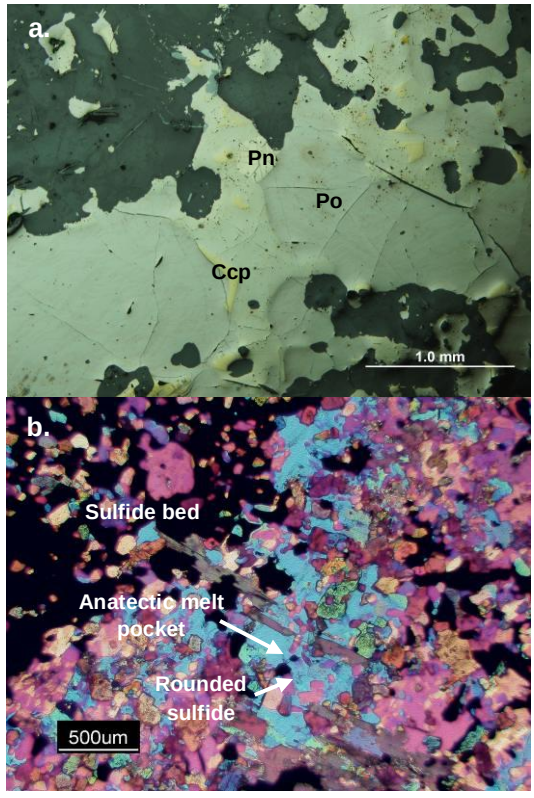

Figure 1. Sulfides textures of xenoliths of the Bedded Pyrrhotite Unit. a) Sulfide bed with pyrrhotite (Po), chalcopyrite (Ccp) and pentlandite (Pn). b) Sulfide droplets trapped in a pocket of former anatectic melt. Both from xenolith at the Mesaba Deposit, Partridge River Intrusion.

Mineralization, in the mafic rocks of the basal unit of the intrusion, consists of pyrrhotite, cubanite, chalcopyrite and pentlandite disseminated and massive sulfides. Extensive mineralization is hosted by the norites which occur in the vicinity of the xenoliths and at the contact with the Bedded Pyrrhotite Unit in the country rocks.

3.2 Geochemical results

The Bedded Pyrrhotite Unit has the highest S/Se (~20,000) and $\delta^{34}S$ (~16‰). A progressive decrease of S/Se and $\delta^{34}S$ is observed from xenoliths of the Bedded Pyrrhotite Unit outwards into gabbronorite with intermediate values in the norites, as shown in previous work (Queffurus and Barnes 2014).

The Bedded Pyrrhotite Unit contains the highest concentrations of the semi-metals Sb, As, Bi and Pb. A progressive decrease in Sb, As and Bi concentration occurs from the xenoliths of the Bedded Pyrrhotite Unit out into the mafic rocks (Fig. 2a; left-hand side). Xenoliths of the Bedded Pyrrhotite Unit and the norites have similar contents of semi-metals, but the gabbronorite is depleted in them. These observations are supported by LA-ICP-MS analyses from pyrrhotite, chalcopyrite, cubanite and pentlandite, which show that the sulfide minerals in the Bedded Pyrrhotite Unit are richer in Bi, As and Pb than the sulfide minerals from either the norite or the gabbronorite. This observation suggests that semi-metals from the xenoliths of the Bedded Pyrrhotite Unit contaminated the mafic magma of the intrusion (Fig. 2b).

In contrast PGE, Ni and Cu concentrations are highest in the gabbronorite and lowest in xenoliths of the Bedded Pyrrhotite Unit; intermediate values occur in the norites (Fig. 2a; right-hand side). This relationship suggests that these elements were derived from the mafic magma. Furthermore, xenoliths of the Bedded Pyrrhotite Unit record higher PGE (except Pt), Ni and Cu contents than the Bedded Pyrrhotite Unit in

the country rocks. This indicates the exchange of material is complex; the semi-metals have been transferred from the xenoliths to the mafic rocks, whereas PGE, Ni and Cu have been transferred in the opposite direction from the mafic magma to the xenoliths of the Bedded Pyrrhotite Unit.

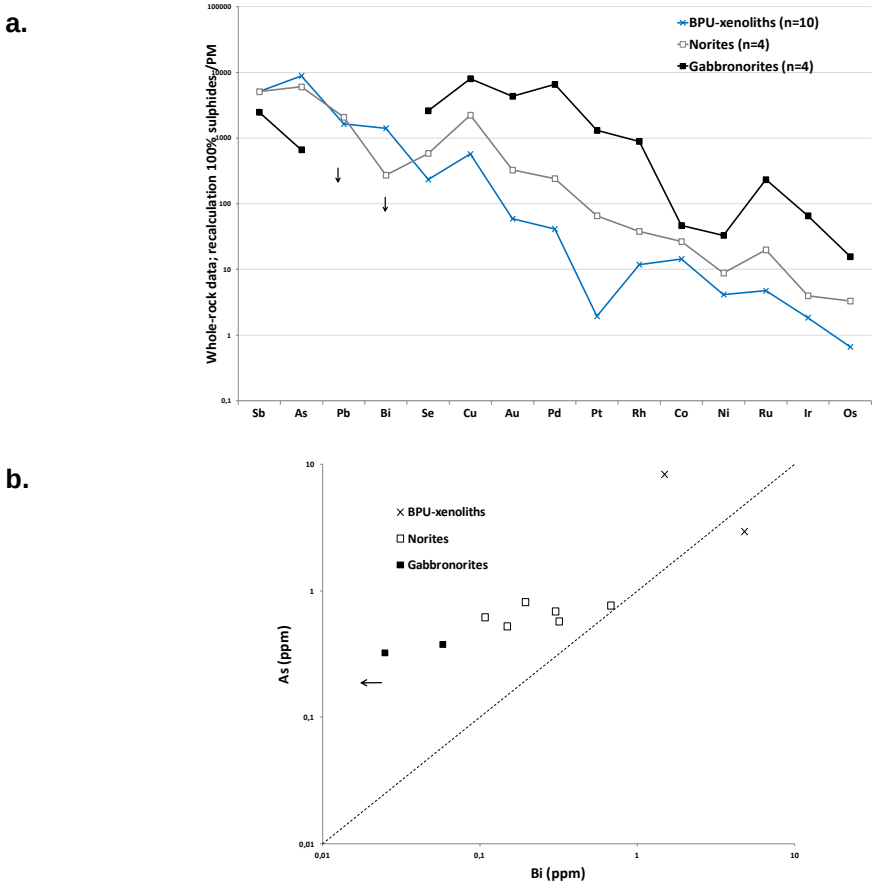

Figure 2. Semi-metals and PGE contents for rocks within the intrusion. a) Semi-metals and PGE whole-rock concentrations in 100 % sulfides and normalized to primitive mantle (Lyubetskaya and Korenaga 2007) for rocks within the intrusion. Note Medians of all series are plotted on diagrams. Arrows indicate values lower than the limit of detection (LOD). b) Arsenic and Bi concentrations from LA-ICP-MS analysis of cubanite for rocks within the intrusion. Arrow indicates values lower than the limit of detection (LOD).

3.3 Platinum-group minerals

Platinum-group minerals (PGM) are found in the cubanite and chalcopyrite from gabbronorites. Back-scattered electron imaging and semi-quantitative analyses were carried out by Scanning Electron Microscopy. Palladium-rich PGM: polarite (Pd-Bi), paolivite (Pd_2Sn), zvyageintsevite (Pd_3Pb) and atokite (Pd_3Sn+Pt) are present.

4 Discussion and Conclusions

Many studies (Ripley and Alawi 1988; Thériault and Barnes 1998; Queffurus and Barnes 2014) show that there was sulfur contamination of the Partridge River Intrusion mafic magma by the Virginia Formation country rocks. A model of *in-situ* assimilation of partial melts from xenoliths of the Bedded Pyrrhotite Unit into the mafic magma has been proposed by Queffurus and Barnes (2014) as a mechanism by which S contamination of the magma occurred. This model is based on comparison of S/Se and $\delta^{34}S$ ratios between Bedded Pyrrhotite Unit xenoliths and magmatic lithologies. In our work, S/Se and $\delta^{34}S$ ratios from xenoliths of the Bedded Pyrrhotite Unit and associated magmatic rocks are in agreement with such a model.

Our work expands on the previous and suggests that *in-situ* assimilation of partial melt from the xenoliths of Bedded Pyrrhotite Unit leads to contamination of the mafic magma by the semi-metals as well. Antimony, Bi, As and Pb are transferred from Bedded Pyrrhotite Unit xenoliths to the mafic magma in droplets of anatectic sulfide melt that were entrained in the more voluminous silicate anatectic melt. Consequently, xenoliths of the Bedded Pyrrhotite Unit xenoliths are impoverished in semi-metals as a result of their transfer (i.e. loss) to the mafic magma.

Semi-metals contamination of the mafic magma by the Bedded Pyrrhotite Unit permits the formation of palladium-rich platinum-group minerals. These could form by two processes. Firstly, a high content of semi-metals in sulfide melt decreases PGE solubility and this results in the crystallization of PGM (Hutchinson and McDonald 2008). Secondly, the PGM exsolve during cooling from base metal sulfides (Barnes et al. 2008). The semi-metal content in sulfide melt is critical to the type of PGM that form.

A new discovery from our work is that sulfur and semi-metal contamination in the mafic magma is coupled with Ni, Cu and PGE transfer from the mafic magma to xenoliths of the Bedded Pyrrhotite Unit. The transfer of nickel accounts for the presence of pentlandite in xenoliths of Bedded Pyrrhotite Unit and for its absence in the samples from outside of the intrusion.

Partial melting in xenoliths of the Bedded Pyrrhotite Unit xenoliths represents a key process in the contamination of mafic magma (Thériault and Barnes 1998; Queffurus and Barnes 2014). Petrological observations from xenoliths of the Bedded Pyrrhotite Unit reveal the occurrence of rounded droplets of sulfides trapped in pockets of crystallized former anatectic melt. We suggest that small droplets of sulfide melt were carried into the mafic magma by silicate anatectic melt expelled from xenoliths of the Bedded Pyrrhotite Unit and thereby transferred S and semi-metals to the mafic magma. On the other hand the enrichment of Ni, Cu and PGE in the xenoliths suggests that these elements have been transferred in the opposite direction from the mafic magma to the xenoliths; exactly how this happens is not yet understood.

Acknowledgments

This research was financed by the NSERC Discovery Grant Program and the Canada Research Chair in Magmatic Metallogeny. We thank Mark Severson for providing some samples of the Bedded Pyrrhotite Unit from outside the contact aureole. Sadia Medhi and Dany Savard from LabMaTer are thanked for help in carrying out analyses.

References

Barnes S-J, Prichard HM, Cox RA, Fisher PC, Godel B (2008) The location of the chalcophile and siderophile elements in platinum-group element ore deposits (a textural, microbeam and whole rock geochemical study): Implications for the formation of the deposits Chemical Geology 248:295-317

Hutchinson D, McDonald I (2008) Laser ablation ICP-MS study of platinum-group elements in sulfides from the Platreef at Turfspruit, northern limb of the Bushveld Complex, South Africa. Mineralium Deposita 43(6):695-711

Lyubetskaya T, Korenaga J (2007) Chemical composition of Earth's primitive mantle and its variance: 1. Method and results. Journal of Geophysical Research: Solid Earth 112(B3):B03211

Ojakangas RW, Morey GB, Green JC (2001) The Mesoproterozoic Midcontinent Rift System, Lake Superior Region, USA. Sedimentary Geology 141–142(0):421-442

Queffurus M, Barnes S-J (2014) Selenium and sulfur concentrations in country rocks from the Duluth Complex, Minnesota, USA: Implications for formation of the Cu-Ni-PGE sulfides. Economic Geology 109(3):785-794

Ripley EM, Alawi JA (1988) Petrogenesis of pelitic xenoliths at the Babbitt Cu-Ni deposit, Duluth Complex, Minnesota, U.S.A. Lithos 21(2):143-159

Ripley EM, Li C (2003) Sulfur isotope exchange and metal enrichment in the formation of magmatic Cu-Ni-(PGE) deposits. Economic Geology 98:635-641

Sawyer EW (2014) The inception and growth of leucosomes: microstructure at the start of melt segregation in migmatites. Journal of Metamorphic Geology 32:695-712

Severson MJ, Hauck SA (2008) Finish Logging of Duluth Complex Drill Core (And a Reinterpretation of the Geology at the Mesaba (Babbitt) deposit). NRRI/TR-2008/17

Thériault RM, Barnes S-J (1998) Compositional variations in Cu-Ni-PGE sulfides of the Dunka road deposit, Duluth Complex, Minnesota: The importance of combined assimilation and magmatic processes. The Canadian Mineralogist 36:869-886

- **SEG Hobart, Australie (Septembre 2015)**

Sulfur Transfer into Mafic Magma from Sediment - Reaction of Sedimentary Sulfides with and into Mafic Magmas.

Sarah-Jane Barnes,[1*] and Nadège Samalens,[1]

[1]Sciences de la Terre, Université du Québec à Chicoutimi, G7H 2B1, Canada

There is ample evidence (e.g. S isotopes and S/Se) that much of the S in that magmatic nickel deposits is derived from sedimentary rocks. However, exactly how the S is transferred from the sediments to the magma is not clearly understood. In part this is because the site of S addition to the magma is generally not the site of the formation of an ore deposit and thus these locations are not as well studied as the ore deposits themselves. In order to understand the process of S transfer to the magma one needs to look at the site of contamination rather than the ore deposits. A suitable example is the basal unit of the Duluth Complex (Minnesota).

The basal unit contains numerous Ni-Cu occurrences and importantly xenoliths of partly melted black shale. Samples of the black shale from outside the intrusion, from the xenoliths and from the magma have all been examined and analyzed. The nature and texture of the sulfide minerals changes from Po+Cp in the contact aureal to droplets in the partial melt in the xenoliths, to Po+Cp+/-Cb+Pn patches in the mafic rocks. Whole rock δS^{34}, S/Se, Ni, Cu PGE, As, Bi and Sb tenors vary with distance from the xenoliths. Samples show a fall in δS^{34}, S/Se, As Bi and Sb tenors and an increase in Ni, Cu and PGE tenor with distance from the xenoliths. The Ni, Cu and PGE tenors are higher in the xenoliths than in black shale of the contact aureal. In situ laser abalation analysis of the chalcopyrites and cubanites from the three different settings show that the chalcopyrite from the black shale in the aureal has the highest As, Bi and Sb concentrations, the xenolith chalcopyrites have intermediate values and the chalcopyrites from the mafic rocks have the lowest values.

Combining all of these observations leads to a model where S is incorporated into the mafic magma when xenoliths undergo partial melting to form a granitoid melt with sulfide droplets. Interestingly the composition of these sulfides is richer in Ni Cu and PGE than the sulfides in the black shales possibly due to diffusion of these elements from the mafic magma through the granitoid melt into the xenolith sulfide melt. As the degree of melting increases some granitoid melt escapes into mafic magma carrying the sulfide droplets with it. These sulfides are rich in As, Bi and Sb and if they are trapped close to the xenolith the resulting rock will be enriched in these elements, but not particularly rich in the Ni and PGE because the sulfide melt has not interacted

with sufficient mafic melt to collect these elements. If the degree of melting of xenolith rises even further large portions of the silicate part of the xenolith melt and dissolve into the mafic magma leaving a residual of refractory material rimmed by semi to massive sulfides, which are poor in metals because they have not interacted with very much mafic magma. If there is some disturbance such as a new injection of magma or an earthquake the sulfide liquid around the xenolith can be transported away from the xenolith and if the sulfide liquid interacts with sufficient magma become rich enough to form a Ni deposit.

➢ **GOLDSCHMIDT Yokohama, Japon (Juin 2016)**

A model of S and semimetals contamination of mafic magma by black-shales for the formation of Ni-Cu-Platinum-group elements deposits

N. SAMALENS[1*], S.-J. BARNES[1], E.W. SAWYER[1]

[1]Université du Québec à Chicoutimi, Chicoutimi, G7H2B1, QC, Canada
(*correspondence: nadege.samalens1@uqac.ca)

The basal unit of the Duluth Complex (Minnesota, USA) contains Ni-Cu sulfides. The S in these is thought to be derived from a sulfide-rich black shale unit known as the Bedded Pyrrhotite Unit (BPU). Partial melting of the BPU xenoliths in the mafic magma represents a key process in its contamination.

Petrographic observation shows that droplets of sulfide melt derived from the BPU were entrained in anatectic silicate melt of the BPU and transferred to the mafic magma by the melt (Fig. 1). Whole rock and laser ablation analysis show that in addition to S the droplets transferred Sb, Bi, As and Pb to the magma. The sulfide droplets closest to the xenoliths are richest in these elements and poor in platinum-group elements (PGE) compared with sulfide droplets farther from the xenoliths. The change in composition of the sulfides with distance from the xenoliths is thought to reflect increasing reaction of the sulfide with mafic magma.

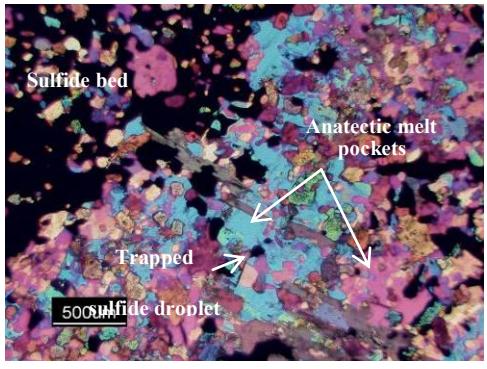

Figure 1: Sulfides droplets in the silicate anatectic melt.

An intriguing complication to this model is that sulfide droplets in the xenolith anatectic melt are richer in Ni, Cu and PGE than sulfides in the contact aureole of the intrusion. This suggests that these elements diffused in from the mafic magma through anatectic melt and into the sulfide droplets before the sulfide droplets transferred to the mafic magma. Diffusion is possibly driven by chemical potential gradients.